Mass Spectrometry Based Quantification of 1, 3-Butadiene Induced DNA Adducts: Potential Biomarkers of Cancer Risk

A DISSERTATION
SUBMITTED TO THE FACULTY OF THE GRADUATE SCHOOL OF THE
UNIVERSITY OF MINNESOTA
BY

Dewakar Sangaraju

IN PARTIAL FULFILLMENT OF THE REQUIREMENTS
FOR THE DEGREE OF
DOCTOR OF PHILOSOPHY

Dr. Natalia Y. Tretyakova, Adviser

November 2014

Acknowledgements

I would like to thank and express my sincere gratitude to my advisor, Dr. Natalia Tretyakova, for her constant support, guidance and source of inspiration over the last five years. I am also thankful to Dr. Stephen Hecht, Dr. Rodney Johnson and Dr. William Pomerantz for agreeing to serve as my thesis committee members and for their valuable feedback and suggestions. I would also like to express my thanks to our collaborators Dr. Vernon Walker (University of Vermont-Burlington, VT), Dr. James Swenberg (University of North Carolina-Chapel Hill, NC) and Dr. Colin Campbell (University of Minnesota, Minneapolis, MN) for their help and support in this research work. I would also like to thank the NIH and the Department of Medicinal Chemistry at University of Minnesota, Minneapolis for their financial support.

I also want to express my sincere thanks to Dr. Peter Villalta for his help and training with the new LTQ Orbitrap instrumentation and high resolution mass spectrometry. I am thankful to Brock Matter for training me in HPLC and MS instrumentation and all my current and past lab members for their valuable discussions and suggestions during research progress meetings that played a key role in the thesis progress. I am especially thankful to Dr. Melissa Goggin, Dr. Srikanth Kotapati, Maria O. Agunsoye, Arnie Groehler, Dr. Susith Wickramaratne and Emily Boldry for making significant contributions to my thesis. I am also thankful to Dr. Delshanee Kotandeniya, Xun Ming, Dr. Bhaskar Malayappan, Chris Seiler, Dr. Teshome Gherezghiher and Dr. Jung-Eun Yeo for their helpful insights and technical discussions during my Ph.D. studies.

I would also thank Bob Carlson for his valuable help in preparing graphics for this thesis and other publications. I am also thankful to members of Hecht lab, Murphy lab and Peterson lab for allowing me to use their labs instrumentation.

Last but not least, I could not have accomplished this work without the support of my family and friends, especially my parents Late S. Chiranjeevi and S. Radha. I would also like to thank my brother Damodar Raju Swamy, my cousins Kiran Kumar Koneti, Divya Koneti and their family, my uncles Raja Muppala, Narasaraju Muppala and their families for their support during my graduate studies. Special thanks to all my friends in the US and India for their continuous support and encouragement.

Dedication

This work is dedicated to my beloved father Chiranjeevi, my mother Radha and my grandmother Jayamma.

Abstract

Chemical carcinogenesis involves metabolic activation of carcinogens to electrophilic species which can react with important cellular biomolecules including DNA to form covalent adducts. Covalent carcinogen-DNA adducts which are not removed by DNA repair mechanisms can induce transforming mutations, ultimately leading to cancer. Hence, carcinogen-DNA adducts are deemed the ultimate biomarkers of carcinogen exposure, metabolic activation, and possibly of cancer risk.

1,3-Butadiene (BD) is a recognized human and animal carcinogen present in cigarette smoke, automobile exhaust, wood fires, and also in some occupational settings such as BD monomer and polymer plants. BD is metabolically activated by CYP2E1 to form three electrophilic epoxides: 3,4-epoxy-1-butene (EB), 3,4-epoxy-1,2-butanediol (EBD), and 1,2,3,4-diepoxybutane (DEB). EB, EBD, and DEB can modify DNA bases to form covalent DNA adducts such as N-7-(1-hydroxy-3-buten-2-yl) guanine (EB-GII), N7-(2, 3, 4-trihydroxybut-1-yl)-guanine (N7-THBG) and 1,4-*bis*-(guan-7-yl)-2,3-butanediol (*bis*-N7G-BD). Although BD-DNA adducts had been successfully detected and quantified in tissues of laboratory animals exposed to relatively high concentrations of BD ($\geq$ 6.25 ppm), they had not been previously quantified in humans, preventing their use as biomarkers of BD exposure, metabolic activation, and cancer risk. The main purpose of this research was to develop ultra-sensitive bioanalytical methodologies based on mass spectrometry to enable the detection and quantitation of BD-DNA adducts in animals treated with sup-ppm levels of BD and in exposed human populations.

In Chapter 2 of the thesis, a novel nanoHPLC-nanoESI$^+$-MS/MS method was developed for sensitive, accurate, and precise quantitation of BD-induced guanine-guanine cross-links (1,4-*bis*-(guan-7-yl)-2,3,-butanediol, *bis*-N7G-BD) in tissues of laboratory mice treated with low - sub-ppm concentrations of BD (0.5-1.5 ppm) which approximate human occupational exposure to BD (1 ppm). *Bis*-N7G-BD concentrations increased in a concentration-dependent manner in mouse liver DNA as a function of BD exposure. In Chapter 3 of this Thesis, we investigated DNA repair mechanisms responsible for *bis*-N7G-BD repair using isogenic Chinese hamster lung fibroblasts proficient or deficient in nucleotide excision repair (NER) and Fanconi Anemia (FA) repair pathways. We found that while both pathways contributed to *bis*-N7G-BD removal, FA pathway was most effective at alleviating the toxicity and replication blockage imposed by *bis*-N7G-BD cross-links.

To enable BD-DNA adduct detection in humans, we developed an isotope dilution capillary HPLC-ESI$^+$-HRMS/MS methodology for the most abundant BD-DNA adducts identified in vivo: N7-(2,3,4-trihydroxybut-1-yl)-guanine (N7-THBG) (Chapter 4). This method was successfully applied to quantify N7-THBG adducts in blood leukocyte DNA of smokers, nonsmokers, and occupationally exposed workers. In addition, we have developed an isotope dilution nanoLC/ESI$^+$-HRMS^3 methodology for the quantitation of BD-induced N-7-(1-hydroxy-3-buten-2-yl) guanine (EB-GII) adducts in human blood leukocyte DNA and human urine (Chapters 5 and 6). This method was applied to quantify EB-GII adducts in blood and urine of BD-exposed populations such as smokers, nonsmokers, and occupationally exposed workers.

Overall, during the course of the studies described in this Thesis, we have developed a range of novel mass spectrometry-based quantitative methods which have excellent sensitivity, accuracy, and precision, and can be used for future human BD exposure biomonitoring studies. Furthermore, these methodologies are now being employed in epidemiological studies to identify any ethnic/racial differences in BD bioactivation and to help understand the origins of ethnic/racial differences in lung cancer risk in smokers.

Table of Contents

List of Tables

List of Figures

Schemes

Figures

List of Abbreviations

1,N^6-α-HMHP-dA	1,*N*^{6}-(1-hydroxymethyl-2-hydroxypropan-1,3-diyl)-2′-deoxyadenosine
	1,*N2*-etheno-2'-deoxyguanosine
1,N^2-ε -dGuo	1,*N*^{2}-etheno-2'-deoxyguanosine
1,N^6-γ-HMHP-dA	1,*N*^{6}-(2-hydroxy-3-hydroxymethylpropan-1,3-diyl)-2′-deoxyadenosine
4-ABP	4-aminobiphenyl
A	Adenine
AA	Acrylamide
ADH	alcohol dehydrogenase
APCI	atmospheric pressure chemical ionization
BD	1,3-butadiene
bis-BDMA	1,4-bis-(N-acetylcysteinyl)butane-2,3-diol
bis-N7G-BD	1,4-*bis*-(guan-7-yl)-2,3,-butanediol
BP-6-N7Gua	N7-(benzo[a]pyrene-6-yl)guanine
BPDE	*trans*-7,8-dihydroxy-*anti*-9,10-epoxy-7,8,9,10-tetrahydrobenzo[a]pyrene
C	cytosine
C8(1-HE)g	C8-(1-hydroxyethyl)guanine
C8-dG-MeIQx	N-(deoxyguanosine-8-yl) MeIQx; *N2*-dG-MeIQx, 5-(deoxyguanosin-*N2*-yl) MeIQx
capLC-nanoESI	capillary HPLC-nanoelectrospray ionization-tandem mass spectrometry
CedG	N2-(1-carboxyethyl)-2'-deoxyguanosine
CNL	constant neutral loss
CP-d(GpG)	cisplatin 1,2-guanine-guanine intrastrand cross-link
CID	collision induced dissociation
CYP 450	cytochrome P450 monooxygenase
DEB	1,2,3,4-diepoxybutane

dG-BPDE	10-(deoxyguanosin-N^2-yl)-7,8,9-trihydroxy-7,8,9,10-tetrahydrobenzo[a]pyrene
dG-C8-4-ABP	*N*-(deoxyguanosin-8-yl)-4-ABP
dG-C8-IQ	*N*-(deoxyguanosine-8-yl)-2-amino-3-methylimidazo [4,5-*f*] quinoline
dG-desMeTam	(*E*)-α-(deoxyguanosin-*N2*-yl)-N-desmethyl tamoxifen
dG-Tam	(*E*)-α-(deoxyguanosin-*N2*-yl) tamoxifen
DHBMA	dihydroxybutyl mercapturic acid [4-(*N*-acetyl-L-cystein-S-yl)-1,2-dihydroxybutane]
DNA	deoxyribonucleic acid
EB	3,4-epoxy-1-butene
EBD	3,4-epoxy-1,2-diol
EB-GI, EB-Guanine I	N-7-(2-hydroxy-3-buten-1-yl) guanine
EB-GII, EB-Guanine II	N-7-(1-hydroxy-3-buten-2-yl) guanine
EH	epoxide hydrolase
ESI	electro spray ionization
FTMS	fourier transform mass spectrometry
fmol	Femto mole (10^{-15} mole)
G	Guanine
GST	glutathione S-transferase
GWAS	genome-wide association study
Hb	Hemoglobin
HB-Val	*N*-(2-hydroxy-3-butenyl)–valine
HILIC	hydrophilic interaction liquid chromatography
HMVK	Hydroxymethylvinylketone
His	histidine
HPLC-ESI+-MS/MS	high pressure liquid chromatography-electrospray ionization tandem mass spectrometry
IDMS	isotope dilution mass spectrometry
IS	internal standard
LOD	limit of detection

LOQ	limit of quantitation
MeIQx	2-amino-3,8-dimethylimidazo-[4,5f]quinoxaline
MHBMA	monohydroxybutenyl mercapturic acid [2-(*N*-acetyl-L-cystein-S-yl)-1-hydroxybut-3-ene + 1-(*N*-acetyl-L-cystein-S-yl)-2-hydroxybut-3-ene]
MS/MS	tandem mass spectrometry
nmol	nano mole (10^{-9} mole)
NMR	nuclear magnetic resonance
N1-THBA	N1-(2,3,4-trihydroxybut-1-yl)-adenine
N7G-N1A-BD	1-(guan-7-yl)-4-(aden-1-yl)-2,3-butanediol
N7G-N3A-BD	1-(guan-7-yl)-4-(aden-3-yl)-2,3-butanediol
N7G-N6A-BD	1-(guan-7-yl)-4-(aden-6-yl)-2,3-butanediol
N7G-N7A-BD	1-(guan-7-yl)-4-(aden-7-yl)-2,3-butanediol
N7-THBG	N7-(2,3,4-trihydroxybut-1-yl)-guanine
nanoLC-nanoESIMS/MS	nanoflow liquid chromatography-nanoelectrospray ionizationtandem mass spectrometry
OHEG	O^6-2-hydroxyethyl-2'-doexyguanosine
ppm	parts per million
Pyr-Val	N,N-(2,3-dihydroxy-1,4-butadiyl)-valine
pmol	Pico mole (10^{-12} mole)
ROS	reactive oxygen species
SPE	solid phase extraction
SRM	selected reaction monitoring
T	thymine
THB	trihydroxybutyl
THBMA	trihydroxybutyl mercapturic acid [4-(*N*-acetyl-L-cystein-S-yl)-1,2,3-trihydroxybutane]
THB-Val	1,2,3-trihydroxybutyl-valine
Tyr	tyrosine
U	Uracil
UDG	uracil DNA glycosylase

TOF	time of flight
TSQ	triple stage quadrupole

I. LITERATURE REVIEW

1.1 Carcinogen induced DNA adducts as biomarkers of exposure and cancer risk

1.1.1 Role of DNA adducts in chemical carcinogenesis

Humans are exposed to multiple chemical carcinogens from various exogenous sources such as air *(1)*, water *(2)*, and food *(3)*, as well as endogenous reactive oxygen species (ROS) *(4)* and lipid peroxidation products *(5)*. These reactive species can either directly or indirectly react with essential cellular biomolecules such as proteins, DNA, RNA, and lipids, producing undesirable biological effects such as cellular toxicity and genetic mutations *(6)*.

Directly acting DNA modifying agents include reactive alkylating agents, reactive oxygen species, aldehydes and α, β-unsaturated carbonyl compounds *(6;7)*. In contrast, carcinogenic molecules known as *pre-carcinogens* require some form of metabolic activation to be converted to the ultimate reactive electrophilic metabolites, which modify cellular biomolecules *(8)*. Electrophilic carcinogen metabolites can undergo detoxification to nontoxic metabolites which are excreted in blood and urine *(9)*.

If not detoxified, activated carcinogen metabolites can react with DNA nucleobases (A, T, G, and C) to form covalent adducts *(10)*. Depending on their chemical structure, DNA adducts have variable stability and persistence in DNA *(11)*. They may or may not be recognized by specialized DNA repair mechanisms such as base excision repair (BER), nucleotide repair (NER), and homologous recombination repair (HRR) that restore DNA to its original state *(12)*. Unrepaired DNA adducts can interfere with DNA replication *(13;14)*, causing toxicity and inducing irreversible genetic changes (mutations). Non-viable mutations can lead to apoptosis / programmed cell death *(15)*.

Viable mutations occurring within tumor suppressor genes *(16)* and protooncogenes *(17)* such as *Kras* and *p53* can lead to an uncontrolled cell growth and the initiation of cancer *(10)* (Scheme 1.1). Because of their direct role in the development of cancer, DNA adducts represent a biologically relevant dose of the carcinogen exposure and can be used as mechanism-based biomarkers of carcinogen exposure and metabolic activation *(18)*.

Some examples of DNA adducts induced by known carcinogens include alflatoxin B1 induced 8,9-dihydro-8-(N7-guanyl)-9-hydroxy aflatoxin B1(AFB1-N7-Gua) *(19)*, tobacco specific nitrosamine 4-(methylnitrosamino)-1-(3-pyridyl)-1-butanone (NNK) induced 7-[4-(3-pyridyl)-4-oxobut-1-yl]-2'-deoxyguanosine (7-pobdG) and O^2-[4-(3-pyridyl)-4-oxobut-1-yl]-2'-deoxycytosine (O^2-pobdC) *(20)*, polycyclic aromatic hydrocarbon benzo[a]pyrene induced *(+/-)-cis/trans-*N^2- benzo[a]pyrene dihydrodiol epoxide-2'-deoxyguanosine (N^2-BPDE-dG) *(21)*, heterocyclic amine 2-amino-1-methyl-6-phenylimidazo[4,5-b]pyridine (PhIP) induced N-(2'-deoxyguanosin-8-yl)-PhIP (dG-C8–PhIP) *(22)*, acrolein induced α/γ-hydroxypropano-2'-deoxyguanosine (HOP-dG) *(23)* and aristocholic acid (AA) induced 7-(deoxyadenosin-N^6-yl)aristolactam and 7-(deoxy-guanosin-N^2-yl)aristolactam adducts (Figure 1.1). Many common anticancer drugs act by forming toxic DNA adducts which are responsible for the pharmacological activity of these drugs. Some examples include cisplatin-induced N7-guanine-N7-guanine intrastrand cross-links (cis-Pt$(NH_3)_2$d(pGpG)) or Pt-(GG)) *(24)*, temozolomide-induced O^6 and N7-methyl guanine adducts *(25)*, and cyclophosphamide-induced interstrand DNA-DNA cross-links (G-NOR-G) *(26)* (Figure 1.1).

Scheme 1.1. Role of DNA adducts in chemical carcinogenesis *(27)*.

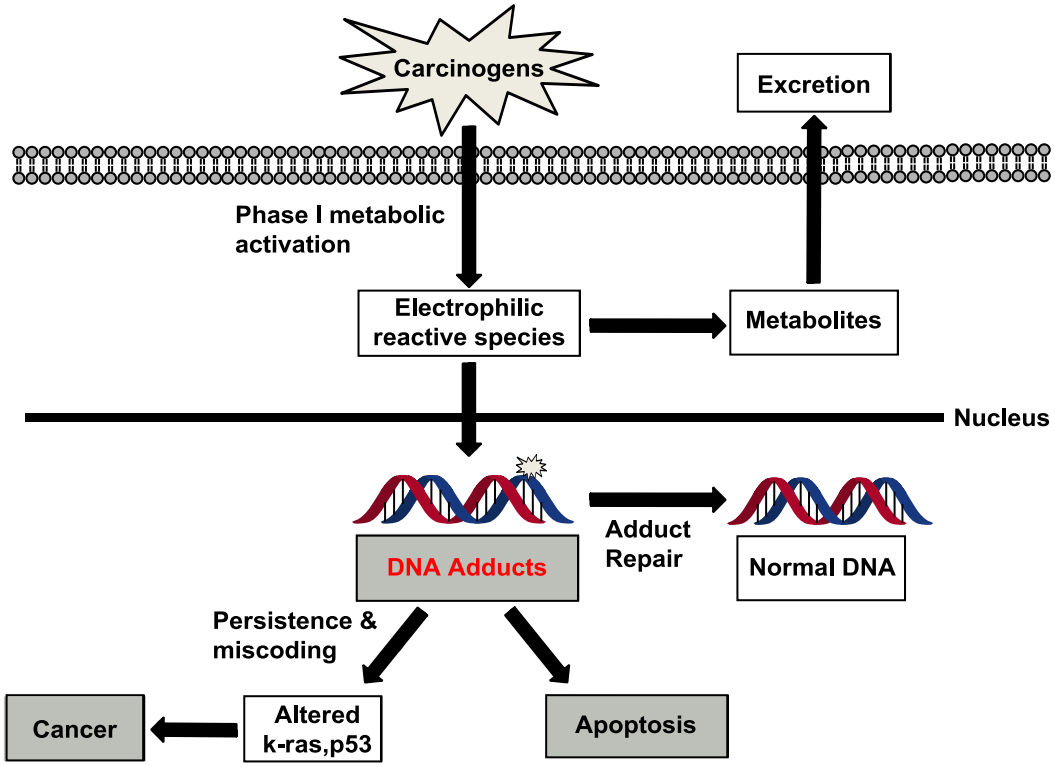

DNA adducts can also be formed by endogenously generated reactive oxygen species (ROS) such as superoxide, hydrogen peroxide, and hydroxyl radical *(28)*. ROS can oxidatively damage DNA nucleobases to form 8-oxo-2'-deoxyguanosine (8-oxo-dG), 8-oxo-2'-deoxyadenosine (8-oxo-dA), ring opened 4,6-diamino-5-formamidopyrimidine (FapyAdenine) adducts, and 2,6-diamino-4- hydroxy- 5-formamidopyrimidine (FapyGuanine) adducts *(29)* (Figure 1.1). 4-hydroxynonenal (HNE) formed as result of endogenous lipid peroxidation induces etheno-DNA adducts such as N^2-3-ethenodeoxyguanosine *(30)*. Endogenously formed estrogen metabolites, particularly catechol estrogens, form bulky DNA adducts such as 4-hydroxyestradiol-1(α,β)-N7-guanine (4-OHE2-N7-G) and 4- hydroxyestradiol-1(α,β)-N3-adenine (4-OHE2-N3-Ade) *(4;31;32)* (Figure 1.1).

Figure 1.1 Examples of DNA adducts formed by chemical carcinogens, drugs and endogenous electrophiles.

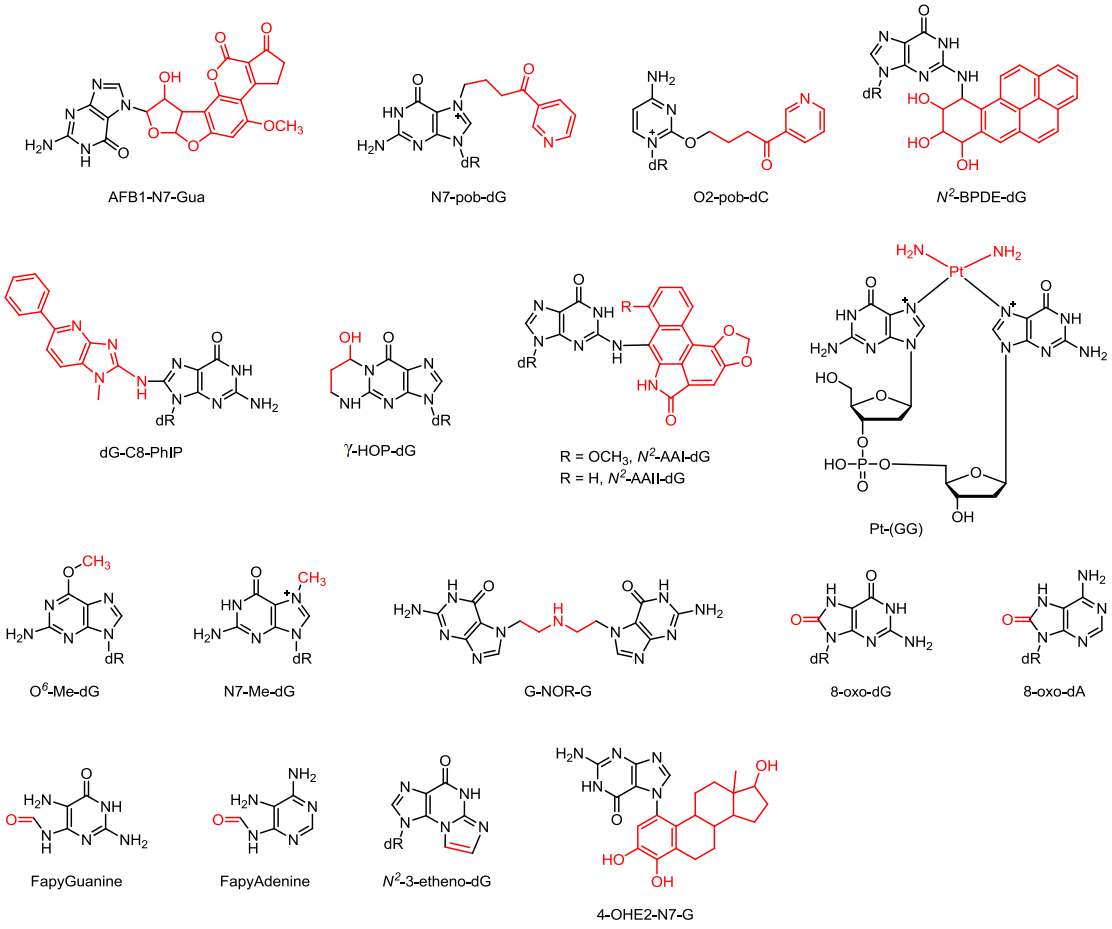

DNA adducts as biomarkers of carcinogen exposure, metabolic activation, and cancer risk.

Human exposure to carcinogens can be quantified using carcinogen specific biomarkers. As mentioned above, many chemical carcinogens require metabolic activation to DNA-reactive species, which can be detoxified via hydrolysis and conjugation steps. Therefore, the health outcomes of chemical exposures are defined in part by the balance of carcinogen bioactivation and detoxification *(33)*. Useful biomarkers of carcinogen exposure include urinary metabolites, DNA, and protein adducts. While urinary metabolites and protein adducts mostly reflect the extent of carcinogen exposure and bioactivation to reactive species, DNA adducts can be considered biomarkers of risk because of their central role in the carcinogenic process *(18) (34)*.

Among various enzymes responsible for carcinogen bioactivation, cytochrome P450 monooxygenases are the most important, based on their ability to perform complex oxidation and reduction reactions on a wide range of substrates. Electrophilic metabolites generated by P450-mediated reactions can undergo detoxification via hydrolysis or conjugation reactions with endogenous nucleophiles such as glutathione *(35)*. Both bioactivation and detoxification pathways are important to consider, as cancer risk is defined by a balance between the two pathways (Scheme 1.2).

For example, benzo[a]pyrene (B[a]P) is a carcinogenic polyaromatic hydrocarbon (PAH) present in tobacco smoke, automobile exhaust, and cooked foods. B[a]P is known to be metabolically activated by cytochrome (CYP) P450 enzymes 1A1 and 1B1 to B[a]P-9,10-oxide and B[a]P-7,8-oxide, which are hydrolyzed by epoxide hydrolase to the

corresponding diols. Further oxidation of the B[a]P-7,8-diol by CYP450s produces carcinogenic diolepoxide metabolite, B[a]P-7,8-diol,9,10-epoxide, which reacts with guanine and adenine bases of DNA to form DNA adducts capable of inducing mutations and cancer *(36)*. Detoxification pathways of B[a]P include glucuronidation of B[a]P-9,10-diol and B[a]P-7,8-diol and glutathione conjugation of 7, 8-diol 9, 10 –epoxides of B[a]P, followed by mercapturic acid formation and urinary excretion *(37;38)*. Quantification of urinary metabolites of benzo[a]pyrene gives an estimate of carcinogen exposure, while the quantification of B[a]P-DNA adducts exclusively measures the extent of metabolic activation and carcinogenic risk posed by B[a]P (Scheme 1.2).

Scheme 1.2 Partial metabolic bioactivation (in red) and detoxification products of B[a]P (Green). UDPGT: uridine diphosphate glucuronyltransferase, GST: Glutathione S-transferase.

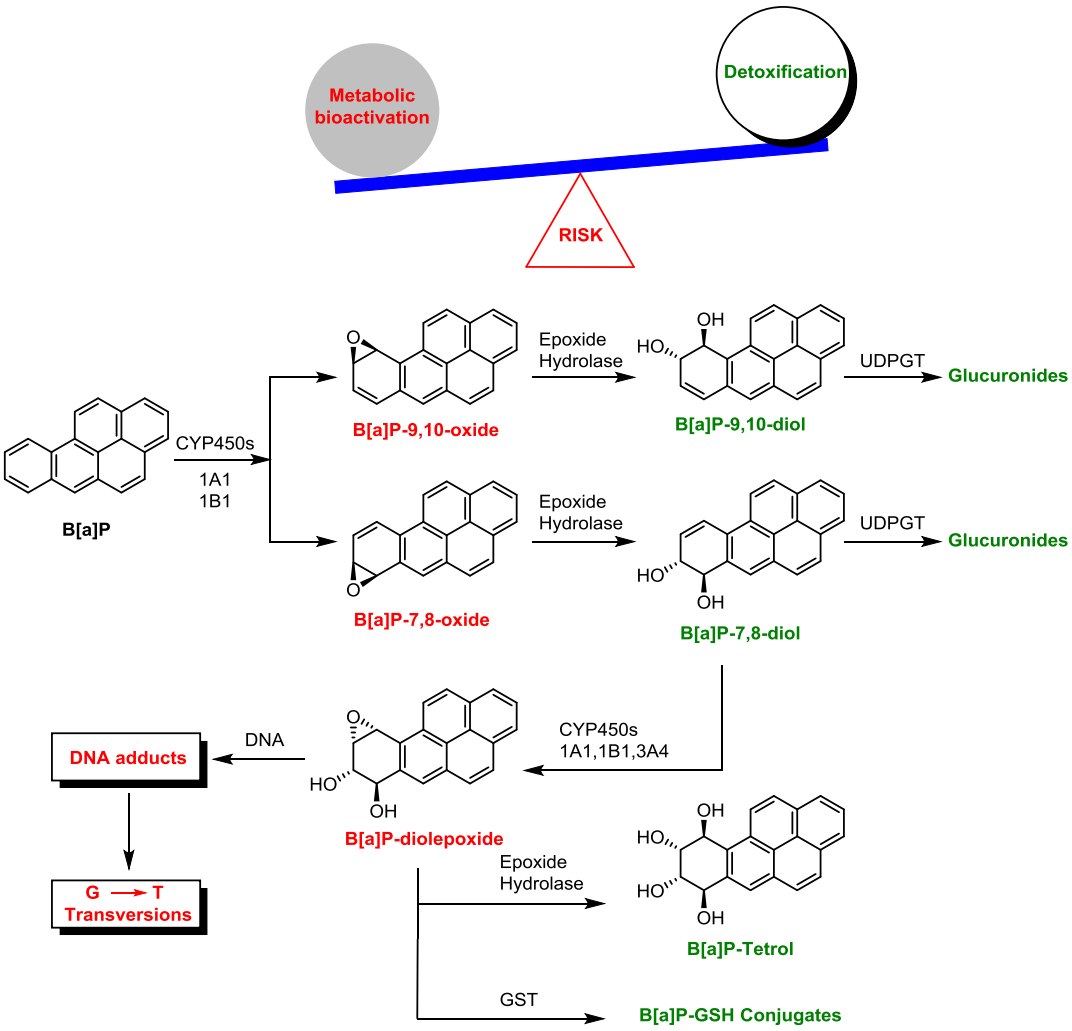

Typical biomarkers of carcinogen exposure include inactivated metabolites which no longer possess DNA-reactive functional groups (such as B[a]P tetrols in the previous example (Scheme 1.2)). Although these metabolites provide a measure of carcinogen exposure and metabolism, they do not quantify the extent of DNA damage induced by the carcinogen *(39)*. In contrast, DNA adducts represent carcinogen bioactivation markers because nucleobase adducts are ultimately responsible for causing mutations and cancer. Hence, carcinogen-induced DNA adducts are considered the ultimate biomarkers for estimating the extent of pharmacologically relevant carcinogen exposure, bioactivation, and potentially of cancer risk.

DNA adducts are commonly used as biomarkers to estimate the pharmacological activity of some important anticancer drugs. For example *N,N*-bis[2-(*N7*-guaninyl) ethyl] amine (G-NOR-G) DNA-DNA cross-links were quantified in blood leukocyte DNA of cancer patients treated with nitrogen mustard prodrug cyclophosphamide (CPA) for the treatment of lymphoma, leukemia, and solid tumors *(40)*. CPA-induced cytotoxic G-NOR-G cross-links (Figure 1.1) represent a measure of CPA metabolic activation to DNA-reactive species. Hence, G-NOR-G crosslinks are useful for biomonitoring the pharmacological activity of CPA in individual patients *(40)*. Other examples of biomarkers useful for biomonitoring the potency of drugs include DNA-DNA crosslinks induced by cisplatin *(41)* and N7-Me-dG adducts induced by temozolomide (Figure 1.1) *(42)*. On the other hand, DNA adducts were also used as biomarkers to monitor the extent of undesirable bioactivation *(43)*. For example, DNA adducts formed by reactive metabolites of tamoxifen are believed to be responsible for its ability to induce endometrial cancer *(44)*.

DNA adducts can also used as biomarkers of exposure and metabolic activation of environmental carcinogens. For example, 7-(deoxyadenosin-N6-yl) aristolactam I (dA-AL-I) and 7-(deoxyguanosin-N2-yl) aristolactam I (dG-AL-I) DNA adducts were used as biomarkers of exposure to aristolochic acids, which are implicated in Chinese herbs nephropathy and Balkan endemic nephropathy *(45)*(Figure 1.1). Urinary aflatoxin-N7-guanine adducts, which is formed by aflatoxin B1, a food contaminant and a liver carcinogen, were used as biomarkers of exposure and metabolic activation in aflatoxin exposure cohort studies in China *(46;47)*(Figure 1.1). Acrolein and crotonaldehyde-derived 1,N^2-propanodeoxyguanosine DNA adducts were used as biomarkers of smoking-mediated DNA damage in human oral tissue *(48)*. Hence, carcinogen induced DNA adducts are of significant biological interest and can be used as biomarkers of exposure, metabolic activation, and cancer risk. Increased levels of DNA adducts in target tissues have been correlated to the carcinogenicity of carcinogens such as aflatoxin B1, dimethylnitrosamine, ethylene oxide, and 4-aminobiphenyl in exposed animals *(49;50)*.

1.2 Mass spectrometry based quantitation of DNA adducts

1.2.1 Mass spectrometry methods for DNA adducts analysis in humans

Among various methodologies available for DNA adduct analysis, mass spectrometry has a number of advantages such as excellent sensitivity, selectivity and robustness when compared to traditional ^{32}P-postlabeling and high performance liquid chromatography–ultraviolet visible light absorbance detection (HPLC-UV-vis) methods *(51)*. In particular, isotope dilution mass spectrometric methods are generally considered the best approach for absolute quantitation of DNA adducts *(51)*. In this approach, naturally occurring isotopes of carbon, nitrogen or hydrogen within the adduct structure are replaced by stable isotopes such as ^{13}C, ^{15}N, ^{2}H, respectively to generate stable isotope analogues of the adducts which have distinct molecular mass, but similar physicochemical properties as compared to the analyte of interest. A known amount of this isotopomer is added to samples at the beginning of sample preparation to be used as an internal standard to account for any analyte losses during the DNA adduct enrichment and to allow for absolute quantitation. Based on the known amounts of the internal standard added, the amount of DNA adduct is quantified by using the ratio of areas under the HPLC-MS/MS peaks corresponding to analyte and its internal standard (Scheme 1.3).

Scheme 1.3 General scheme for the mass spectrometry (MS) based analysis of DNA adducts.

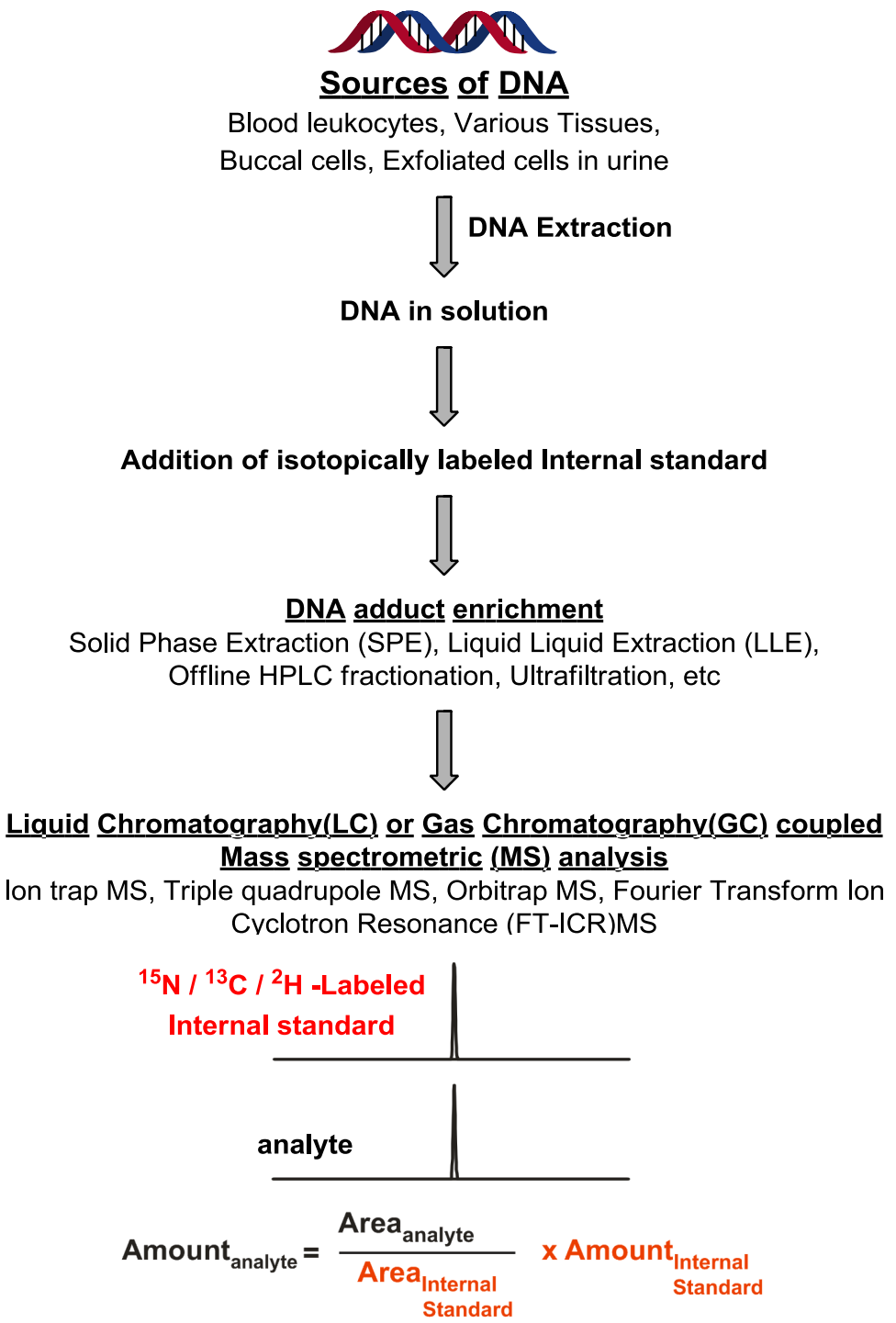

1.2.1.1 DNA adduct enrichment and sample preparation procedures

Carcinogen-DNA adducts can be quantified in DNA extracted from various biological sources/matrices. These include DNA extracted from target tissues such as liver, lung, and kidney. Surrogate matrices from accessible tissues include DNA from white blood cells in blood *(23;52;53)*, saliva/buccal cells *(54;55)*, exfoliated cells from human breast milk *(56)*, and exfoliated urothelial cells from human urine *(57)*. Carcinogen-induced DNA adducts can also be quantified in human urine as free bases *(58;59)* after they are released from DNA following active repair or spontaneous hydrolysis. DNA adducts can be enriched using sample enrichment strategies. Hydrolytically labile DNA adducts such as N7-guanine and N3-adenine adducts can be released from the DNA backbone by neutral thermal hydrolysis by heating at 70-90 °C *(60)*. N7-guanine or N3-adenine alkylation generates a positive charge, which destabilizes the N-glycosidic bond of the modified nucleoside, leading to spontaneous depurination of adducts from the DNA, and this process can be accelerated by heating (Scheme 1.4). Some DNA adducts can also be released by selective enzymatic treatment with formamidopyrimidine [fapy]-DNA glycosylase (Fpg) which releases 8-oxodG *(61)* and N7-substituted *(62)* and unsubstituted FAPY bases *(63)*. Nonselective DNA adduct release strategies include mild acid hydrolysis to liberate all purine nucleobases form DNA backbone *(64)* and enzymatic hydrolysis of DNA to individual 2'-deoxynucleosides. Specific enzymes used for enzymatic hydrolysis of DNA to deoxynucleotides include deoxyribonucleases (DNAse I and II), phosphodiesterases (PDE I and II), and nuclease P1, which cleave either at the 3' end or 5' end of DNA to

generate 3' or 5' phosphates. The use of alkaline phosphatase removes the phosphate groups, generating 2'-deoxynucleosides *(65-67)*(Scheme 1.4).

Scheme 1.4 (A) Neutral thermal hydrolysis to release N7-guanine and N3-adenine adducts from DNA. (B) Mild acidic hydrolysis to release nucleobases in DNA. (C) Enzymatic hydrolysis of DNA to 2'-deoxynucleosides.

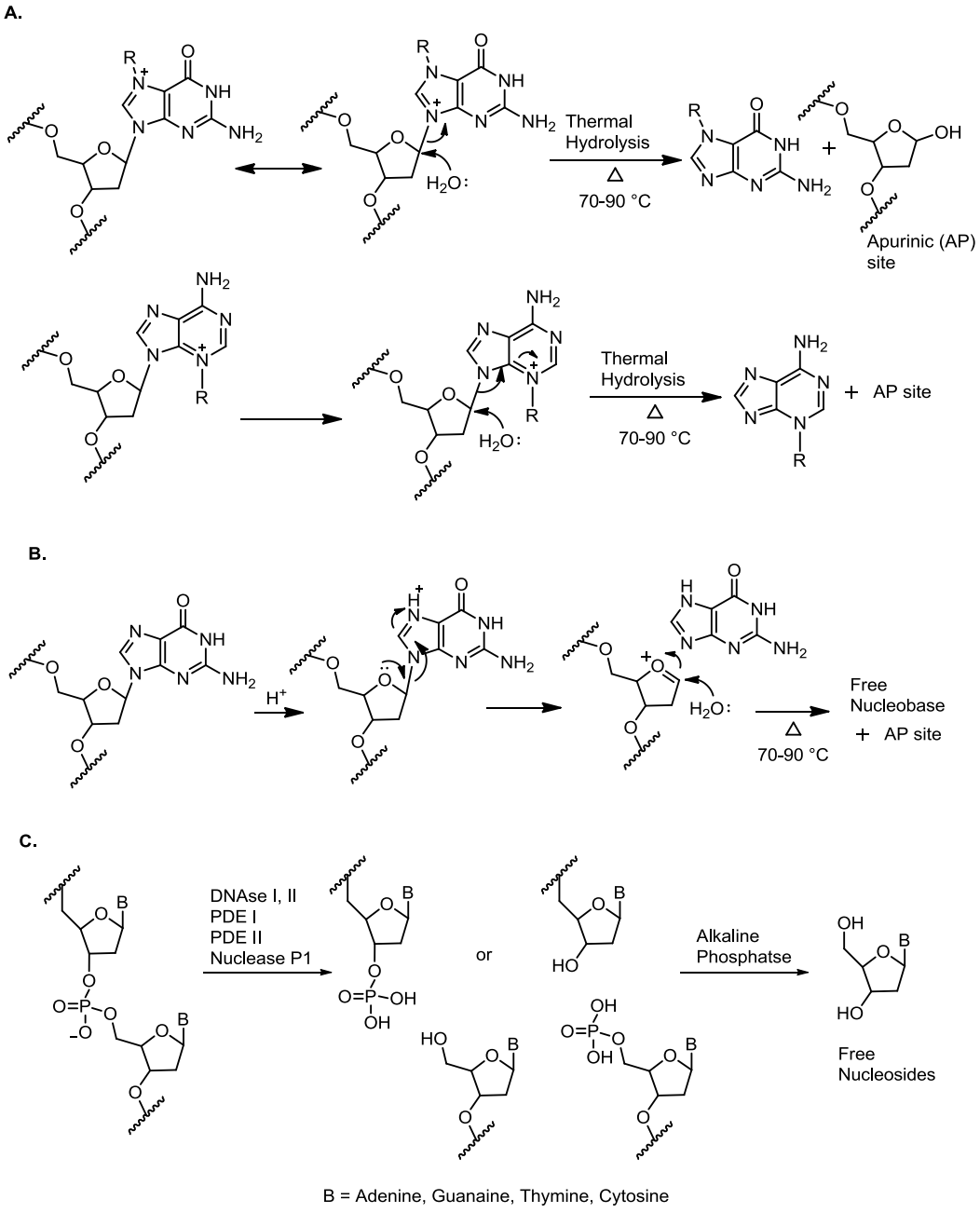

The liberated nucleoside or nucleobase adducts can be enriched using specialized sample preparation techniques such as ultrafiltration, solid phase extraction (SPE), liquid-liquid extraction (LLE), immunoaffinity purification, or offline HPLC fractionation. These enrichments are performed to remove interfering unmodified nucleobases, nucleosides, proteins, and salts which are present in large excess. Interfering compounds can increase ion background and lead to signal suppression during mass spectrometry analysis *(68)*. During ultra-filtration, the samples are loaded onto filters with specific molecular weight cut off (10000, 30000 Da) and then subjected to centrifugation to remove high molecular weight constituents such as proteins and unhydrolyzed DNA *(51)*. For some DNA adducts, liquid-liquid extraction can be used for enrichment. Liquid-liquid extraction using mixture of organic solvents such as ethyl acetate and hexanes has been used for the enrichment of hydrophobic DNA adducts such as aristolactam-DNA adducts *(67)*.

Solid phase extraction (SPE) is the most popular method for DNA sample enrichment because of its versatility. DNA adducts can be retained on the SPE stationary phases based on their hydrophobicity or ionizability. Various SPE catridges packed with stationary phases such as reverse phase C18, phenyl, cation and anion exchange phases are commercially available. Cation exchange and anion exchange SPE methods can be employed for the enrichment of DNA adducts that are ionized at specific pH. The pKa values of adducts must be considered. As a rule of thumb, a weak acid is fully ionized (negatively charged) at a pH valve 2 units above the pKa and unionized at 2 units below pKa. In contrast, a weak base is fully ionized (positively charged) at a pH value 2 units below the pKa and uncharged at pH 2 units above pKa. Since nucleobase adducts are

generally weak bases due to the presence of nitrogen containing heterocycles in their structures, they can be protonated and retained on cation exchange SPE cartridges under acidic conditions. Following retention, any interfering compounds can be removed by washing with buffer of weak solvents, while adducts of interest are retained. Finally, the analyte and its internal standard are released from the cation exchange resin by increasing the pH to favor uncharged form of the adduct. Mixed mode SPE cartridges which possess both reverse phase and ion exchange capabilities can also be used.

Off-line HPLC can be efficiently employed for the enrichment of DNA adducts. HPLC fractions containing the analyte are collected, concentrated, and reconstituted for liquid chromatography-mass spectrometry (LC-MS) analysis. HPLC cleanup methods provide a more efficient separation of DNA adducts from interfering compounds than SPE and can be more cost efficient. Fraction collection is performed using retention time markers (e.g. 2'-deoxythymidine and 2'-deoxycytidine) to accurately determine the elution times. Since the analytes are typically present in low picogram amounts, their chromatographic peaks are not visible by UV absorption. Retention time markers can be used to adjust the fraction collection times because of the influence of sample matrix on HPLC retention times. Offline HPLC fraction collection have been previously used for the enrichment of a range of DNA adducts such as 1,4-*bis*-(guan-7-yl)-2,3-butanediol (*bis*-N7G-BD) *(69)* and N-7-(1-hydroxy-3-buten-2-yl) guanine (EB-GII) *(70)* adducts in our laboratory.

1.2.1.2 Quantitative mass spectrometric methods for DNA adducts

Mass spectrometry is the preferred method for the quantification of DNA adducts in biological matrices as it offers structural information, accurate detection, and absolute quantitation of the analytes. A number of mass spectrometry-based methods are reported in literature for the quantitation of nucleoside adducts. The majority of the recent reports employ liquid chromatography (LC)-mass spectrometry, although GC-MS can be useful for some applications.

Liquid Chromatography -Mass Spectrometry

High performance liquid chromatography (HPLC) is the preferred method of choice for sample introduction into the mass spectrometers for quantitative analysis of DNA adducts *(34)*. Mass spectrometers determine the mass to the charge ratios (*m/z*) of the analyte following *sample ionization*. HPLC provides an efficient way to separate DNA adducts from interfering compounds in the biological matrices before introduction into the mass spectrometer for sample ionization and *m/z* measurements. DNA adducts are typically present in very low concentrations (1-3 adducts/10^8 nucleotides or 5-10 pg/100 μg DNA), and HPLC provides a way to reduce MS signal suppression caused by interfering matrix components. A variety of HPLC stationary phases are commercially available, including reverse phase C12, C18, C8, polyphenyl, and others. For extremely polar DNA adducts that are not retained on reverse phase HPLC packing, hydrophilic interaction liquid chromatography (HILIC) may be a viable option. HILIC is variant of normal phase liquid chromatography which uses hydrophilic stationary phases with reversed-phase type eluents and thus has the ability to retain polar DNA adducts. Flow

rates typically used in LC-MS analysis include normal analytical flow (0.1-0.2 mL/min), capillary flow (5-15 μL/min), and nanoflow (100-400 nL/min). As described below, better sensitivity is attained using lower flow rates due to the higher efficiency of ionization *(51)*.

The first critical step in mass spectrometry based analysis of DNA adducts is analyte ionization. One of the most common methods of ionization for LC-MS analysis is electrospray ionization (ESI) (Figure 1.2) *(71)*. ESI can be conducted in the positive or negative ion modes to generate positive and negative ions, depending on voltage polarity. DNA adducts such as N^2-(1-carboxyethyl)-2'-deoxyguanosine (CEdG), 8-nitroguanine, N^6-(1-carboxyethyl)-2'-deoxyadenosine *(72)*, and cisplatin-DNA adducts *(73)* are quantified in negative mode because of their propensity to lose a proton and to become negatively charged. However, the majority of nucleobase adducts are readily protonated under mildly acidic buffer conditions, hence enabling their detection in the positive ion mode. Aqueous and organic mobile phases containing volatile acids such as 0.05% acetic acid, 0.1% formic acid, 0.01% trifluoroacetic acid, or buffers containing 5-10 mM ammonium acetate are typically used in HPLC of structurally modified nucleosides and nucleobases to aid in the separation and ionization of the analyte. An alternative ionization method for the analysis of DNA adducts is atmospheric pressure chemical ionization (APCI), typically used with higher HPLC flow rates (0.2-1.0 mL/min) *(51)*.

Tandem mass spectrometry analysis (LC-MS/MS or SRM analysis)

Tandem mass spectrometry (MS/MS) in the selected reaction monitoring mode (SRM) is by far the most efficient method used for the accurate quantitation of DNA adducts. Tandem mass spectrometry experiments are most commonly conducted on triple

quadrupole mass analyzers. Triple quadrupole MS consists of three quadrupole mass analyzers made up of four parallel metal rods with alternating radio frequency voltages and can filter specific ions based on the *m/z* ratio. Triple quadrupole MS is used for quantitation by monitoring the gas phase fragmentation of the parent protonated molecule to its fragment ions and this mode is called selected reaction monitoring (SRM) or multiple reactions monitoring (MRM). As shown in Scheme 1.5 A and B, the sample is introduced by HPLC and ionized by ESI, and the resulting ions move through the triple quadrupole mass spectrometer. For example, consider the case of guanine and $^{15}N_5$ labeled guanine spiked as internal standard in the sample. Following ionization in the ESI source, quadrupole 1 (Q1) is used for initial mass selection of *m/z* 152 $[(M+H)^+]$ for guanine and *m/z* 157 $[(M+5+H)^+]$ for its internal standard. Q2 is used for fragmentation of the ions selected in Q1 using high energy collisions with an inert gas such as argon or nitrogen (collision-induced dissociation). After fragmentation, Q3 is used for mass analysis of specific product ions. In the case of guanine and $^{15}N_5$ guanine, fragment ions corresponding to cleavage of the exocyclic amino group can be employed: *m/z* 135.1 $[(M+H-NH_2)^+]$ for guanine and *m/z* 139.1 $[(M+5+H-NH_2)^+]$ for $^{15}N_5$ internal standard. The selected fragment ions are finally detected by the mass detector to produce the MS signal. The MS signal for selected reaction monitoring of *m/z* 152 → 135 and *m/z* 157 →139.1 is transformed into the corresponding peaks for analyte and the internal standard. The analyte amounts can be accurately determined using the ratios of areas under the peaks and the known amount of internal standard added before starting the sample preparation (Scheme 1.5 A, B). Apart from SRM/MRM modes, triple quadrupole MS can also be used for single ion monitoring (SIM) mode for selecting and monitoring only

ionized analyte ions, or in the precursor ion or neutral loss mode to detect a range of structurally related adducts. Triple quadrupole MS are ideally suited for trace analysis of DNA adducts due to their high duty cycle in SIM and SRM modes, relatively good resolution power (1000-3000), their low cost, and the ease of operation. Resolution power (R) of a mass spectrometer is defined as its ability to distinguish between two ions with close *m/z* ratios and it calculated as the ratio of nominal mass (M) to the mass difference between two ions (ΔM) (R = M/ΔM). Typically limits of quantitation for DNA adducts measured using triple quadrupole LC-MS based SRM analysis are in the range of 1-4 adducts per 10^7 to 10^8 nucleotides *(74;75)*.

Ion trap mass spectrometric analysis (LC-MS^n)

Linear ion trap (LTQ) MS instruments are designed to store ions within specified mass range. Generally, LC-ion trap (IT) MS/MS operated in the "collision activated dissociation" (CID) mode can be used for analysis of DNA adducts. For example, N-(deoxyguanosin-8-yl) (dG-C8) DNA adducts formed by alkylation of guanine by aromatic amines such as 2-amino-1-methyl-6-phenylimidazo[4,5-b]pyridine (PhIP), 2-amino-9H-pyrido[2,3-b]indole (AαC), 2-amino-3,8-dimethylmidazo[4,5-f]quinoxaline (MeIQx) and 4-aminobiphenyl (4-ABP) were successfully identified in human salivary DNA using Linear Quadrupole Ion Trap/Multistage Tandem Mass Spectrometry *(55)*. Another advantage of ion trap MS includes the multi stage fragmentation (MS^n) of ions. MS/MS fragment ions can be selected and further fragmented to generate MS^3 ions, which can to provide rich structural information for the analyte. This can theoretically be continued to yield even smaller fragments (MS^n) (Scheme 1.6 A, B). Monitoring the

fragmentations of the analyte ions in the MS^3 mode can provide increased signal to noise ratios due to an increased selectivity. Liquid chromatography-stable isotope dilution mass spectrometry on linear ion trap mass spectrometer (LC- ITMS) has been used successfully for detection and quantitation of aristolactam-DNA adducts in human biomonitoring studies *(45)*.

Major differences between ion trap MS and triple quadrupole MS include type of fragmentation of ions in gas phase. Triple quadrupoles are only capable of fragmentation of ions until MS^2 stage to generate fragments while ion trap MS can perform sequential fragmentation reactions from a single precursor ion, generating up to approximately 10cycles of fragments or theoretically MS^n fragmentation. Hence ion traps can perform multi-stage tandem mass spectrometry experiments (MS^n) as compared to triple quadrupoles, which can provide additional rich structural information of the molecule *(55)*. In iontrap MS, fragmentation is achieved by Collision Induced Dissociation (CID) which can be acquired by ejection of all ions other than the ion with required *m/z* ratio of interest, and then fragmenting the selected ions with inert gases such as helium or argon followed by mass analysis of the resulting fragment ions. In triple quadrupole MS, SRM based fragmentation is achieved in the second quadrupole collision cell (Q2) using inert gas such as nitrogen after precursor mass selection in first quadrupole (Q1) mass analyzer and final MS^2 fragment mass analysis in third quadrupole (Q3). In case on adducted DNA nucleosides the major MS/MS fragmentation is the neutral loss of the sugar moiety, which provides little structural information; in contrast, MS^3 and MS^4 fragmentation experiments using ion trap MS can reveal rich structural details for the modified base allowing for its identification. Use of ion traps in trace quantitative analysis of DNA

adducts is limited as compared to triple quadrupole MS due to their relatively low duty cycle and nonlinear response to MS fragmentation. But modern LTQ ion traps have improved sensitivity, specificity, and S/N ratios for DNA adduct analysis which can be achieved by monitoring specific MS^3 transitions *(45)*.

Scheme 1.5 A. Schematic representation of a triple quadrupole mass spectrometer (A) operated in the selected reaction monitoring mode to detect guanine and its $^{15}N_5$-labeled analog (B).

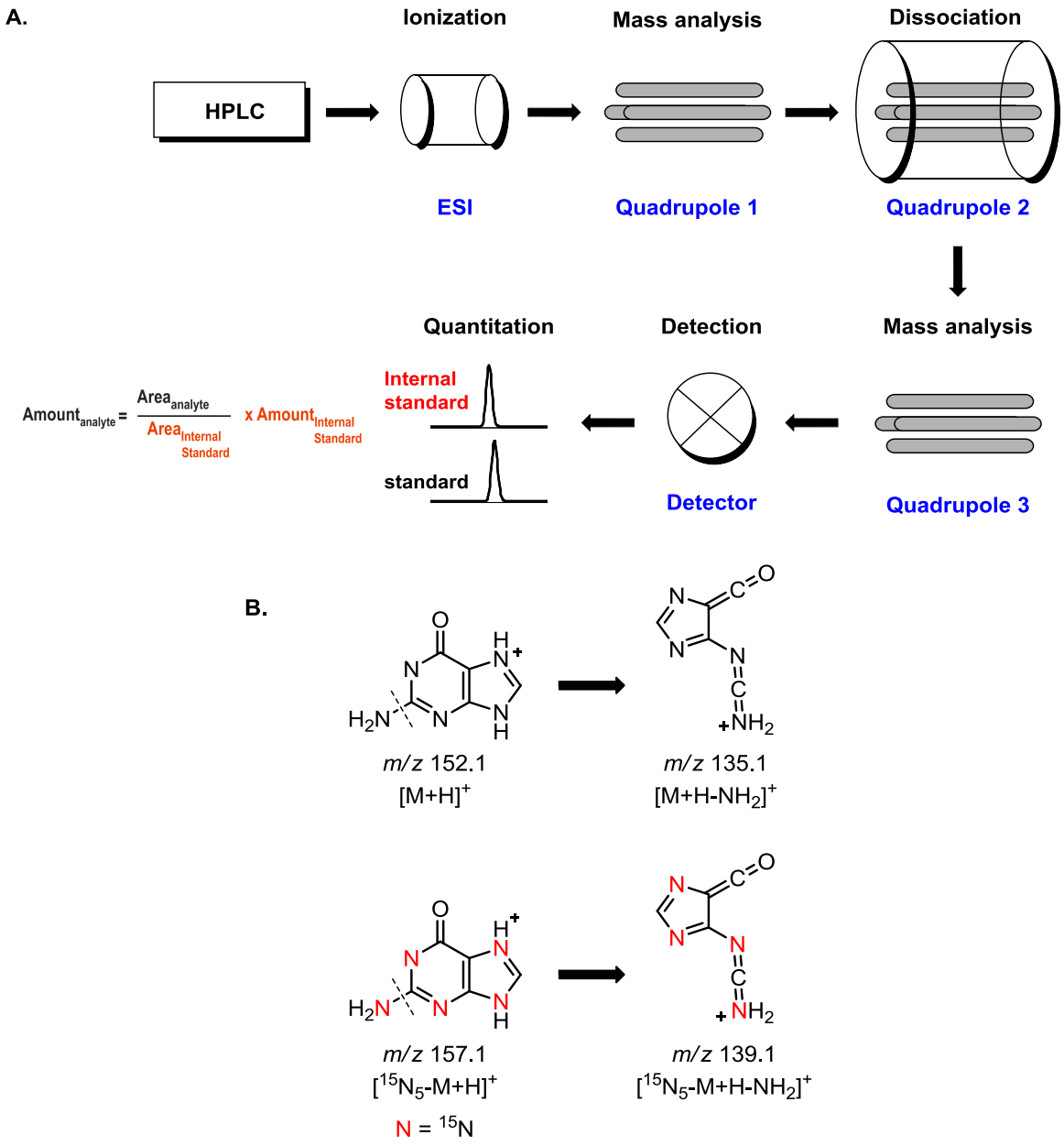

Scheme 1.6 A. Schematic of a HPLC-ion trap MS/MS system (A) and MS^3 dissociation of N7-methyl guanine and its ^{15}N-labeled internal standard (B).

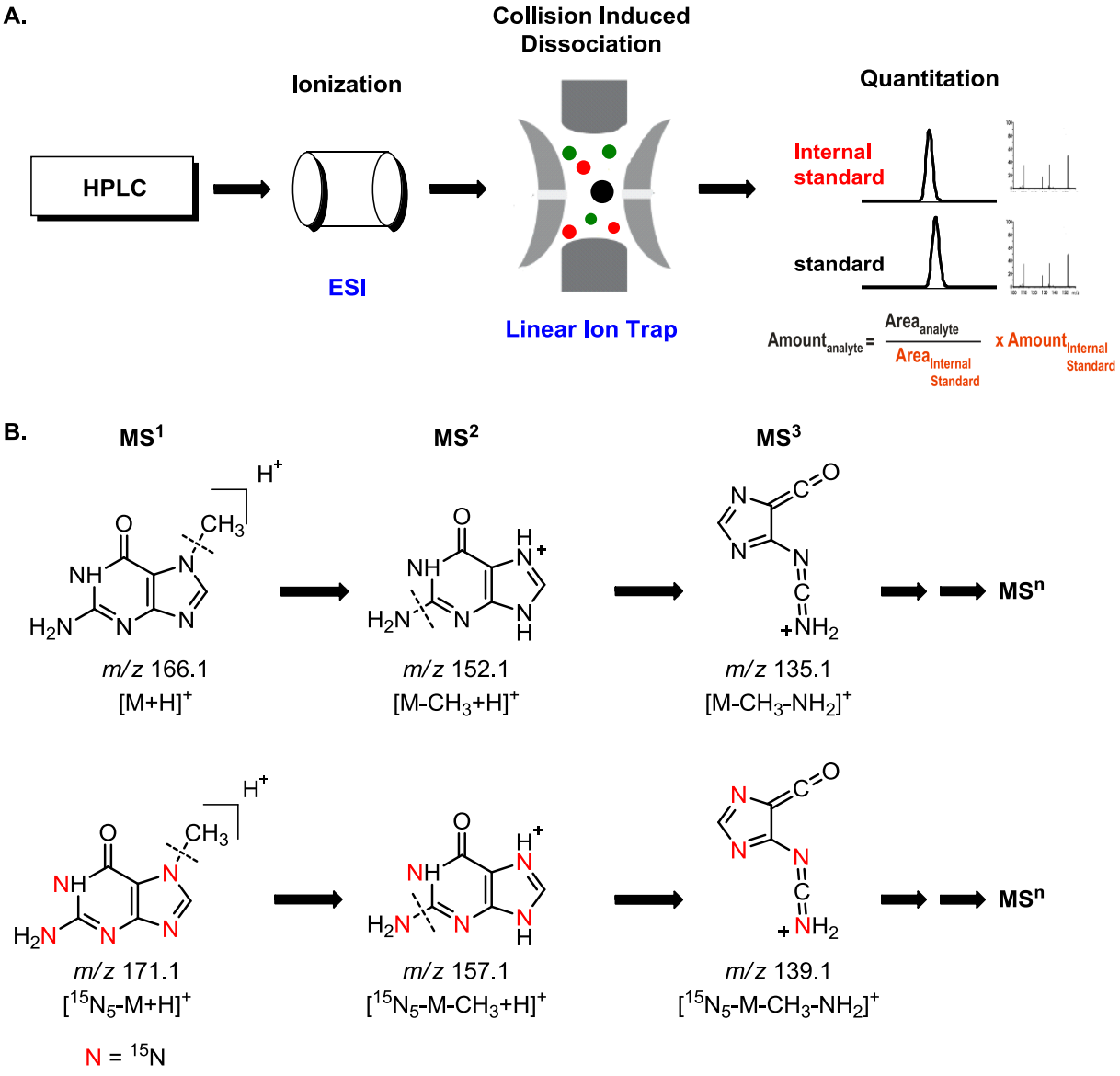

1.2.2 Ultra-sensitive advanced mass spectrometry based methods

Human biomonitoring of trace levels of DNA adducts requires higher sensitivity and selectivity for accurate quantitation. For example, 1,N^2-propano-2'-deoxyguanosine DNA adducts derived from environmental carcinogens such as acrolein (AdG) and crotonaldehyde (CdG) are present in very low amounts in the range of 78 ± 23, 6.2 ± 3.8 adducts per 10^8 nucleotides (5-50 fmol) in human blood leukocyte DNA and 108 ± 2.6, 26 ± 3.1 adducts per 10^8 nucleotides in human placental DNA *(76)*. The amounts of ethylated thymidine DNA adducts such as O(2)-ethyl dT, N(3)-ethyl dT, and O(4)-ethyl dT in smokers were found to be 44.8 ± 52.0, 41.1 ± 43.8, 48.3 ± 53.9 per 10^8 normal nucleotides respectively *(77)*.

1.2.2.1 Capillary and nanospray LC-MS analysis of DNA adducts

Electrospray ionization (ESI) is the most common form of ionization method used for the analysis of DNA adducts as it is conducive to liquid chromatography. Flow rate and ion transmission into the mass spectrometer play a major role in the sensitivity of the method *(78)*. Capillary LC-MS methods which employ columns with internal diameters of 0.3-0.5 mm and flow rates typically in the range of 5-10 µL/min are used for the quantitation of DNA adducts. Also, with the advent of nanoLC-MS systems, which operate at very low flow rates (100-400 nL/min) and use nano columns with diameters of 50-100 µm in combination with nanoESI source, it is possible to develop highly sensitive methods for DNA adduct analysis. Smith RD et al. reported that use of low flow rates in the range of 200 nL/min improves ESI sensitivity. Nanoflow rates lead to efficient ion spray, better ionization and highly efficient ion transfers as the ions can be introduced directly into the MS ion transfer tube of the mass spectrometer, thereby increasing the

overall ion current *(78)*. Nanospray emitters are commercially available with different configurations such as metal coated tip for application of voltage at the front end of the tip and emitters with frit at the front end which can be packed in house with desired stationary phases etc.

Figure 1.2 Electrospray ionization using capillary LC flow (A) and nanoLC flow rates (B).

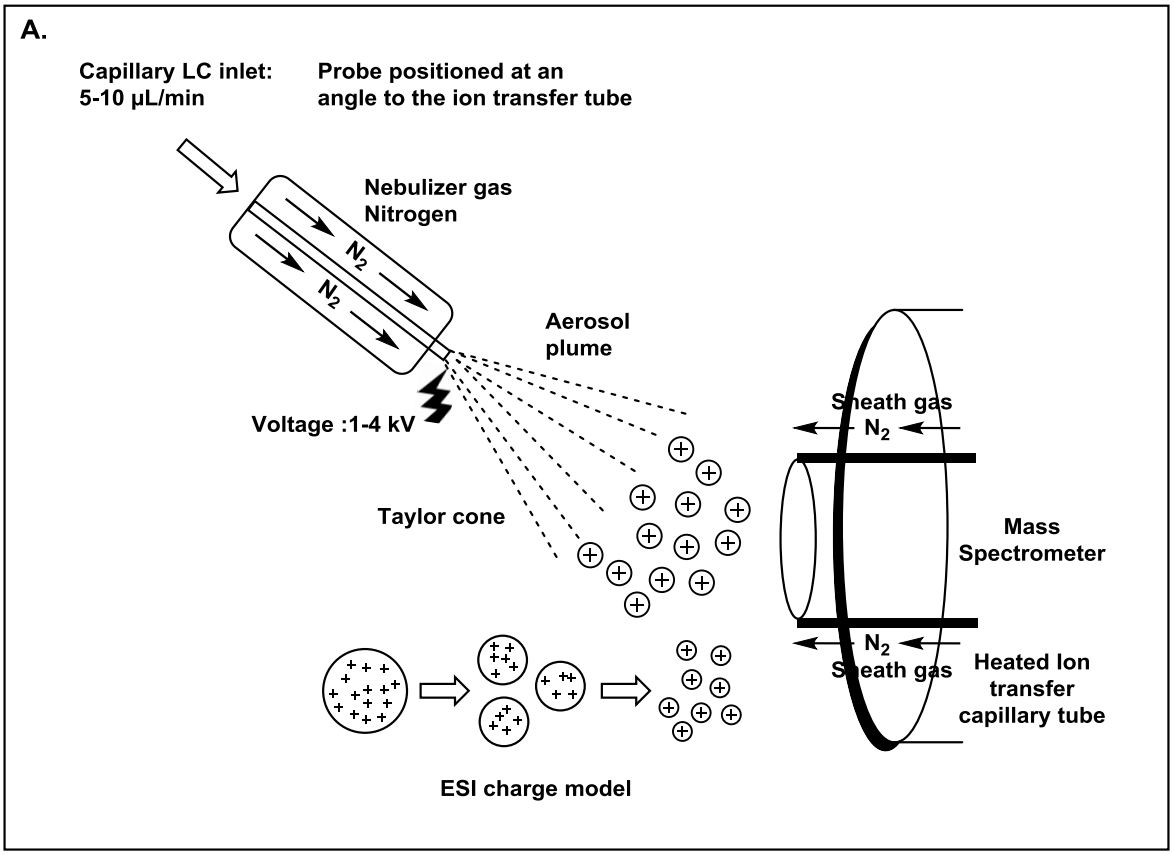

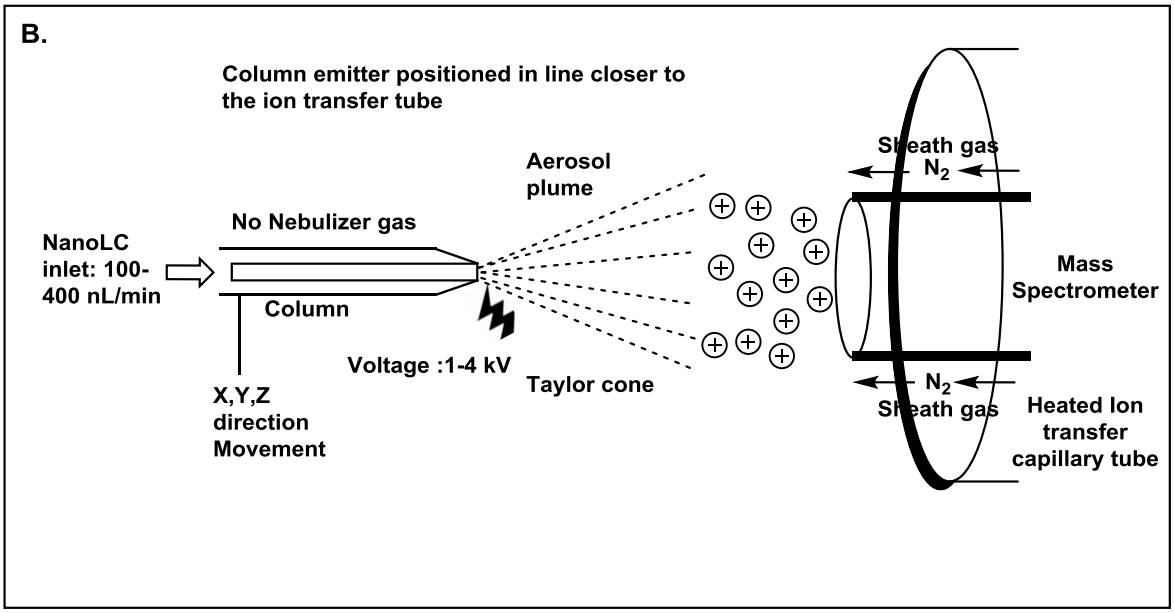

1.2.2.2 Accurate mass quantitation of DNA adducts

Accurate mass quantitation is the determination of mass of the molecule such that its elemental composition of the molecule can be determined unambiguously. For example, consider the protonated guanine molecular ion ($[Gua +H]^+$). Mass spectrometers such as triple quadrupoles and ion traps determine the mass of guanine as *m/z* 152.05, for which there are numerous possible elemental compositions. But, accurate mass spectrometers are capable of measuring the exact mass of protonated guanine as *m/z* 152.05669 with mass error less than 5 ppm, for which there is only one plausible elemental composition. Mass error is defined as the difference between the experimental mass (M_{exp}) and the theoretical value (M_{theo}), calculated from elemental composition. It is generally reported in relative terms as ppm calculated using $(M_{exp}-M_{theo})/ M_{theo}$. Accurate mass measurement instruments are also capable of distinguishing two close masses which is defined as mass resolution factor (R), calculated as nominal mass (M)/ mass difference (ΔM). ΔM can be calculated using full width at half maximum (FWHM) measurements. FWHM is a measure of width of a single peak measured at 50% peak apex *(79)*.

One of the popular accurate mass measurement (high resolution) mass spectrometers uses orbitrap mass analyzers. Orbitrap mass analyzers are basically ion traps developed by Marakov A et al. *(80)*. Orbitrap mass analyzers are made up of outer barrel-like and coaxial inner spindle-like electrodes that traps ions, move in an orbital motion following ion injection and, finally the ion current frequency signal is Fourier transformed (FT) into a mass spectrum. It works on the principle that the angular frequency of the orbital motion of ions is related to the mass to the charge ratio by the equation $\omega=\sqrt{(k/(m/z))}$, where k=force constant. Most of the modern mass spectrometers

are hybrid/ tandem instruments assembled with linear ion traps or quadrupole with orbitrap mass analyzers or linear ion traps and quadrupoles with orbitrap mass analyzers. For example the orbitrap Velos (Thermo scientific, Waltham, MA, USA) instrument has linear ion trap (LTQ) mass analyzer upfront of the orbitrap mass analyzer. Hence, there is an option for detection of ions in low resolution mode using ion trap or high resolution (HRMS) mode using orbitrap mass analyzer after efficient ion transmission into the instrument.

Orbitrap HR-MS^n scanning analysis of DNA adducts

Instruments such as orbitrap Velos can be efficiently used for the analysis of DNA adducts in trace amounts by using ion trap MS^n fragmentation followed by detection of the final product ions in high resolution mode using the orbitrap mass analyzer (Figure 1.3). Analyzing the ions in high resolution mode significantly improves the signal to noise ratio as compared to conventional triple quadrupole based tandem MS (SRM or MS/MS) analysis. HRMS detection also increases the confidence in the analysis of DNA adducts because of non-interference of other masses and absence of artifacts or co elution problems. For example use of orbitrap HRMS analysis was reported by Zhang NR et al. for the identification and quantitation of small molecules in biomatrices with comparable assay precision, accuracy, linearity and better sensitivity as compared to triple quadrupole SRM based analysis *(81)*. Nanospray LC with nanoESI ionization can be used in combination with HRMS detection to increase the sensitivity of analysis of DNA adducts. For example, nanoLC-ESI in combination with orbitrap HRMS analysis was used for the quantitation of N7-ethylguanine using isotope dilution with $^{15}N_5$-N7-ethyl guanine internal standard in blood leukocyte DNA of smokers. In this method the

protonated adduct of *m/z* 180 $(M+H)^+$ was fragmented in the LTQ ion trap and the MS^2 (MS/MS) fragment of protonated guanine with *m/z* 152.05669 $(Gua+H)^+$ was detected using HRMS detection by orbitrap mass analyzer. Similar transition of *m/z* 185 ($^{15}N_5$-$M+H)^+$ →*m/z* 157.04187($^{15}N_5$-$Gua+H)^+$ was used for the internal standard. In orbitrap Velos, MS fragmentation of ions can be achieved either by CID in LTQ ion trap or by high collision dissociation (HCD), also known as C-trap assisted dissociation *(82)*. Hence, with the help of hybrid instruments such as orbitrap Velos, MS^n fragmentation can be performed either in LTQ ion trap or in HCD collision cell, and the ions can be detected using ion trap nominal mass or orbitrap mass analyzer (HRMS) (Figure 1.3).

Figure 1.3 Schematic of a hybrid/Linear ion trap-Orbitrap Velos HRMS instrument

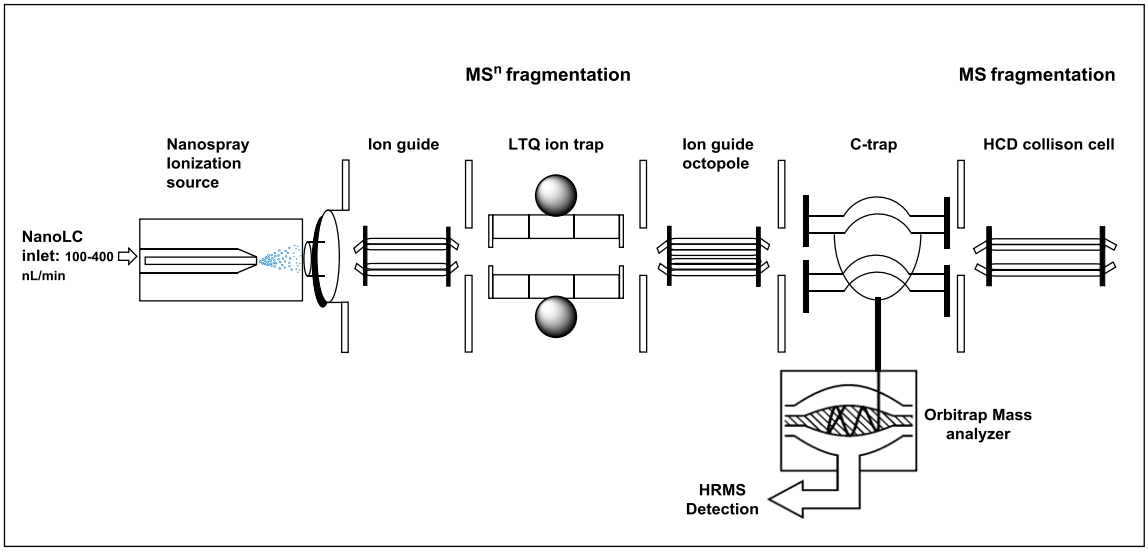

1.3 1,3-Butadiene (BD) an human and animal carcinogen: An Overview

1.3.1 Sources of exposure, metabolism and toxicity of BD

1,3-Butadiene (BD) is a volatile and colorless gas used in polymer industries for the production of rubber *(83)*. BD is a classified as a carcinogen based on studies in laboratory rodents, which developed tumors in multiple organs after exposure to BD *(84;85)*. Studies in humans occupationally exposed to BD in the butadiene-monomer industry and polymer rubber industries showed increased risk of leukemia *(86-88)*. The general human population is exposed to sub ppm (1-10 ppb) concentrations of BD in urban air from automobile exhaust *(89)*, mainstream (20-75 μg), and sidestream (205-360 μg) cigarette smoke, wood burning and forest fires *(90;91)*.

Metabolism and toxicity of 1,3-butadiene (BD)

BD is known to be metabolically activated by cytochrome P450 monoxygenases CYP 2E1 and CYP 2A6 to 3,4-epoxy-1-butene (EB) *(92)*. EB is further oxidized by CYP P450 2E1, 3A4 to form the diepoxide 1, 2, 3, 4-diepoxybutane (DEB) *(92;93)*. DEB is reported to undergo hydrolysis by epoxide hydrolase (EH) to another mono epoxide 3,4-epoxy-1,2-butanediol (EBD). EB can also undergo hydrolysis by epoxide hydrolase (EH) to form EB-diol which can further undergo metabolic activation by CYP 2E1 to form 3,4-epoxy-1,2-butanediol (EBD) (Scheme 1.7) *(94;95)*.

BD toxicity is mainly attributed to its three reactive epoxides EB, EBD and DEB which all can react with nucleophilic biomolecules such as DNA and proteins to form covalent adducts. Among the three BD epoxides, EBD is the most abundant epoxide formed *in vitro* and *in vivo* followed by EB and DEB. Though DEB is the least abundant epoxide, it is the most mutagenic and genotoxic epoxide probably because of its

Scheme 1.7 Metabolism of BD to DNA reactive epoxides.

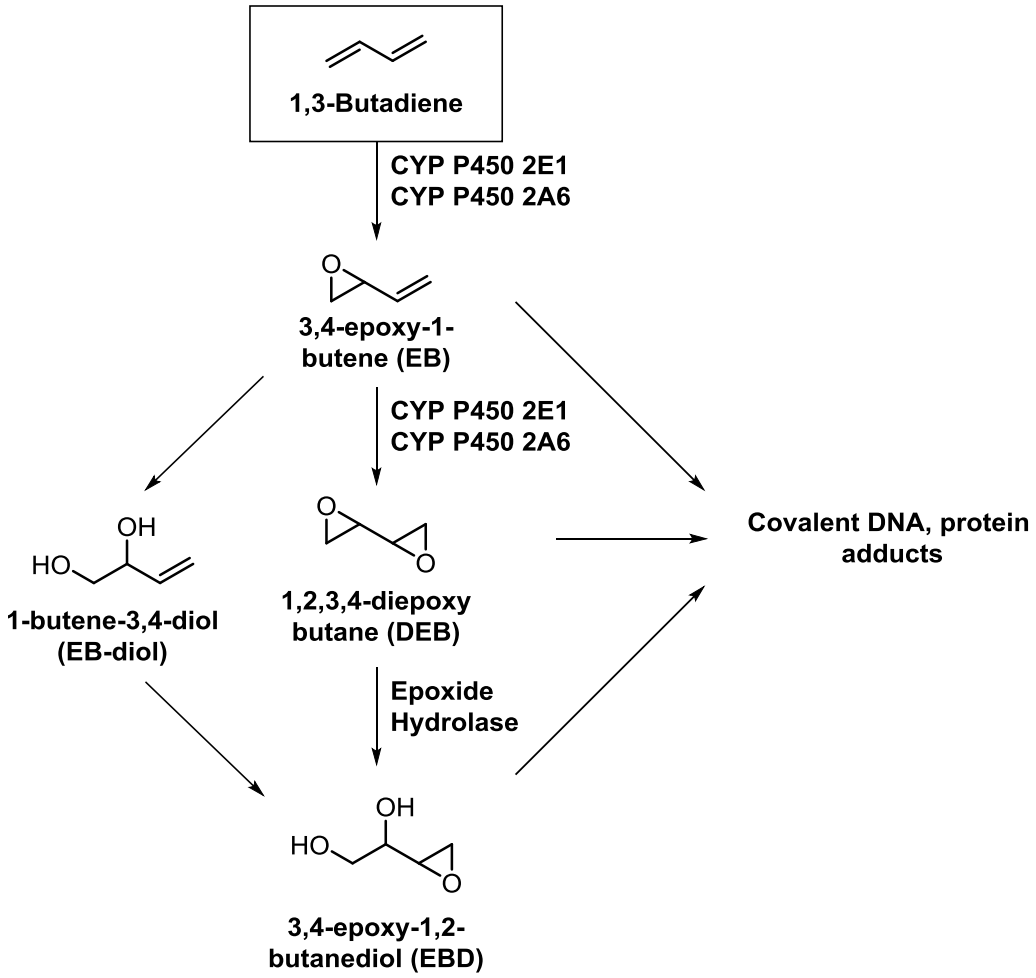

bifunctional crosslinking nature *(96)*. The mutagenic ability of various sterioisomers of DEB (*RR*, *SS* and *meso*) is also different with *S,S*-DEB being the most mutagenic epoxide *(97)*. *In vitro* studies in human lymphoblastoid TK6 cells have shown that DEB is mutagenic at concentration levels less than 5 μM. In comparison, EB and EBD were mutagenic at higher concentration levels of 100–800 μM *(98)*. DEB induced A→T transversions and partial deletions in *hprt* gene of TK6 lymphoblasts exposed to 4 μM of DEB for 24h, while EB required at least 100 fold higher concentrations (400 μM, 24h) to induce GC→AT point mutations and AT→TA transversions *(98)*. *In vivo* studies in B6C3F1 *laci* transgenic mice exposed to higher concentrations of BD (62.5 – 1250 ppm, 6 h/day, 5 days/week for 4 weeks) reported that BD induced AT→GC or AT→TA point mutations in spleen and bone marrow *(96)*. A significant increase in frequency of exon deletions in *hprt* gene *(99)* and increased AT→TA transversions and frameshift mutations were observed in workers exposed to BD *(100)*. However, other research studies found no statistically significant differences in *hprt* gene mutation frequencies between exposed and control workers *(101;102)*.

1.3.2 Biomarkers of BD exposure and metabolic activation

BD is metabolized to its reactive epoxides which can react with biomolecules such as DNA and proteins. Alternatively, BD reactive epoxides can potentially be detoxified by glutathione conjugation followed by conversion to mercapturic acids which are finally excreted in urine. To assess the extent of toxicity by BD, biomarkers of bioactivation and detoxification pathways can be used.

1.3.1.1 BD-DNA adducts

BD reactive epoxides are electrophilic and therefore can react with nucleophilic groups on DNA bases guanine, adenine, thymidine and cytosine to form covalent DNA adducts. For example, the most abundant BD epoxide 3,4-epoxy-1,2-butanediol (EBD) is known to react with DNA bases such as guanine and adenine to form N7-(2',3',4'-trihydroxybut-1'-yl)guanine (N7-THBG) (meso and racemic), N6-(2',3',4'-trihydroxybut-1'-yl)adenine (N6-THB-Ade), and N3-(2',3',4'-trihydroxybut-1'-yl)adenine (N3-THB-Ade) *(75;103;104)* (Scheme 1.8). 3,4-Epoxy-1-butene (EB) is also reported to form DNA adducts N7-(2-hydroxy-3-buten-1-yl)guanine (EB-GI), N7-(1-hydroxy-3-buten-2-yl)guanine (EB-GII), N1-(2-hydroxy-3-buten-1-yl)adenine (EB-Ade I) and N1-(1-hydroxy-3-buten-2-yl)adenine (EB-Ade II) *(75;103;104)*(Scheme 1.8). 1, 2, 3, 4-Diepoxy butane (DEB), the most mutagenic of the BD epoxides is a bis electrophile and can sequentially react with two DNA bases to form inter-strand and intra-strand DNA-DNA crosslinks such as 1,4-bis-(guan-7-yl)-2,3-butanediol (bis-N7G-BD), 1-(guan-7-yl)-4-(aden-1-yl)-2,3-butanediol (N7G-N1A-BD), 1-(guan-7-yl)-4-(aden-3-yl)-2,3-butanediol (N7G-N3A-BD), 1-(guan-7-yl)-4-(aden-7-yl)-2,3-butanediol (N7G-N7A-BD) and 1-(guan-7-yl)-4-(aden-N6-yl)-2,3-butanediol (N7G-N6A-BD) cross-links *(105;106)*(Scheme 1.8). DEB is also known to react with two different sites on the same nucleobase to form exocyclic DNA adducts such as 1,N6-(2-hydroxy-3-hydroxymethylpropan-1,3-diyl)-2'-deoxyadenosine (1,N6-γ-HMHP-dA) and 1,N6-(1-hydroxymethyl-2-hydroxypropan-1,3-diyl)-2'-deoxyadenosine (1,N6-α-HMHP-dA) *(107)*(Scheme 1.8). BD DNA adducts are regarded as the ultimate biomarkers of BD

induced carcinogenesis and cancer risk, as they are directly responsible for DNA damage and mutations leading to cancer.

In the literature, there is an increased interest to develop BD induced DNA adducts as biomarkers to estimate the extent of bioactivation, biologically effective dose and cancer risk of BD. Rodents such as rats and mice exposed to BD by inhalation were used as models to identify DNA adducts that can potentially be used as biomarkers to quantify BD exposure and metabolic activation. Initially, ^{32}P-post labeling and HPLC methodologies were used to quantify several DNA adducts induced by BD and its metabolites. Koivisto et al. used ^{32}P-post labeling methodologies to identify N7-gunaine and N6-adenine adducts of 3,4-epoxy-1-butene, N7-guanine adducts of EBD and DEB in liver, lung and testis of mice and rats exposed to BD *(108-111)*. N1-THB-Ade adducts of EBD were quantified in human blood leukocyte DNA and were present in higher concentrations in BD-exposed workers as compared to unexposed workers or controls *(112)*. With the advent of isotope dilution mass spectrometry and LC-ESI-MS/MS (SRM) analysis, 3,4-epoxy-1-butene specific EB-GI, EB-GII and EBD specific N7-THBG were quantified in liver tissues of mice and rats exposed to 1250 ppm BD for 10 days *(104)*. Koc et al. observed a clear dose-response relationship between EB-GI, II and N7-THBG and BD concentrations in liver, lung and kidney tissues of mice and rats *(75)*.

Ultra sensitive HPLC-ESI$^+$-MS/MS methods for quantification of DEB-specific DNA adducts *in vivo* were developed in our laboratory. Goggin et al. found significantly increased levels of guanine-guanine crosslink (*bis*-N7G-BD) adducts in the liver (3.2 ± 0.4 adducts per 10^6 dG) and lung (1.8 ± 0.5 adducts per 10^6 dG) tissues of C57BL/6 mice exposed to 625 ppm BD for 7h/day for 5 days *(74)*.

Scheme 1.8 DNA adducts formed by various BD epoxides (EB, DEB, EBD)

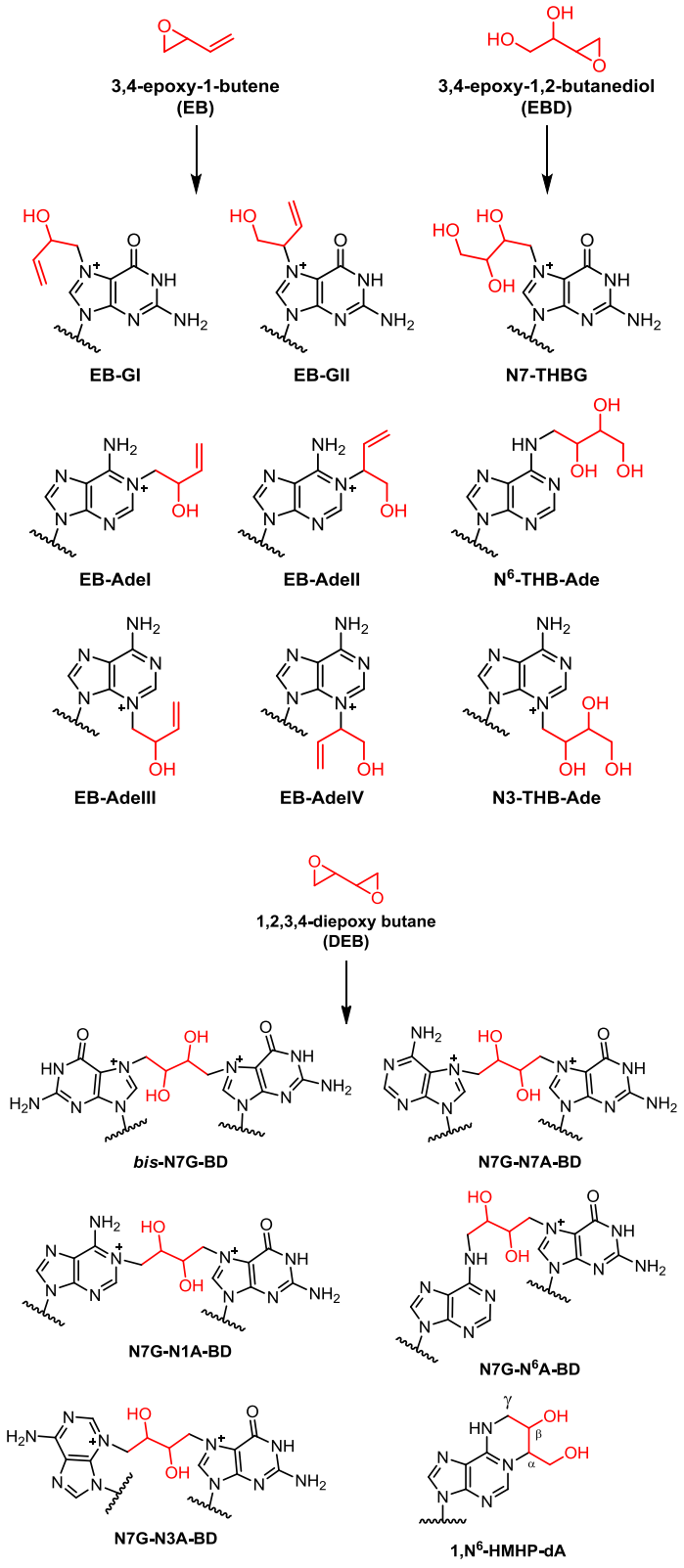

BD induced Guanine-adenine crosslinks (N7G-N1A-BD) were also quantified in liver DNA of B6C3F1 mice exposed to 625 ppm BD for 2 weeks *(113)*. *Bis*-N7G-BD and N7G-N1A-BD adducts increased linearly with BD concentrations in tissues of laboratory mice exposed to BD by inhalation (0-625 ppm) *(114)*. In contrast, the same adduct levels in tissues of rats reached a plateau at 62.5 ppm, indicating saturation in metabolism in rats *(114)*. Goggin et al. developed a highly sensitive column switching HPLC-ESI^+-MS/MS method, for the quantitation of $1,N^6$-HMHP-dA exocyclic adducts (0.44 ± 0.08 adducts per 10^8 nucleotides) induced by DEB in liver DNA of B6C3F1 mice exposed to 625 ppm BD. Persistence, repair and tissue distribution of BD induced guanine-guanine crosslinks (*bis*-N7G-BD), guanine-adenine crosslinks (N7G-N1A-BD) and exocyclic ($1,N^6$-HMHP-dA) adducts were also investigated in B6C3F1mice and F344 rats. When compared to *bis*-N7G-BD adducts, N7G-N1A-BD and $1,N^6$-HMHP-dA were found to be persistent with a half life greater than 30 days in various tissues such as liver, lung and kidney *(115)*.

So far, BD-DNA adducts have been detected and quantified in laboratory animals exposed to BD in a dose dependent manner, but they have not been successfully quantified in humans to evaluate BD exposure. Humans are exposed to very low amounts of BD (occupational BD exposure: 2-4 ppm), leading to formation of very low levels of BD-DNA adducts and, hence bioanalytical quantitation of BD-DNA adducts in humans is a challenge.

1.3.2.2 BD-protein adducts

BD electrophilic epoxides are known to react with N-terminal valine of hemoglobin to form hemoglobin protein adducts *(116)*. EB is known to react with N-terminal valine in globin to form N-(2-hydroxy-3-butenyl)–valine (HB-Val) adducts (Scheme 1.9) *(117)*. Similarly, EBD and DEB are also known to react with N-terminal valine of hemoglobin to form N-(2,3,4-trihydroxybutyl)–valine (THB-Val) and N,N-(2,3-dihydroxy-1,4-butadiyl)-valine (*pyr*-Val) protein adducts, respectively (Scheme 1.9) *(118)*. Unlike DNA adducts, protein adducts do not represent actual risk of mutations and cancer. However, BD hemoglobin adducts are known to be relatively more abundant than DNA adducts as they accumulate over lifetime of red blood cells and hence can be relatively easily quantified *(119)*. BD induced hemoglobin adducts were quantified as biomarkers of exposure in humans occupationally exposed to BD in rubber production industries. All three N-terminal valine adducts were quantified in hemoglobin isolated from blood erythrocytes of laboratory animals and humans. HB-Val and THB-Val adducts were quantified by a methodology which involves modified Edman protein degradation, followed by derivatization to pentafluorophenyl thiohydantoins and stable isotope dilution GC-MS/MS analysis *(117;120)*. As *pyr*-Val does not have a free amine for thiohydantoin derivatization, it was quantified as a 7- or 11-mer peptide, generated by proteolytic trypsin digestion of blood hemoglobin, followed by HPLC or immunoaffinity enrichment and stable isotope dilution LC-MS/MS analysis *(116;121)*. HB-Val adduct levels increased linearly with BD exposure (0-1000 ppm) in Wister rats exposed to BD for 6 h/day for 2 weeks *(122)*.

Scheme 1.9: N-terminal valine hemoglobin adducts of BD-derived epoxides.

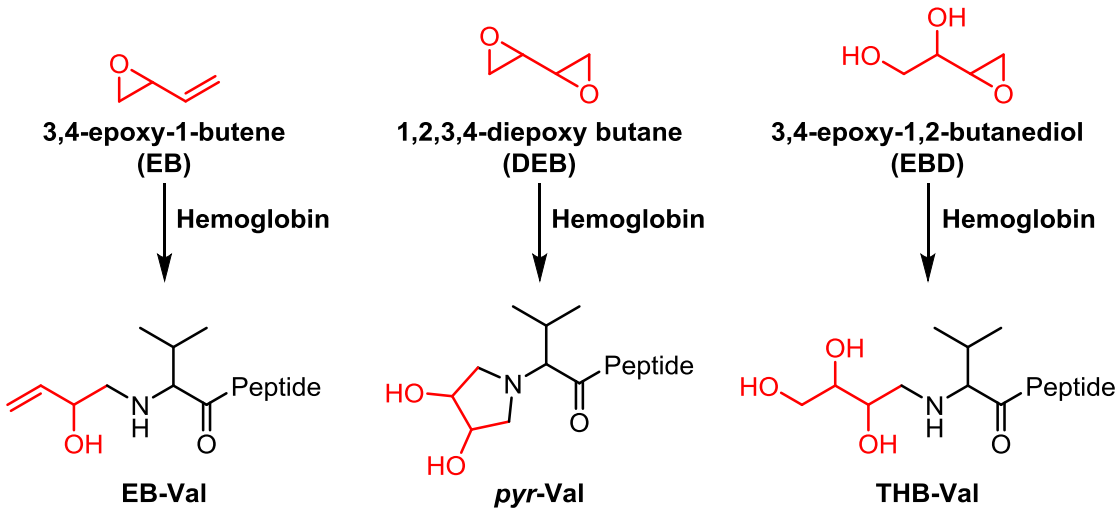

A similar linear dose response relationship was also observed for THB-Val. THB-Val hemoglobin adducts were also quantified in workers occupationally exposed to BD in the polymer industry (1 ppm) and the mean THB-Val concentrations in these workers were reported to be 1-3 pmol HB-Val/g of hemoglobin *(123)*. DEB specific *pyr*-Val adducts were also detected and quantified in mice and rats treated with DEB *(124)*. BD induced hemoglobin adducts have been used to evaluate the species differences in metabolic activation in mice, rats and humans. HB-Val and THB-Val adducts were at least 2-8 times higher in mice than rats after exposure to BD (1,000 ppm at 6 h/day, 5 days/week for 13 weeks), indicating interspecies differences in BD metabolism. Statistically significant differences in THB-Val amounts were observed between occupationally exposed Chinese workers (88 ± 59 pmol/g Hb) and unexposed workers (39 ± 13 pmol/g Hb) ($P < 0.001$) *(119)*. In another study HB-Val and THB-Val adduct levels were compared between male workers in administration (BD, 0.010 ppm), monomer production (BD, 0.29 ppm) and polymer production (BD, 0.811 ppm) in a BD and styrene-butadiene rubber production facility in the Czech Republic and it was reported that the hemoglobin adduct levels correlated with BD exposure *(125;126)*. In human male versus females comparison study, THB-Val adduct levels were found to be significantly higher in males as compared to females. In contrast, female rats or mice were reported to have higher levels of THB-Val as compared to males exposed to the same dose of BD *(127)*. No significant differences in THB-Val levels were observed between control workers and workers occupationally exposed to very low concentrations of BD (0.014 ppm) in a BD plant in Italy *(128;129)*.

Pyr-Val adducts represent a biomarker for the most genotoxic BD epoxide, DEB. *pyr*-Val was quantified in B6C3F1 mice and F344 rats exposed to 3, 62.5, 1250 ppm BD (6 h/day for 2 weeks) and its levels were compared with HB-Val and THB-Val adducts. THB-Val was the major adduct in both species, which indicated that EBD is the most abundant BD-epoxide in both the species. The concentrations of Pyr-Val were found to be higher in mice than rats because of the efficient formation of DEB in mice as compared to rats *(130)*. Recently, a highly sensitive nanoLC-ESI^+-MS/MS method was developed and validated for the quantification of *pyr*-Val in mice and rats exposed to sub ppm concentrations of BD in the range of 0, 0.5, 1, 1.5 ppm *(131)*. The concentrations of *pyr*-Val adducts in control, monomer, and polymer production workers were found to be 0.11 ± 0.07, 0.16 ± 0.12, and 0.29 ± 0.20 pmol/g globin, respectively *(132)*.

1.3.2.3 Urinary mercapturic acid biomarkers of BD exposure

Detoxification pathways of BD involve reaction of electrophilc BD epoxides with endogenous nucleophilic molecules such as glutathione (GSH). Glutathione adducts are known to be biotransformed to polar mercapturic acids which are finally excreted in urine (Scheme 1.10). Four mercapturic acids of BD were reported in literature as biomarkers of BD exposure. EB, HMVK (formed after oxidation of 1-butene-3,4-diol (EB-diol) by alcohol dehydrogenase (ADH)), EBD, DEB can be conjugated with glutathione and excreted in urine as the corresponding mercapturic acids 2-(N-acetyl-L-cystein-S-yl)-1-hydroxybut-3-ene/1-(N-acetyl-L-cystein-S-yl)-2-hydroxybut-3-ene (MHBMA), N-acetyl-S-(3,4-dihydroxybutyl)-L-cysteine (DHBMA), 4-(N-acetyl-L-cystein-S-yl)-1,2,3-trihydroxybutane (THBMA) and bis-butanediol-mercapturic acid (bis-BDMA)

respectively (Scheme 1.10) *(133-135)*. One advantage of analysis of urinary biomarkers is that the urine collection is non-invasive and human urine sample is readily available as compared to blood samples. Urinary BD metabolites can be used as a measure of BD detoxification, which can further be used as an indicator of BD induced carcinogenesis.

MHBMA and DHMA were quantified in various animal species including Sprague-Dawley rats, B6C3F1 mice, syrian hamsters, and cynomolgus monkeys exposed to 8000 ppm for 2h of radioactive ^{14}C-BD. MHBMA and DHBMA concentrations were highest in mouse, followed by the hamster and the rat, and are lowest in the monkey, indicating that the monoepoxide availability is inversely related to the hepatic activity of epoxide hydrolase enzyme. The concentration epoxide hydrolase is highest in monkeys as compared to the other three species *(136)*.

Among the two metabolites quantified in human urine of workers exposed to BD, DHBMA was found to be significantly more abundant than MHBMA since the majority of EB is hydrolyzed by epoxide hydrolase *(137)*. Another study in rats and mice exposed to 200 ppm radioactive ^{14}C-BD for 6 h confirmed the formation of another minor BD mercapturic acid 4-(N-acetyl-L-cystein-S-yl)-1,2,3-trihydroxybutane (THBMA) and its regio-isomer 3-(N-acetyl-L-cystein-S-yl)-1,2,4-trihydroxybutane *(138)*. Boogaard et al. found the evidence for the formation of bis-glutathione conjugate of DEB, which can ultimately be converted via mercapturic acid pathway to *bis*-BDMA and excreted in urine *(139)*.

Scheme 1.10 Formation of BD- mercapturic acids and their excretion in urine.

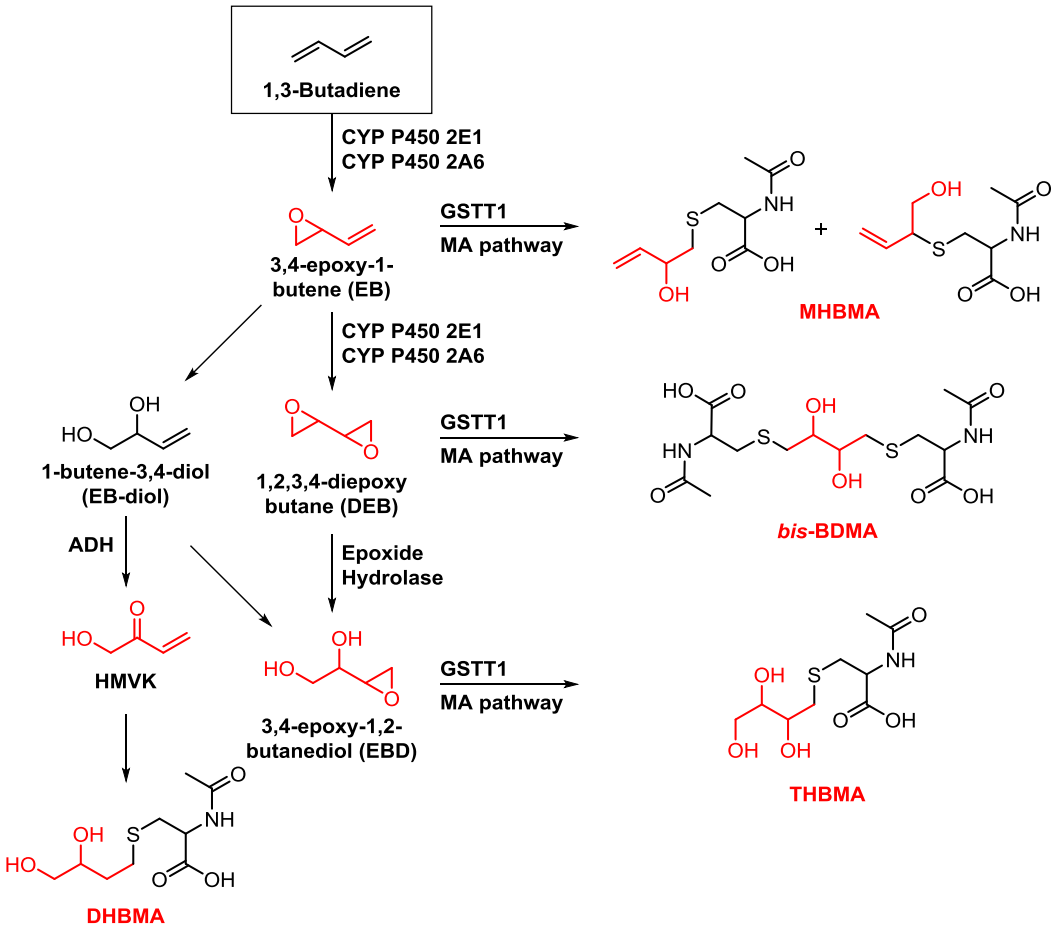

Mercapturic Acid (MA) Pathway:

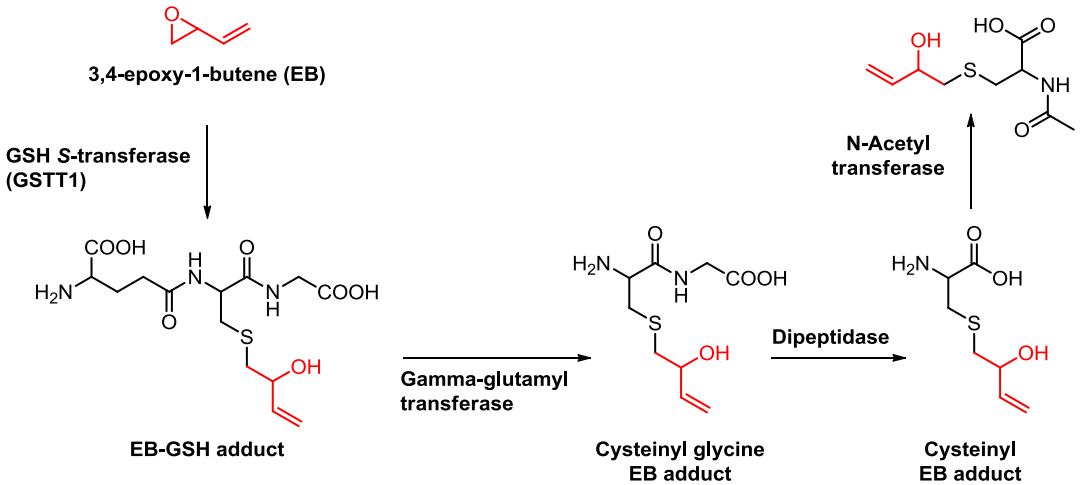

Recently bis-BDMA was quantified in the urine of rats exposed to BD by inhalation (0, 62.5 and 200 ppm) in dose dependent manner *(135)*. MHBMA (2 ng/mL) and DHBMA (524 ng/mL) were quantified in the urine of workers in the rubber industry from the Netherlands and Czech Republic using a sensitive GC-MS/MS method (LOD: 0.1 ng/ml) *(140)*. The median values of MHBMA and DHBMA were highest in polymer workers as compared to monomer workers and the least in controls. Metabolic ratio calculated as DHBMA/(MHBMA+DHBMA) is used as a measure of hydrolysis of BD epoxides by epoxide hydrolase. The metabolic ratio in humans was determined to be 0.98 as compared to 0.5 and 0.3 in rats and mice, respectively. Hence humans were reported to be more efficient at hydrolysis of BD epoxides than rats and mice *(120)*.

Albertini et al. found positive correlations between MHBMA, DHBMA levels and BD induced hemoglobin adducts. No significant associations were found between either of the urinary metabolites and polymorphisms in CYP2E1, EH and ADH, *hprt* gene mutations and cytogenetic end points *(126)*. MHBMA levels decreased significantly (>80%) 3 days after smokers quit smoking and >95% after 56 days post smoking cessation indicating strong correlation between MHBMA and cigarette smoking. However, DHBMA levels remained constant after smoking cessation *(141)*. Our laboratory also developed a sensitive isotope dilution MS method for the quantitation of THBMA and bis-BDMA in human urine after BD exposure *(134;135)*. Several other isotope dilution mass spectrometric methods using triple quadrupole MS were developed for the quantitation of MHBMA, DHBMA in smokers, nonsmokers, control and occupationally exposed workers *(129;133;142-146)* and humans exposed to BD in the environment *(147)*, and automobile exhaust *(148)*.

1.3.3 Species and gender differences in BD metabolism

Animal models to study the effects of BD exposure uncovered species differences in BD carcinogenesis and metabolism. Mice developed tumors even at 6.25 ppm BD exposure, while rats developed only a small number of tumors even at 150-200 fold higher BD exposures *(84;85)*. In another study, female mice developed lung tumors at 10 fold lower concentrations of BD than male mice *(91)*. *In vivo* concentrations of EB and DEB in blood were at least 5 fold higher in mice as compared to rats showing species differences in BD metabolism *(149;150)*. Female rats were also found to have 4.75-fold higher blood concentrations of DEB as compared to male rats exposed when exposed to 62.5 ppm BD for 6h by inhalation *(150)*. Similarly, female mice had greater DEB concentrations in several tissues such as blood, femur, lung and fat tissue as compared to male mice receiving the same BD exposure *(150)*. These results clearly confirm the presence of species differences in BD metabolism. *In vitro* studies that determined catalytic V_{max}/K_m values for the epoxidation of EB to DEB in mice, rat and human liver microsomes revealed that the rates of conversion in mice were 3.5 fold faster than rats, and 3-60 fold greater than humans *(151) (152)*. Furthermore, the catalytic activity of the enzymes responsible for hydrolysis of DEB and detoxification of EB to EB-diol were higher is humans followed by rats and least in mice explaining the higher concentrations of BD epoxides in mice *(93;94)*.There is also evidence that rat CYP P450 2E1 monooxygenase, the major enzyme responsible for BD metabolism to EB and DEB is inactivated by phosphorylation of ser residues by PKA/cAMP *(153)*or by covalent binding of BD metabolites, especially EB to Tyr and His residues within its active site *(154)* and hence leading to decreased bioactivation of BD.

The rates of detoxification by GST of BD epoxides are higher in rats as compared to mice *(93)*. BD metabolic detoxification ratio [DHBMA/(DHBMA +MHBMA)] is an indicator of EB metabolism by epoxide hydrolase (EH) or GST. The ratio was observed to be 0.20, 0.52 and 0.98 in mice, rats and humans, respectively *(137)*. No statistically significant differences were observed in MHBMA and DHBMA concentrations per unit of BD exposure between occupationally exposed female and male workers. Furthermore, the DHBMA/(DHBMA +MHBMA) ratio was similar for males and females, reflecting the same relative utilization of the hydrolytic (DHBMA) and the conjugation (MHBMA) detoxification pathways in both genders *(155)*.

BD-hemoglobin adducts HB-Val and *pyr*-Val levels were also 4-10 fold higher in B6C3F1 mice as compared to F344 rats exposed to BD. THB-Val adduct was present in higher amounts as compared to HB-Val and *pyr*-Val adducts, and the ratio of THB-val to total BD-hemoglobin adduct formation in rats and mice was found to be 2-6 and the corresponding ratio in humans was >500 *(116;118)*. THB-Val adduct levels were significantly higher in male workers than female workers (in both control and exposed groups) which in contrast to the gender differences observed in mice and rats *(127)*. At low occupationally relevant exposure of 1 ppm BD in mice, rats and humans, HB-Val and *pyr*-Val adducts were the highest in mice indicating a highly efficient metabolic activation in this species. The percentage of THB-Val to the total BD-hemoglobin adducts was highest in humans (99.6%) indicating the highly efficient hydrolysis of BD epoxides by epoxide hydrolase to EBD *(116)*.

Concentrations of DEB are highest in mice as compared to rats and humans as indicated by the higher DEB specific *pyr*-Val adduct levels in mice *(132)*. Even DEB specific DNA crosslinks *bis*-N7G-BD adduct levels were also higher in mice as compared to rats exposed to the same concentration of BD *(114)*. Gender differences were also observed in mice, where females have significantly higher levels of DEB specific bis-N7G-BD, N7G-N6A-BD adducts as compared to males. However, these differences were not observed in rats. EBD specific N7-TBHG adducts were also significantly higher in liver, lung and kidney tissues of mice as compared to rats exposed to same dose of BD (625 ppm) *(75)*. Hence, significant inter-species and gender differences were observed in metabolism of BD. Among the rodent species examined, mice were known to form higher levels of DEB, followed by rats and humans exposed to BD which is consistent with the greater carcinogenicity of BD in mice as compared to rats and humans. Gender differences in BD hemoglobin adduct formation were observed at relatively high exposure of BD but not at low BD exposures in laboratory rodents *(131)*. These species and gender differences in BD metabolism make BD risk assessment challenging and complex.

1.3.4 BD exposure in cigarette smoke and lung cancer risk in various ethnic groups

Lung cancer accounts for 14% of all cancer deaths worldwide and 27% of all cancer deaths in the US *(156)*. Cigarette smoking is one of the major risk factors for lung cancer development, accounting for approximately 87% of lung cancer deaths and 30% of all other cancer deaths *(157;158)*. Other environmental exposure risk factors for lung cancer include radon, secondhand smoke, asbestos, chromium, cadmium, arsenic, ionizing radiation, air pollutants, and diesel exhaust *(157)*. Cigarette smoke is a complex mix of known carcinogens such as polycyclic aromatic hydrocarbons (PAHs), heterocyclic compounds, aromatic amines, heterocyclic aromatic amines, N-nitrosamines, phenolic compounds, volatile hydrocarbons, nitrohydrocarbons, metals, inorganic compounds, and other small molecule aldehydes such as acetaldehyde, formaldehyde and volatile organic compounds such as benzene, 1,3-butadiene and isoprene. Among various carcinogens in cigarette smoke, 1,3-butadiene has one of the highest cancer risk index per cigarette per day *(159)*. BD is generated as a gas in mainstream smoke either from incomplete combustion or thermal cracking process of complex molecules such as carbohydrates, amino acids, phytosterols, paraffins, and many other tobacco components in tobacco *(160;161)*.

Ethnic differences in lung cancer risk due to smoking

Smoking related lung cancer risk and incidence was found to be different among various ethnic groups in the United States. In a study of 740 lung cancer patients and 1616 controls, the age adjusted lung cancer incidence rates in males were found to be in the order of Hawaiian > Caucasian > Chinese > Japanese > Filipino *(162)*. In the same study lung cancer incidence rates in females were Hawaiian > Caucasian > Chinese >

Filipino > Japanese *(162)*. From this study, it was hypothesized that the differences in lung cancer risk among various ethnic groups might be due to differences in diet and metabolic differences in activation and detoxification of carcinogens present in cigarette smoke due to genetic polymorphisms *(162)*. Hinds et al. also conducted a multi-ethnic cohort study involving 375 lung cancer subjects and 2404 controls in Japanese, Chinese and Hawaiian women from Hawaii and found the lung cancer risk among the ethnic groups to be Hawaiian > Japanese > Chinese women *(163)*. An independent study was conducted to identify ethnic differences in lung cancer risk among African American and European Americans smokers including 5588 lung cancer cases and 3692 controls *(164)*. It was concluded that African Americans have 2-4 times higher risk of lung cancer than European American smokers in the 40-54 age group *(164)*. Stellman et al. found that the lung cancer risk was at least 10 times higher in Americans than Japanese Americans *(165)*. In another study conducted by Stellman et al. in European American and African American smokers, no statistically significant differences in lung cancer risk were identified *(166)*.

In a large multi ethnic cohort study by Haiman and co workers involving 180,000 smokers (≤ 10 cigarettes/day) belonging to African-American, Japanese-American, Latino, Native Hawaiian, European American ethnicity, the relative risk of lung cancer was found to be 1.00, 0.25, 0.21, 0.88 and 0.45, respectively. But, at a higher smoking level (>30 cigarettes/day), the relative risks were 1.00, 0.75, 0.79, 0.95 and 0.82, respectively *(167)*. This study hypothesized that the ethnic differences might be due to differences in metabolism of tobacco carcinogens *(167)*. Five year (2006-2010) lung cancer incidence rate statistics from National Cancer Institute among different ethnic

groups were African American > European American > American Indian > Asian > Hispanic in males. In females, the corresponding lung cancer incidence rates were European American > African American > American Indian > Asian > Hispanic *(158)*.

1.4 Carcinogen induced small molecule DNA adducts repair mechanisms

DNA damage is an important step in mutagenesis and the development of cancer. DNA damage induced by exogenous and endogenous carcinogens is known to be repaired by cellular DNA repair mechanisms such as base excision, nucleotide excision and homologous recombination repair pathways.

For example, O6-methylguanine DNA methyltransferase (MGMT, DNA alkyltransferase) cleaves both methyl and ethyl adducts from methyl/ethyl guanine adducts. MGMT reaction is noncatalytic but is rather stoichiometric consuming one molecule of MGMT for each adduct removed *(168)*. DNA polymerases such as pol-δ contain proofreading activities and are involved in the repair of DNA adducts *(169)*. pol-δ is known to halt the process of DNA replication when it encounters bulky DNA adducts such as 1,N6-ethenoadenine and works backward to excise nucleotides with the adduct from the growing DNA chain and, then starts the forward replication process. Point mutations of a conserved active site residue in pol-δ significantly elevates the frequency of insertion errors of pol-δ *(169)*. Another type of repair called mismatch excision repair (MMR) is capable of correcting errors of DNA replication not detected by the proofreading activities of replicative DNA polymerases. MMR enzymes excise an incorrect nucleotide from the daughter DNA and repair the strand using watson and crick base pairing of parent DNA strand as the correct template *(170)*.

1.4.1 Base Excision Repair and Nucleotide Excision Repair of DNA adducts

Base excision repair (BER) of DNA adducts involves several enzymes depending on the nature of DNA adduct. DNA adduct base modifications primarily repaired by BER enzymes include 7,8-dihydro-8-oxoguanine (8-oxoG) *(171)*, uracil in DNA due to cytosine deamination *(172)*, ring opened N7 substituted and unsubstituted guanine and adenine bases also called formamidopyrimidine (Fapy) adducts *(173)*, and psoralen induced DNA adducts by UV radiation *(174)*. BER enzymes are typically DNA glycosylases and cleave the N-glycosidic bond between the nucleotide base and ribose resulting in an apurinic or apyrimidinic (AP) site. 8-Oxoguanine DNA glycosylase I (Ogg1) is known to remove 7,8-dihydro-8-oxoguanine (8-oxoG) *(175)*. Mutations or polymorphisms in the human OGG1 gene are associated with the risk of lung and colorectal cancer *(176;177)*. Uracil DNA glycosylase, another BER enzyme, excises the uracil in the DNA that is the product of unnecessary cytosine deamination, thereby preventing the subsequent C→T point mutations *(172)*. BER enzyme N-methylpurine DNA glycosylase (MPG) is able to remove a variety of adducted purine bases *(178)*, and the enzyme formamidopyrimidine [fapy]-DNA glycosylase (fpg) is known to remove various fapy adducts such as fapy-guanine, methy-fapy-guanine, fapy-adenine, aflatoxin B1-fapy-guanine *(179)* . AP sites generated by the action of BER enzymes are known to be repaired by the action of AP-endonuclease 1 (APE1) and DNA polymerase β (Polβ). Other proteins such as X-ray repair cross-complementing group 1 (XRCC1), a scaffold protein and DNA ligase III (LIG3) are also involved in ligation of the correct base and this process is known as short patch BER pathway *(180;181)*. Long-patch BER replaces a strand of nucleotides with a minimum length of 2 nucleotides and up to 12 nucleotides

next to the AP site and this process involves scaffolding protein proliferation cell nuclear antigen (PCNA), DNA polymerases such as Polδ and Polε, flap endonuclease-1 (FEN1) and DNA ligase I (LIG1) *(182)*.

Nucleotide excision repair (NER) is another common DNA repair pathway capable of removing bulky base modifications from DNA. NER involves cleavage at two phosphodiester bonds, 3′ and 5′ of the site of damage, followed by excision from single-stranded fragment *(183;184)*. The excised oligonucleotide is replaced by DNA repair, synthesis, and ligation. NER deficiency in humans results in xeroderma pigmentosum (XP), a genetic disorder characterized by photosensitivity to UV light, leading to increased incidence of skin cancer *(185)*. XP patients are impaired in the removal of radiation products and DNA adducts induced by the UV component of sunlight *(185)*. Somatic cell lines created from these patients have also been reported to have decreased efficiency in NER of bulky DNA adducts resulting from genotoxic chemicals *(184)*. *In vitro* studies in cellular extracts showed that the range of base lesions detected by mammalian NER extends to nonbulky adducts, and even abasic sites *(186)*.

Several biological experiments demonstrated that mammalian NER process involves over 20 proteins including XPA, XPC, replication protein A (RPA), XPB and XPD DNA helicases, ERCC1-XPF and XPG, Polδ, Polε, PCNA etc. with defined roles in detection, removal and repair of DNA adducts *(187)*. Detailed molecular mechanisms by which several NER proteins distinguish a large number of chemically unrelated DNA lesions as substrates for NER are unknown. However, NER is believed to be involved in repair of DNA lesions when the system recognizes conformational changes imposed on DNA. Even within NER, Global genomic NER (GGR) repairs damage throughout the

genome, while another specific NER pathway called Transcription Coupled Repair (TCR) is known to repair genes during active RNA polymerase transcription *(188)*.

Recombination and fanconi anemia (FA) repair pathways of DNA adducts

Many bifunctional crosslinking agents such cisplatin and nitrogen mustards form interstrand crosslinks in DNA which in turn lead to the formation of DNA double strand breaks during replication to initiate various repair pathways such as recombination and FA repair pathways *(189)*.

Recombination repair can happen either by homologous recombination (HR) or nonhomologous end-joining (NHEJ). The HR pathway requires the presence of an identical or partially identical sequence linked to the damaged DNA region via the use of a repair template. The nucleotide sequences are exchanged between two similar or identical molecules of DNA to initiate the recombination *(190)*. Non-homologous end joining occurs when no homologous template is available and the break ends are directly ligated. NHEJ generates single-stranded overhangs on the ends of double-strand breaks and when completely repaired, the overhangs are removed without loss of genetic information *(191)*. Imprecise repair can cause loss of nucleotides which can further lead to translocations and frame shift mutations. In NHEJ, either the Ku heterodimeric proteins or other multiple enzymes (Ku independent pathway) are involved in the rejoining process, including DNA ligase IV, XRCC4, and DNA-dependent protein kinase (DNA-PK) *(192)*.

Fanconi anemia (FA) repair pathway is associated with the repair of interstrand DNA crosslinks formed by bifunctional crosslinking agents *(193)*. FA pathway is known to work in coordination with three other DNA repair pathways such as homologous

recombination, nucleotide excision repair, and mutagenic translesion bypass DNA synthesis in response to the DNA modification produced by carcinogens *(194)*. Fanconi Anemia (FA) is a rare autosomal recessive or X-linked genetic disease condition and patients with FA are hyper-sensitive to bifunctional DNA damaging agents such as mitomycin C (MMC) or diepoxybutane (DEB) that create DNA interstrand crosslinks (ICLs) *(195)*. FA pathway is activated not only by bifunctional DNA damaging chemicals, but also by other agents, such as ultraviolet radiation (UV), ionizing radiation (IR) or spontaneously during replication *(196;197)*. FA pathway is a complex process involving unique nuclear protein complex consisting of at least 13 complementation groups FANCA to N, leading to formation of DNA repair structures either upstream or downstream of the pathway *(193)*.

1.5 Development of novel DNA adducts as biomarkers

Mass spectrometry is used as a tool for the identification of novel DNA adducts as biomarkers of exposure, metabolic activation and cancer risk in DNA adductomics *(198)*. Previously, MS analysis of DNA adducts was a bottom-up approach where predetermined and structurally known DNA adducts were quantified in both *in vitro* and *in vivo* studies. DNA adductomics approach is a top down generalized procedure to characterize overall DNA damage induced by carcinogens by identifying structurally known or unknown DNA adducts

In MS based DNA adductomics approach, MS based fragmentation of a common structural feature of nucleosides, a deoxyribose sugar moiety bonded to the nucleobase through a N-glycosidic bond is performed. MS based fragmentation reactions for the neutral loss of 2′ deoxyribose sugar (dR = 116 amu) ($[M\text{-}B\text{-}dR+H]^+ \rightarrow [M\text{-}B+H]^+$ - dR, M = modification, B = nucleobase) are monitored using different MS scanning modes (Scheme 1.11) *(199)*.

Scanning modes to determine loss of dR (116 amu)

Constant neutral loss (CNL) scanning for the neutral loss of 116 amu has been performed on a triple quadrupole MS for determination of polycyclic aromatic hydrocarbon DNA adducts *(200)*. In this type of scanning, quadrupole 1 (Q1) and Q3 scan were offset from each other by the neutral loss of dR (*m/z* = 116 amu). Collision cell (q2) filled with inert gas such as argon or nitrogen is used to induce fragmentation. Finally, only ions that fragment with the specific neutral loss of dR (*m/z* = 116 amu) will pass through Q1, q2, and Q3 and be recorded as an MS signal (Scheme 1.11). A variant of the above CNL scan method known as the pseudo-CNL approach was used to assess

and comprehensively detect DNA adducts in human lung, esophagus *(201)* and food derived modified nucleosides *(202)*. In this approach, instead of CNL scanning, the system is set to monitor a number of sequential selected reaction monitoring (SRM) transitions, all involving a loss of 116 amu. Although time consuming, the pseudo-CNL approach is proposed to have better sensitivity over the normal CNL approach because triple quadrupole instruments are good at performing multiple SRMs rather than scanning over a wide mass range.

Another advanced MS-based DNA adductomics method involved usage of data-dependent (DD) scanning approach to monitor the CNL of dR (116 amu) using newer MS instruments such as linear ion trap quadrupole (LTQ) and orbitrap velos, for high resolution accurate mass analysis. DD scanning is optimized software dependent scanning performed in real time and provides increased DNA adduct coverage by preventing the repeated fragmentation of the most abundant ions using dynamic exclusion of already fragmented ions. In addition, a predetermined reject mass list can be included to exclude interfering high abundant background ions from fragmentation *(199)*. Examples of the use of this approach include DD analysis in MS^2 mode *(203)* or in MS^3 mode for fragmentation *(204-206)*. In DD-MS^3 mode, adducts that have a neutral loss of *m/z* 116 can be further fragmented via MS^3 mode to obtain structural information from MS^3 fragments (Scheme 1.11). Recently Balbo et al. used DD-MS^3 scanning to monitor the accurate neutral loss of dR (*m/z* 116.0474) using the Orbitrap Velos HRMS instrument. This method has advantages over previous methods as the high resolution accurate mass measurement significantly decreases the nonspecific fragmentation. Furthermore, more than 10 adducts were identified in liver DNA of mice exposed to the

tobacco-specific nitrosamine 4-(methylnitrosamino)-1-(3-pyridyl)-1-butanone (NNK) *(205)*. Hence, with advancing MS instructions, it is possible to adopt top down DNA adductomics based approaches to identify novel DNA adducts as biomarkers.

Scheme 1.11 MS/MS fragmentation based neutral loss of deoxyribose sugar from adducted DNA nucleosides (dR = 116 amu) (A), triple quadrupole based scanning of the neutral loss of sugar from nucleosides (B), Data dependent constant neutral loss based scanning of sugar (C).

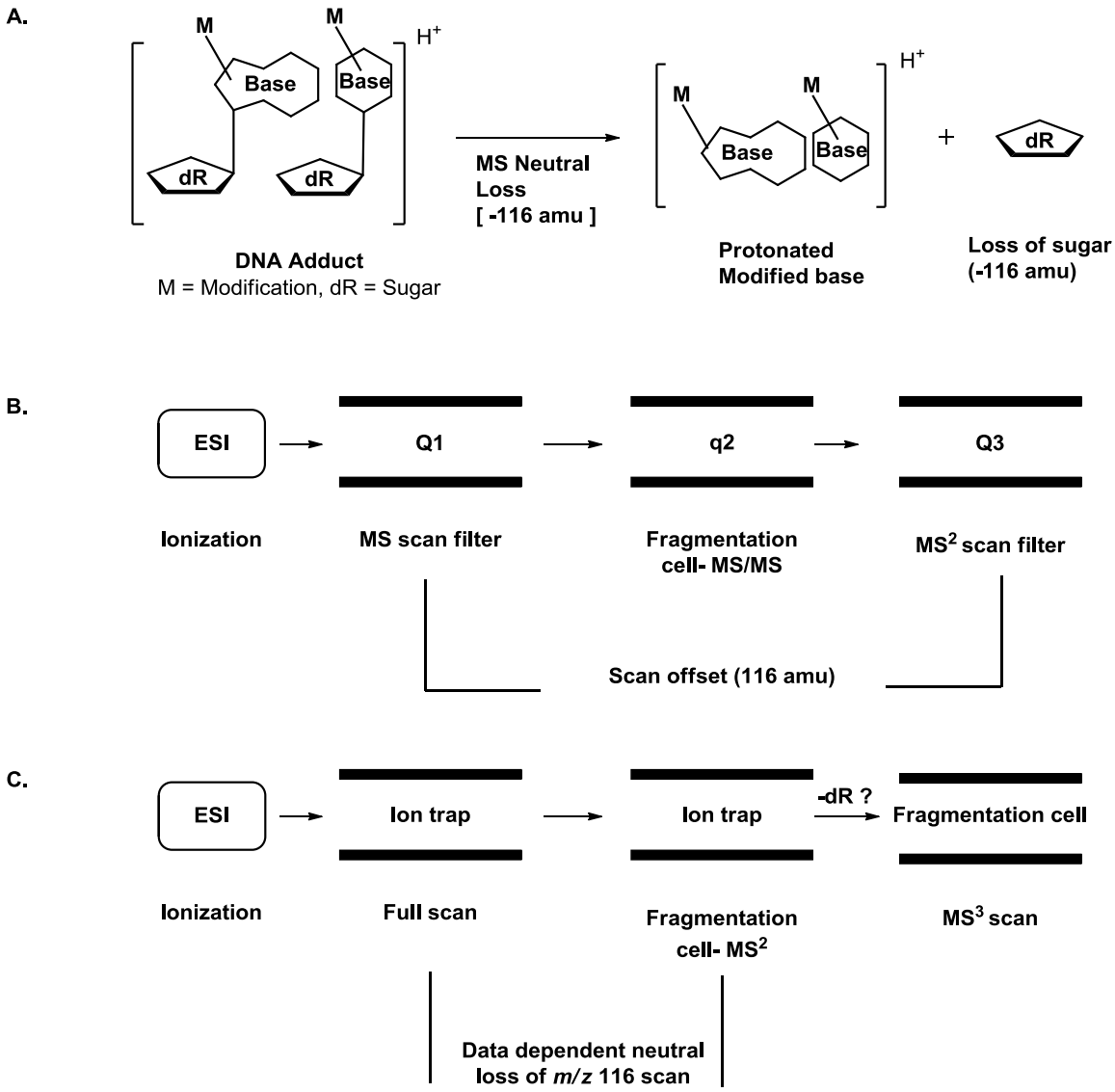

1.6 Summary and thesis goals

BD is a carcinogen known for its widespread human exposure in polymer and monomer rubber industries and environmental exposure due to automobile exhaust, cigarette smoke, and wood burning due to forest fires. The metabolically activated BD-epoxides EB, EBD and DEB are responsible for BD carcinogenicity (Scheme 1.7). BD electrophilic metabolites are known to react with DNA to form various DNA adducts which can cause mutations that are ultimately responsible for the carcinogenicity of BD (Scheme 1.8). Though there are various biomarkers of BD exposure such as protein adducts and mercapturic acids, DNA adducts are known as ultimate biomarkers as they represent biologically relevant dose of exposure, and are a direct measure of metabolic activation and cancer risk. Though BD induced DNA adducts are quantified in animals exposed to relatively high concentrations of BD (> 6.25 ppm), they have not been quantified in humans exposed to sub ppm concentrations of BD (< 1-3 ppm BD). Hence the initial goals of this thesis work were to develop highly sensitive isotope MS methods for the absolute quantification of DEB specific *bis*-N7G-BD in animal model exposed to low sub ppm (0.5 – 1.5 ppm) concentrations of BD.

We have developed sensitive accurate mass spectrometric methods using advanced capillary and nanospray LC-MS techniques for the quantitation of BD DNA adducts such as N7-THBG and EB-guanine. N7-THBG and EB-guanine adducts were quantified in human blood leukocyte DNA of smokers, nonsmokers, occupationally exposed individuals and control administrative workers. As blood leukocyte DNA is limited and the levels of BD-DNA adducts are very low in blood (1-3 adducts/10^8 to 10^9 nucleotides), we worked on the development of a novel high resolution accurate MS

method for the quantitation of the BD-DNA adducts in urine. Differences in smoking related lung cancer risk in various ethnic/racial differences has been hypothesized to be because of the differences in genetic polymorphisms of the genes involved in the metabolic activation and deactivation of carcinogens. Though cigarette smoke contains more than 70 different carcinogens, BD is one of the most potent and abundant carcinogens present in mainstream and sidestream cigarette smoke. We tested this hypothesis by quantification of BD-DNA adducts in urine of European American and African American smokers to evaluate the ethnic/racial differences in metabolism of BD .

Additional studies were performed on isogenic repair deficient cell lines from Chinese hamster lung fibroblasts to understand the repair of DNA–DNA crosslinks induced by DEB. We also investigated the formation of novel ring opened formamidopyrimidine (Fapy) BD-DNA adducts.

II. NANO HPLC-NANO ESI$^+$-MS/MS QUANTITATION OF *BIS*-N7-GUANINE DNA-DNA CROSS-LINKS IN TISSUES OF B6C3F1 MICE EXPOSED TO SUB-PPM LEVELS OF 1,3-BUTADIENE

Reprinted with permission from: Dewakar Sangaraju , Melissa Goggin, Vernon Walker , James Swenberg, Natalia Tretyakova. Anal Chem. 2012, 84(3), 1732-9.

2.1 Introduction

1,3-Butadiene (BD) is an important industrial chemical commonly used in rubber and plastic manufacturing *(83)* and an environmental pollutant present in automobile exhaust *(207)* and in cigarette smoke *(208)*. BD is classified as human carcinogen based on epidemiological studies in occupationally exposed workers that revealed an increased incidence of leukemia *(86;87;91;209)*. Furthermore, inhalation experiments with laboratory animals have shown that BD is a multi-site carcinogen, inducing lung, liver, heart stomach and other solid tumors in mice *(84)* and thyroid, pancreas, uterus, testes and other tissue tumors in rats *(85)*. BD requires metabolic activation to DNA-reactive epoxides 3,4-epoxy-1-butene (EB), 1, 2, 3, 4-diepoxybutane (DEB), and 1,2-dihydroxy-3,4-epoxybutane (EBD) *(95;210)*. Among these, DEB is the most genotoxic, inducing large numbers of base substitutions, sister chromatid exchanges, and chromosomal aberrations *in vitro* and *in vivo (95;98;211)*. Large interspecies differences in carcinogenicity of BD in mouse and rat animal models *(84;85)* have been attributed to more efficient metabolic activation of BD to DEB in the mouse *(212-214)*. Because of its key role in carcinogenicity of BD, there is a need for sensitive biomarkers of DEB formation *in vivo.*

Georgieva et al. have developed DEB-specific biomarkers based on N-terminal valine hemoglobin adducts (Hb) adducts, namely N,N[2,3-dihydroxy-1,4-butyl]valine (*pyr*-Val) *(127;131)*. *Pyr*-Val adducts have been detected in blood of B6C3F1 mice and F344 rats exposed to BD as low as 0.5 ppm BD *(131)*. More recently, *Pyr*-Val adducts were observed in blood of occupationally exposed workers at concentrations of 0.08 to 0.86 pmol/g globin *(116)*. Hb-based biomarkers are valuable because these adducts are not repaired and therefore are representative of cumulative exposure over time(the lifetime of red blood cells is ~120 days in humans, 45 days in mice, and 63 days in rats). However, Hb based biomarkers may not represent a biologically relevant dose of DEB since protein adducts do not lead to mutations, and DNA rather than cellular proteins is the ultimate biological target of genotoxic carcinogens such as DEB.

Our laboratory previously identified several DEB-specific DNA adducts including DNA-DNA cross-links, 1,4-*bis*-(guan-7-yl)-2,3-butanediol (*bis*-N7G-BD) (Scheme 2.1) and 1-(guan-7-yl)-4-(aden-1-yl)-2,3-butanediol (N7G-N1A-BD), and an exocyclic DEB-dA adduct, *1,*N^6-(1-hydroxymethyl-2-hydroxypropan-1,3-diyl)-2'-deoxyadenosine *(65;74;107;113;215;215)*. DEB-specific bifunctional DNA adducts have been quantified in tissues of laboratory rats and mice that were exposed to 6.25-625 ppm of BD by inhalation *(114)*. Among DEB-DNA adducts, *bis*-N7G-BD were present at the highest concentration (3.95 ± 0.89 adducts/10^7 nucleosides (nts) in livers of mice exposed to 625 ppm BD), followed by N7G-N1A-BD (0.27 ± 0.07 adducts/10^7 nts), *1,*N^6-HMHP-dA (0.044 ± 0.008 adducts/10^7 nts) *(65;114)*.

Scheme 2.1 Metabolism of 1,3-butadiene to DEB and its reactions with DNA to form *bis*-N7G-BD crosslinks.

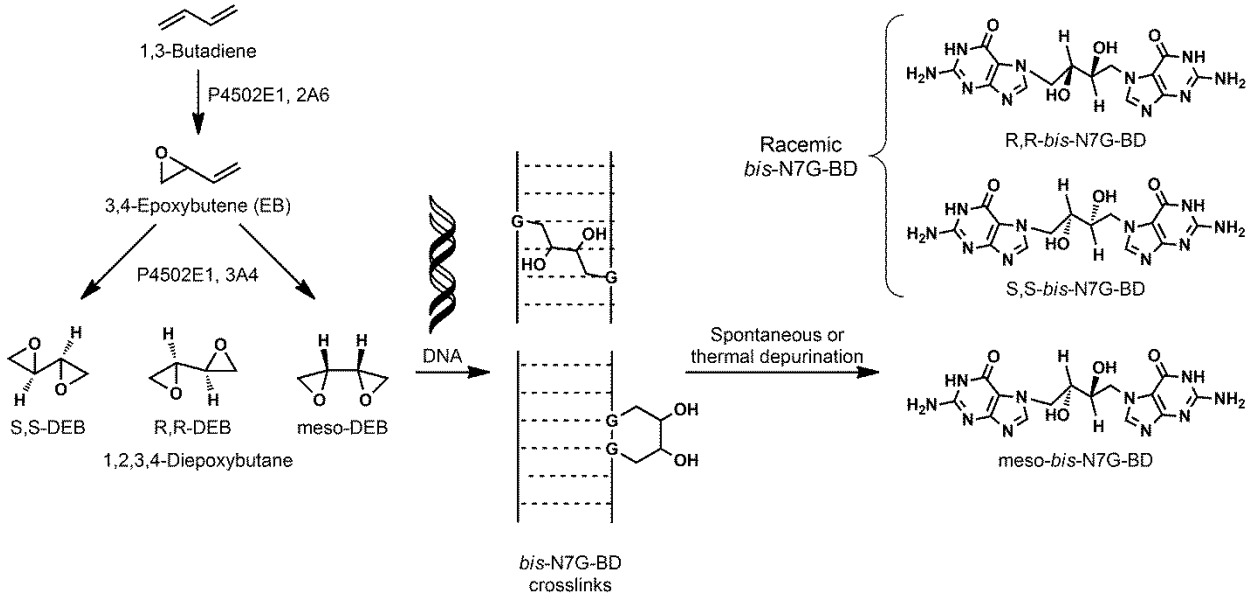

While our previously capillary HPLC-ESI$^+$-MS/MS methods were adequate for detection of *bis*-N7G-BD in tissues of laboratory animals exposed to 6.25 ppm BD and higher, *(114)* greater sensitivity is required in order to detect DEB-DNA adducts following typical human exposures (1 ppm and lower). In the present work, we have developed and validated a nanoHPLC-nanoESI$^+$-MS/MS method for the quantitation of *bis*-N7G-BD *in vivo*. The sensitivity and accuracy of the new method are as follows: LOD: 0.5 fmol/ 100 μg DNA, LOQ: 1.0 fmol/ 100 μg DNA, and accuracy: 97.1 ± 6.3 % (n = 5). To our knowledge, this is the first quantitative analysis of DEB-specific DNA adducts following exposure to occupationally relevant BD concentrations (OSHA limit = 1 ppm) *(216)*. Our results indicate that *bis*-N7G-BD formation is more efficient at low BD exposure levels (< 1.5 ppm), probably because a greater fraction of BD is metabolized to DEB. These results will be useful for human risk assessment from exposure to BD.

2.2 Materials and Methods

Note: *DEB is a known carcinogen and must be handled with adequate safety precautions. Phenol and chloroform are toxic chemicals that should be handled in a well-ventilated fume hood with appropriate personal protective equipment.*

LC-MS grade water, methanol and acetonitrile were obtained from Fisher Scientific (Pittsburgh, PA). All other chemicals and solvents were obtained from Sigma-Aldrich (Millwaukee, WI, St. Louis, MO) with the exception of *bis*-N7G-BD and [$^{15}N_{10}$]-*bis*-N7G-BD, which were prepared in our laboratory as described elsewhere *(74;105;215)*.

Animals and treatment

BD inhalation exposure experiments were performed at the Lovelace Respiratory Research Institute (Albuquerque, NM) as previously reported *(114)*. Briefly, B6C3F1 female mice (5 per group) were exposed to 0, 0.5, 1.0, or 1.5 ppm BD by inhalation for 2 weeks (6 h/day, 5 days/week). Animals were euthanized by CO_2 and cardiac puncture at the end of the exposure period. Liver tissues were collected, flash frozen, and shipped to the University of Minnesota on dry ice, where they were stored at -80 ºC.

Cell culture

V79 chinese hamster lung fibroblasts were obtained from the Coriell institute (Camden, NJ, USA). Cells were grown to confluence on 15 cm dishes in Ham's F-12 modified essential Eagle's media supplemented with 9% fetal bovine serum. The cell culture was maintained in a humidified environment containing 5% carbon dioxide and 95% air at 37°C. Cells were subjected to serial passage at a dilution of 1:10 following brief exposure to porcine pancreatic trypsin and mechanical agitation. All experiments were performed on cells at low passage number.

DNA isolation

DNA was isolated from mouse liver tissue using NucleoBond AXG500 anion exchange cartridges (Macherey-Nagel) according to the manufacturer's instructions. DNA employed for method validation was isolated from CHL-V79 cells by standard phenol-chloroform extraction. DNA concentrations were estimated using UV spectrophotometry. DNA purity was assessed from A_{260}/A_{280} absorbance ratio, which was typically between 1.7 and 1.8. DNA amounts were determined by quantitation of dG in enzymatic hydrolysates as described below.

dG quantitation

DNA aliquots (~10 μg) were enzymatically digested with phosphodiesterase I (6.0 mU/μg DNA), phosphodiesterase II (8.0 mU/μg DNA), DNase (3.0 U/μg DNA), and alkaline phosphatase (6.69 U/μg DNA) in 10 mM Tris-HCl/15 mM $MgCl_2$ (pH 7.2) at 37 °C overnight. HPLC-UV analysis of dG was conducted by HPLC-UV using a Zorbax SB-C8 column (4.6 x 150 mm, 5 μm, from Agilent Technologies, Palo Alto, CA) eluted with a gradient of 150 mM ammonium acetate (A) and acetonitrile (B) described previously *(217)*.

Neutral thermal hydrolysis and isolation of *bis*-N7G-BD adducts

DNA samples (100 μg) were spiked with 50 fmol of *S,S;R,R* $^{15}N_{10}$- *bis*-N7G-BD (racemic $^{15}N_{10}$- *bis*-N7G-BD, internal standard for mass spectrometry) and incubated at 70 ºC for 1 hour to release *bis*-N7G-BD from the DNA backbone as a free base conjugate. Partially depurinated DNA was removed by ultrafiltration with Nanosep 10K filters (Pall Life Sciences, Ann Arbor, MI). The filtrates containing *bis*-N7G-BD and its internal standard were purified by offline HPLC. A Zorbax Eclipse XDB-C18 (4.6 x 150

mm, 5 μm, from Agilent Technologies, Palo Alto, CA) column was eluted at 1 mL/min with a gradient of 0.4% formic acid in Milli-Q water (A) and HPLC grade acetonitrile (B). Solvent composition was maintained at 0% B for 5 min and then increased to 3% B in 10 min and further to 40% B in 5 min. The solvent composition was returned to 0% B in 5 min and maintained at 0% B for 15 min. 2'-deoxythymidine (dT) and 2'-deoxyadenosine (dA) (12.0 nmol each) were added as retention time markers, eluting at 13.7 and 18.8 min, respectively. HPLC fractions containing *bis*-N7G-BD (14 – 18 min, about 1.25 mL) were collected, dried under vacuum, and dissolved in water (25 μL) for nanoHPLC-nanoESI$^+$-MS/MS analysis.

NanoLC-nanoESI$^+$-MS/MS analysis of *bis*-N7G-BD

A Waters nanoAcquity UPLC system (Waters Corp., Millford, MA) interfaced to a Thermo-Finnigan TSQ Quantum UltraAM mass spectrometer (Thermo Fisher Scientific Corp., Waltham, MA) was used in all analyses. HPLC solvents were 0.01% acetic acid in LC-MS grade water (A) and LC-MS grade methanol: acetonitrile (1:1) (B). Samples (8 μL) were loaded on a trapping column (Symmetry C18 nanoAcquity, 0.18 x 20 mm, Waters Corp., Millford, MA) for 1 min at 0% B at a flow rate of 10 μL/min. The chromatographic separation was achieved with a nano-HPLC column (75μm x 200 mm) manually packed with Zorbax SB-C18, 5 μm chromatographic packing (Agilent Tech. Santa Clara, CA). The column was eluted at a flow rate of 0.4 μL/min. Solvent gradient started at 0% B for 1 min and was increased to 10% B in 2 min, further to 50% B in 8 min, and finally to 80% B in 5 min. Solvent composition returned to 0 %B for 14 min equilibration at a flow rate of 0.4 μL/min. Under these conditions, *bis*-N7G-BD eluted as a sharp peak at ~15 min.

The triple quadrupole mass spectrometer was fitted with a nanospray source from Thermo Fisher Scientific Corp. (Waltham, MA). The instrument was operated in the positive ion mode ESI mode with Ar as a collision gas (1.4 mTorr). The mass spectrometer was tuned upon infusion of authentic *bis*-N7G-BD solution to achieve maximum sensitivity. Quantitative analyses were conducted in the selected reaction monitoring (SRM) mode by following the MS/MS transitions corresponding to the neutral loss of guanine from protonated molecules of the analyte (*m/z* 389.1 $[M + H]^+ \rightarrow$ *m/z* 238.1 $[M + H - Gua]^+$), and the formation of protonated guanine (*m/z* 389.1 $[M + H]^+ \rightarrow$ *m/z* 152.1 $[Gua + H]^+$). Typical instrument settings included a spray voltage of 2.0 kV, capillary temperature at 300 °C, and collision energy at 32 and 22 V for the first and the second SRM transition, respectively. The corresponding transitions for the $^{15}N_{10}$-isotopically-labeled internal standard were *m/z* 399.1 $[^{15}N_{10}\text{-}M + H]^+ \rightarrow$ *m/z* 243.1 $[M + H - [^{15}N_5]Gua]^+$ and *m/z* 157.1 $[^{15}N_5\text{-}Gua + H]^+$. The Q1 peak width was 0.4 amu, while the peak width for Q2 was 0.7 amu. The scan width was 0.4 amu, and the scan time was 0.5 s. NanoHPLC-nanoESI$^+$-MS/MS quantitation was based on the areas of the peaks in the extracted ion chromatograms corresponding to the analyte and the internal standard.

Method standard curves were constructed by analyzing solutions containing a fixed amount of $^{15}N_{10}$-*bis*-N7G-BD (50 fmol) and increasing amounts of *bis*-N7G-BD (0.5, 1.0, 5.0, 10.0, 15.0, 25.0, and 50.0 fmol) in water (in triplicate), followed by regression analysis of the actual and observed amounts of *bis*-N7G-BD (Figure 2.1). Solvent blanks were periodically injected to monitor for potential analyte carry-over.

Figure 2.1: NanoHPLC-nanoESI^{+}-MS/MS method standard curve.

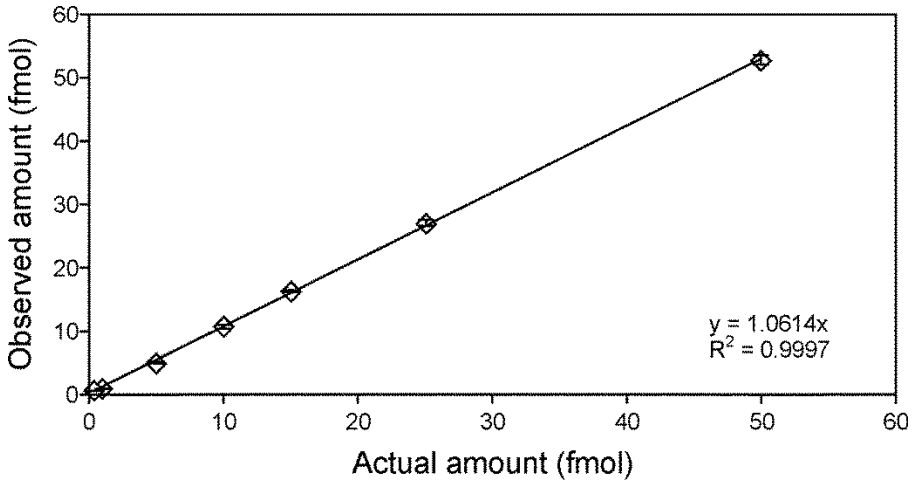

Method validation

DNA isolated from CHL V-79 cells (100 μg, in triplicate) was spiked with 0, 1, 5, 10, 15, 25 or 50 fmol of *bis*-N7G-BD and 50 fmol $^{15}N_{10}$-*bis*-N7G-BD internal standard. Following heating at 70 ºC for 1 hour (neutral thermal hydrolysis), samples were filtered through Nanosep-10K ultra- centrifugation devices to remove partially depurinated DNA. *Bis*-N7G-BD and its internal standard were purified by off-line HPLC as described above and subjected to nanoHPLC-nanoESI$^+$-MS/MS analysis by usual methods. Regression analysis was conducted to compare the measured and the spiked amounts of *bis*-N7G-BD.

Determination of LOD/LOQ, precession, and accuracy.

DNA extracted from CHL V-79 cells (100 μg) was spiked with 1, 0.75, 0.5, or 0.1 fmol of *bis*-N7G-BD and 50.0 fmol of $^{15}N_{10}$-*bis*-N7G-BD. Samples were subjected to thermal hydrolysis, ultrafiltration, purified by offline HPLC, and analyzed by nanoHPLC-nanoESI$^+$-MS/MS as described above. Method limit of quantification (LOQ) was estimated as the amount of analyte which gave a signal-to-noise ratio (S/N) greater than 10 and % CV < 15%. Limit of detection (LOD) was determined as the amount of analyte that produced a signal-to-noise ratio > 3.

To evaluate the interday and intraday accuracy and precision of the new method, *bis*-N7G-BD (2.0 fmol) and $^{15}N_{10}$-*bis*-N7G-BD (50.0 fmol) were spiked into blank DNA from CHL cells (100 μg). Samples were processed as described above and analyzed three times per day on three consecutive days. Method accuracy was calculated from the equation ($A_m/A_a \times 100\%$), where A_m is the measured amount of *bis*-N7G-BD and A_a is the actual amount added.

Analysis of *bis*-N7G-BD in mouse liver samples:

DNA was extracted from livers of B6C3F1 mice exposed to either 0, 0.5, 1.0 or 1.5 ppm BD by inhalation (2 weeks at 6 h/day, 5 days/week) using methodology described above. DNA aliquots (100 μg in 200 μL water) were subjected to neutral thermal hydrolysis (70 °C for 1 hr), followed by Nanosep10K ultra filtration and offline HPLC as described above. Our previous experiments confirmed that these conditions efficiently release *bis*-N7G-BD adducts form the DNA backbone *(74;105)*. *Bis*-N7G-BD adducts were quantified using the newly validated nanoHPLC-nanoESI$^+$-MS/MS method. Adduct numbers were expressed as number of adducts per 10^9 nucleotides. DNA amounts were determined by HPLC-UV analysis of dG in DNA hydrolysates as described above.

Method Reproducibility

DNA was extracted from six 100 mg aliquots of liver from F344 rat treated with 62.5 ppm BD by inhalation and analyzed by the standard methodology. An additional two aliquots were extracted by the Qiagen DNA extraction kit and analyzed for comparison. A good agreement was observed between these separate analyses (CV 9.4%).

2.3 Results

2.3.1 Experimental Approach

The goal of the present study was to develop ultra-sensitive methodologies to quantify *bis*-N7G-BD adducts in tissues of mice exposed to low ppm and sub-ppm levels of BD. In our approach (Scheme 2.2), genomic DNA extracted from tissue is spiked with [$^{15}N_{10}$]-*bis*-N7G-BD internal standard, and *bis*-N7G-BD lesions are released from the DNA backbone by neutral thermal hydrolysis. Our previous results indicate that heating at 70 °C for 1 h results in a quantitative release of *bis*-N7G-BD cross-links *(74;114)*. Following the removal of partially depurinated DNA via ultrafiltration, *bis*-N7G-BD and its internal standard are isolated from the bulk of the sample matrix using offline HPLC. HPLC fractions containing analyte are then dried, reconstituted in buffer, and subjected to nanoHPLC-nanoESI$^+$-MS/MS analysis on a triple quadrupole mass spectrometer. Our new method employs a flow rate of 0.4 μL/min and nanoESI MS/MS detection as compared to the earlier capillary HPLC-ESI-MS/MS method that uses a flow rate of 10 μL/min *(114)*.

2.3.2 NanoHPLC-nanoESI$^+$-MS/MS method development and validation.

MS/MS fragmentation pattern of *bis*-N7GBD in a triple quadrupole mass spectrometer is characterized by predominant product ion peaks at *m/z* 238.1 corresponding to neutral loss of guanine base from protonated molecules of the adduct $[M + H - Gua]^+$ *(74;215)*. Another abundant fragment of *m/z* 152.1 corresponds to the protonated guanine $[Gua + H]^+$ (Figure 2.2).

Scheme 2.2. *Bis*-N7G-BD Analytical Procedure

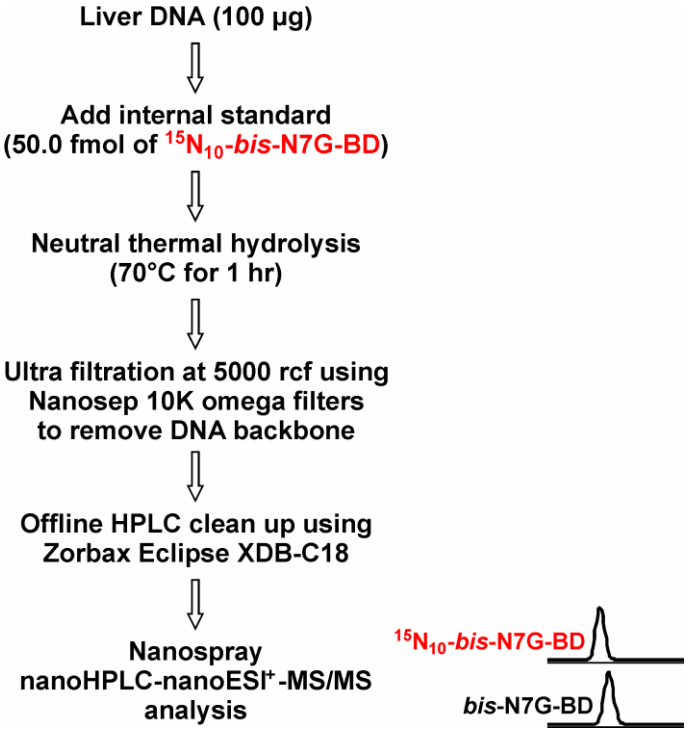

Figure 2.2 NanoLC-nanoESI^{+}-MS/MS analysis of a mixture of pure *bis*-N7G-BD (1.0 fmol) and $^{15}N_{10}$-bis-N7G-BD (10 fmol).

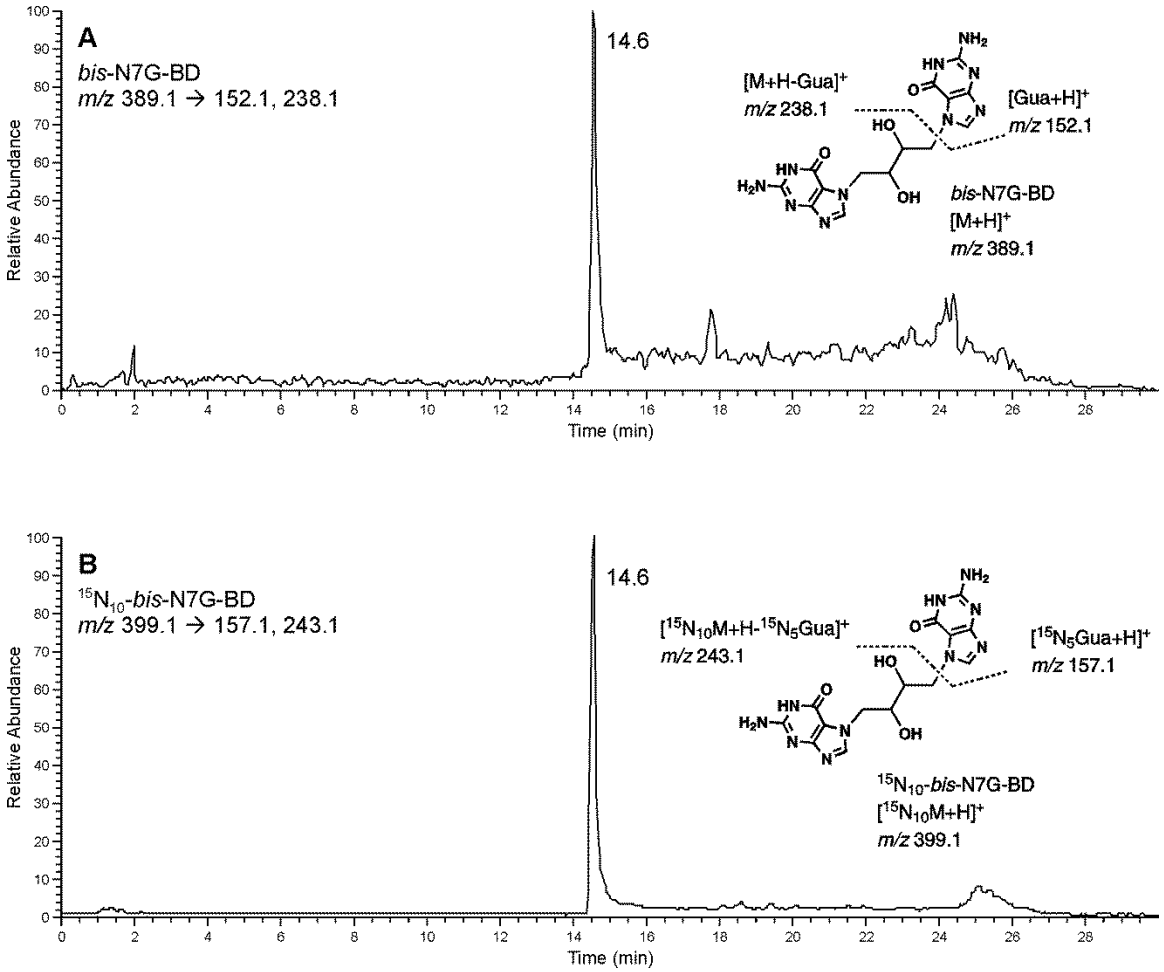

The corresponding fragments for the corresponding $^{15}N_{10}$ isotopically labeled internal standard are *m/z* 243.1 [M + H - [$^{15}N_5$]Gua]$^+$ and *m/z* 157.1 [$^{15}N_5$-Gua + H]$^+$.The quantitative method for *bis*-N7G-BD is based on selected reaction monitoring of the MS/MS transitions *m/z* 389.1 [M + H]$^+$ → *m/z* 238.1 [M + H - Gua]$^+$ and *m/z* 389.1 [M + H]$^+$ → *m/z* 152.1 [Gua + H]$^+$. The corresponding transitions for the $^{15}N_{10}$-isotopically-labeled internal standard are *m/z* 399.1 [$^{15}N_{10}$-M + H]$^+$ → *m/z* 243.1 [M + H - [$^{15}N_5$]Gua]$^+$ and *m/z* 157.1 [$^{15}N_5$-Gua + H]. A sum of the two transitions is used for quantitation to improve sensitivity.

To optimize analyte separation from interfering components of the biological matrix, the new method employs an offline HPLC sample cleanup. dT and dA were spiked in each sample as retention time markers eluting at 13.7 and 18.8 min, respectively, while the retention time of *bis*-N7G-BD and its internal standard is ∼16 min. HPLC fractions containing *bis*-N7G-BD and $^{15}N_{10}$-*bis*-N7G-BD (14−18 min, about 1.25 mL) were collected and concentrated for nanoLC-nanoESI+-MS/MS analysis.

We have chosen nanospray LC-MS method over conventional capillary flow LC-MS because of its greater sensitivity. When HPLC flow rate is reduced to < 1 μL/min, droplet formation in the electrospray source occurs more readily, requiring only the applied voltage (typically 2000V) to generate a spray *(218)*. The efficiency of electrospray ionization is greatly improved under nanoflow conditions, because a smaller amount of mobile phase passes through the emitter, producing fine aerosol droplets. Consequently, the stability of ion spray, and therefore MS signal, is improved, thus leading to improved detection sensitivity *(219;220)*. As an additional benefit, nanoHPLC methods consume very small amounts of solvents as compared to conventional capillary

flow LC MS methods. Several laboratories have previously reported the use of nanospray for sensitive quantitation of DNA adducts *(76;221-224)*.

Several HPLC stationary phases were evaluated during nanoHPLC method development, including Symmetry C18 (Waters Corp., Millford, MA), Luna C18 (Phenomenex, Torrance, CA), HILIC-NH_2 (Phenomenex, Torrance, CA), Synergi Polar RP and Hydro RP (Phenomenex, Torrance, CA). The best analyte retention and peak shape were obtained with Zorbax SB-C18 stationary phase (Agilent Technologies, Santa Clara, CA). We found that the best sensitivity was achieved with a gradient of 0.01% aqueous acetic acid (solvent A) and acetonitrile:methanol (1:1, solvent B). All solvents were LC-MS grade. Using a linear gradient between 10% and 100% B, *bis*-N7G-BD adducts eluted at 14.5 min and were resolved from the impurities present in DNA hydrolysates (Figure 2.3)

Figure 2.3: NanoLC-nanoESI^{+}-MS/MS analysis of *bis*-N7G-BD in liver DNA from a mouse exposed to 1.0 ppm BD for 2 weeks.

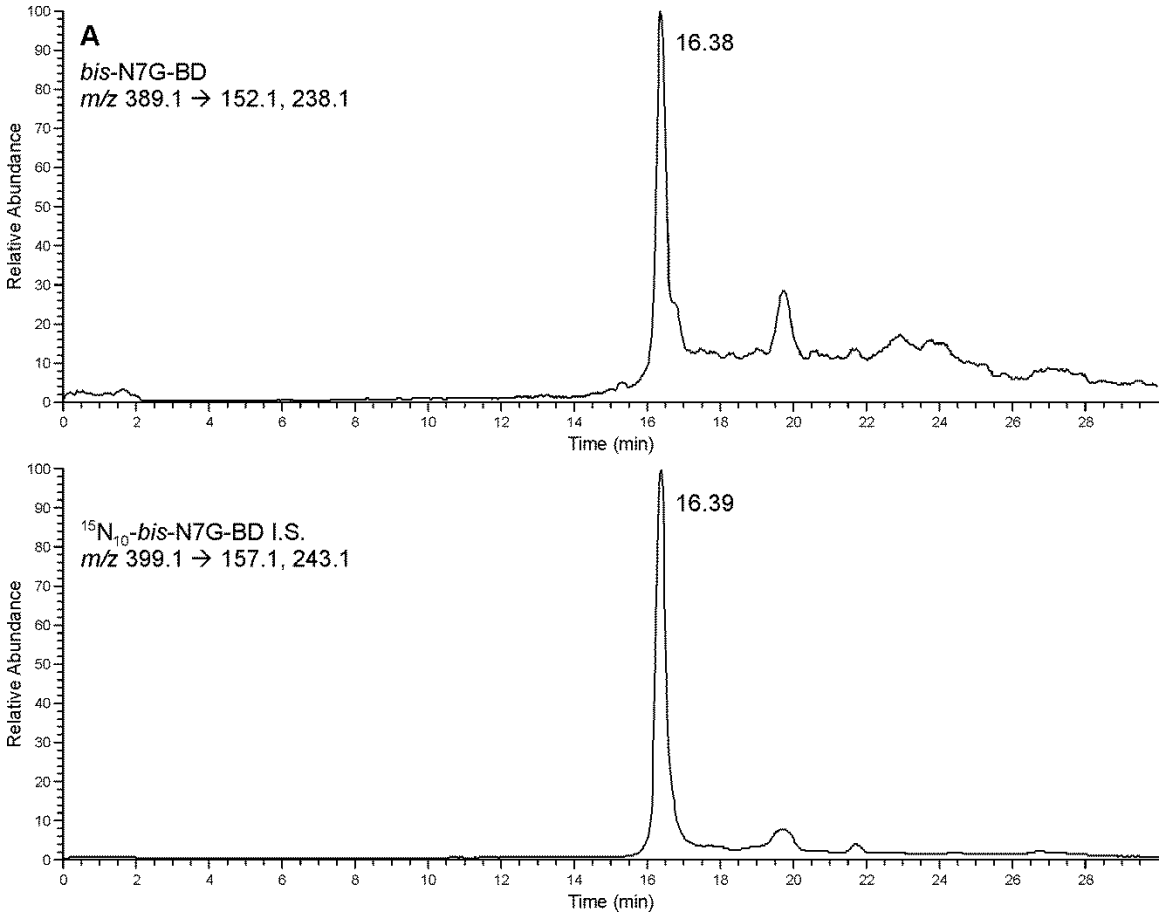

2.3.3 Method Validation

The limit of detection of the new method was estimated as 50 amol *bis*-N7G-BD on column, a significant increase in sensitivity as compared to our previous capillary HPLC-ESI$^+$-MS/MS method *(114)*.To validate the new methodology, aliquots of DNA from Chinese hamster lung fibroblasts (100 μg) was spiked with known amounts of *bis*-N7G-BD and corresponding $^{15}N_{10}$-labelled internal standard, followed by sample processing and nanoHPLC-nanoESI$^+$-MS/MS analysis as described above. An excellent correlation was observed between the expected and observed concentrations of *bis*-N7G-BD, with an R^2 value of 0.999 (Figure 2.4). We found that the method's lower limit of quantitation (S/N ratio of 10 or better) was 1.0 fmol *bis*-N7G-BD in 0.1 mg DNA (3 *bis*-N7G-BD adducts per 10^9 nts), and the LOD value was 0.5 fmol/0.1 mg DNA. The LOD value for pure standard of *bis*-N7G-BD was 0.1 fmol. Method accuracy (n = 5) and precision (n = 3) were determined for replicates of *bis*-N7G-BD (2.0 fmol) spiked into 0.1 mg of DNA. Accuracy was determined to be 97.1 ± 6.3 % (n = 5) and the interday and intraday precision were less than 8 % RSD (n = 3) (Table 2.1).

2.3.4 Analysis of bis-N7G-BD in mouse liver DNA

The newly validated quantitative nanoHPLC-nanoESI$^+$-MS/MS method was employed to analyze the formation of *bis*-N7G-BD adducts in liver DNA of B6C3F1 mice that were exposed to 0.5 – 1.5 ppm BD by inhalation for 2 weeks. Representative extracted ion chromatogram from nanoHPLC-nanoESI$^+$-MS/MS analysis of *bis*-N7G-BD in liver DNA samples from a mouse exposed to 1.0 ppm BD is shown in Figure 2.3.

Figure 2.4: NanoHPLC-nanoESI^{+}-MS/MS method validation curve

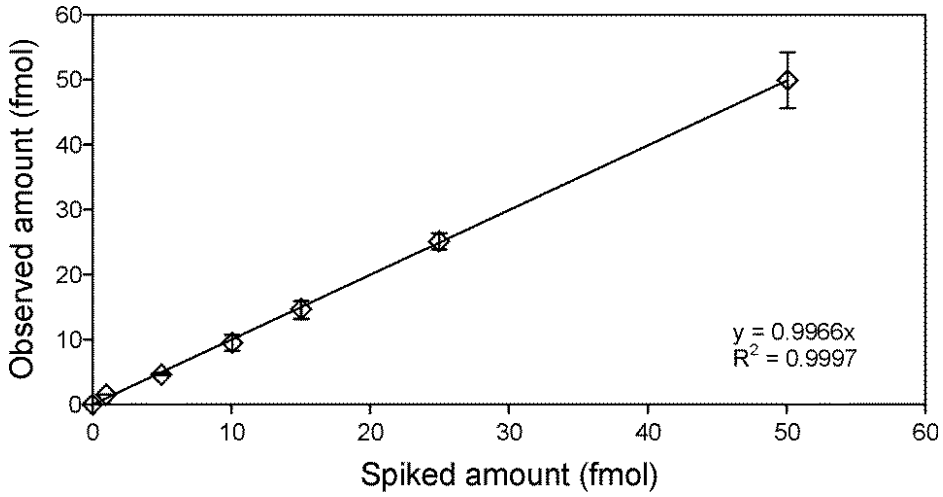

Table 2-1. Accuracy and precision of nanoHPLC-nanoESI$^+$-MS/MS analysis for *bis*-N7G-BD (2 fmol) in DNA (0.1 mg).

Day	Parameter	value
Day 1	Mean	1.9
	RSD (%)	5.4
	Accuracy (%)	93.5
	N	3
Day 2	Mean	2.1
	RSD (%)	6.7
	Accuracy (%)	106.0
	N	3
Day 3	Mean	2.2
	RSD (%)	0.9
	Accuracy (%)	108.1
	N	3
Interday	Mean	2.1
	RSD (%)	7.9
	Accuracy (%)	102.6
	N	9

We found that DNA extracted from tissues of mice treated with 0.5 ppm BD for 2 weeks contained 5.7 ± 3.3 *bis*-N7G-BD adducts per 10^9 normal nucleotides (N = 3), while animals exposed to 1.0 ppm BD contained 9.2 ± 1.5 *bis*-N7G-BD adducts per 10^9 ntds (N = 4) and those exposed to 1.5 ppm BD contained 18.6 ± 6.9 *bis*-N7G-BD adducts per 10^9 normal nucleotides (N = 4). DNA of control animals (N = 5) did not contain detectable amounts of *bis*-N7G-BD (N = 5) (Figure 2.5).

Figure 2.5: *Bis*-N7G-BD adduct levels in mice treated with 0, 0.5, 1.0 and 1.5 ppm 1,3-butadiene

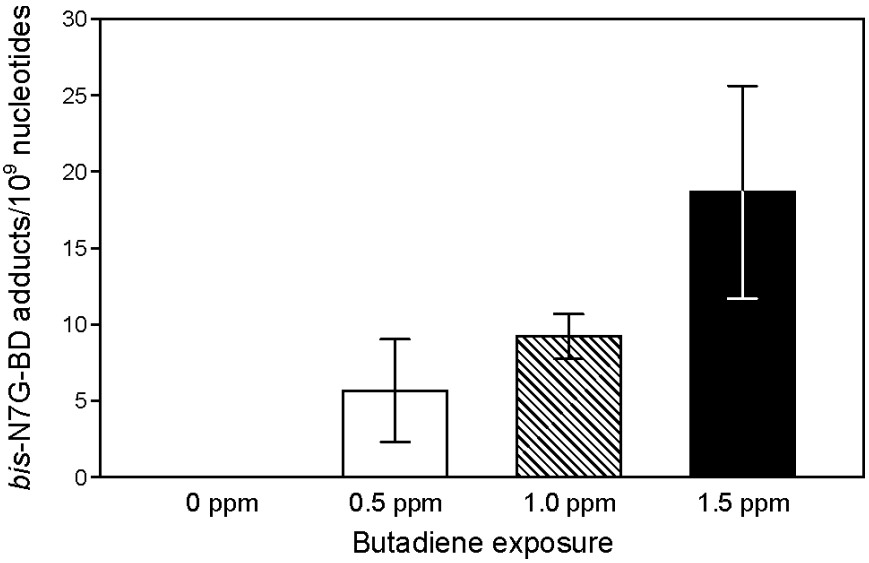

2.4 Discussion

A potent human and animal carcinogen, BD is metabolically activated to DEB, which reacts with DNA to form DNA-DNA cross links, e.g. 1,4-*bis*-(guan-7-yl)-2,3-butanediol (*bis*-N7G-BD) *(65;74;113;215)*. If not repaired, the interstrand *bis*-N7G-BD adducts can block DNA replication and lead to genotoxicity, while the corresponding intrastrand lesions are likely to be mutagenic *(105)*. It is important to have specific biomarkers of DEB formation *in vivo* because of its central role in BD-mediated adverse health effects. In particular, DEB is 100−200-fold more mutagenic than other epoxide metabolites of BD *(95)* and is thought to be responsible for most of the genotoxic effects of BD at low exposure concentrations(<62.5 ppm BD) *(211)*.

Bis-N7G-BD lesions have been previously identified and quantified in laboratory animals exposed to relatively high concentrations of BD 6.25-625 ppm *(114)*. However, DEB-specific DNA adducts have not been previously analyzed in animals subjected to BD exposures approaching the human Occupational Safety and Health Administration (OSHA) time weighted average levels (1 ppm) *(216)*. Ambient BD concentrations in monomer and polymer work places range from 0.3 to 3 ppm. New and improved bioanalytical methods were required in order to quantify *bis*-N7G-BD adducts in tissues following low ppm and subppm exposures.

In the present study, an ultra sensitive nanoHPLC-nanoESI$^+$-MS/MS was developed for quantitation of *bis*-N7G-BD in liver DNA of mice exposed to sub-ppm levels of BD. Capillary flow HPLC-ESI-MS based methods typically employed for DNA adduct analysis are limited in their sensitivity due to the presence of relatively large amounts of solvent, which reduces the efficiency of ion formation in the ESI source. In

contrast, nanospray analysis is characterized by more efficient ionization and improved sensitivity *(218;225)*. Therefore, we adopted a nanospray LC-MS/MS methodology for quantitative analysis of *bis*-N7G-BD *in vivo*. Our new analytical method is more sensitive than our previous capillary HPLC-ESI-MS/MS methodology (LOQ, 1.0 fmol) because of an improved sample clean up by offline HPLC and the inherent advantages of nanospray HPLC-ESI-MS/MS.

NanoHPLC-nanospray MS/MS methodology has been recently employed for the detection of 7-ethylguanine adducts in leukocyte DNA isolated from smokers and non smokers *(223)*. Solid phase extraction was employed for sample cleanup following DNA hydrolysis, and MS analyses were conducted with an Orbitrap LTQ Velos mass spectrometer using an accurate mass mode *(223)*. The LOD and LOQ values of the method were reported as 0.1 fmol on column and 8 fmol per 180μg DNA, respectively *(223)*. Zarbl et al. employed nanoHPLC-nanospray MS to detect and quantitate DNA adducts in bronchial epithelial cells treated with 10^{-5}–10^{-8} M concentrations of 1-methyl-6-phenylimidazo[4,5-b]pyridine (PhIP), a potent food carcinogen present in overcooked meat *(224)*.

In another recent study, Chen et al. employed nanoHPLC-nanospray MS/MS technique to analyze 1,N^2-propano-2′-deoxy-guanosine adducts derived from acrolein (AdG) and crotonaldehyde (CdG) in various human DNA samples from saliva, human placenta and blood leukocytes *(76;221;222)*. Three lipid peroxidation-related etheno adducts:1,N^6-etheno-2′-deoxyadenosine (εdAdo), 3,N^4-etheno-2′-deoxycytidine (εdCyt), and 1,N^2-etheno-2′-deoxyguanosine (1,N2-εdGuo) were also analyzed by nanoHPLC-nanospray MS/MS *(222)*. The limits of quantification per 5 μg of DNA were reported as

0.31 fmol, 1.5 fmol, 0.36 fmol, 2.0 fmol, and 1.7 fmol for AdG and CdG, εdAdo, εdCyd, and 1,N^2-εdGuo, respectively *(221)*.

Our nanoHPLC-nanospray MS/MS methodology for *bis*-N7G-BD in tissue DNA described herein is comparable or better than previously reported methods in sensitivity (LOD: 0.5 fmol and LOQ: 1.0 fmol in 100μg DNA), accuracy, and precision (Table 2.1). With this methodology, it is possible to detect 3 adducts per 10^9 nucleotides. Since DNA-DNA cross-links are less abundant in DNA than DNA monoadducts such as 7-ethylguanine, an offline HPLC sample cleanup was required to provide a higher degree of separation than can be afforded by solid phase extraction. While such a cleanup step increases the overall analysis time, minimal operator involvement is required with the use of an automated HPLC system incorporating an autosampler and a fraction collector.

Using the validated nanoHPLC-nanospray MS/MS method, *bis*-N7G-BD adduct amounts were determined in livers of B6C3F1 mice following a 2 week exposure to 0.5, 1.0, or 1.5 ppm BD (6 h/day, 5 days/week, see Figure 2.5). No *bis*-N7G-BD was detected in liver DNA of control mice (n = 5) which have not been exposed to BD. A comparison of the numbers of *bis*-N7G-BD adducts/10^7 nucleotides/ppm of BD under low ppm exposure conditions determined in the present study to our earlier data for animals exposed to higher BD concentrations (6.25−625 ppm) *(114)* shows that there is a higher ratio of *bis*-N7G-BD adduct numbers per ppm of BD at low levels of BD exposure as compared to BD exposures greater than 62.5 ppm (Figure 2.6). Table 2.2 provides a comparison of *bis*-N7G-BD adduct levels per unit dose of BD to *pyr*-Val adducts (picomoles per gram of globin) per ppm of BD exposure in female mice.

Table 2-2 *Bis*-N7G-BD adduct concentrations in mouse liver DNA per unit dose of BD. Concentrations of *pyr*-Val adducts (picomoles per gram of globin) in the same animals are shown for comparison.

BD exposure (ppm)	*Bis*-N7G-BD adducts per 10^7 nucleotides/ppm BD	*Pyr*-Val adducts, picomoles per gram of globin/ppm of BD[c]
0	ND[a]	ND[a]
0.5	0.170	21.0
1.0	0.142	20.0
1.5	0.144	26.0
6.25 [b]	0.051[b]	12.0
62.5 [b]	0.013 [b]	6.7
200 [b]	0.009 [b]	3.7
625 [b]	0.006 [b]	2.5

[a] ND, not detected, [b]From literature reference number *(114)*, [c] Pyr-val adducts from *(131)*.

Figure 2.6 Dose-dependent formation of *bis*-N7G-BD in liver DNA of female B6C3F1mice exposed to BD by inhalation (6.25 and 62.5 ppm values are taken from literature*(114)*)

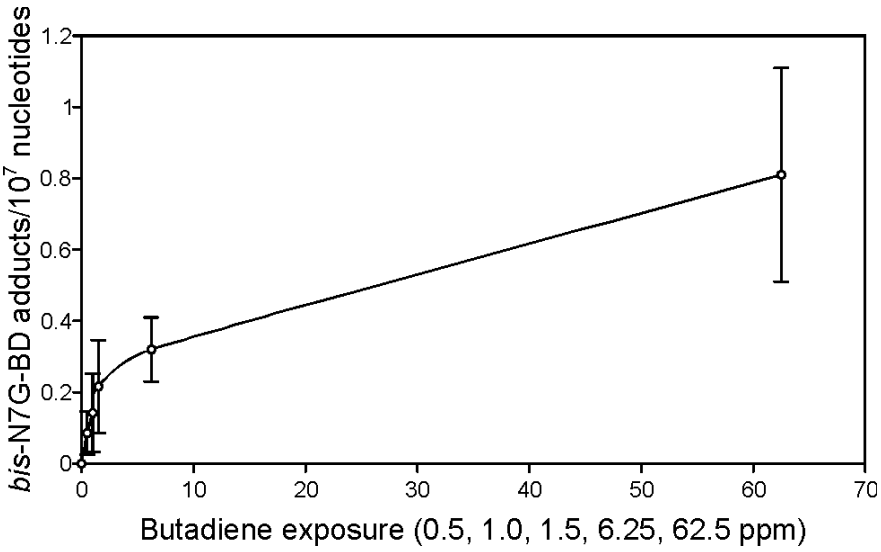

Taken together, our results indicate that *bis*-N7G-BD adduct formation is more efficient at low concentrations of BD (≤6.25 ppm) as compared to higher exposure concentrations (≥62.5 ppm), probably a result of an increased bioactivation of BD to DEB under low exposure conditions. These results are relevant because typical occupational or environmental exposure of humans to BD is 2 ppm or less.

III. CELLULAR REPAIR OF DNA-DNA CROSSLINKS INDUCED BY 1,2,3,4-DIEPOXYBUTANE

3.1 Introduction

DNA-DNA interstrand cross-links (ICLs) are among the most toxic types of DNA damage known because of their ability to block DNA strand separation, interfering with DNA replication and transcription *(226;227)*. The anticancer activity of many clinically useful drugs including platinum compounds, mitomycin C, psoralens, and antitumor nitrogen mustards is attributed to ICL formation and toxicity in rapidly proliferating tumor cells *(228-231)*. However, ICLs can also be induced by endogenous lipid peroxidation products such as α, β-unsaturated aldehydes *(232;233)* and carcinogen metabolites such as 1,2,3,4-diepoxybutane (DEB), the ultimate carcinogenic species of industrial and environmental chemical 1,3-butadiene *(95;95)*. DEB sequentially alkylates two nucleophilic sites within DNA to form interstrand and intrastrand 4-*bis*-(guan-7-yl)-2,3-butanediol cross-links (*bis*-N7G-BD). Previous studies conducted in our laboratory have revealed that the cross-linking specificity of DEB is dependent on its stereochemistry: while *SS* and *RR* DEB preferentially form interstrand lesions, the *meso* isomer generates equal numbers of intrastrand and interstrand lesions (Scheme 3.1) *(105;215;234)*. Both intrastrand and interstrand lesions are hydrolytically labile, with average half-lives of 3.5-4 days under physiological conditions *(115)*.

Scheme 3.1 Metabolic activation of BD to its three reactive epoxides and formation of *bis*-N7G-BD DEB-DNA crosslinks.

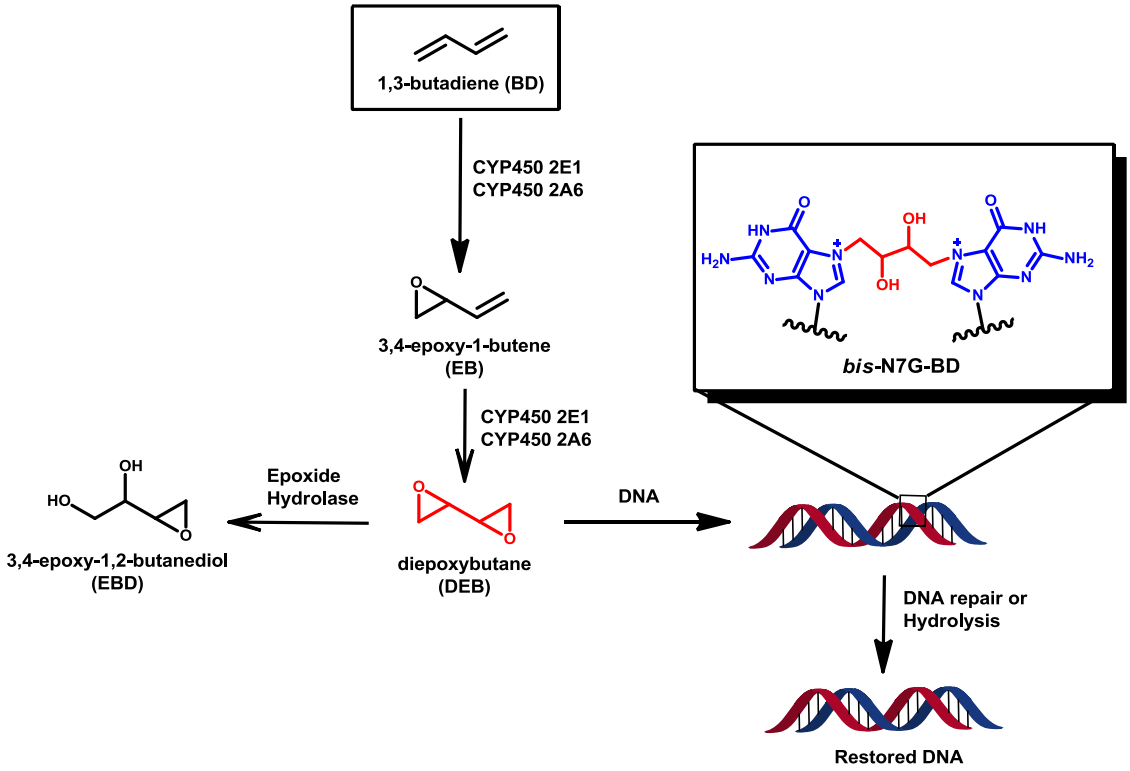

Cellular repair of ICLs such as *bis*-N7G-BD is complicated because they inhibit local duplex melting at the site of adduct *(235)*. Furthermore, both DNA strands at the site of cross-link are damaged, potentially compromising their use as templates for accurate repair synthesis. The mechanism of ICL repair is strongly dependent on the specific stage of the cell cycle. For cells in G0/G1 phase of the cell cycle, helix distorting ICLs may be removed by nucleotide excision repair (NER) of one of the strands and translesion synthesis past the "flipped out" ICL *(236)*. Details regarding mechanisms of ICL repair in G0/G1 remain largely to be discovered, however. Fanconi Anemia (FA) repair pathway appears to play a central role in ICL removal for cells in the S phase of the cell cycle *(227)*. FA repair pathway involves at least 16 different genes. It has been reported that replication forks stalled ahead of an ICL are recognized by FANCM, triggering the recruitment of the FA core complex (FANC A to F) to the site of damage. Following monoubiquitination of FANCD2-FANCI complex, the replication fork is stabilized, and the nascent strand is extended via the homologous recombination (HR) mechanism. Double incisions on each side of the cross-link are made by nucleases such as FANC1 and EME1/MUS81, and the unhooked intermediate is bypassed via translesion synthesis that may involve Pol ν, θ, and ζ *(227)*. FA pathway acts in coordination with other DNA repair pathways such as recombination repair *(227;237)*, nucleotide excision repair (NER) *(238)*, and mismatch repair *(239;240)*. ICL repair deficiency in FA patients leads to an increased cancer risk because of genomic instability *(241)*, increased cell death, *(242)* and genetic damage in tumor suppressor genes such as p53 *(243)*.

Incomplete ICL repair leads to the formation of DNA double strand breaks (DSBs) *(226;244)*. DSBs are serious types of DNA damage that have the potential to cause deletions and chromosomal aberrations, if not repaired by recombination repair pathways such as homologous recombination (HR) *(245)* or nonhomologous DNA end joining (NHEJ) *(246)*, which are mediated by nucleotide excision repair proteins ERCC1–XPF *(247;248)*. Since ICL formation is thought to be responsible for the efficacy of bifunctional alkylating agents used as anticancer drugs *(249)*, complete understanding of the mechanisms of ICL repair is important for efforts to improve their efficacy and to combat tumor resistance.

In the present work, we examined the kinetics of formation and repair of DEB induced *bis*-N7G-BD crosslinks and DNA double strand breaks in isogenic Chinese hamster lung fibroblasts proficient or deficient in NER and FA recombination repair pathways in an effort to identify specific repair pathways involved.

3.2 Materials and methods

Note: *DEB is a known carcinogen and, should be handled with adequate safety precautions in a well ventilated fume hood strictly following its material safety data sheet.*

Materials

LC-MS grade acetonitrile, methanol, and water were obtained from Fisher Scientific (Pittsburgh, PA). All other chemicals and solvents were obtained from Sigma-Aldrich (Millwaukee, WI, St. Louis, MO). *bis*-N7G-BD and $^{15}N_{10}$-*bis*-N7G-BD internal standard was prepared in our laboratory as described previously *(74;105;215)* and their concentration was determined by UV spectrophotometry (ε_{252} = 15700, pH 1).

Cell Culture

Cell lines: V79 Chinese hamster lung fibroblasts (wild type, Catalog ID: GM16136), V-H4 (Catalog ID: GM16142) Chinese hamster lung mutant cell line derived from V79 wild type cells possess phenotype similar to that of cells derived from Fanconi anemia individuals were produced by ethylnitrosourea-induced mutagenesis of V79 cells *(250-252)*. Arwert, F. et al. (1991) Cytogenetics and Cell Genetics studies established that V-H4 cells are homologous to the human Fanconi anemia complementation group A *(253)*. V-H1 (Catalog ID: GM16141) cells are derived from V79 by ethylnitrosourea-induced mutagenesis and are UV hypersensitive with reduced excision repair of photoproducts and belongs to complementation group 2 of UV-sensitive rodent mutants. V-H1 is mutated in the *ERCC2* gene which codes for XPD protein involved in the helicase activity for unwinding DNA during NER *(254)*. All of the above cell lines were obtained from the Coriell Institute (Camden, NJ, USA). Cells were grown to 80-90%

confluence on tissue culture dishes in Ham's F-12 modified essential Eagle's media (Life Technologies, Grand Island, NY, USA) supplemented with 9% fetal bovine serum. Cells were then cultured in a humidified atmosphere of 5% carbon dioxide, 95% air, at 37 °C.

Cytotoxicity Assays

The cytotoxic effects of DEB were examined by direct counting and clonogenic assays. For direct-counting assays, cells (V79, V-H1 and VH-4) were seeded into 6 cm dishes at a density of 0.5 x 10^6 cells/dish. The following day, the cells were exposed to various concentrations of DEB for three hrs in serum free media. Following DEB treatment, the media was replaced with drug-free normal growth media. Twenty-four hours later, cells were harvested and counted using a haemocytometer. Trypan blue exclusion confirmed that $\geq$ 99% of recovered cells were viable. The percent cell death was calculated by dividing the number of recovered cells obtained from drug-treated cultures by the corresponding number of cells recovered from control cultures not exposed to DEB. Experiments were performed in triplicate, and the results represent the average +/- the standard error of the mean (SEM) from three or more independent sets of experiments. For clonogenic assays, V79, V-H1 and V-H4 cells were plated in triplicate in 6 cm dishes at a density of 500 cells/dish. The following day, the cells were exposed to various concentrations of DEB for 3 hrs in serum free media. Following this incubation period the media was replaced with drug-free normal growth media. After 7 days the colonies were fixed and stained with 1% crystal violet in 95% ethanol. Colonies (>50 cells) were counted manually. The surviving fraction was calculated as follows: number of colonies in drug treatment/number of colonies in non-drug treatment. Results depict mean value +/- SEM, N = 3.

Concentration dependence for bis-N7G-BD adduct formation:

V79 cells (6-8 million, in duplicate) were treated with 0, 10, 15, 25, 50 and 100 μM DEB in media in duplicate for 3 hrs. DEB-containing media was removed, and the cells were washed with phosphate buffered saline (PBS). Cells were harvested with PBS, pelleted, and stored at - 20 °C until DNA extraction and adduct analysis.

Time dependent adduct formation and repair studies of bis-N7G-BD adducts in cell lines

V79, V-H4, and V-H1 cells (6-8 million, in duplicate) were treated with 15 μM DEB for 0, 1, 2 and 3 hrs. Following treatment, DEB-containing media was replaced with fresh media, and the cells were allowed to recover for 2, 24 or 48 hrs to allow for adduct removal. To quantify the remaining *bis*-N7G-BD adducts, cells were harvested with 5 mL of PBS, pelleted, and stored at -20 °C until DNA extraction and adduct analysis as described below.

Inhibitor treatment

V79 cells in culture (6-8 million, in duplicate) were pre-treated with 20 nM UCN-01 (7-hydroxystaurosporin, NER inhibitor) *(255)* for 2 hrs. Following treatment with the inhibitor, cells were exposed to 15 μM DEB for 0, 1, 2, or 3 hrs. DEB-containing media supplemented with UCN-01, was replaced with fresh media containing 20 nM UCN-01, and the cells were allowed to recover for 2, 24, or 48 hrs post DEB treatment. Following repair incubation, the cells were harvested, pelleted, and stored at -20 °C until DNA extraction and adduct analysis as described below.

NanoLC-ESI$^+$-MS/MS analysis of *bis*-N7G-BD adducts in DEB-treated cells

DNA extraction from cells was performed using standard phenol-chloroform extraction as described previously *(217)*. DNA concentrations were determined by UV spectrophotometry (Thermo Scientific, Waltham, MA, USA) based on the UV absorbance at 260 nm. DNA purity was assessed from A_{260}/A_{280} absorbance ratios, which were typically between 1.8 and 1.9, indicating minimal protein contamination.

DNA (50-150 μg) was re-suspended in water (200 μL) and spiked with $^{15}N_5$-*bis*-N7G-BD (50 fmol, internal standard for mass spectrometry). Samples were subjected to neutral thermal hydrolysis (70 °C for 1 h) to release *bis*-N7G-BD adducts from the DNA backbone as a free base conjugate. Following ultrafiltration to remove partially depurinated DNA, the solutions were subjected to offline HPLC cleanup as described previously *(69)*. HPLC fractions corresponding to *bis*-N7G-BD and its internal standard were dried under reduced pressure, reconstituted in water (25 μL), and subjected to nanoLC-ESI$^+$-MS/MS analysis as described previously *(69)*. Selected reaction monitoring (SRM) transitions used for quantitation were *m/z* 389.1 $[M + H]^+ \rightarrow$*m/z* 238.1 $[M + H - Gua]^+$, *m/z* 152.1 $[Gua + H]^+$ for *bis*-N7G-BD and *m/z* 399.1 $[^{15}N_{10}\text{-}M + H]^+$ → *m/z* 243.1 $[M + H - [^{15}N_5]Gua]^+$, *m/z* 157.1 $[^{15}N_5\text{-}Gua + H]^+$ for $^{15}N_5$-*bis*-N7G-BD internal standard. Quantitation was conducted using nanoLC-ESI$^+$-MS/MS areas corresponding to the analyte and the internal standard using standard curves constructed with authentic standards.

Native Comet Assay

Chromosomal DNA strand breaks were estimated by performing comet assays under neutral conditions using the a CometAssay kit (Trevigen, Gaithersburg, MD) *(256)*.

V79, V-H4 and VH-1 cells were incubated in the presence or absence of 15 μM DEB in serum free media for 3 hrs at 37 °C. Culture media was removed, and the cells incubated at 37 °C in drug-free growth media for times indicated (0, 3 and 24 hrs). Cells were harvested and suspended in PBS at a density of approximately 1 x 10^6 cells/mL. Briefly, 10 μL of cell suspension was mixed with 90 μL of 0.5% low melting temperature agarose (GIBCOBRL, Grand Island, NY) in PBS and layered on top of microscope slides pre-coated with 1% normal agarose. Slides were placed flat at 4 °C in the dark for 15 min. Cells were lysed overnight at 4 °C in the dark in lysis buffer (Tris-EDTA buffer, sodium chloride, sodium lauryl sulfate, 1% Triton-X 100) overnight at 4 °C in the dark. After electrophoresis in TRIS Borate EDTA buffer [10.8% (w/v) TRIS base, 5.5% (w/v) boric acid, and 0.93% (w/v) EDTA] for 30 minutes at 1V/cm, slides were washed in DNA precipitation solution (7.5 M ammonium acetate in 95% ethanol) for 30 minutes at room temperature. Slides were immersed in 70% ethanol for 30 minutes at room temperature. Slides were dried at 37 °C for 15 min then stained with 100 μL of diluted SYBR Green (1:10,000 in TE Buffer) for 30 min in the dark. Comets were imaged using a Zeiss Axioplan 2 upright microscope. At least 50 cells were randomly selected from each treatment and blindly scored into five categories (0-4) *(257)* based upon the intensity of the comet tail relative to the head.

γH2AX immunocytochemistry for visualization of double strand breaks

The immunocytochemistry assay was performed as described before with some modifications *(258)*. For all cell lines, 1 x 10^5 cells were seeded in 3.5 cm dishes that contained sterilized glass cover slips (22 x 22 mm, No.1 Thickness, ThermoScientific) and incubated over night at 37 °C in normal growth media. On the following day,

individual dishes were treated with 15 μM DEB in serum free medium for 3 hrs at 37 °C. Drug-containing media was replaced with normal growth media and the cells maintained at 37 °C for recovery at various times (0, 3 and 24 hrs). Following removal of the media, ice cold 50% methanol: 50% acetone was added, and the cells were incubated for 8 min at 4 °C. Cells were then washed with ice-cold PBS three times and permeabilized with 0.1% Triton X-100 in PBS for 5 min at room temperature. Cells were incubated in blocking buffer (0.1% Triton X-100, 0.2% skimmed dry milk in PBS) at 4 °C overnight in a humidified chamber. The following day samples were incubated with rabbit polyclonal antibody specific for phosphorylated H2AX (γH2AX, Bethyl Scientific, Montgomery, TX) at 1:10,000 dilution in blocking buffer for 1h at room temperature. After washing 3 times with 0.1% Triton X-100 in PBS, cells were then incubated with Alexa Fluor 633 conjugated goat anti-rabbit secondary antibody (Invitrogen, Grand Island, NY) at a dilution of 1:2000 in blocking buffer for 1h at 4 °C in the dark. Cells were washed with PBS and counterstained with 4',6-diamidino-2-phenylindole dihydrochloride dihydrate, DAPI (Sigma) at 1:10,000 dilutions in PBS for 3 min. Stained cells were washed with ice-cold PBS three times and the slides mounted with Fluoromount-G (SouthernBiotech, Birmingham, AL), using a #1 glass cover slips and the edges were sealed with clear nail polish.

Images were visualized with an Olympus FluoView FV1000 BX2 Upright confocal microscope (60x oil immersion objective), equipped with 633 nm HeNe excitation laser. Foci were counted in at least 50 cells per time point and results from three independent experiments averaged. Cells were scored into two categories, i.e. ≤10

and >10. The γH2AX foci were scored manually on coded samples in a blind manner. Data are expressed as the mean percentage of γH2AX-positive cells (± SEM).

3.3 Results

3.3.1 Experimental Overview

To gain insight into the dynamics of drug-induced ICL formation and removal in cultured mammalian cells we simultaneously pursued a number of distinct strategies: 1. Quantitation of ICL formation and removal in drug-treated cells, 2. Measurement of drug-induced acute cell death and irreversible cell cycle arrest, and 3. Determination of drug-induced DNA double-strand break formation and rejoining. We focused on the bifunctional alkylating agent 1,2,3,4-diepoxybutane (DEB) and performed this analysis on wild-type Chinese hamster clones (V79) and two isogenic clones derived from these cells that are deficient in the hamster homologs of the human FANCA gene (V-H4) *(253)* or ERCC2/XPD gene (V-H1) *(254)*. V-H4 cells were selected because they are hypersensitive to cell death induced by a variety of cross-linking agents, including DEB. Importantly, human-derived clones with inactivating mutations in the FANCA gene also display hypersensitivity to death induced by these agents. While NER has not been implicated directly in ICL repair in mammalian cells, and clones deficient in this repair pathway are generally not recognized to be hypersensitive to DNA crosslinking agents, we chose to include the NER-deficient V-H1 cell line in our analysis because this DNA repair pathway plays an essential role in ICL in prokaryotes and lower eukaryotes.

3.3.2 Cytotoxicity assays

In order to compare the sensitivity of wild type and repair deficient cells to DEB exposure, cells were treated with increasing concentrations of DEB for three hours in serum-free growth media, and cellular drug sensitivity was analyzed using a clonogenic (colony forming) assay *(259)*.

The results presented in Figure 3.1A show that DEB exposure exerted a substantially greater inhibitory effect on colony formation in V-H4 cells as compared to the parental V79 cell line. For example, while exposure to 25 μM DEB for three hours reduced colony formation by 50% (IC_{50}) in V-79 cells, a similar magnitude effect was observed in V-H4 cells following exposure to 1.4 μM DEB, indicative of a ~18-fold enhanced DEB sensitivity of the latter cell line (Figure 3.1A). This result confirms an earlier report by Zdzienicka et al. that the V-H4 clone was hypersensitive to cell death induced by *bis*-electrophiles, and is consistent with the drug-sensitivity phenotype associated with V-H4 cells harboring loss of function mutations in the human homolog of the FANCA gene *(251)*. In contrast, the NER-deficient V-H1 clone exhibited a modest ~1.3-fold increased sensitivity to DEB than the parental V79 clone, with an IC_{50} value in the clonogenic assay of 19 μM (Figure 3.1A). This latter result is consistent with previous observation of De Silva et al that Chinese hamster-derived clones defective in the XPD gene are only slightly more sensitive to nitrogen mustard-induced cell death *(260;261)*.

While drug-induced reductions in colony forming ability are generally interpreted to indicate cell death, this assay also reflects drug-induced loss of replicative potential in cells that otherwise remain viable following drug exposure *(259)*. Indeed, it has been known for decades that a substantial population of cells exposed to *bis*-electrophiles such as mitomycin C or DEB remain viable, yet permanently exit the cell cycle *(262;263)*. This phenomenon has been exploited to create non-dividing so-called 'feeder' cells used to support the cultivation of specialized cell lineages, including embryonic stem cells *(264)*. It thus seemed likely that the reductions in colony formation associated with

exposure to DEB and the formation of ICLs (Figure 3.1A) over-estimated the direct cytotoxic effect of DEB exposure on V79, V-H1 and V-H4 cells. We therefore repeated the drug exposure experiments depicted in Figure 3.1A and analyzed cellular sensitivity to DEB by direct cell counting of trypan blue-excluding cells 24 hours post-drug treatment (Figure 3.1B). The results from this experiment revealed that all three cell lines examined were substantially less sensitive to DEB-induced cell death than might have been anticipated based on the results of the clonogenic assay (Figure 3.1B). LC_{50} values from direct cell counts were estimated as 165 μM (V79, based on extrapolation), 65 μM (V-H1), and 30 μM (V-H4). Comparison of the respective IC_{50} (clonogenic assay) and LC_{50} (direct cell count assay) values indicates that the DEB sensitivity of V-H4 cells in the clonogenic assay was approximately 20-fold greater than that measured in the direct cell counting method. In contrast, when a similar comparison is made in V79 and V-H1 clones, one observes a substantially lower ~3-7-fold increased DEB sensitivity in the clonogenic assay, relative to direct cell count assay.

These results indicate that the FANCA-deficient V-H4 clones are substantially more sensitive to acute DEB-induced cell death, and are also significantly more sensitive to DEB-induced loss of proliferative capacity than are wild-type cells. While V-H1 clones display an intermediate sensitivity to acute DEB-induced cell death, they display only a very mostly enhanced sensitivity to DEB-induced loss of proliferative capacity, relative to wild-type cells. Taken together, these results support the interpretation that both the FA pathway and the NER pathway are involved in the repair of DEB-induced DNA damage.

Figure 3.1 Effect of exposure to DEB on colony formation and survival of V79 (circles), V-H1 (squares) and V-H4 (diamonds) cells. The influence of exposure to various concentrations of DEB for three hours on colony forming activity was determined using the clonogenic assay (A) and direct cell counting of trypan blue-excluding cells (B) as described in the methods section. Results represent average +/- S.D. N= 3 or more.

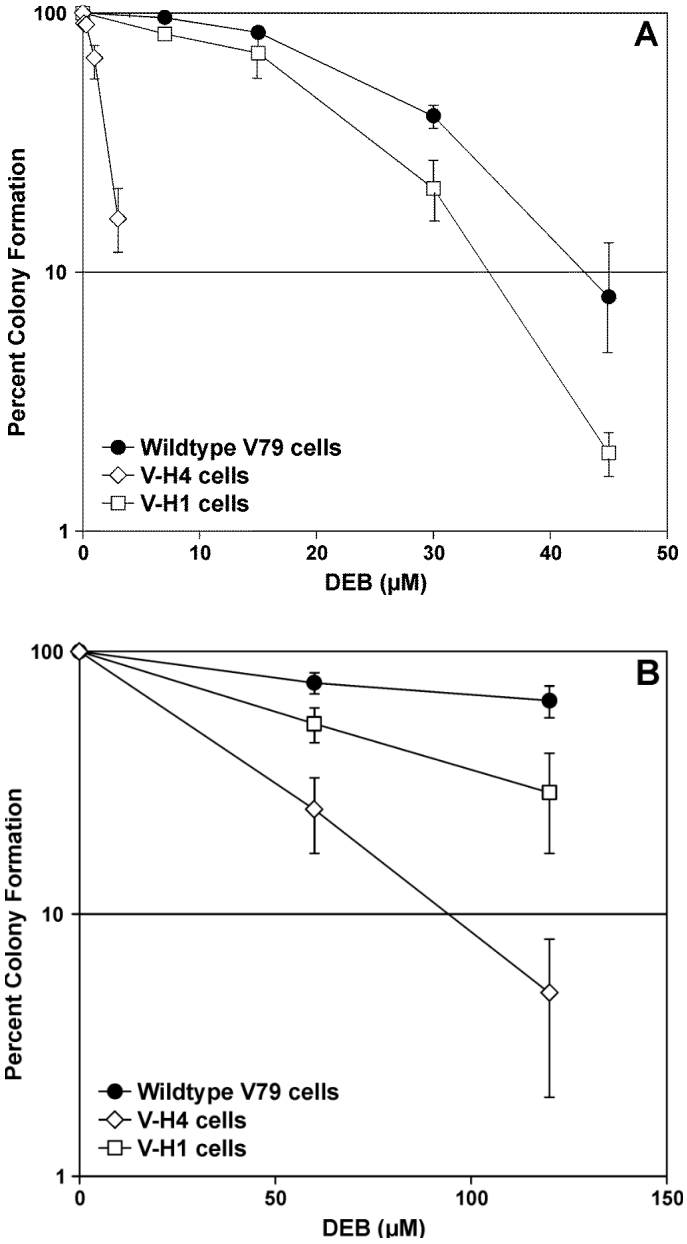

3.3.3 *Bis*-N7G-BD Adduct Formation and Removal

As discussed above, DEB induces a variety of DNA lesions including DNA monoadducts, DNA-protein cross-links, and both intrastrand and interstrand DNA-DNA cross-links. DNA monoadducts are the most abundant DEB-induced DNA lesions, representing about 90% of the total number of covalent chromosomal modifications. DNA-DNA and DNA-protein crosslinks are thought to represent 5 and 1-2% of the total adducts, respectively *(104;114;265;266)*, *(115;267)*.

Interstrand DNA-DNA crosslinks (ICLs) are considered the most lethal and genotoxic among DEB-mediated DNA lesions and are believed to be largely responsible for its adverse health effects *(226;227;231)*. DEB-induced ICLs predominately involve the N-7 residues on guanines in the opposite strands of 5'-GNC-3' trinucleotides, and their structures have been established as 1,4-*bis*-(guan-7-yl)-2,3-butanediol (*bis*-N7G-BD) *(215)*. These lesions can be quantitatively released from the DNA backbone as nucleobase conjugates upon heating because N7-guanine alkylation creates a positive charge on N-7 and destabilizes the glycosidic bond (t ½ = 84-96 h under physiological conditions) *(115)*.

We employed a sensitive and specific mass spectrometry-based methodology developed in our laboratory to quantitatively assay the time-dependent formation and removal of *bis*-N7G-BD from the chromatin of wild-type and mutant Chinese hamster lung fibroblasts V-79, V-H1, and V-H4 *(69;74)*. Preliminary studies in V-79 cells treated with increasing concentrations of DEB (0, 10, 15, 25 and 100 μM) have shown that *bis*-N7G-BD formation was concentration-dependent, with adduct numbers ranging between 0.5 and 3 adducts per 10^6 nucleotides depending on exposure concentration (Figure 3.2).

Figure 3.2 Concentration-dependent formation of *bis*-N7G-BD adducts in wild type V79 cells treated with increasing amounts of DEB (10-100 μM).

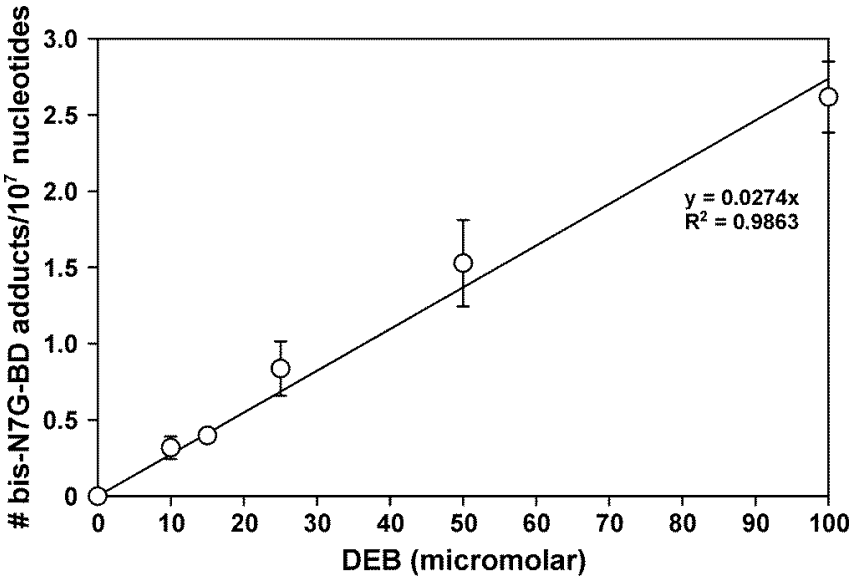

In order to compare the kinetics of *bis*-N7G-BD cross-link repair in control and repair deficient cells, wild-type V79 and mutant Chinese hamster fibroblasts were exposed to DEB for 3 hours, and the cells were allowed to recover in carcinogen free media for 1- 48 hrs. At various time points, cells were harvested, and the amounts of *bis*-N7G-BD in chromosomal DNA were determined by nanoLC-ESI$^+$-MS/MS (Figure 3.3) *(69)*. While this approach does not allow us to distinguish amongst interstrand versus intrastrand *bis*-N7G-BD crosslinks, our previous studies have shown that *SS,RR* DEB almost exclusively forms interstrand ICLs *(105;215)*.

We found that *bis*-N7G-BD adduct numbers in fibroblasts exposed to 15 μM DEB for 0-3 hrs increased nearly linearly during the exposure period (Figure 3.3A). At the end of the three hour exposure period, adduct numbers were 0.40 ± 0.01(V79), 0.76 ± 0.07 (V-H1), and 0.62 ± 0.01 *bis*-N7G-BD adducts/10^7 nucleotides (V-H4), respectively. The rate of crosslink formation (calculated from the slope of linear regression curves obtained using the data from Figure 3.3B) was the lowest in the V79 cells, corresponding to approximately ~ 80 GG crosslinks formed per cell per hr (based on an estimated Chinese hamster genome size of 2.8 gigabases). By comparison, the rate of cross-link formation in V-H1 and V-H4 clones were ~140 and ~110 crosslinks/cell/hr, respectively. Given that these latter clones are isogenic to V79, it is unlikely that the differences in rates of crosslink formation reflect altered drug pharmacokinetics. Instead, these differences in levels of *bis*-N7G-BD adducts present in these cells reflect diminished rates of lesion *removal* from the V-H1 and V-H4 clones, relative to the wild-type V79 clone. Thus, the data depicted in Figure 3.3B most likely reflect the functioning of a robust and fast-acting DNA ICL repair pathway that is functional in wild-type cells but is impaired to

Figure 3.3 Time course of *bis*-N7G-BD adduct accumulation in V79, V-H1, and V-H4 cells. Cells were exposed to 15 μMolar DEB for three hours and subsequently drug was removed and replaced with fresh growth media. At the indicated times chromosomal DNA was isolated and *bis*-N7G-BD adduct levels determined as described in the methods section. A; Full time course, B; expanded view of the first three hours of DEB exposure.

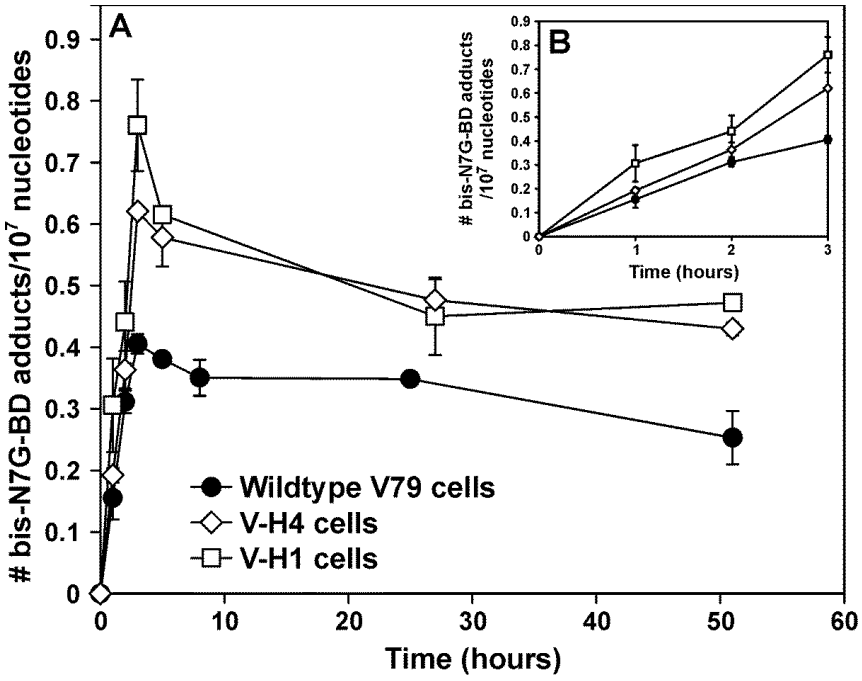

different extents in the V-H1 and V-H4 clones. Interestingly, the defect in this pathway(s) is substantially more pronounced in the V-H1 cells, compared to V-H4, despite the observation that V-H1 cells are substantially less sensitive to the cytotoxic and growth-arresting effects of DEB than are V-H4 cells (Figure 3.1).

Following carcinogen removal at the 3 hr time point, adduct numbers initially dropped off at a significant rate, but then decreased gradually, with substantial numbers of apparently stable crosslinks remaining up to 48 hours post-DEB exposure. This slow decrease at the later time points likely reflects spontaneous depurination of *bis*-N7G-BD from the DNA backbone. Our previous studies in calf thymus DNA have estimated the half-life of *bis*-N7G-BD under physiological conditions in the absence of repair as 84-96 h *(115)*. Overall although repair deficient cells (V-H1 and V-H4) exhibited slower removal of *bis*-N7G-BD cross-links (Figure 3.3), the rates of adduct removal did not correlate with DEB toxicity in these three clones (Figure 3.1), suggesting that ICL numbers *per se* are not predictive of cellular toxicity and that other DNA lesions or processes play a role in the mechanisms of *bis*-N7G-BD-mediated cell death.

Pharmacological inhibition of NER was employed to further evaluate the contribution of this pathway to *bis*-N7G-BD removal. Similar to the kinetics observed in VH-1 cells, V79 cells pretreated with NER inhibitor UCN-01 demonstrated a rapid increase in adduct formation (0.52 +/- 0.04 adducts/10^7 nucleotides after 3 hour treatment), following with a slower rate of adduct removal (0.43 +/- 0.03 adducts/10^7 nucleotides at 48 hour post exposure) (Figure 3.4 A, B). While the 2 hr pre-treatment of V79 cells with the NER inhibitor UCN-01 did not fully recapitulate the ICL removal deficit observed in V-H1 cells, it is conceivable that a longer period of preincubation may

Figure 3.4 Time course of bis-N7G-BD adduct accumulation in V79 (circles), V-H1 (squares) and V79+20 nM UCN-01 (diamonds) cells. Cells were pretreated with 20nM UCN-01 for 2h and the NER inhibitor is present during and after treatment with DEB. Cells were exposed to 15 μM DEB for three hours and subsequently drug was removed and replaced with fresh growth media with 20nM UCN-01. At the indicated times chromosomal DNA was isolated and *bis*-N7G-BD adduct levels determined as described in the methods section A; Full time course, B; expanded view of the first three hours of DEB exposure.

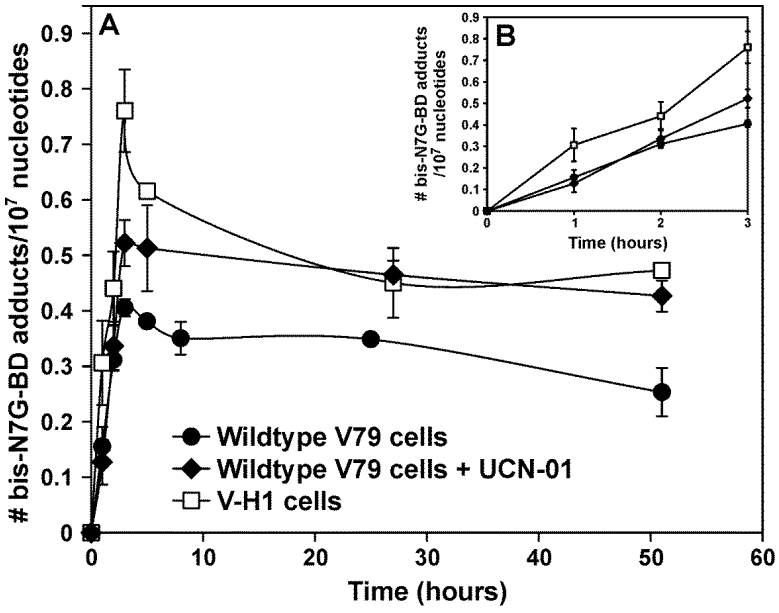

have enhanced the effect of inhibitor on ICL removal. In any event, the data in Figure 3.4 confirm the existence of a rapid-acting NER-dependent ICL removal pathway in Chinese hamster fibroblast clones.

3.3.4 Formation and Repair of DEB-induced DNA Double Strand Breaks

To gain further insight into the mechanism(s) underlying differential ICL removal kinetics observed in DEB-treated V79, V-H1 and V-H4 clones (Figure 3.3, 3.4) we performed a series of experiments to examine chromosomal DNA double-strand break formation and rejoining in drug-treated cells. First we performed single cell gel electrophoresis experiments. It is generally accepted in the literature that an increased amount of DNA in the so-called comet tails detected following neutral electrophoresis reflects elevated levels of chromosomal DNA double strand breaks *(257)*. We therefore performed comet assays on V-79, V-H1, and V-H4 clones prior to drug addition (T0), at the conclusion of the three hour DEB exposure (T3), and at three (R3) and 24 (R24) hours post-drug removal. The results depicted in Figure 3.5 show that immediately following exposure to DEB, V79 cells display a very small increase in comet tail DNA-indicating the presence of slightly elevated levels of chromosomal DNA double-strand breaks. This increase in comet tail DNA appears to peak at or shortly after the end of the three-hour DEB treatment and diminishes to nearly undetectable levels by 24 hours post-drug treatment. We speculate that the basal levels of strand breaks observed in cells prior to DEB treatment reflect normal chromosomal breaks formed by cells in S-phase. As is addressed in the discussion, very low levels of tail DNA detected 24 hours post-DEB exposure may reflects a cell population that is largely arrested in G1 phase of the cell cycle.

Figure 3.5 Formation and repair of DEB-induced DNA double strand breaks in V79, V-H1, and V-H4 cells. Single cell electrophoresis (Comet assays) was performed on cells prior to and following exposure to 15 μMolar DEB as described in the methods section. The data represent the percent of cellular DNA present in the 'comet tail' plus the SEM, N=3 or more. T0; pre-drug exposure, T3; following three hours of DEB exposure, R3; three hours post-drug exposure, R24; 24 hours post-drug exposure.

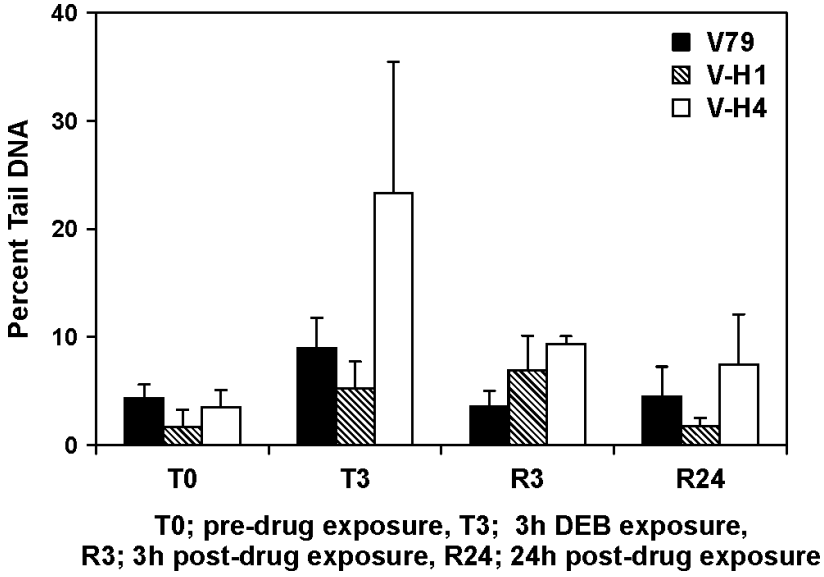

In contrast, drug-treated V-H4 cells displayed dramatically elevated levels of comet tail DNA that peaked at the time corresponding to DEB removal (Figure 3.5). While comet tail DNA levels rapidly declined, they were still substantially elevated 24 hours post DEB treatment. The comet tail analysis of DEB-treated V-H1 cells broadly resembled that observed for V79 cells, with perhaps a slightly enhanced, and somewhat delayed time course. However, in contrast to the V-H4 cells, the kinetics of chromosomal DNA double-strand break formation and rejoining in V-H1 cells did not appear to be substantially different from that seen in V79 cells (Figure 3.5). These results are consistent with the interpretation that chromosomal DNA double-strand breaks accumulate in V-H4 clones immediately following DEB exposure at levels that are substantially higher than those observed in either V-H1 or wild-type V79 clones. Since DEB does not directly induce DNA strand breaks, these differences in chromosomal double strand breaks reflect differences in the cellular DNA damage response to ICLs in these three clones.

To further explore the relationship between ICL removal kinetics and chromosome double strand break formation, we examined the kinetics of phospho-H2AX foci formation in V79, V-H1 and V-H4 cell lines during and after three hour treatment with 15 μM DEB (Figure 3.6A). Immunocytochemistry was performed using an antibody specific for phosphorylated histone H2AX (commonly referred to as γH2AX), and the percentage of cells within randomly-selected microscope fields that contained ten or more foci was determined as described in the Materials and Methods section. In these experiments foci containing phosphorylated H2AX are depicted as pink puncta within a nucleus visualized in blue due to counterstaining with the dye DAPI. This analysis was

performed prior to drug exposure (T0) and at one (T1), two (T2), and three (T3) hours after exposure to DEB, as well as at three (R3) 24 (R24) and 48 (R48) hours post-DEB exposure. Examination of the dynamics of focus formation in V79 cells reveals that γH2AX foci form rapidly in DEB-treated cells, and equally rapidly disappear (Figure 3.6B). The peak of focus formation is centered around the second and third hour of DEB treatment, and by 24 hours post-drug treatment foci levels have returned to basal levels. In contrast, while foci rapidly form in DEB-treated V-H4 cells, their levels continue to increase even after drug is removed, peaking at a time point three hours post-drug exposure. Inspection of the data in Figure 3.6 B reveals that even at 24 and 48 hours post-drug removal, V-H4 cells still harbor elevated levels of γH2AX foci. Again, as was observed using the comet assay, double strand break formation in V-H1 cells, as assessed by γH2AX focus formation, was somewhat delayed, and displayed a much more broadened peak compared to wild-type cells. The data in Figure 3.6 B indicate that γH2AX foci levels in V-H1 clones remain at peak levels a full day post-drug removal. Interestingly, despite harboring substantially elevated levels of γH2AX foci at 24 hours post-drug removal, by the end of the following day, foci levels in these clones had returned to basal levels. Intriguingly, direct cell counting experiments performed on V79, V-H1 and V-H4 cells 24, 48 and 72 hours post-DEB exposure revealed that at these latter time points the V79 and V-H1 cells were increasing in numbers whereas the V-H4 cells were continuing to die (data not shown).

Figure 3.6 (A) Images of phosphorylated histone H2AX-containing foci in V79, V-H1 and V-H4 cells prior to and following exposure to 15 μM DEB. At the indicated times immunocytochemistry was performed using a mouse monoclonal antibody specific for phospho-H2AX, as described in the methods section. Time points same as Figure 3.3, except R48; 48 hours post-DEB exposure.

A.

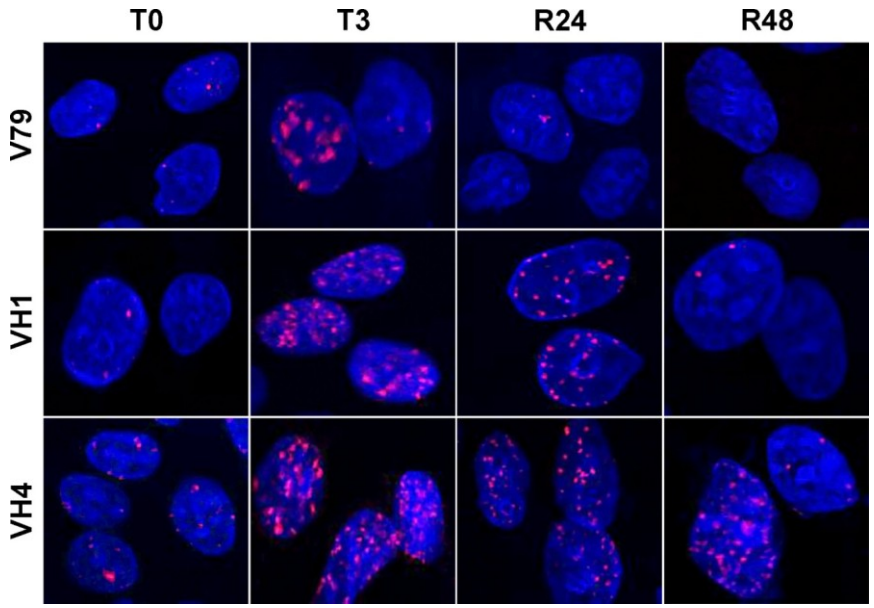

B. Dynamics of phosphorylated histone H2AX-containing foci in V79 (black bars), V-H1(cross-hatched bars) and V-H4 (white bars) cells prior to and following exposure to DEB. Cells were exposed to 15 μM DEB for three hours and subsequently drug was removed and replaced with fresh growth media. The data represent the percentage of cells within randomly-selected microscope fields that contained 10 or more foci, plus the SEM, N=3.

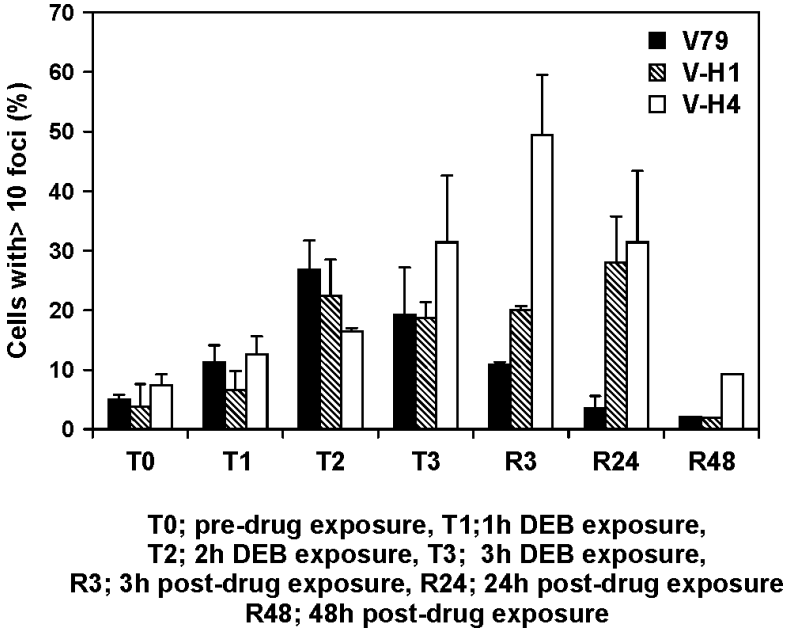

T0; pre-drug exposure, T1;1h DEB exposure,
T2; 2h DEB exposure, T3; 3h DEB exposure,
R3; 3h post-drug exposure, R24; 24h post-drug exposure
R48; 48h post-drug exposure

3.4 Discussion

In the present study, we investigated the dynamics of DEB-induced ICL formation and DNA double-strand break formation and removal in isogenic Chinese hamster lung fibroblasts. We focused on a wild type parental clone (V79) and two isogenic derivative cell lines with defects, respectively, in the NER gene XPD/ERCC2 (V-H1) or the FANCA gene (V-H4). We focused on the latter clone because of the well-known hypersensitivity of cells derived from FA patients to DNA cross-linking agents, as well as a number of recently published models postulating a role for the FA gene products in ICL *(251;252)*. While, most models of ICL suggest that, with the exception of the XPF/ERCC1 heterodimer, NER proteins do not play a prominent role in ICL repair it is clear that in prokaryotes and lower eukaryotes NER is known to play an essential role in ICL repair, thus prompting us to include the V-H1 clone in this study *(254;268-270)*.

Our results confirmed previous studies based on clonogenic cytotoxicity assays that the FANCA-deficient V-H4 cells were hypersensitive to cell death induced by DEB, compared to wild-type cells while the NER-deficient V-H1 cells were only slightly more sensitive than their wild-type counterparts *(254;271;272)*. Interestingly, when a direct cell counting assay was used, our analysis revealed that while the V-H4 clones were again the most sensitive to DEB-induced cell death, the V-H1 clones were substantially more sensitive than were the wild-type V-79 cells. It is unclear, however, whether the enhanced sensitivity of V-H1 cells to DEB is due to a relative inability of these cells to repair drug-induced ICLs, or if it instead reflects a defect in NER-dependent repair of drug-induced monoadducts *(75;267)*.

To gain further insight into this question we employed a sensitive and precise nanoLC/ESI$^+$-MS/MS methodology developed in our laboratory to directly quantify the formation and removal of DEB induced *bis*-N7G-BD crosslinks in V79, V-H1, and V-H4 cells. Based on analysis of the linear regression curves generated from the data in the inset in Figure 3.3B we estimated the rates of ICL formation to be 80 110 and 140 GG crosslinks /cell/hr in the V79, V-H4, and V-H1 cells respectively. Since the mutant clones are isogenic to the parental V79 cells, the enhanced rate of formation in those clones is mostly due to the absence or malfunctioning of a robust, rapid ICL removal pathway that is functional in the wild-type V79 cells.

Further analysis of the data in Figure 3.3 revealed a second, slower phase of adduct removal occurring during the initial 2 hrs post-drug removal. We noted that in V-H1 clones *bis*-N7G-BD adducts were removed approximately three times as fast as compared to either V-H4 or wild-type cells. We further noted that between 2 and 48 hrs post DEB treatment there was a further slow decline in *bis*-N7G-BD crosslinks between. We hypothesize that this latter removal of adducts is due to spontaneous depurination of *bis*-N7G-BD from the DNA backbone *(115)*. It is notable that a substantial amount of *bis*-N7G-BD crosslinks remain present in all three cell lines 48 h post DEB exposure. We postulate that this represents a reservoir of crosslinks in cells that have survived the initial wave of DEB-induced cell death but have permanently exited the cell cycle (i.e. cells that are present and viable in the direct-cell counting experiment, but which do not proliferate and form colonies).

Interestingly, ICLs accumulated to the highest levels in V-H1 cells which exhibited only a slightly elevated sensitivity to DEB as measured in the clonogenic assay, while adduct levels were closer to those detected in wild-type cells, yet V-H4 cells were dramatically more sensitive to the colony-inhibiting effects of DEB than were the other lines (Figure 3.1A). It seems plausible that the increased sensitivity to DEB in V-H4 cells is due to a relative inability to rejoin double strand breaks formed during *bis*-N7G-BD removal, an interpretation consistent with our data (Figure 3.5) revealing increased accumulations of DNA in comet tails in V-H4 cells as compared to either V-H1 or V79 cells showing increased DSB levels both during DEB treatment (15μM, 3h) and higher DSB accumulation post exposure to DEB until 24hr (Figure 3.5). Immunocytochemical detection of γH2AX foci also support the interpretation that DNA double strand breaks accumulate in V-H4 cells following DEB treatment (Figure 3.6).

Based on our results we propose a working model for ICL repair induced by DEB. Our model postulates that the majority of ICL repair occurs in cells in the S, and G2 phases of the cell cycle, and that minimal repair occurs in cells that are in the G1 phase of the cell cycle when exposed to DEB. Our working assumption is that cells that sustain significant numbers of interstrand DNA adducts arrest at the G1/S boundary and/or enter G0. We propose that it this population of cells that are the reservoir of *bis*-N7G-BD adducts that persist at time points 24-48 hrs post-DEB exposure (Figure 3.3, 3.4), and that these are the cells–which are no longer capable of cell division–that are responsible for the higher apparent cell viability when direct cell counting is used to assess DEB-induced cytotoxicity.

Our model further proposes that ICL repair in cells in the S and G2 phases of the cell cycle occurs via two at least partially distinct pathways. While both pathways are critically dependent on the Fanconi anemia recombinational repair machinery, there are some key differences. As outlined in Figure 3.7, our model postulates that the key factor determining which of these two pathways is pursued is whether the relevant portion of the genome in which the ICL forms has undergone replication or not. As the cartoon depicts, lesions within replicated portions of the chromosome–for which an undamaged sister chromatid exists (depicted as the ICL lesion on the right hand side of Figure 3.7)–undergo recombinational repair between the damaged chromatid and the undamaged sister chromatid, *triggered by an initial NER-dependent initiation event*. The mechanism *via* which the double-strand break is formed remains unclear, but we propose the XPF-ERCC1 nuclease as an attractive candidate *(247)*. As was mentioned above, our model points that this recombination repair process is perturbed in FA cells.

For lesions occurring within portions of the genome that have yet to be replicated, we propose that ICL repair is initiated by collision of replication forks, associated with translesion synthesis, which is followed by a recombination-mediated gap-repair. Our model is not specific regarding the identity of the nuclease(s) responsible for endonucleolytic cleavage, however a number of candidates including FAN1, XPF/ERCC1, MUS81-EME1 and SLX1-SLX4 have been proposed *(227;244;273)*. As others have suggested, we propose that this process is disrupted in cells lacking a functional FA pathway.

We postulate that the SCE-mediated repair pathway (right-hand lesion in Figure 3.7) is responsible for the initial rapid phase of ICL removal that occurs during the three

hr DEB exposure. Notably, this pathway of removal appears to be absent-or at least significantly inactivated in NER-deficient XPD cells, suggesting that an initiating event may involve endonucleolytic cleavage by NER proteins at the site of the ICL.

FANCA-deficient V-H4 cells display an intermediate rate of ICL removal during this initial drug-treatment period, leading us to postulate that conversion of the NER-processed duplex into a double-strand break is at least partially dependent on the FA pathway. (It is noteworthy that the reaction intermediate depicted on the right hand side of figure 3.7C retains a chromosomal *bis*-N7G-BD crosslink.) Our model proposes that the SCE repair event depicted in Figure 3.7 D-F is dependent on a functional FA pathway and that in FANCA-deficient V-H4 cells DNA double-strand breaks accumulate that ultimately trigger cell death. This is consistent with the elevated numbers, and prolonged kinetics of comet tails and γH2AX foci in V-H4 cells.

We postulate that the second, delayed onset phase of ICL removal in cells treated with DEB occurs as outlined in the left-hand side of the cartoon shown in Figure 3.7. We suggest that the replication fork collision pathway occurs more slowly than the more rapid SCE based recombination repair pathway depicted on the right-hand side of the cartoon, thus explaining the delay kinetics of removal. We further postulate that this latter repair pathway is able to remove ICLs that are not recognized via the NER-dependent pathway, perhaps as part of the G2/M checkpoint machinery. This would be consistent with the observation (Figure 3.3, 3.4) that while V-H1 clones exhibit a severely diminished 'fast' ICL repair phase, the subsequent phase of GG-crosslink removal occurs extremely efficiently, compared to that detected in either wild-type or V-H4 clones.

Figure 3.7 Model of ICL repair in Chinese hamster lung fibroblasts. The cartoon depicts a chromosome in mid-replication, containing duplicated regions, as well as a central, un-replicated portion. (A.) The Gray lines indicate the newly synthesized strands of DNA with arrowheads indicating the growing 3' ends. The red slashes depict interstrand crosslinks, one each within non-replicated or replicated portions of the chromosome. Right Hand Side: (B.) The NER machinery introduces endonucleolytic nicks bracketing the lesion on one strand of the affected duplex. (C. -D.) The reaction intermediate from (B) is converted to a double-strand break with protruding 3' ends. (E.-F.) Recombinational repair dependent on a functioning cellular FA machinery mediates double-strand break repair via sister chromatid exchange. Left Hand Side: (B.) Replication forks stall on either side of the ICL lesion. (C.) A currently unidentified nuclease (see text) unhooks the ICL, followed by (D.) translesion synthesis, and (E.-F.) FA machinery mediated recombinational repair.

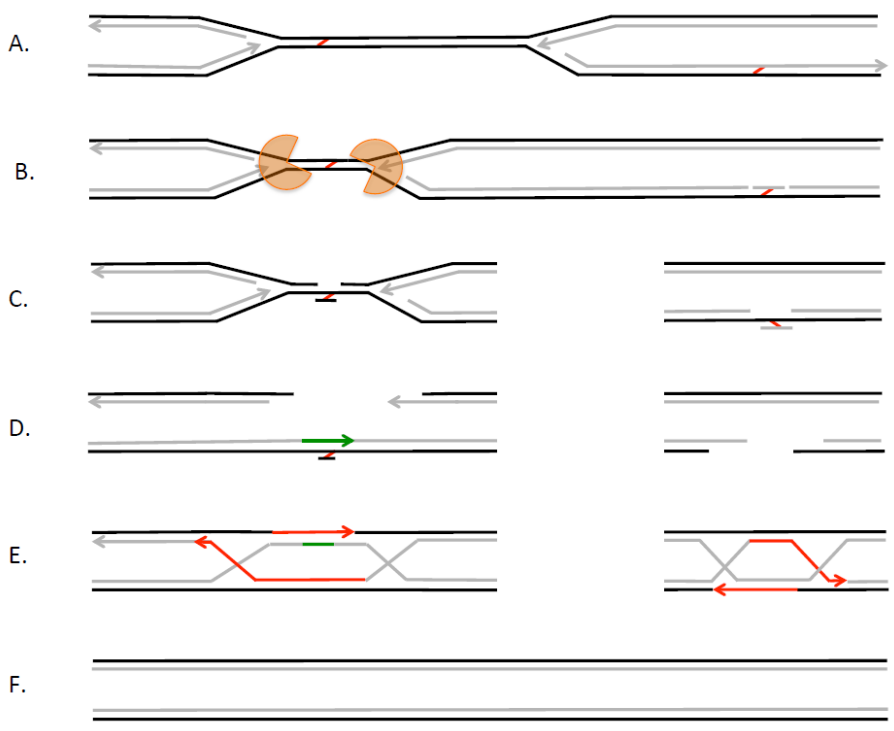

The most significant distinction between the model outlined in Figure 3.7 and those previously proposed to explain ICL repair *(227;240;244;273)* involves the incorporation of a NER-dependent 'fast' ICL repair pathway distinct from the previously developed 'replication fork' dependent ICL repair model. It is noteworthy that it was only through the development of methodology to quantitatively monitor chromosomal *bis*-N7G-BD adducts that we were able to detect this novel connection between the NER pathway and removal of interstrand DNA crosslinks. We note that this pathway of ICL repair appears to be functionally redundant with respect to cellular survival following exposure to DNA crosslinking agents such as DEB–at least when rapidly dividing immortalized cells are examined using a clonogenic assay–thereby explaining why others have failed to detect the NER-ICL connection highlighted by our data. We are currently pursuing additional experiments to gain further insight into the potential interplay between the newly identify NER-dependent ICL repair pathway and the FA machinery. Hence, from our results we postulate the involvement of NER and FA pathway in the repair of DEB induced ICLs.

IV. CAPILLARY HPLC-ACCURATE MASS MS/MS QUANTITATION OF N7-(2, 3, 4-TRIHYDROXYBUT-1-YL)-GUANINE ADDUCTS OF 1,3-BUTADIENE IN HUMAN LEUKOCYTE DNA

Reprinted with permission from: Dewakar Sangaraju, Peter Villalta, Melissa Goggin, Maria O. Agunsoye, Colin Campbell, and Natalia Tretyakova. Chem. Res. Toxicol. 2013, 26(10), 1486-97.

4.1 Introduction

1,3- Butadiene (BD) is an important industrial and environmental chemical classified as an animal *(84;85)* and human carcinogen *(86;87;91;209)*. Humans are commonly exposed to BD due to its widespread use in polymer industries *(274)*, its presence in cigarette smoke *(208)*, urban environment *(275)*, automobile exhaust *(207)*, and its formation upon wood burning and forest fires *(276)*. Inhalation exposure to BD causes multi-site tumors in laboratory rats and mice *(84;85)* and is associated with an increased incidence of leukemia in occupationally exposed workers *(86;87;91;209)*. The adverse health effects of BD are mainly attributed to its cytochrome P450-mediated metabolism to electrophilic epoxides 3,4-epoxy-1-butene (EB) and 1,2-dihydroxy-3,4-epoxybutane (EBD), and 1,2,3,4-diepoxybutane (DEB) *(95;210)*. DEB and EBD are known to exist in either racemic or meso forms of isomers *in vivo (75;108;117;119)*.(Scheme 4.1). Among these, EBD is the most abundant *in vivo (105;151;267)*.

Epoxide metabolites of 1, 3-butadiene can alkylate DNA to form a range of nucleobase adducts *(65;75;105;107;113;215)*. Specifically, EBD binds to the N7 position of guanine to give N7-(2, 3, 4 –trihydroxybut-1-yl) guanine (N7-THBG) adducts (Scheme 4.1) *(75)*.

N7-THBG are also induced by DEB via a two-step process including hydrolysis of one of the two epoxide rings *(104)*. Both meso and racemic forms of N7-THBG are observed *in vivo (94;105;267)*. N7-THBG are the most abundant nucleobase adducts in DNA treated with EBD or DEB *in vitro (104;215)* and in tissues of laboratory animals exposed to BD by inhalation *(75;115;215)*. Because N7-guanine alkylation generates a positive charge on the modified nucleobase, it destabilizes the *N*-glycosidic bond, leading to spontaneous depurination of N7-THBG and the formation of abasic site (Scheme 4.1) *(115)*. The hydrolytic half-lives of N7-THBG adducts *in vivo* (mouse and rat liver DNA) are 3.6-5.5 days, depending on chirality *(277)*. In the laboratory, N7-THBG nucleobases can be readily released from the DNA backbone by heating, facilitating their analysis by mass spectrometry *(104)*. Although N7-THBG adducts may not be mutagenic because they retain normal Watson-Crick base pairing with C *(278)*, they can be used as mechanism based biomarkers of BD metabolism to DNA-reactive epoxides. In the present study, N7-THBG was selected as a DNA based biomarker of human exposure to BD due to its high prevalence *in vivo* as compared to other BD-DNA lesions *(75;215)*. Previous studies have quantified N7-THBG adducts in tissues of laboratory mice and rats exposed to BD by inhalation using HPLC-ESI^+-MS/MS *(75;104)*. However, the sensitivity of existing methods is insufficient for studies in humans due to significantly lower amounts of DNA adducts observed in human tissues (< 1-2 adducts per 10^9 nucleotides in humans versus 1-10 adducts per 10^7 nucleotides in laboratory animals exposed to BD).

Scheme 4.1: BD bioactivation to epoxide metabolites and the formation of thermally labile N7-THBG adducts in DNA.

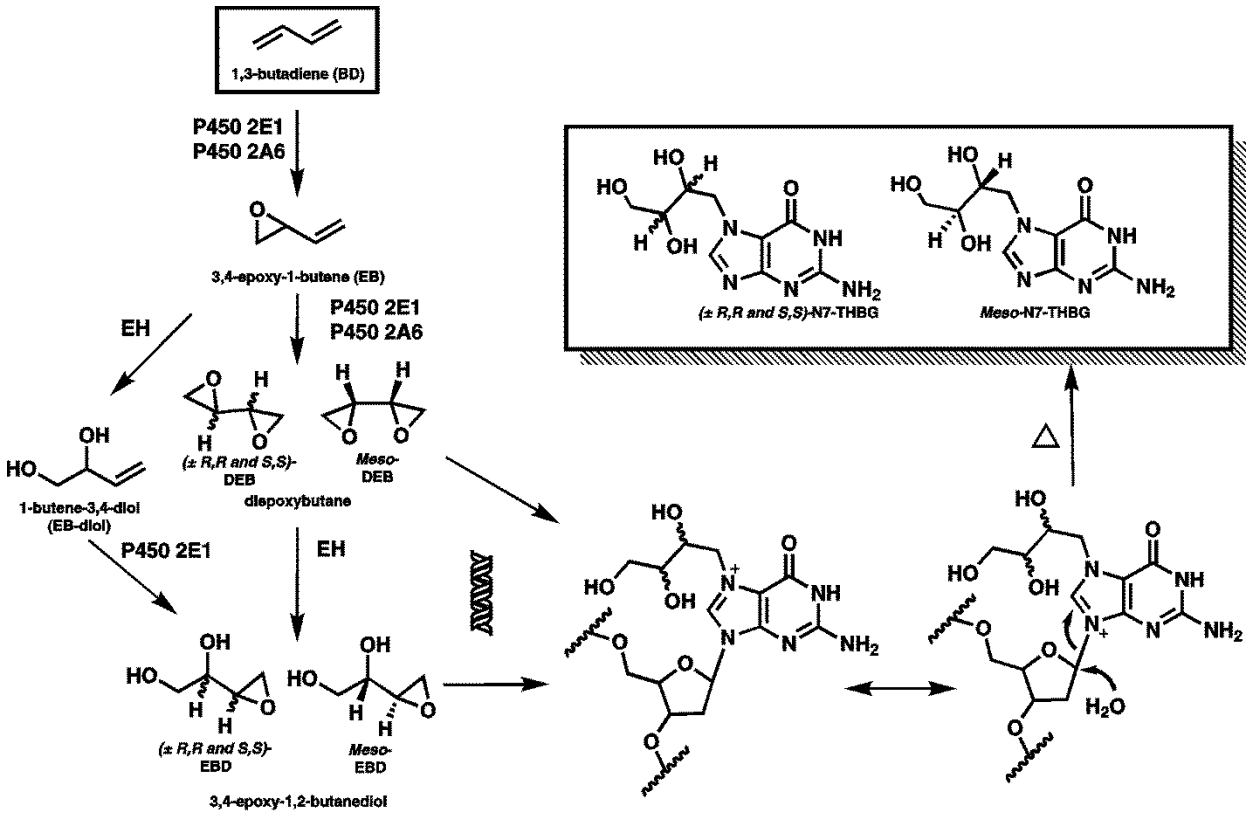

EH, epoxide hydrolase; N7-THBG,N7-(2', 3', 4'-trihydroxybut-1-yl) guanine
For simplicity, the (R,S)-form of meso-THBG is shown.

In the present work, a highly sensitive and specific capillary HPLC - accurate mass ESI^+ MS/MS methodology utilizing an Orbitrap Velos mass spectrometer was developed for quantitation of N7-THBG adducts in human white blood cells (WBCs). Separation of the two isomeric forms of N7-THBG adduct was not achieved and we quantified total N7-THBG formed as single peak in various *in vivo* samples. The method was initially applied to human fibrosarcoma (HT1080) cells treated with sub-micromolar concentrations of DEB (10 nM – 100 μM). The validated method was subsequently used to determine the concentrations of N7-THBG adducts in DNA isolated from PBLs of smokers, nonsmokers, occupationally exposed workers, and individuals participating in a smoking cessation study.

4.2 Materials and methods

Note: *DEB is a known human carcinogen and must be handled with adequate safety precautions. Phenol and chloroform are toxic chemicals that should be used only in a well-ventilated fume hood with appropriate personal protective equipment.*

N7-THBG and [$^{15}N_5$]-N7-THBG were synthesized in our laboratory as described elsewhere *(215)*. Puregene DNA purification reagents were obtained from Qiagen (Valencia, CA). LC-MS grade water, methanol and acetonitrile were purchased from Fisher Scientific (Pittsburgh, PA). Isolute ENV+ 50 mg/1 mL SPE cartridges were provided by Biotage (Charlotte, NC). DNA oligodeoxynucleotides (5'-TCAGATTCGCGCCGGCTGCGATAAGCT-3') were purchased from Integrated DNA Technologies (Coraville, IA) or synthesized in our laboratory using automated solid phase synthesis. All other chemicals and solvents were obtained from Sigma-Aldrich (Millwaukee, WI, St. Louis, MO). Human blood buffy coat samples were acquired from the Biorespository Facility, Masonic Cancer Center, University of Minnesota, Minneapolis, the NCI CRCHD repository, and the American Chemistry Council, Washington DC.

Cell culture

Human fibrosarcoma cells **(**HT1080) were grown in Dulbecco's modified Eagle's media supplemented with 9% fetal bovine serum (Atlanta Biologicals). Cells were cultured in a humidified atmosphere of 5% carbon dioxide, 95% air, at 37 °C.

N7-THBG formation in human cell culture

HT1080 cells were plated in 15 cm dishes using Dulbecco's modified Eagle's medium containing 9% FBS and permitted to adhere overnight. On the following morning, cells (in duplicate) were treated with increasing concentrations of DEB (0, 10 nM, 50 nM, 100 nM, 1 μM, 10 μM, 50 μM or 100 μM) for 3 h at 37 °C. Control and treated cells (N = 2) were harvested, washed with ice cold phosphate-buffered saline (PBS), and suspended in PBS for DNA extraction as described below.

Study subjects

The study was approved by the University of Minnesota Human Research Protection Programs Institutional Review Board. Blood samples from 13 smokers and 13 nonsmokers were obtained from the Tobacco Research Biorepository Facility, Masonic Cancer Center, University of Minnesota. All human subjects were age 18 years or older, not pregnant or breast feeding. They consumed less than 21 alcoholic drinks per week, and were in good physical and mental health. Smokers included in the study had been smoking for at least 5 years and consumed at least 7 cigarettes per day (CPD), with no change greater than 50% in CPD or brand within the last year, and had not used any other tobacco products in the last 6 months. Individuals with nonsmoking status were required to have smoked less than 100 cigarettes in their lifetime and were not using any tobacco products regularly. Individual smoking status was confirmed by expired carbon monoxide (CO) levels. CO levels were determined by having participants take a deep breath and hold it for 20 s before exhaling into a carbon monoxide monitor (Bedfont Scientific, Upchurch, UK). Smokers had CO levels of ≥10 ppm (range 7-29 ppm), while

nonsmokers had CO levels ≤ 3 ppm (range 0-3 ppm). The average age of smokers was 41 ± 12 (range 19-61) and that of nonsmokers was 35 ± 12 years (range 20-61).

Human blood buffy coat samples from a smoking cessation study were obtained from National Cancer Institute. Subjects included were between the ages of 18 and 65, smoked at least 10 cigarettes daily for the past year, had carbon monoxide (CO) levels of >10, and were in good physical and mental health. Fasting blood was collected through venipuncture at various time points during the study. Blood buffy coat samples were obtained at 14 and 7 days prior to smoking cessation (baseline levels) and at two time points post smoking cessation (28 and 84 days). Smoking status was confirmed through CO measures and self-reported tobacco use diaries. To obtain sufficient sample size, buffy coat samples from 5 subjects were pooled for each time point (N = 2). DNA was isolated as described above. Samples were stored at – 80 °C until further analysis.

Human blood buffy coat samples from 10 workers with known occupational exposure to BD and 10 matched controls (administrative workers) were obtained from the American Chemistry Council, Washington DC. BD exposures were determined by personal monitoring tubes for 8-h work shifts on 10 separate occasions over a 4-month interval for each study subject. Ambient air samples were analyzed for BD concentrations. Co-exposures to toluene, styrene, and benzene were measured by personal monitoring in a subset of subjects on a single occasion and by ambient air sampling and other details of the study population are previously reported *(125;132)*. The experimental protocol was approved by the Institutional Review Boards at Regional Institute of Hygiene of Central Bohemia, the University of Vermont. Samples were

shipped to the University of Minnesota on dry ice and stored at – 80 °C until further analysis.

DNA isolation

DNA isolation from human blood samples was performed using the commercial protocol for DNA purification from buffy coat (Qiagen, Valencia, CA), *(223)* with the following modifications. Human whole blood buffy coat fractions obtained from 10 mL of whole blood were lyzed in the presence of RBC lysis solution (3 mL). White blood cells were collected as a pellet via centrifugation at 2000 g for 10 min. RBC lysis solution (3 mL) was added to the pellet, and the samples were centrifugated at 2000g for 10 min. The WBC pellet was mixed with 2 mL of cell lysis solution and 8 μL of proteinase K solution (20 mg/mL) and incubated at room temperature overnight upon slow mixing. On the following day, a solution of RNase A (4 mg/mL) was added (8 μL), and the samples were incubated at room temperature for 2 h. Protein precipitation solution (700 μL) was added to the cell lysate, and the mixture is vortexed at a high speed for 20 seconds and centrifugated at 2000g for 15 min to remove proteins. DNA was precipitated with cold isopropyl alcohol (3 mL) and washed twice with 1 mL of 70% ethanol in water. DNA was dried under a stream of nitrogen and stored at - 20°C until further analysis. Typical DNA yields from 10 mL of whole blood were 0.1-0.15 mg.

DNA from control and DEB-treated human fibrosarcoma (HT1080) cells was isolated using standard phenol-chloroform extraction *(217)*. DNA concentrations were estimated by UV spectrophotometry, and DNA purity was assessed from A_{260} /A_{280} absorbance ratios, which was typically between 1.6 and 1.7. DNA amounts were determined by dG quantitation in enzymatic hydrolysates as described below.

dG quantitation

DNA aliquots (~ 2 μg) were enzymatically digested with DNA Degradase Plus (Zymo Research, Irvine, CA) at 37 °C overnight. HPLC-UV analysis of dG was conducted by HPLC-UV using Eclipse XDB-C8 column (4.6 x 150 mm, 5 μm, from Agilent Technologies, Palo Alto, CA) eluted with a gradient of 150 mM ammonium acetate (A) and acetonitrile (B) *(217)*.

Sample preparation and adduct enrichment

DNA samples (35-150 μg in water) were spiked with 50 fmol of $^{15}N_5$-N7-THBG (99.9% purity, internal standard for mass spectrometry) and heated at 70 ºC for 1 h to release N7-THBG adducts from the DNA backbone. Partially depurinated DNA was removed by ultrafiltration with Nanosep 10K filters (Pall Life Sciences, Ann Arbor, MI) at 5000 g for 10 min. The filtrates containing N7-THBG and its internal standard were subjected to solid phase extraction (SPE) on Isolute ENV+ 50 mg/1 mL cartridges from Biotage (Charlotte, NC). SPE cartridges were conditioned with 2 mL of CH_3OH and 2 mL of H_2O. Samples were loaded at neutral pH, washed with 1 mL of H_2O and 1 mL of 0.1% formic acid in water, and eluted with 50% CH_3CN in water. SPE fractions containing N7-THBG were collected, evaporated to dryness, and dissolved in water (24 μL) for HPLC-ESI$^+$-HRMS/MS analysis. One third of the sample (8 μL, containing between 10 and 50 μg DNA) was injected on the column for HPLC-ESI$^+$-HRMS/MS analysis as described below.

HPLC-ESI$^+$-HRMS/MS analysis of N7-THBG

A Nano2D-LC HPLC system (Eksigent, Dublin, CA) was interfaced to an LTQ Orbitrap Velos instrument (Thermo Scientific, Waltham, MA). HPLC solvents were LC-MS grade water containing 0.05% acetic acid (A) and LC-MS grade acetonitrile (B). Samples (8 μL) were injected on to Synergi Hydro RP 80R (250 × 0.5 mm, 4 μm) analytical column (Phenomenex, Torrance, CA). The column was eluted at a flow rate of 10 μL/min. Solvent composition was maintained at 1% B for 3 min and then linearly increased to 7% B in 12 min, further to 12% B in 1 min, to 20 % B in 2 min, to 50% B in 1 min, and kept at 50% B for 2 min. Solvent composition returned to 1% B for an 8 min equilibration period at a flow rate of 10 μL/min. Under these conditions, both meso and racemic isomers of N7-THBG eluted as a single sharp peak at 17 and 18 min.

Samples were analyzed in the ESI$^+$ mode using an LTQ Orbitrap Velos instrument (Thermo Scientific, Waltham, MA). The source temperature was set at 350°C, sheath gas was at 40.0, the ESI source voltage was at 4.0 kV, and S-Lens RF level was set at 80%. N7-THBG adducts were quantified in the SRM mode by monitoring the transitions *m/z* 256.1 $[M + H]^+ \rightarrow$ *m/z* 152.05669 $[Gua + H]^+$ and $[^{15}N_5]$-N7-THBG at *m/z* 261.1 → *m/z* 157.04187 for the analyte and its $^{15}N_5$ labeled internal standard, respectively. CID was achieved using the HCD collision cell at the isolation width of 1 amu, collision energy of 50%, and mass resolution of 27,000.Accurate mass monitoring of the specified fragment ions was conducted at 5 ppm mass accuracy (152.05669 ± 0.0008 and 157.04187 ± 0.0008, respectively) with the Orbitrap Velos FTMS detector. A full scan event was also performed over *m/z* 50-270 to monitor for any co-eluting matrix

components. HPLC-ESI$^+$-HRMS/MS quantitation was conducted using the peak areas in extracted ion chromatograms corresponding to the analyte and the internal standard.

HPLC-ESI$^+$-HRMS/MS standard curves were constructed by analyzing aqueous solutions containing fixed amount of $^{15}N_5$-N7-THBG (50 fmol) and increasing amounts of N7-THBG (1.0, 5.0, 10.0, 15.0, 25.0, and 50.0 fmol) (in triplicate), followed by regression analysis of the actual and the observed amounts of N7-THBG. Solvent blanks were periodically injected to monitor for potential analyte carry-over.

Method validation

DNA from untreated human fibrosarcoma (HT1080) cells (150 μg aliquots, in triplicate) was spiked with 0, 1, 5, 10, 15, 25 or 50 fmol of N7-THBG and 50 fmol of $^{15}N_5$-N7-THBG internal standard. Following neutral thermal hydrolysis at 70 °C for 1 h, samples were filtered through Nanosep-10K ultra centrifugation devices to remove partially depurinated DNA. Samples were then enriched for N7-THBG and its internal standard by solid phase extraction on Isolute ENV+ and subjected to capillary HPLC-ESI$^+$-HRMS/MS analysis as described above. N7-THBG amounts were expressed as adduct numbers per 10^9 normal nucleotides, and N7-THBG amounts endogenously present in human HT1080 cells (2.03 fmol/150 μg DNA) were subtracted from each value. The observed amounts of N7-THBG were plotted against the theoretical values, followed by regression analysis. DNA amounts were determined by HPLC-UV analysis of dG in DNA hydrolysates.[26]

Determination of LOD/LOQ, precession, and accuracy

The LOD values of the new HPLC-ESI$^+$-HRMS/MS method were determined by spikingsynthetic oligodeoxynucleotide (5'-TCAGATTCGCGCCGGCTGCGATAAGCT-3',150 μg) with increasing amounts of N7-THBG (0, 0.3, 0.5, or 1 fmol) and a fixed amount of $^{15}N_5$-N7-THBG (50 fmol, internal standard for mass spectrometry), followed by sample processing and HPLC-ESI$^+$-HRMS/MS analysis by the standard methodology. Synthetic DNA was employed in these experiments because DNA from all biological sources examined contained endogenous N7-THBG (2 -3 fmol/150 μg DNA). The LOD value was determined as the analyte amount that consistently produced HPLC-ESI$^+$-HRMS/MS signal-to-noise ratios above 3. The limit of quantitation was defined by identifying minimum analyte amounts that produced a coefficient of variation less than 15% and a signal-to-noise ratio (S/N) greater than 10. To evaluate the inter-day and intra-day accuracy and precision of the new method, N7-THBG (1.0 fmol) and $^{15}N_5$-N7-THBG (50.0 fmol) were spiked into synthetic oligodeoxy-nucleotide solution (150 μg). Samples were processed as described above and analyzed three times per day on three consecutive days. Method accuracy was calculated from the equation ($A_m/A_a \times 100\%$), where A_m is the measured amount of N7-THBG and A_a is the actual amount added.

SPE recovery was determined by adding [$^{15}N_5$]-N7-THBG (50 fmol) to synthetic oligodeoxynucleotide solution (150 μg) and processing the samples as described above. N7-THBG standard (75 fmol) was added immediately prior to HPLC-ESI$^+$-HRMS/MS analysis, and the recovery was determined by comparing the theoretical and the observed [$^{15}N_5$]-N7-THBG:N7-THBG peak area ratios.

4.3 Results

4.3.1 Experimental approach

Human exposure to BD is common due to it ubiquitous presence in urban air *(207;275;276)*, cigarette smoke *(208;279)*, and its extensive use in plastic and rubber industries *(86;87;209;274)*. Classified as a human carcinogen, BD induces tumors in laboratory animals and increases the risk for hematopoietic cancer in occupationally exposed individuals *(91)*. The goal of the present study was to develop a non-invasive, mechanism-based biomarker of BD exposure and metabolism to DNA-reactive epoxides. N7-THBG adducts (Scheme 4.1) have been chosen because they are the most abundant BD-DNA lesions *in vivo (75;104;115;215)*.

Ultra-sensitive analytical methodology was required to enable the detection and accurate quantification of N7-THBG in human samples. In our approach, DNA isolated from human blood buffy coat (35-150 μg) is spiked with $^{15}N_5$-N7-THBG internal standard, and the adducts of interest are released from the DNA backbone by thermal hydrolysis (Scheme 4.2) *(74;75;104;215)*. This is possible due to the intrinsic instability of the *N*-glycosidic bond on N7-alkylguanine lesions in DNA *(278)*. Initial experiments have compared the efficiency of N7-THBG release following neutral thermal hydrolysis for 1 h at 70 °C versus heating at 80 °C for 1 h as reported previously *(215)*. We found that thermal hydrolysis at a lower temperature (70 °C) was equally effective at releasing N7-THBG, but produced lower background of unmodified bases than hydrolysis at 80 °C (results not shown). Following thermal hydrolysis, partially depurinated DNA was removed by ultrafiltration, and N7-THBG and its internal standard were purified by solid phase extraction on Isolute ENV+ (50 mg/1 mL) cartridges (Scheme 4.2). SPE recovery

(92.6 ± 1.8%) was determined by spiking synthetic oligodeoxynucleotide (150 μg) with known amounts of the analyte. We found that Isolute ENV+ cartridges (Biotage) provided the best recovery as compared to other SPE stationary phases tested.

4.3.2 HPLC-ESI$^+$-HRMS/MS method development for N7-THBG

N7-THBG is a highly polar molecule due to the presence of hydrophilic 2,3,4-trihydroxybut-1-yl substituent on the guanine base, leading to its poor retention on reversed phase HPLC columns. Our HPLC-ESI$^+$-HRMS/MS method development efforts for N7-THBG have explored a wide range of stationary phases, including Synergi Polar RP, Synergi Max RP, and Synergi Hydro RP from Phenomenex (Torrance, CA), Hypercarb (Thermo Fisher Scientific, West Palm Beach, FL), and Zorbax SB C18 (Agilent Technologies, Palo Alto, CA). The best results in terms of analyte retention and HPLC peak shape were achieved with Synergi Hydro RP column (Phenomenex). Among HPLC mobile phases tested, a gradient of 0.05% acetic acid in water and acetonitrile has afforded the best chromatography and optimal ionization efficiency.

Our initial HPLC-ESI$^+$-MS/MS method for N7-THBG was based on column switching, with Synergi Max RP 80R (150 × 0.5 mm, 4 μm) as a trap column (5 min at 10 μL/min of 0.05% acetic acid in water) and Synergi Hydro RP (250 × 0.5 mm, 4 μm) as an analytical column. HPLC separation was achieved using gradient elution with acetonitrile and 0.05% acetic acid in water at 10 μL/min. A TSQ Vantage triple quadrupole mass spectrometer was operated in the SRM mode by monitoring the neutral loss of guanine from the analyte and the $^{15}N_5$-lebeled internal standard, respectively (*m/z* 256.1$[M+H]^+ \rightarrow$ 152.1 $[Gua + H]^+$) and $^{15}N_5$ -guanine (*m/z* 261.1 $[^{15}N_5\text{-}M + H]^+ \rightarrow$ *m/z* 157.1 $[^{15}N_5\text{-}Gua + H]^+$).

Scheme 4.2: Analytical procedure for isotope dilution HPLC-ESI$^+$-HRMS/MS analysis of N7-THBG in human leukocyte DNA.

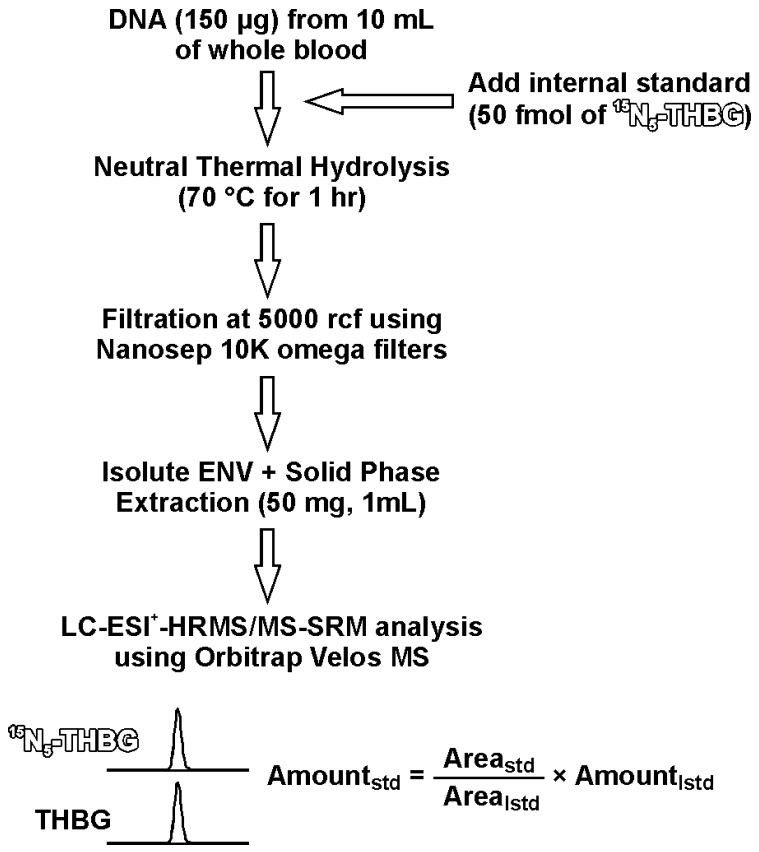

These SRM transitions were selected based on ESI-MS/MS infusion results for authentic standards *(74;75;104;215)*. However, the sensitivity of this method (LOQ, 5 fmol) was insufficient for human biomonitoring due to poor signal to noise ratios and the high sample matrix background in human samples (Figure 4.1). To enable N7-THBG quantification in human DNA, we have developed a new method that takes advantage of the high resolution capabilities of the Orbitrap Velos mass spectrometer (HPLC-ESI^+-HRMS/MS-MS). In our approach, SPE-purified samples (8 µL out of the total 24 µL) are directly injected onto capillary HPLC column for ESI^+-HRMS/MS analysis, avoiding the need for lengthy column switching. The same SRM transitions listed above are monitored, but the fragment ions are detected in the accurate mass mode: *m/z* 256.1$[M+H]^+ \rightarrow$ 152.05669 $[Gua + H]^+$ for N7-THBG and *m/z* 261.1 $[^{15}N_5\text{-}M + H]^+ \rightarrow$ 157.04187 $[^{15}N_5\text{-}Gua + H]^+$ (Figure 4.2). As shown in Figure 4.3, the use of high resolution MS dramatically improves the signal to noise ratios for N7-THBG (LOD, 100 amol), facilitating its detection in human DNA. An additional SRM transition (*m/z* 256.1$[M+H]^+ \rightarrow$ 135.03014 $[Gua -NH_2 + H]^+$ and *m/z* 261.1 $[^{15}N_5\text{-}M + H]^+ \rightarrow$ 139.01828 $[^{15}N_5\text{-}Gua -NH_2 + H]^+$ was employed for confirmation purposes.

Figure 4.1: Chromatogram of N7-THBG in smokers DNA sample with poor sensitivity and S/N ratio of a column switching TSQ vantage triple quadrupole SRM method. S/N ratio is 4 for 1.82 fmol on column.

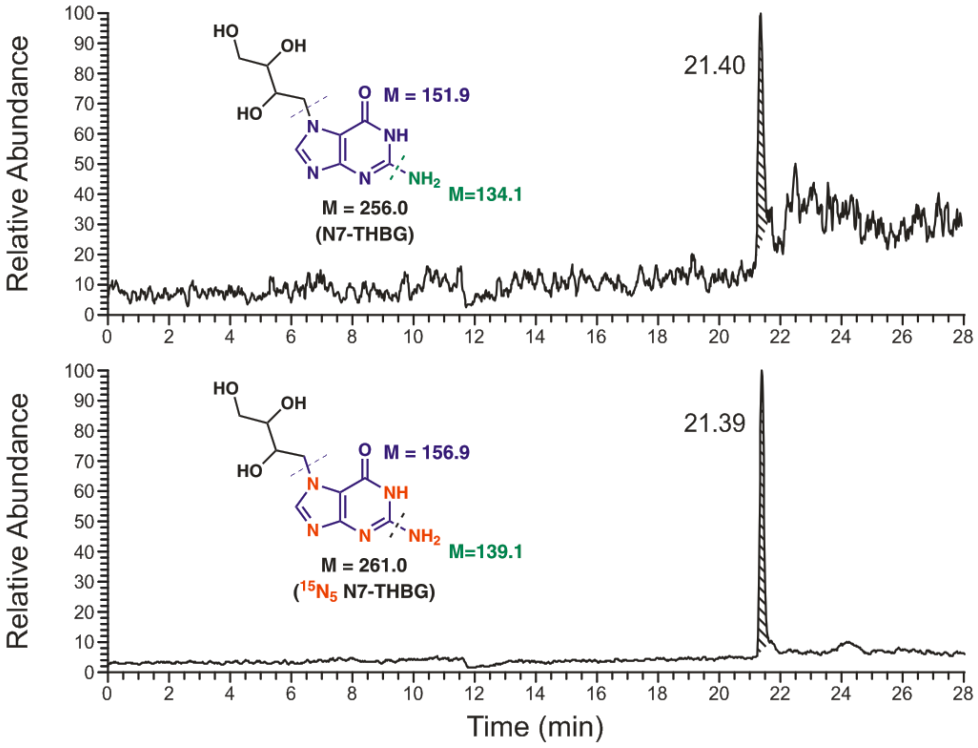

Figure 4.2 HPLC-ESI^{+}-HRMS/MS extracted ion chromatograms (A) and MS/MS spectra of synthetic N7-THBG (4 fmol) and [$^{15}N_5$]-N7-THBG (50 fmol) (B).

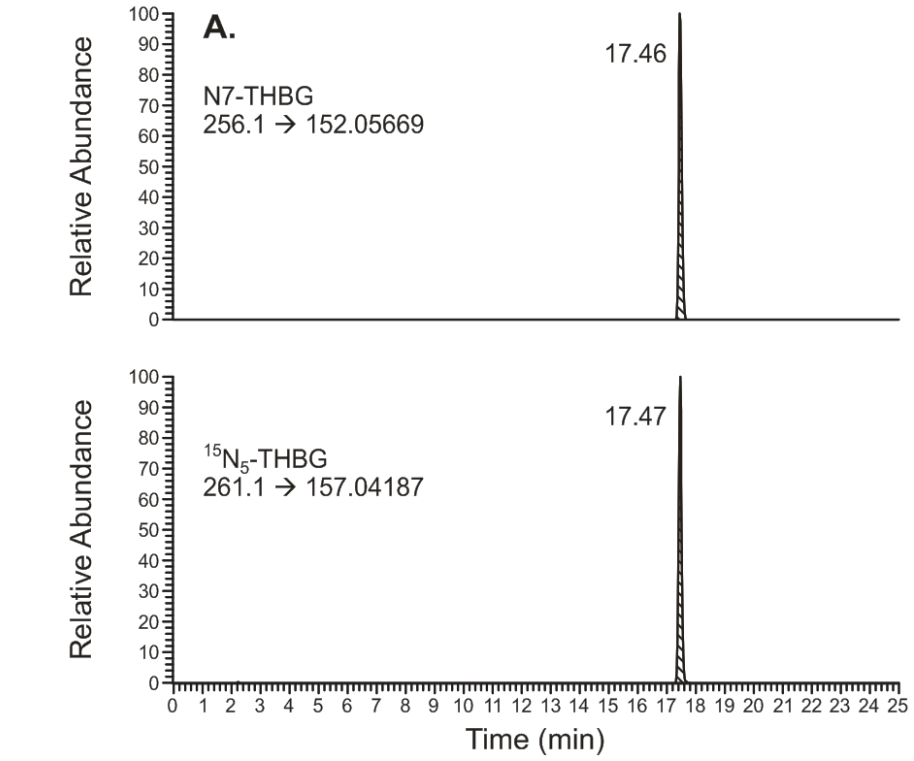

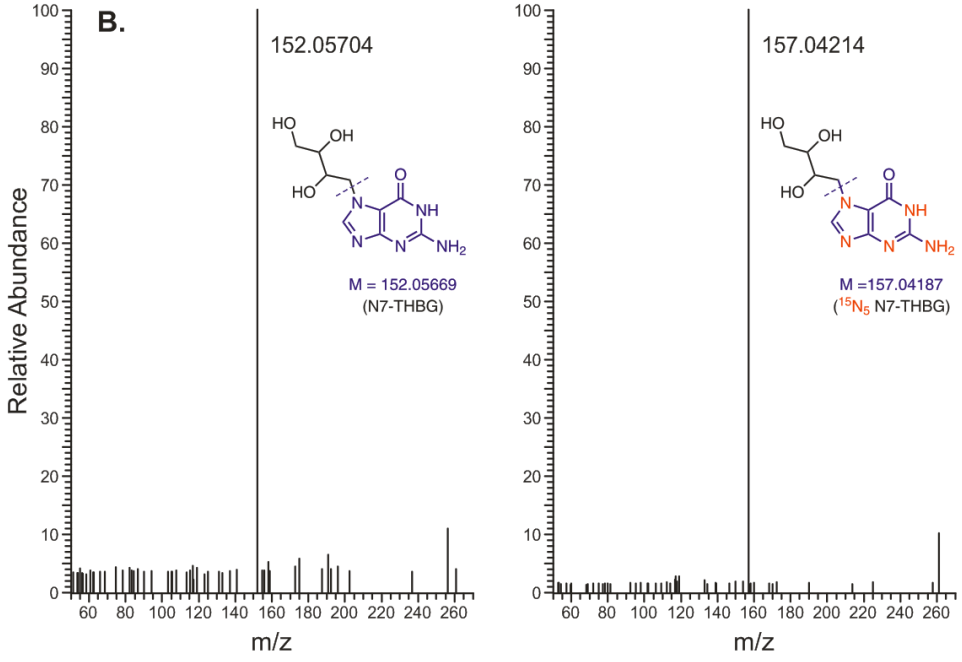

Figure 4.3 HPLC-ESI$^+$-HRMS/MS analysis of N7-THBG in leukocyte DNA of a smoker (A, 34 μg DNA hydrolysate on column) and an occupationally BD exposed worker (B, 25 μg DNA on column). DNA isolated from human blood buffy coat (80-100 μg total) was spiked with $^{15}N_5$-N7-THBG internal standard and subjected to thermal hydrolysis, sample processing, and high resolution HPLC-ESI$^+$-MS/MS analysis on an Obitrap Velos mass spectrometer.

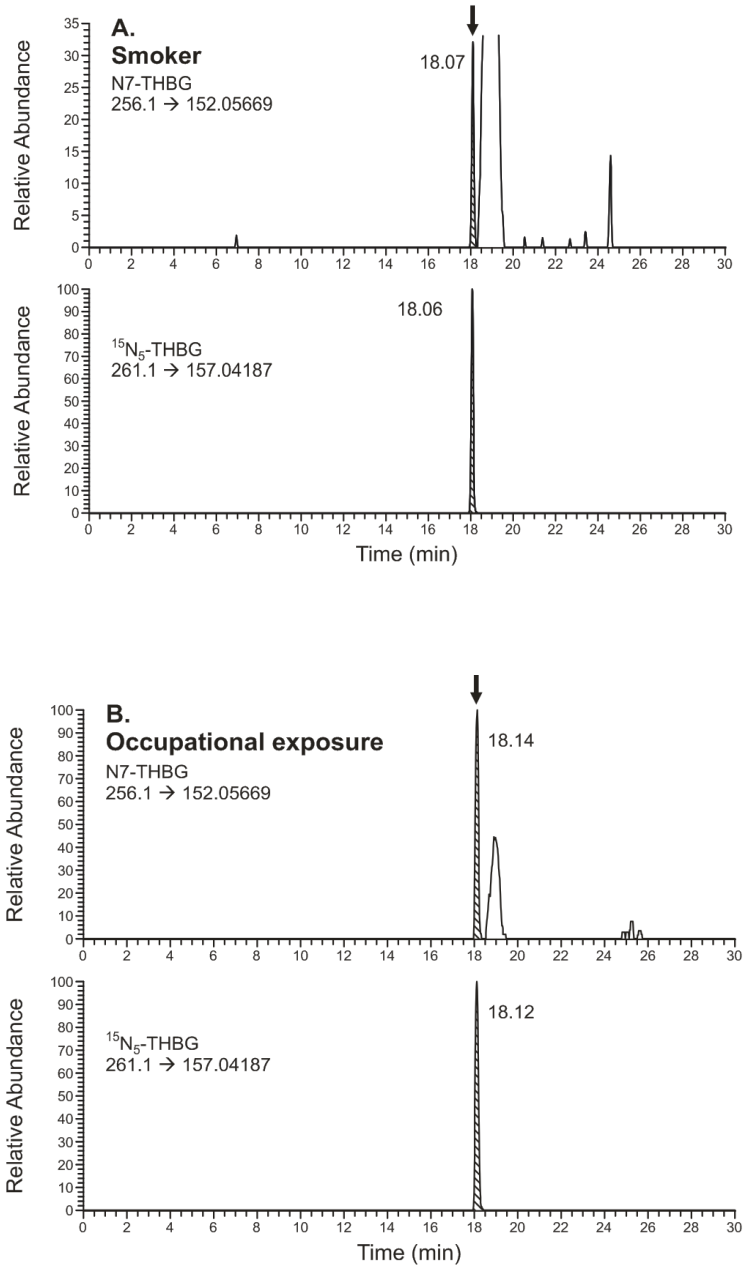

4.3.3 Method validation

The new capillary HPLC-ESI$^+$-HRMS/MS method was validated by analyzing control DNA from untreated human fibrosarcoma (HT1080) cells spiked with 1.0 -50.0 fmol N7-THBG and 50.0 fmol $^{15}N_5$-N7-THBG internal standard. The calculated N7-THBG amounts were corrected for the analyte endogenously present in HT1080 cells (2.03 fmol/150 μg DNA). An excellent correlation between the spiked and the observed amounts of the analyte was obtained, with an R^2 value of 0.998 (Figure 4.4). Method accuracy and precision were determined by analyzing replicate samples of N7-THBG (1.0 fmol) spiked into 150 μg of synthetic oligonucleotide solution. Method accuracy was calculated as 92.3 ± 6.7% (n = 5), with the interday and intraday precision less than 13% RSD (Table 4.1).

In order to evaluate HPLC-ESI$^+$-HRMS/MS method sensitivity, aliquots of synthetic DNA oligodeoxynucleotide (150 μg) were spiked with known amounts of N7-THBG standard (0.1, 0.3. 0.5, or 1.0 fmol), followed by hydrolysis and sample processing by standard methodology (Scheme 4.2). We chose synthetic DNA for these experiments because all DNA samples of biological origin, e.g. calf thymus DNA, salmon sperm DNA, human placental DNA, and DNA isolated from human fibrosarcoma (HT1080) cells, contained significant amounts of N7-THBG (20-40 N7-THBG adducts /10^9 nucleotides).

Table 4-1 Accuracy and precision results for N7-THBG at 1 fmol spiked in 150µg of oligonucleotide solution.

Day	Parameter	value
Day 1	Mean	0.99
	RSD (%)	3.35
	Accuracy (%)	99.8
	N	3
Day 2	Mean	1.10
	RSD (%)	12.3
	Accuracy (%)	110.2
	N	3
Day 3	Mean	1.01
	RSD (%)	12.99
	Accuracy (%)	101.7
	N	3
Interday	Mean	1.03
	RSD (%)	10.3
	Accuracy (%)	103.9
	N	9

Figure 4.4 Correlation between the theoretical and the observed amounts of N7-THBG in spiked DNA. DNA isolated from untreated human fibrosarcoma cells (150 μg) was spiked with 0, 1, 5, 10, 15, 25, or 50 fmol of N7-THBG and 50 fmol of $^{15}N_5$-N7-THBG internal standard, followed by sample processing and capillary HPLC-ESI$^+$-HRMS/MS analysis as shown in Scheme 4.2 and described in text. N7-THBG amounts observed in control sample (20 adducts/10^9 nucleotides) were subtracted from each value. The calculated N7-THBG amounts were plotted against the theoretical values.

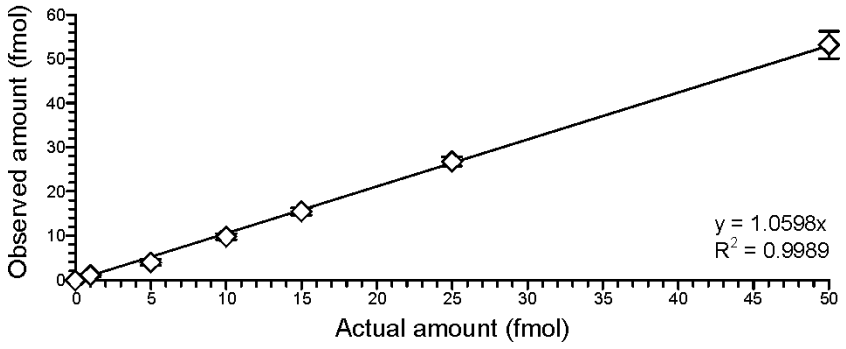

The HPLC-ESI$^+$-HRMS/MS limit of detection for N7-THBG spiked into 150 μg synthetic oligodeoxynucleotide solution was determined as 0.3 fmol (0.6 adducts/10^9 nucleotides), which gave the signal to noise ratio ≥ 3. No N7-THBG was detected in unfortified oligodeoxynucleotide samples, confirming that there was no analyte carryover and no artifactual N7-THBG production during the sample preparation and analysis. Method limit of quantitation was defined as the lowest N7-THBG amounts that afforded the signal to noise ratios of > 10 and intra/inter day precision within 15 % CV. We found that the LOQ value of our capillary HPLC-ESI$^+$-HRMS/MS method for N7-THBG was 1 fmol analyte in 150 μg of DNA (2 adducts per 10^9 nucleotides).

4.3.4 N7-THBG quantitation in HT1080 cell culture

To examine N7-THBG formation in a cell culture model, HT1080 cells were treated with increasing concentrations of DEB (10 nM – 100 μM). DNA was extracted and analyzed by HPLC-ESI$^+$-HRMS/MS methods described above. Adduct concentrations were unchanged from the background values in cells treated with 0 - 100 nM DEB, but increased linearly from 31.48 ± 4.84 adducts /10^9 nucleotides in cells treated with 1 μM DEB to 966.55 ± 128.05 adducts/10^9 nucleotides in cells treated with 100 μM DEB (Figure 4.5).

Figure 4.5 Concentration-dependent formation of N7-THBG adduct levels in HT1080 cells treated with increasing amounts of DEB (1-100 μM). N7-THBG amounts observed in control sample (20 adducts/10^9 nucleotides) were subtracted from each value.

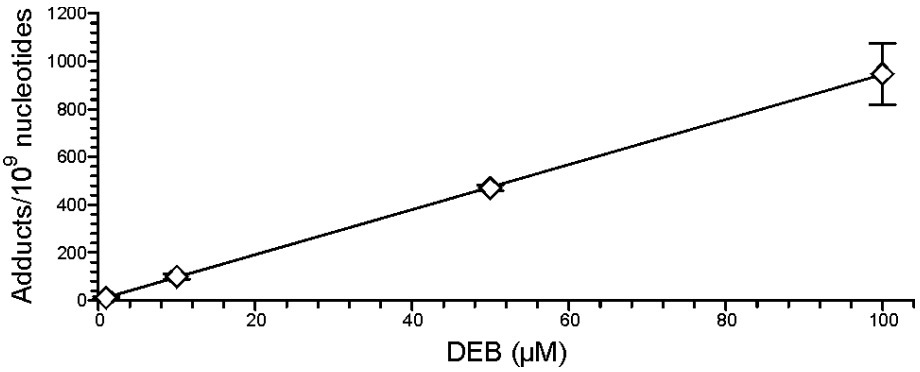

4.3.5 N7-THBG quantitation in blood of confirmed smokers and non-smokers and the effect of smoking cessation

Having confirmed the effectiveness of the new method in a cell culture model (Figure 4.5), we proceeded to quantify N7-THBG adducts in leukocyte DNA of known smokers and the corresponding controls. Cigarette smoke contains high amounts of BD (~ 46 μg/ cigarette in main-stream smoke and 283 μg/cigarette in side-stream smoke) *(90)*, leading to significant exposure of smokers to this carcinogen. DNA samples from smokers and nonsmokers (13 per group) were analyzed.

HPLC-ESI^+-HRMS/MS analysis has revealed the presence of N7-THBG in DNA hydrolysates from human samples (Figure 4.2). N7-THBG amounts in DNA were expressed as the number of adducts per 10^9 nucleotides, with DNA amounts determined from HPLC analysis of dG in DNA hydrolysates. *(113)* The concentrations of N7-THBG in leukocyte DNA of smokers were 8.20 ± 5.12 adducts /10^9 nucleotides (range 2.22 – 19.03), while the corresponding values for nonsmokers were 7.08 ± 5.29 adducts /10^9 nucleotides (range 0.77 – 15.73) (Table 4.2). Although smoker DNA contained higher numbers of adducts, the differences in N7-THBG concentrations in DNA of smokers and non-smokers were not statistically significant in this pilot study ($p = 0.60$, two-sample t-test).

Table 4-2 Effect of smoking on N7-THBG concentration in human leukocyte DNA

Smokers					
sample	**gender**	**age**	**DNA analyzed (µg)[a]**	**Cigarettes /day**	**Adducts/10^9 nucleotides**
1	M	52	77.3	11	11.23
2	F	35	77.8	26	<0.9
3	M	57	82.6	7	2.22
4	M	48	38.3	9	5.73
5	F	19	79.6	23	2.71
6	F	32	73.9	13	6.03
7	F	61	78.8	24	19.03
8	M	23	89.9	19	6.39
9	F	51	101.6	12	14.97
10	F	54	107.5	26	10.28
11	M	43	100.7	29	5.36
12[c]	F	33	38.8	19	3.97
13[c]	F	44	42.1	15	10.58
Mean ± SD		42.5 ± 13.1	144.2 ± 20.8	17.9 ± 7.3	8.20 ± 5.12

nonsmokers				
sample	**gender**	**Age**	**DNA analyzed (µg)[a]**	**Adducts/10^9 nucleotides**
14	F	27	93.3	0.79[b]
15	M	24	87.2	3.01
16	F	33	92.7	5.92
17	F	20	103.0	1.17[b]
18	F	34	92.9	<0.9
19	M	24	108.2	15.73
20	F	22	154.5	11.54
21	M	53	122.9	8.45
22	F	53	111.7	16.05
23[c]	F	44	102.4	6.83
24[c]	M	28	107.9	0.91[b]
25[c]	M	28	59.7	7.40
26[c]	M	35	35.9	7.14
Mean ± SD		32.7 ± 11.0	97.9 ± 28.5	7.07 ± 5.29

[a] One third of the total DNA amount was injected on column for HPLC-accurate mass MS/MS analysis. [b] Adduct amounts less than LOQ but greater than LOD. [c] Samples analyzed using an N7-THBG internal standard contaminated with 0.72 fmol of N7-THBG analyte which was subtracted from the quantified amount.

In order to directly evaluate the influence of smoking on N7-THBG adduct concentrations, N7-THBG was quantified in DNA of 10 individuals participating in a smoking cessation study. Two baseline samples were obtained before smoking cessation, and two additional samples were collected 28 and 84 days post smoking cessation. To afford sufficient DNA amounts (150 μg), samples from five smokers were pooled prior to DNA extraction, and combined samples were subjected to HPLC-ESI$^+$-HRMS/MS analysis of N7-THBG as described above. N7-THBG amounts post cessation were normalized to the baseline values. As shown in Figure 4.6, smoking cessation did not influence N7-THBG concentrations in human leukocyte DNA, suggesting that N7-THBG adducts in humans are not associated with smoking.

4.3.6 Influence of Occupational BD Exposure on N7-THBG Levels in Human DNA

To evaluate the effects of occupational exposure on adduct N7-THBG prevalence in human DNA, blood samples were obtained from ten individuals exposed to BD in a workplace (average BD concentration, 1.51 ± 1.12 ppm) and the corresponding controls (average BD concentration, 0.009 ± 0.012 ppm). We found that N7-THBG adduct concentrations were significantly elevated in leukocyte DNA of individuals occupationally exposed to BD (9.72 ± 3.80 adducts/ 10^9 nucleotides) as compared to matched controls (3.08 ± 2.15 adducts/ 10^9 nucleotides, $p = 0.00014$) (Table 4.3).

Figure 4.6 Percent reduction in N7-THBG adducts in leukocyte DNA of 10 individuals following smoking cessation. For each time point, DNA from 5 different subjects was pooled together to obtain sufficient sample size. Samples were collected 2 times before smoking cessation and 28, and 84 days following smoking cessation. The day when the smokers quit smoking is designated as day 0. Number of adducts per 109 nucleotides (mean ± SD) are shown below each point.

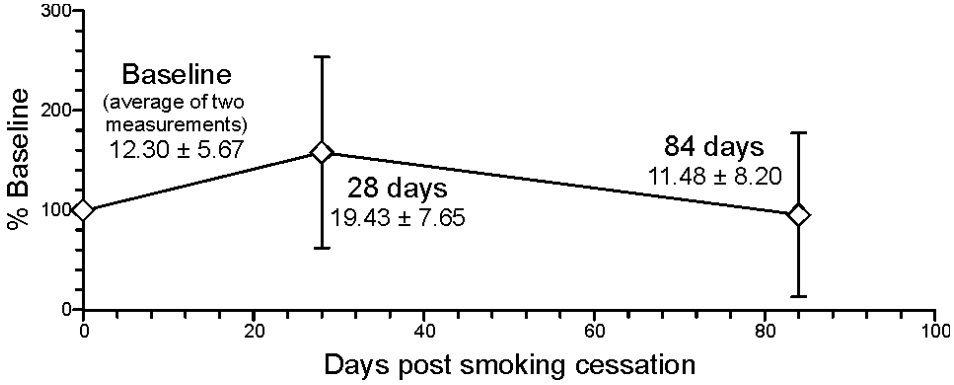

Table 4-3 Effect of occupational BD exposure on of N7-THBG concentrations in human leukocyte DNA

Controls				BD exposed			
sample	**BD exposure (ppm)**	**DNA analyzed (µg)[a]**	**Adducts/10^9 nucleotides**	**sample**	**BD exposure (ppm)**	**DNA analyzed (µg)[a]**	**Adducts/10^9 nucleotides**
1	0.005	91.7	1.02[b]	**11**	2.2	83.3	6.55
2	0.003	94.6	0.55[b]	**12**	3.1	103.9	9.93
3	0.004	94.8	6.64	**13**	1.2	86.6	6.65
4	0.005	98.7	1.56[b]	**14**	3.3	69.1	7.29
5	0.006	81.9	3.81	**15**	2.1	71.3	10.11
6	0.040	76.84	2.64	**16**	0.92	82.98	8.68
7	0.005	78.80	5.97	**17**	0.21	76.84	15.7
8	0.007	45.94	3.07	**18**	0.24	78.80	4.37
9	0.010	84.65	4.61	**19**	0.99	45.94	12.8
10	0.007	75.84	0.90[b]	**20**	0.83	84.65	15.1
Mean ± SD	0.009 ± 0.01	82.4 ± 15.2	3.08 ± 2.15		1.51 ± 1.11	78.3 ± 14.9	9.72 ± 3.79

[a] One third of total DNA amount was injected on column for HPLC-accurate mass MS/MS analysis. [b] Adduct amounts less than LOQ but greater than LOD.

4.4 Discussion

A recognized human and animal carcinogen, BD is metabolically activated to DNA-reactive epoxides which produce a range of nucleobase adducts including nucleobase monoadducts N7-(2-hydroxy-3-buten-1-yl)guanine (HB-Gua I), N7-(1-hydroxy-3-buten-2-yl)guanine (HB-Gua II), N7-(2,3,4-trihydroxy-3-buten-2-yl)guanine (THB-G), *1,N*^{6}-(2-hydroxy-3-hydroxymethylpropan-1,3-diyl)-2'-deoxyadenosine (1,*N*^{6}-*γ* HMHP-dA), *1,N*^{6}-(1-hydroxymethyl-2-hydroxypropan-1,3-diyl)-2'-deoxyadenosine (1,*N*^{6}-*α* HMHP-dA), DNA-DNA cross-links such as 4-*bis*-(guan-7-yl)-2,3-butanediol (*bis*-N7G-BD) and 1-(guan-7-yl)-4-(aden-1-yl)-2,3-butanediol (N7G-N1A-BD), and numerous DNA-protein cross-links *(91;107;115;116;198;266)*. If not repaired, BD-induced lesions can lead to heritable mutations by inducing polymerase errors *(14;280;281)*. N7-THBG are the most abundant DNA adducts generated upon exposure to BD *(75;104;115;215)*, and thus have been selected for development of mechanism-based human biomarkers of BD exposure and activation to DNA-reactive epoxides in the present study.

Several reports have previously quantified N7-THBG formation in tissues of laboratory rats and mice exposed to BD by inhalation. The first method for N7-THBG employed analytical flow HPLC-ESI$^+$-MS/MS to detect these adducts in livers of rats and mice exposed to 1250 ppm BD for 14 days *(104)*. Neutral thermal hydrolysis was used to release N7-THBG bases from the DNA backbone, followed by ultra-filtration, solid phase extraction, and HPLC-ESI$^+$-MS/MS analysis *(104)*. N7-THBG adducts were observed in liver DNA of mice (7.6 ± 1.5 adducts/10^6 nucleotides) and rats (4.1 ± 1.5 adducts/10^6 nucleotides) *(104)*. Oe et al. further optimized the HPLC-ESI$^+$-MS/MS methodology to separately quantify *SS,RR* and *meso* forms of N7-THBG in DNA of rats

and mice treated with 1250 ppm of BD *(267)*. (±) N7-THBG concentrations in liver DNA increased from 0.1 per 10^6 nucleotides to 1.6 adducts per 10^6 nucleotides in rats and from 1.3 adducts per 10^6 nucleotides to 3.9 adducts per 10^6 adducts in mice between 1 and 10 days of inhalation exposure to BD. *Meso* N7-THBG levels in the liver increased from 0.1 per 10^6 nucleotides to 0.8 adducts per 10^6 per 10^6 nucleotides in rats and from 0.6 per 10^6 nucleotides to 2.2 adducts per 10^6 nucleotides in mice upon continuous exposure to 1250 ppm BD for 1 or 10 days, respectively. Koc et al conducted a molecular dosimetry study of N7-THBG in mice and rats exposed to 0-625 ppm BD *(75)*. They observed a non-linear increase in N7-THBG adduct levels in liver, lung and kidney DNA of laboratory mice and rats exposed to BD. This was attributed to saturation of metabolic activation of BD starting at 62.5 ppm *(75)*. However, to our knowledge, N7-THBG has not been previously detected in humans.

N7-THBG adducts are relatively stable in double-stranded DNA, with an in vitro hydrolytic half-life is about 50h *in vitro* by first order kinetics *(215)*. *In vivo* half-lives of N7-THBG in tissues of laboratory mice and rats exposed to 1250 ppm of 1,3-butadiene are between 3.6 to 5.5 days, depending on adduct stereochemistry *(277)*. N7 guanine adducts are shown to be repaired and removed either by spontaneous hydrolysis or base excision repair generating abasic sites in the DNA *(282)*.

Human exposure to BD includes environmental sources (1-10 ppb in urban air) *(283;284)*, automobile exhaust (20-60 ppb) *(207;284)*, smoking (on average 46 μg/ cigarette in main-stream smoke and 283 μg/cigarette in side-stream smoke) *(90)* and workplace sources at butadiene monomer and polymer plants (< 2 ppm in the workplace) *(216)*. Since these levels of exposure are orders of magnitude lower than those employed

in inhalation studies of laboratory animals, human studies of BD-DNA adducts demand significantly more sensitive analytical methodologies.

Our initial studies have revealed that traditional HPLC-ESI$^+$-MS/MS analysis on a triple quadrupole mass spectrometer did not have adequate sensitivity and specificity for N7-THBG detection in DNA isolated from human leukocytes (Figure 4.1). This difficulty may be a result of low N7-THBG concentrations, the polar nature of the analyte, and its relatively low molecular weight (*m/z* 256.1), leading to increased background and poor HPLC-ESI$^+$-MS/MS signal to noise ratios. To overcome this challenge, we have taken advantage of the high resolution capabilities of the Orbitrap Velos mass spectrometer. A highly sensitive isotope dilution HPLC-ESI$^+$-HRMS/MS method has been developed that is characterized by greatly improved signal to noise ratios, high accuracy, and excellent precision as compared to traditional HPLC-ESI$^+$-MS/MS (compare Figures 4.1 and 4.3). To our knowledge, this the first report of N7-THBG formation in human DNA. The LOD and LOQ values of the new method (0.3 fmol and 1 fmol, respectively, when spiked into 150 μg of DNA) are sufficiently low to enable sensitive and accurate N7-THBG quantitation in humans. Our HPLC-ESI$^+$-HRMS/MS method does not separate two isomeric forms of N7-THBG, so the total amount of adducts were determined.

The new method was first employed to quantify N7-THBG in DNA of human fibrosarcoma (HT1080) cells treated with a range of DEB concentrations (0, 10 nM, 50 nM, 100 nM, 1 μM, 10 μM, 50 μM and 100 μM). Unexpectedly, we found that untreated cells contained measurable amounts of N7-THBG (~ 20 adducts per 10^9 nucleotides). Careful method validation and multiple control experiments have confirmed that this was not a result of contamination or analyte carryover. These results suggest N7-THBG

adduct can be formed endogenously. It has been hypothesized that 1,2-dihydroxy-3,4-epoxybutane (EBD) might be formed from dietary and/or endogenous sources linked to catabolism of carbohydrates *(129;140)*. Consistent with this observation, structurally analogous N-(2,3,4-trihydroxy-butyl)valine (THB-Val) hemoglobin adducts have been detected in control subjects with no known exposure to BD *(127)*. Similarly, DNA adducts such as N7-methylguanine *(285)*, N7-ethylguanine *(223)*, 1,N^2-etheno-2'-deoxyguanosine *(221;222)*, 1,N^2-propanodeoxyguanosine *(23)*, etheno adducts such as 1,N^6-ethenodeoxyadenosine (εdA), heptanone-etheno-2'-deoxyguanosine *(286)*, and 3,N^4-ethenodeoxycytine (εdC) are also endogenously found in human DNA *(287;288)*.

To determine the influence of smoking on N7-THBG concentrations in human DNA, HPLC-ESI$^+$-HRMS/MS analysis was conducted using DNA isolated from blood of 13 smokers and 13 non-smokers. N7-THBG concentrations were similar in DNA of smokers and non-smokers (8.21 ± 5.12 and 7.08 ± 5.29 adducts /10^9 nucleotides, respectively; P = 0.60, based on a two-sample t test) (Table 4.2). Furthermore, N7-THBG levels remained unchanged upon smoking cessation (Figure 4.6), suggesting that N7-THBG adduct levels in human leukocytes are not related to smoking. Environmental and/or endogenous sources may be responsible for this observation. In contrast, N7-THBG levels were significantly increased in leukocyte DNA of occupationally exposed individuals (9.73 ± 3.80 adducts/ 10^9 nucleotides in workers exposed to 1.51 ± 1.12 ppm, N = 10) as compared to matched controls exposed to 0.009 ± 0.012 ppm (3.07 ± 2.15 adducts/ 10^9 nucleotides, N = 10) (Table 4.3). This is not unexpected because occupational exposures to BD (~ 1- 2 ppm in our study) are much higher than those associated with smoking. However, it should be noted that in addition to BD, smokers are

exposed to ~ 60 of other known carcinogens, which can act in a synergistic manner to contribute to lung cancer development *(208;279)*.

Our quantitative results for N7-THBG in human leukocyte DNA are consistent with previously published results for other human BD-DNA adducts. For example, Hemminki et al. have employed ^{32}P-post-labelling to quantify N1-(2, 3, 4-trihydroxybut-1-yl)adenine (N1-THB-Ade) adducts in occupationally exposed individuals *(112)*. These authors have found statistically higher levels of N1-THB-Ade adducts in male workers occupationally exposed (4.5 ± 7.7 adducts/10^9 nucleotides) as compared to controls (0.8 ± 1.2 adducts/10^9 nucleotides) *(112)*. The differences in N1-THB-Ade adduct levels in smokers and nonsmokers were not statistically significant *(112)*. Since N7-THBG concentrations in DNA of smokers and non-smokers determined in our study are similar (Table 4.2) and are not influenced by smoking cessation (Figure 4.6), this suggests the presence of an endogenous source of N7-THBG in humans. Indeed, background levels of N7-THBG were also found in DNA isolated from freshly cultured human fibrosarcoma (HT1080) cells. Future studies are needed to establish the origins of endogenous N7-THBG in humans. However, occupational exposure to BD does increase N7-THBG concentrations in human blood (Table 4.3), suggesting that it can be a useful biomarker useful in BD risk assessment.

In summary, we have developed and validated an isotope dilution HPLC-ESI$^+$-HRMS/MS method for N7-THBG in human leukocyte DNA. The method has adequate accuracy and sensitivity for human biomonitoring. Future studies involving larger numbers of subjects need to be performed to further validate N7-THBG as a biomarker for BD exposure and metabolic activation to DNA-reactive metabolites.

V. NANO LC/ESI$^+$-HRMS^3 QUANTITATION OF DNA ADDUCTS INDUCED BY 1,3-BUTADIENE

Reprinted with permission from: Dewakar Sangaraju, Peter W. Villalta, Susith Wickramaratne, James Swenberg, and Natalia Tretyakova . J Am Soc Mass Spectrom. 2014, 25(7), 1124-35 © 2014 Springer, Part of Springer Science + Business Media

5.1 Introduction

Humans are exposed to numerous exogenous and endogenous chemicals present in automobile exhaust, urban air, water, food, and cigarette smoke *(1-3)*. Among these is 1,3-butadiene (BD), a prominent industrial and environmental pollutant classified as a known carcinogen *(84;85;91;276)*. Human exposure to BD is due to its presence in automobile exhaust (20-60 ppb) *(284)*, cigarette smoke (8.5-48.2 μg/cigarette) *(289)*, wood fires (0.14-0.17 ppb) *(290)*, and occupational sources in BD monomer and polymer industries *(127;216;274)*.

BD undergoes cytochrome P450-mediated metabolic activation to three epoxide metabolites: 3,4-epoxy-1-butene (EB), 1,2,3,4-diepoxybutane (DEB), and 1,2-dihydroxy-3,4-epoxybutane (EBD) (Scheme 5.1) *(92)*. These electrophilic epoxides are held responsible for the carcinogenicity and mutagenicity of BD because of their propensity to react with DNA to form covalent nucleobase adducts *(104;105;114;115;267)*, which can cause DNA polymerase errors *(14;98;291;292)*. Sensitive and specific quantitative methods for BD-DNA adducts *in vivo* are needed because they can be used in human cancer risk assessment *(18;293)*.

3,4-Epoxy-1-butene (EB) is the second most abundant epoxide formed upon metabolic activation of BD. EB reacts with the N7-position of guanine in DNA to form N-7-(2-hydroxy-3-buten-1-yl) guanine (EB-GI) and N-7-(1-hydroxy-3-buten-2-yl) guanine (EB-GII) adducts (Scheme 5.1) *(104;265)*. EB-GI and EB-GII can be used as biomarkers of BD exposure and bioactivation, along with the corresponding hemoglobin adducts (N-(2-hydroxy-3-buten-1-yl)-valine (HB-Val)) *(119)* and urinary metabolites (2-(N-acetyl-L-cystein-S-yl)-1-hydroxybut-3-ene and 1-(N-acetyl-L-cystein-S-yl)-2-hydroxybut-3-ene (MHBMA) *(140)*. While globin adducts and urinary metabolites have been extensively used as biomarkers of BD exposure and metabolic activation *(116;117;119;120;140;141)*, one important advantage of DNA adducts is that they represent the biologically relevant dose of BD and thus are directly associated with BD-mediated mutagenesis and cancer.

Scheme 5.1 Bioactivation of BD to electrophilic epoxides and the formation of EB Guanine adducts in DNA. EH, epoxide hydrolase; EB-GI, N-7-(2-hydroxy-3-buten-1-yl) guanine; EB-GII, N-7-(1-hydroxy-3-buten-2-yl) guanine.

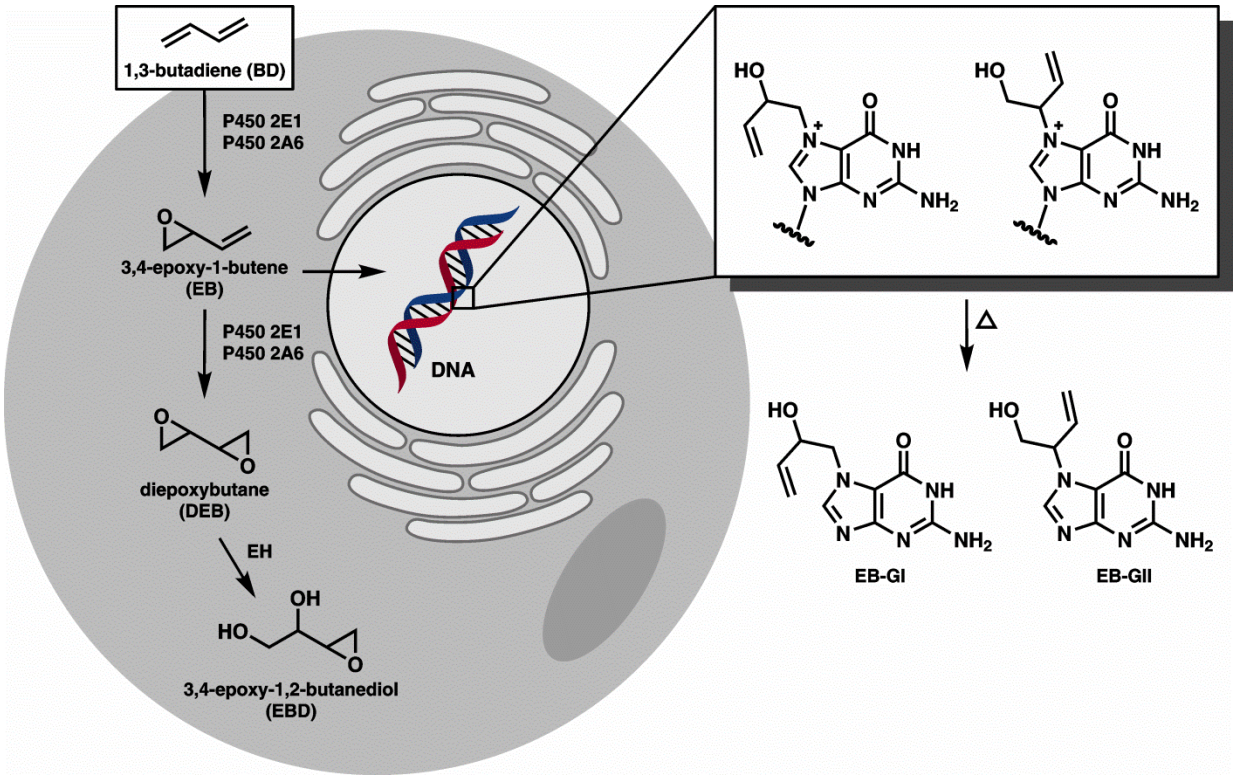

In the present study, a nanoHPLC-high resolution tandem mass spectrometry (nanoLC/ESI$^+$-HRMS^3) methodology utilizing an Orbitrap Velos mass spectrometer was developed to allow for sensitive and specific quantitation of EB-GII adducts *in vivo*. EB-GII adducts were quantified by isotope dilution with the corresponding ^{15}N-labeled internal standard. The new method was fully validated and applied to determine the concentrations of EB-GII in human fibrosarcoma (HT1080) cells treated with increasing concentrations of EB (50 nM to 10 μM), in liver tissues of laboratory rats exposed to BD by inhalation, and in human blood DNA.

5.2 Materials and Methods

Note: *EB is a known carcinogen and must be handled with adequate safety precautions. Phenol and chloroform are toxic chemicals which should be used only in a well-ventilated fume hood with appropriate personal protective equipment.*

Puregene DNA purification reagents were obtained from Qiagen (Valencia, CA). LC-MS grade water, methanol and acetonitrile were purchased from Fisher Scientific (Pittsburgh, PA). All other chemicals and solvents were obtained from Sigma-Aldrich (Millwaukee, WI, St. Louis, MO). Nonsmoker blood buffy coat fractions were purchased from BioChemed (Winchester, VA). Blood samples from known smokers and nonsmokers were acquired from the NCI CRCHD repository (PI: Dr. Peter Shields).

Synthesis of EB-guanine standards and the corresponding $^{15}N_5$ internal standards

EB-GI and EB-GII were prepared as previously reported *(265;294)*. Briefly, dG (105 mg, 0.393 mmol) was reacted with 3,4-epoxy-1-butene (EB) (266 mg, 3.93 mmol) in 5 mL of glacial acetic acid at 50 °C for 5 h. The reaction mixture was precipitated with one volume of acetone and 4 volumes of ether, and the resulting white precipitate was air dried and dissolved in 1.5 mL of 1N HCl. The reaction mixtures was heated at 80 °C for 5 h to induce depurination, cooled down, and neutralized with NaOH. EB-GI and EB-GII were isolated by reverse phase HPLC on a Synergi Hydro RP 80R semipreparative column (250 mm × 10 mm, 4μ) (Phenomenex, Torrance, CA) using a gradient of water and acetonitrile at 2 mL/min. Under these conditions, EB-GI and EB-GII eluted at 22.5 and 24.1 min, respectively. Both adducts were characterized by UV spectrophotometry, ^{1}H NMR, and MS/MS, which were consistent with literature data *(265)*. $^{15}N_5$-EB-GI and $^{15}N_5$-EB-GII were prepared analogously starting with $^{15}N_5$–dG. Molar concentrations of

EB-G and $^{15}N_5$-EB-G standard solutions were determined by UV spectrophotometry using the molar extinction coefficient (ε) of 8030 M^{-1} cm^{-1} at 284 nm at neutral pH *(294)*. Isotopic purity of $^{15}N_5$-EB-GI and II as determined by mass spectrometry was 99.97 and 99.93 %, respectively.

HT1080 cell culture experiments

Human fibrosarcoma cells **(**HT1080) were grown in Dulbecco's modified Eagle's media supplemented with 9% fetal bovine serum (Life technologies, Grand Island, NY). Cells were cultured in a humidified atmosphere of 5% carbon dioxide and 95% air, at 37 °C. HT1080 cells were plated into 15 cm dishes using Dulbecco's modified Eagle's medium containing 9% FBS and permitted to adhere overnight at 37 °C. On the following morning, cells (in duplicate) were treated with increasing concentrations of EB (0, 500 nM, 1 μM, 5 μM or 10 μM) for 3 h at 37 °C. The EC_{50} for EB in HT1080 cells treated with 0.25 to 50 m for 48 h was 13.8 mM as determined by the alamar blue assay (Life technologies, Grand Island, NY). Control and treated cells (N = 3) were harvested, washed with ice cold phosphate-buffered saline (PBS), and suspended in 5mL of PBS for DNA extraction as described below.

Animals and Treatment

In the first study, male and female F344 rats (N = 3 per group) were exposed to 0.5, 1.0, or 1.5 ppm for 2 weeks (6 h/day, 5 days/week) using whole-body exposure chambers at the Lovelace Respiratory Research Institute (LRRI, Albuquerque, NM) as reported previously *(131)*.

In a separate study, female F344 rats (3 per group) were exposed to 1250 ppm BD by whole-body exposure chamber inhalation for 10 days (7 h/day) at LRRI. The animals

were sacrificed either immediately at the end of the exposure period or 1, 3, or 6 days post exposure as reported previously *(115)*. Liver tissue was collected, flash frozen, and shipped to the University of MN on dry ice, where they were stored at – 80 ℃ until DNA extraction. All protocols are approved by the Institutional Animal Care and Use Committee at LRRI.

Human study subjects

Human smoker and nonsmoker blood buffy coat (white blood cells) samples were obtained from the National Cancer Institute. These samples were a part of the NCI 3ARM study supported by National Cancer Institute contract HHSN261200644002 (Laboratory Assessment of Tobacco Use Behavior and Exposure to Toxins Among Users of New Tobacco Products Promoted to Reduce Harm; PI: Peter Shields, M.D.). National Cancer Institute, Washington, DC. Nonsmoker (N = 5) and smoker subjects (N = 3) were between the ages of 18 and 65. Smokers smoked at least 10 cigarettes daily for the past year had exhaled carbon monoxide (CO) levels of > 10 ppm. The nonsmokers have smoked less than 100 cigarettes in their life time. Smoking status was confirmed through CO measures and self-reported tobacco use diaries. All subjects were in good physical and mental health. Fasting blood was collected through venipuncture at various time points during the study. Samples were stored at − 80 °C until further analysis.

DNA isolation

DNA from control and EB-treated human fibrosarcoma (HT1080) cells was isolated using standard phenol-chloroform extraction *(217)*. DNA concentrations were estimated by nanodrop UV spectrophotometer (Thermo Scientific, Waltham, MA), and the DNA purity was assessed from A_{260} /A_{280} absorbance ratios, which was typically between 1.8 and 1.9. DNA amounts were accurately determined by dG quantitation in enzymatic hydrolysates as described previously *(217;295)*.

DNA from human blood samples was isolated using the manufacturer's protocol for DNA purification from buffy coat (Qiagen, Valencia, CA) *(223)* with minor modifications *(295)*. DNA isolation from rat liver was performed using the manufacturer's protocol for DNA purification from tissue (Qiagen, Valencia, CA). Briefly, 100-200 mg of liver tissue was homogenized in 4 mL of cell lysis buffer. Cell lysis was performed overnight following addition of 15 μL of proteinase K solution (20 mg/mL). On the following day, RNA digestion was performed by addition of 15 μL of RNase A solution (4 mg/mL) and incubation at room temperature for 2 h. Protein precipitation solution (1 mL) was added to the cell lysate, and the mixture was vortexed at a high speed for 20 s and centrifuged at 2000g for 15 min for removal of proteins. DNA was precipitated with isopropyl alcohol (5 mL) and washed twice with 1 mL of 70% ethanol in water.

Sample preparation and EB-GII enrichment (Scheme 5.2)

DNA samples (3-76 μg in water) were spiked with 3 fmol of $^{15}N_5$-EB-GII internal standard and heated at 90 ºC for 0.5 h to release EB-GII adducts from the DNA backbone as free bases. Partially depurinated DNA was removed by ultrafiltration with Nanosep 10K filters (Pall Life Sciences, Ann Arbor, MI) at 5000 g for 10 min. The filtrates containing EB-GII and its internal standard were subjected to offline HPLC purification using an Agilent 1100 series HPLC equipped with a UV detector and an automated fraction collector (Agilent Technologies, Palo Alto, CA). Offline HPLC purification was carried out using Zorbax Eclipse XDB-C18 column (4.6 × 150 mm, 5 μm, from Agilent Technologies, Palo Alto, CA) eluted at flow rate of 1 mL/min with a gradient of 0.4% formic acid in Milli-Q water (A)and HPLC grade acetonitrile (B). UV absorbance was monitored at 254 nm. Solvent composition was maintained at 0% for 5 min and then linearly changed to 3% in 10 min and further to 40% B in 5 min. The solvent composition was returned to 0% acetonitrile in 5 min and held at 0% for 15 min for column equilibration. Either 2′-deoxyadenosine (dA, 0.60 nmol) or 2′-deoxythymidine (dT, 0.62 nmol on column) was added as retention time markers, which eluted at 13.2 or 18.3 min, respectively. EB-GII typically eluted at 16.4 min. HPLC fractions containing EB-GII and its internal standard (15.8 – 17.8 min, 1 mL each) were collected in 1.2 mL MS total recovery vials (Thermo Fischer Scientific, Waltham, MA), concentrated under vacuum, and re-dissolved in water (10 μL) for nano-HPLC-nanoESI$^+$-HRMS^3 analysis. Typical injection volume was 5 μL.

Scheme 5.2 Analytical procedure for isotope dilution nanoLC/ESI$^+$ HRMS^3 analysis of EB-GII in DNA.

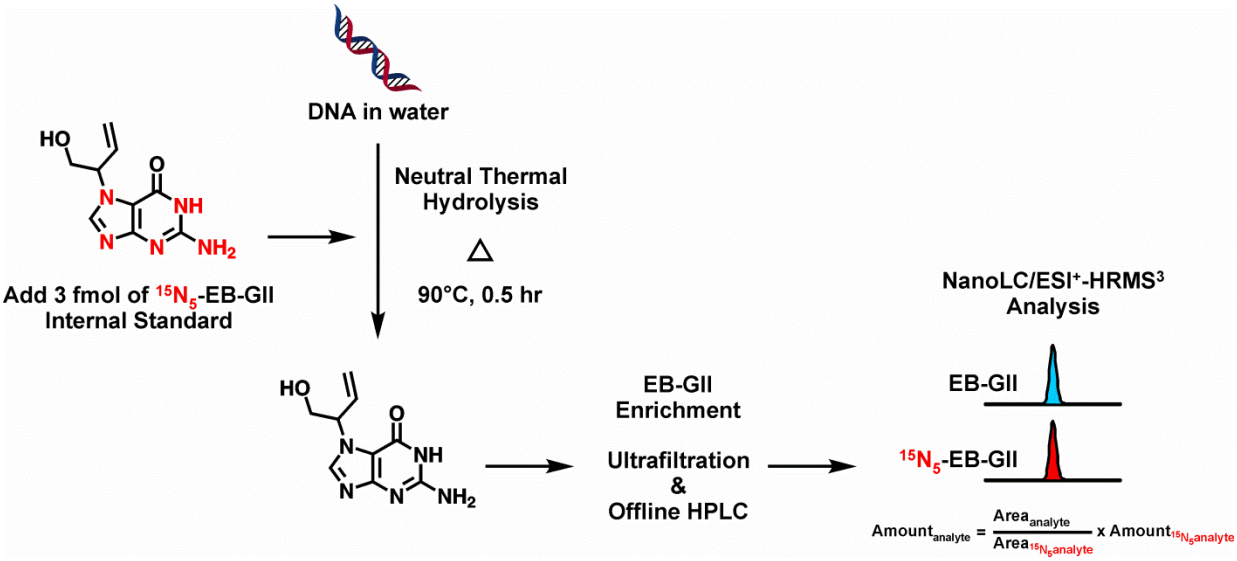

NanoLC/ESI$^+$-HRMS^3 analysis of EB –GII

A Nano2D-LC HPLC system (Eksigent, Dublin, CA) with 5 μL injection loop was interfaced to an LTQ Orbitrap Velos instrument equipped with a nanospray source (Thermo Fisher Scientific Corp., Waltham, MA). HPLC solvents were LC-MS grade water containing 0.01% acetic acid (A) and LC-MS grade acetonitrile containing 0.02% acetic acid (B). Samples (5 μL) were injected onto a trapping column (Symmetry C18 nanoAcquity, 0.18 × 20 mm, Waters Corp., Millford, MA) in line with a nano-LC column (0.075× 200 mm). The nano-LC column was prepared by manually packing a fused-silica emitter (New Objective, Woburn MA) with Synergi Hydro-RP, 80Å, 4 μm chromatographic packing (Phenomenex, Torrance, CA). Following sample injection (5 μL), the HPLC flow (2% B) was maintained at 1 μL/min for 5.5 min to enable sample loading onto the trapping column. The HPLC flow was then decreased to 300 nL/min and maintained at 2% B for 0.5 min. The organic phase content linearly increased to 25% B in 19 min and further to 50% B in 10 min, returned to 2% B in 2 min, and equilibrated for 7 min. Under these conditions, EB-GII eluted as a sharp peak at 20 min.

HPLC/ESI$^+$-HRMS^3 analyses were conducted in the nanoESI$^+$ mode using an LTQ Orbitrap Velos instrument (Thermo Scientific, Waltham, MA). Typical instrument settings included the spray voltage at 2.0 kV, capillary temperature at 350 °C, and S-Lens RF level at 40%. MS analysis was performed by fragmenting $[M + H]^+$ ions of EB-GII (*m/z* 222.1) via collision induced dissociation (CID) in the linear ion trap, with a normalized collision energy set at 25 units and the isolation width of 1.0 amu. The resulting MS/MS fragment ions at *m/z* 152.1 corresponding to protonated guanine $[Gua + H]^+$ were subjected to further fragmentation in the high collision dissociation (HCD) cell

using nitrogen as collision gas, normalized collision energy of 75 units, and an isolation width of 1.0 amu. The resulting MS^3 fragment ions were detected in the mass range of *m/z* 50 to *m/z* 270 using the Orbitrap mass analyzer at a resolution of ~ 25,000. EB-GII was quantified using extracted ion chromatograms from the combined signal of *m/z* 135.0301 ($[Gua - NH_3]^+$) and *m/z* 153.0411 ($[Gua - NH_3 + H_2O]^+$) at a mass tolerance of 5 ppm. The MS^3 fragments at *m/z* 153.0411 ($[Gua - NH_3 + H_2O]^+$) correspond to the adduction of water to *m/z* 135.0301 ($[Gua - NH_3]^+$) in the collision cell *(296)*.The $^{15}N_5$ labeled internal standard ($[^{15}N_5]$-EB-GII) was quantified using an analogous MS^3 scan event consisting of fragmentation of *m/z* 227.1 ($[M + H]^+$) to *m/z* 157.1 $[^{15}N_5$-Gua + $H]^+$ and further to *m/z* 139.0183 ($[^{15}N_5$-Gua – $NH_3]^+$). Extracted ion chromatograms corresponding to the sum of *m/z* 139.0183 ($[^{15}N_5$-Gua – $NH_3]^+$) and *m/z* 157.0283 ($[^{15}N_5$-Gua – $NH_3 + H_2O]^+$) at 5 ppm were generated and used for quantitation (Figure 5.1). A full scan event was also performed over the mass range of *m/z* 100-500 at a resolution of 7500 to monitor for any co-eluting matrix components. EB-GII amounts in DNA were expressed as adduct numbers per 10^8 normal nucleotides.

NanoLC/ESI^+-$HRMS^3$ standard curves were constructed by analyzing aqueous solutions containing fixed amounts of $^{15}N_5$-EB-GII (5 fmol) and increasing amounts of EB-GII (0.1, 0.5, 1, 3, 5, and 10.0 fmol) (in triplicate), followed by regression analysis of the actual and the observed amounts of EB-GII. 5 µL injections were made out of a 25 µL sample volume. Solvent blanks were periodically injected to monitor for any potential analyte carry-over.

Figure 5.1 Nano-HPLC-nanoESI^{+}-HRMS^{3} extracted ion chromatograms and MS^{3} spectra of synthetic EB guanine II (0.1 fmol) (A) and [$^{15}N_5$]-EB guanine II (5 fmol) (B).

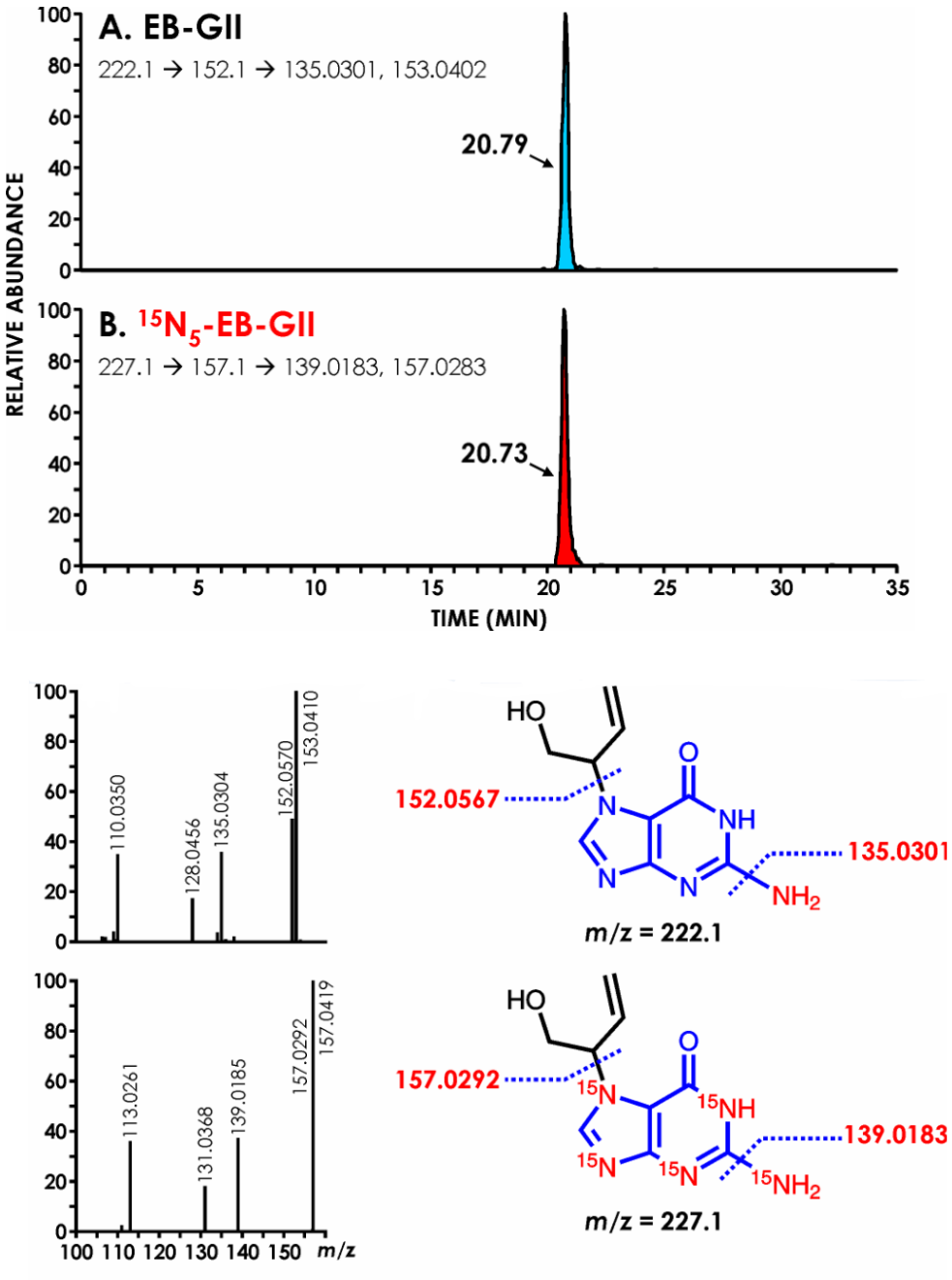

Figure 5.2 Nano-HPLC-nanoESI^{+}-HRMS^{3} method validation: correlation between the spiked and the observed amounts of EB-GII spiked into blank DNA. DNA isolated from nonsmoker blood leukocytes (150 µg) was spiked with 0, 0.2, 0.5, 1, 3, 5, 7 or 10 fmol of EB-GII and 3 fmol of $^{15}N_5$- EB-GII (internal standard), followed by sample processing and nano-HPLC-nanoESI^{+}-HRMS^{3} analysis.

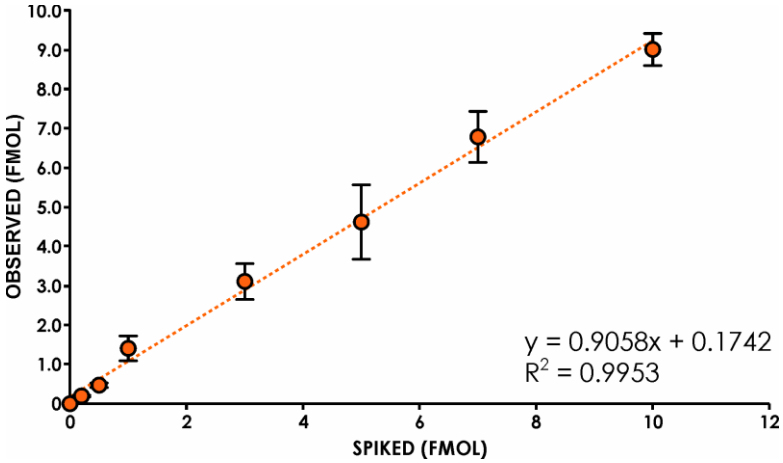

Method validation

DNA isolated from unexposed human leukocyte DNA (150 μg aliquots, in triplicate) was spiked with fixed amount of $^{15}N_5$-EB-GII (3 fmol, internal standard) and increasing amounts of EB-GII (0, 0.2, 0.5, 1, 3, 5, 7 or 10 fmol). Samples were processed by neutral thermal hydrolysis, ultrafiltration, and off-line HPLC as described above and subjected to nanoLC/ESI$^+$-HRMS^3 analysis. The observed amounts of EB-GII were plotted against the theoretical values, followed by regression analysis (Figure 5.2).

Determination of method LOD, LOQ, precision, and accuracy

The LOD values of the quantitative method for EB-GII were determined by spiking blank human DNA (150 μg) with increasing amounts of EB-GII (0, 0.05, 0.1, or 0.2 fmol) and a fixed amount of $^{15}N_5$-EB-GII (3 fmol), followed by sample processing and nanoLC/ESI$^+$-HRMS^3 analysis by standard methodology. The LOD value was determined as the analyte amount that consistently produced signal-to-noise ratios above 3. The limit of quantitation was defined as minimum analyte amount that produced a coefficient of variation less than 15% and a signal-to-noise ratio (S/N) greater than 10.

To evaluate the inter-day and intra-day accuracy and precision of the new method, EB-GII (0.2 fmol) and $^{15}N_5$-EB-GII (3.0 fmol) were spiked into blank human DNA (150 μg). Samples were processed as described above and analyzed three times per day on three consecutive days. Method accuracy was calculated from the equation ($A_m/A_a \times 100\%$), where A_m is the measured amount of EB-GII and A_a is the actual analyte amount added.

5.3 Results and Discussion

Because of their critical role in cancer development, DNA adducts represent mechanism-based biomarkers of carcinogen exposure, and their quantitation is particularly useful for cancer risk assessment. DNA adducts are also valuable in mechanistic studies linking tumorigenic effects of environmental and industrial carcinogens to specific electrophilic species generated from their metabolism. As discussed above, BD is among the most important industrial and environmental chemicals classified as known carcinogens *(87;297)*. Humans can be exposed to BD in an occupational setting at BD monomer/polymer industries *(216)* or as a result of inhaling cigarette smoke *(289)*, automobile exhaust *(284)*, and smoke from cooking and wood fires *(290)*. This is a cause of concern because of the established carcinogenicity of BD *(84;85;91;276)*.

The long term goal of this work is to develop sensitive biomarkers of human exposure to BD. We recently reported an isotope dilution accurate mass spectrometric method for another BD-DNA adduct, N7-(2,3,4-trihydroxybut-1-yl)-guanine (N7-THBG), which was detected in leukocyte DNA of smokers, nonsmokers, and occupationally exposed workers *(295)*. Unexpectedly, N7-THBG was also observed in samples from individuals with no known exposure to BD, and no significant decrease in N7-THBG levels was observed upon smoking cessation *(295)*. Therefore, THBG may be formed endogenously and does not accurately reflect human exposure to BD.

In an effort to develop a new BD-specific DNA biomarker, we turned our attention to structurally analogous EB-G adducts (Scheme 5.1). EB-GI and EB-GII are formed upon N7-guanine alkylation by 3,4-epoxybut-1-ene (EB). Because EB is formed

in lower amounts than 3,4-epoxy-1,2-butanediol (EBD), *in vivo* concentrations EB-GI and EB-GII adducts are approximately 10-fold lower than those of THBG following exposure to BD *(75)*, calling for a highly sensitive methodology.

Our method for quantitative analysis of EB-G adducts *in vivo* starts with DNA extraction from cells or tissues (Scheme 5.2). DNA purity is estimated by UV spectrophotometry (A 260/280 ratios) to minimize any contamination with cellular proteins. DNA samples (7-76 μg) are spiked with isotopically labeled internal standard ($^{15}N_5$-EB-GII) to account for any analyte loss during sample workup and to allow for absolute quantification. Since N7-guanine alkylation generates a positive charge on the adducted base and destabilizes the N-glycosidic bond, EB-G adducts can be selectively released from the DNA backbone as free bases by neutral thermal hydrolysis (Scheme 5.2) *(75;278)*. This step was optimized upon analyzing EB-treated calf thymus DNA. A range of depurination conditions were tested, including heating at 90 °C for 0.5 h (pH 6.8), 70 °C for 1 h (pH 6.8), and acidic thermal hydrolysis at 90 °C for 0.5 h (0.1N HCl). Since all three conditions were equally effective at releasing EB-G adducts from the DNA backbone (not shown), neutral thermal hydrolysis at 90 °C for 0.5 h in water was selected to minimize the depurination of unmodified nucleobases. Following ultrafiltration to remove partially depurinated DNA, EB-GII adducts were enriched by offline HPLC. Retention time markers (dT or dA) were added to account for any sample-dependent retention time shifts. Under our HPLC conditions, dA, EB-GI, EB-GII, and dT typically eluted at 13.2, 15.3, 16.4, and 18.3 min, respectively. In our experience, offline HPLC purification is the best option for isolating trace amounts of DNA adducts from DNA hydrolysates prior to LC-MS analysis because it affords nearly quantitative analyte

recovery, can be readily automated, and avoids the introduction of solid phase particles which can clog nano HPLC columns *(198)*. However, cross-contamination and analyte carryover can be a serious problem, so multiple HPLC blanks must be introduced throughout the analysis.

5.3.1 NanoLC/ESI$^+$-HRMS^3 method development

Our ultimate goal was to develop a quantitative method sensitive enough to detect EB-G adducts in tissues of laboratory animals exposed to sub-ppm levels of BD and in leukocyte DNA of smokers and occupationally exposed individuals. NanoHPLC-nanospray HPLC-MS methodology was employed because of its enhanced sensitivity as compared to conventional capillary LC-MS. Nanospray ionization is more efficient than conventional electrospray because of an improved ionization efficiency and an increased ion transport from the source into the mass spectrometer *(298)*. A number of stationary HPLC phases were tested, including Zorbax SB-C18 (Agilent Technologies), Hypercarb (Phenomenex), Luna C18 (Phenomenex), Synergi Hydro- RP 80Å (Phenomenex), and Synergi Polar-RP (Phenomenex). These solid phases were manually packed into commercial fused-silica Self-Pack PicoFrit emitters (200 mm x 75 μm, New Objective), with a 15 μm tip orifice diameter. The best results in terms of analyte retention and HPLC peak shape were obtained when using a Synergi Hydro-RP column eluted with a gradient of 0.01% acetic acid in water (A) and 0.02% acetic acid in acetonitrile (B) (Figure 5.1) This system has afforded a good EB-GII peak shape (Peak Asymmetry factor=1.16, tailing factor = 1.08), along with good retention time (RT 20.7 min) and theoretical plates (N) close to 40000, without any co-eluting peaks (Figure 5.1).

Our initial method development efforts have attempted to employ nanoHPLC-ESI-MS/MS on a triple quadrupole mass spectrometer. However, preliminary experiments with EB-G I and EB-G II pure standards spiked into synthetic DNA indicated that the sensitivity of this approach was insufficient for BD-DNA adduct detection in human samples. Other published HPLC-ESI-MS/MS methods for EB-guanine adducts *(75)* similarly reported moderate sensitivity for this analyte (typical LOD, 0.5 adducts/10^6nucleotides). To achieve detection limits in the low fmol to amol range (1 per 10^8-1 per 10^9 nucleotides) as required for our *in vivo* studies, we employed nanoLC/ESI^+-$HRMS^3$ methodology on an Orbitrap Velos mass spectrometer. We and others have recently reported the use of high resolution mass spectrometry for DNA adduct analysis in complex samples and have shown that it dramatically reduces the matrix background, leading to greatly improved signal to noise ratios *(54;69;223)*.

An LTQ Orbitrap Velos mass spectrometer was operated in the high resolution MS^3 scan mode to allow for highly selective detection of EB-GII adducts in a complex biological matrix. Protonated molecules of the analyte were trapped and fragmented in the linear ion trap (LTQ), and specific MS^2 fragments were axially ejected, fragmented in the HCD cell, and collected in a C-shaped ion trap (C-Trap) to be analyzed in the Orbitrap for accurate mass analysis. Initial fragmentation of protonated molecules of EB-GII and $^{15}N_5$-EB-GII (*m/z* 222.1 $[M + H]^+ \rightarrow$ *m/z* 152.1 $[Gua + H]^+$ and *m/z* 227.1 $[^{15}N_5\text{-}M + H]^+ \rightarrow$ *m/z* 157.1 $[^{15}N_5\text{-}Gua + H]^+$) was performed in the linear ion trap via CID, while subsequent fragmentation (*m/z* 152.1 $[Gua + H]^+ \rightarrow$ *m/z* 135.0301 $[Gua - NH_3]^+$, 153.0402 $[Gua - NH_3 + H_2O]^+$) and *m/z* 157.1 $[^{15}N_5\text{-}Gua + H]^+ \rightarrow$ *m/z* 139.0183 ($[^{15}N_5\text{-}Gua - NH_3]^+$), 157.0283 ($^{15}N_5$-Gua – $^{15}NH_3 + H_2O$) was performed in the HCD cell

(Scheme 5.3). The ions at 153.0402 $[Gua - NH_3 + H_2O]^+$ are generated via neutral gain of H_2O by $[Gua - NH_3]^+$ ions (Scheme 5.3), a process that have been shown to takes place in the MS collision cell due to the presence of residual water *(296)*. MS^3 fragment ions were analyzed in the accurate mass mode over a range *m/z* 50-270 at a resolution of ~ 25,000. We found that the MS^3 scan mode afforded better signal to noise ratios as compared to the MS^2 due to its selectivity for the analyte of interest in the presence of co-eluting contaminant peaks (Figure 5.3B). Using nanoLC/ESI^+-$HRMS^3$ methodology, the sensitivity for EB-G adducts was dramatically improved as compared to standard SRM on a triple quadrupole mass analyzer (Compare Figures 5.3A and B), with excellent S/N ratios for the low and sub fmol analyte amounts. As an additional benefit, MS^3 spectra are available for each sample, providing additional confirmation of analyte identity. Quantitation is based on peak areas corresponding to the analyte and its internal standard. Standard curves obtained by nanoLC/ESI^+-$HRMS^3$ analysis of known amounts of pure standards of EB-G and its $^{15}N_5$-labeled internal standard (Y = 1.0044X+0.0012, R2 = 0.9984)

Scheme 5.3 Dissociation scheme to explain the formation of fragment ions at 153.04106 [Gua - NH_3 + H_2O]$^+$. Adopted from *(296)*.

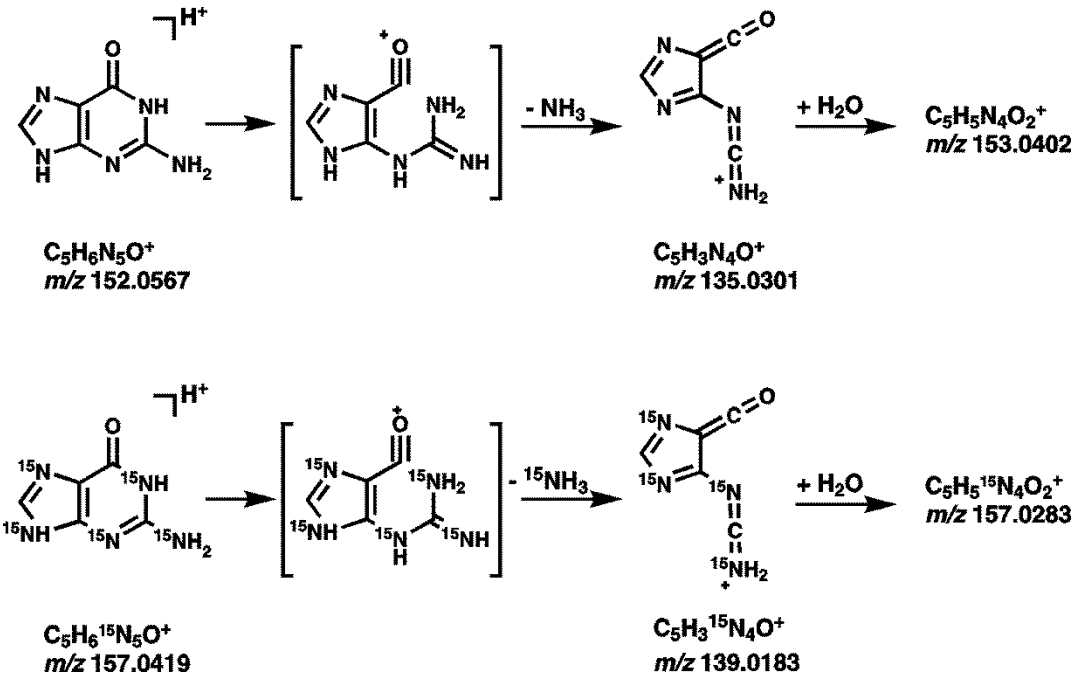

Figure 5.3 Comparision of EB-GII detection using nanoLC-ESI$^+$-MS/MS on a triple quadrupole mass spectrometer (A) and nanoLC/ESI$^+$-HRMS^3 using Orbitrap Velos (B). EB-GII internal standard (3.0 fmol) was spiked into blank DNA oligonucleotide solution (150 µg). The sample was subjected to neutral thermal hydrolysis and HPLC cleanup by standard methods. Sample aliquots (5 µL) were injected on the same nanoHPLC column connected to TSQ Ultra (A) or Orbitrap Velos (B) for mass spectrometry analysis.

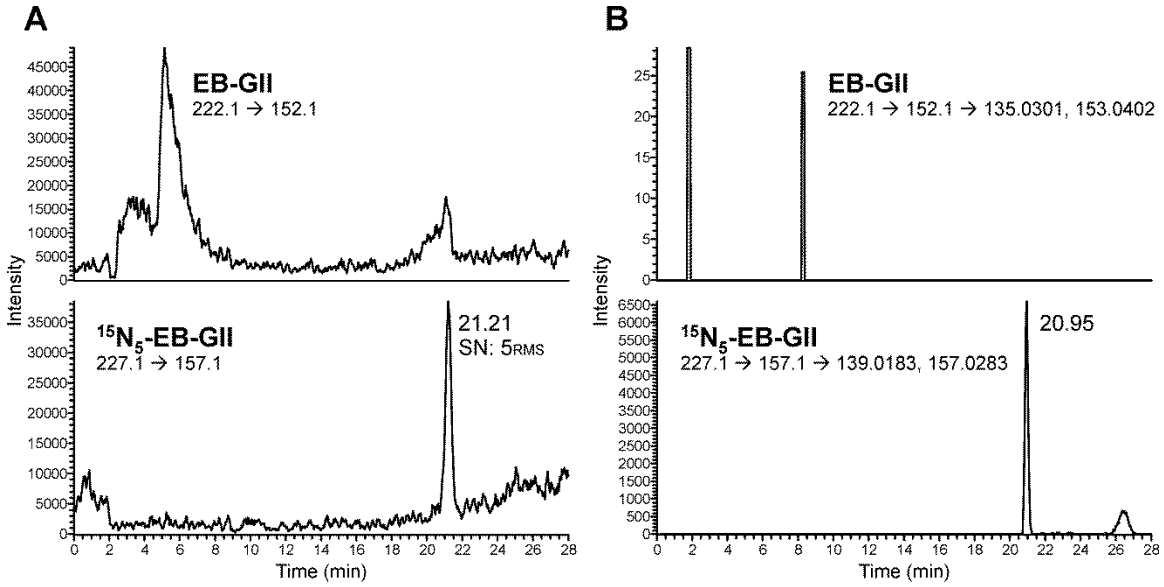

Our initial studies have attempted to quantify both regioisomers of the adduct, EB-GI and EB-GII (Scheme 5.1). Under our offline HPLC conditions, pure standards of EB-GI and EB-GII eluted as sharp peaks well resolved from each other (not shown). However, when the two analytes were spiked in synthetic oligodeoxynucleotide or into blank human DNA (150 μg), processed as described above, and subjected to nanoLC/ESI$^+$-HRMS-SRM analysis, a co-eluting peak was observed at similar HPLC retention time as EB-GI (Figure 5.4). Our efforts to separate EB-GI from this interfering impurity under various chromatographic conditions (a range of HPLC stationary phases, HPLC gradients, and HPLC buffers such as 0.05% formic acid, 5 mM ammonium acetate buffer (pH 6.8) and 0.1% formic acid with a gradient of methanol or acetonitrile as organic phase) were not successful. Although the co-elute signal was somewhat decreased when narrowing the precursor ion (*m/z* 222.1) isolation width from 3.0 amu to 1.0 amu, this also led to a significant loss of sensitivity for the analyte (not shown). MS^2 experiments have revealed that the co-eluting impurity from sample matrix had a different MS^2 fragmentation pattern as compared to authentic EB-GI, but unfortunately shared the same major fragment ion at *m/z* 152.0567 (Figure 5.4). Our efforts to eliminate the interfering peak using MS^3 also proved unsuccessful and the co-eluting impurity interfered with accurate analysis of EB-GI (results not shown). We therefore focused our efforts on EB-GII (Scheme 5.1), which is formed upon nucleophilic attack of N7-guanine at an internal carbon of EB and is produced in similar amounts as its regioisomer *(75)*.

Figure 5.4 Attempts to identify the impurity co-eluting with EB-GI. EB-GI standard (2.5 fmol) and internal standard $^{15}N_5$-EB-GI (2.5 fmol) were spiked in synthetic oligodeoxynucleotide solution (150 µg) and subjected to neutral thermal hydrolysis, sample processing, and nano-HPLC-nanoESI$^+$-HRMS^2 analysis on an Obitrap Velos mass spectrometer (A). MS/MS spectrum of the co-eluting impurity from sample matrix (*m/z* 222.1681, RT 19.39) (B) and MS/MS spectrum of authentic EB-GI (*m/z* 222.0983, RT 20.00) (C). The analyte and the impurity have different fragmentation patterns, but share the same major fragment ion at *m/z* 152.0566.

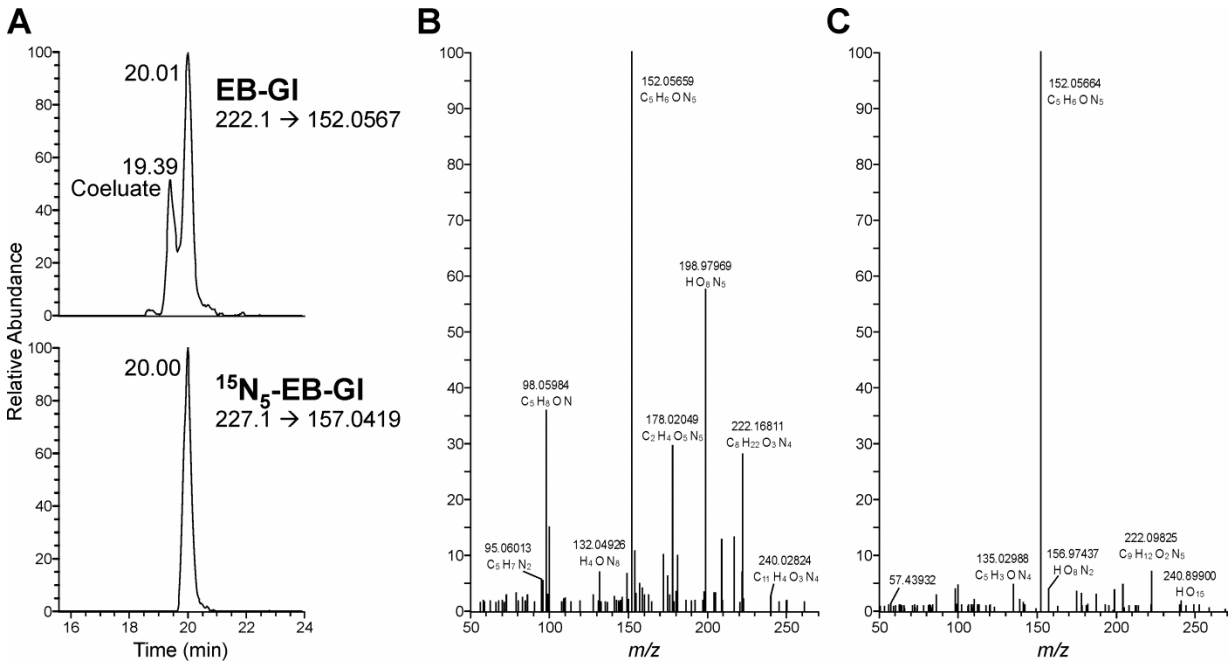

5.3.2 NanoLC/ESI$^+$-HRMS^3 Method Validation

The newly developed method was validated by analyzing samples prepared by spiking known amounts of EB-GII (0.2 - 10 fmol) and 3 fmol of $^{15}N_5$-EB-GII internal standard into 150 μg of blank human buffy coat DNA. Samples were analyzed by the methodology described above. An excellent correlation (R^2 = 0.9953) was observed between the spiked and the observed amounts of EB-GII in the targeted sample matrix analysis (Figure 5.2). Method accuracy and interday/ intraday precision were determined by analyzing replicate samples of EB-GII (0.2 fmol) spiked into blank human DNA. The accuracy of the analytical method for 0.2 fmol spiked into 150 μg of blank human DNA was calculated as 92.9 ± 7.19 % (N = 9), while the interday and intraday precision were less than 8% RSD (Table 5.1). In order to evaluate the method's sensitivity (LOD), aliquots of blank human DNA (150 μg each) were spiked with known amounts of EB-GII standard (0, 0.05, 0.1 or 0.2 fmol), followed by thermal hydrolysis and sample processing as described above (Scheme 5.2). The nanoLC/ESI$^+$-HRMS^3 limit of detection for EB-GII was determined as 0.05 fmol in 150 μg of DNA (0.1 adducts /10^9 nucleotides), which gave the signal-to-noise ratio ≥3. No EB-GII was detected in blank human DNA derived from blood leukocytes of a nonsmoker, confirming that there was no artifactual formation of EB-GII during the sample preparation and analysis. The method's limit of quantitation was defined as the lowest amount of EB-GII spiked into blank human DNA (150 μg) that afforded the signal-to-noise ratios of >10 and intra/inter day precision within 15% CV. We found that the LOQ value of our LC-MS^3 method for EB-guanine II was 0.2 fmol analyte in 150 μg of DNA, corresponding to 0.4 adducts/10^9 nucleosides.

Table 5-1 Accuracy and precision results for NanoLC/ESI$^+$ HRMS^3 analysis of EB-GII (0.2 fmol) spiked into 150 μg of blank human DNA.

Day	Parameter	value
Day 1	Mean	0.17
	RSD (%)	3.75
	Accuracy (%)	86.0
	N	3
Day 2	Mean	0.18
	RSD (%)	1.23
	Accuracy (%)	91.8
	N	3
Day 3	Mean	0.20
	RSD (%)	5.29
	Accuracy (%)	100.8
	N	3
Interday	Mean	0.18
	RSD (%)	7.74
	Accuracy (%)	92.9
	N	9

5.3.3 EB–GII quantitation in Human Cell Culture

The applicability of the new HPLC-MS^3 analytical method for EB-GII was initially tested by quantifying these adducts in human fibrosarcoma (HT1080) cells treated with increasing concentrations of EB (0.5-10 μM) for 3 h. These concentrations are well below the EC50 of EB in HT1080 cells (13.8 mM). Following DNA extraction, EB-GII adducts were released by neutral thermal hydrolysis and analyzed by nanoLC/ESI^+-$HRMS^3$ as described above. Adduct concentrations in cells treated with 0.5 μM -10 μM DEB increased in a concentration-dependent manner from 1.15±0.23 to 10.11±0.45 adducts/10^8 nucleotides (Figure 5.5).

5.3.4 EB–GII quantitation in rat liver tissue DNA

The new method was next used to quantify EB-GII DNA adducts in liver tissue DNA of F344 rats exposed to sub ppm concentrations of BD (0.5 -1.5 ppm). According to literature reports, laboratory rats are a better animal model of human exposure to BD than laboratory mice due to interspecies similarities in the metabolic pathways *(299)*. We chose low to sub-ppm exposures because this concentration range is comparable to occupational BD exposures in polymer or monomer industries *(216)*. NanoLC/ESI^+-$HRMS^3$ analyses of EB-GII in liver DNA of BD-exposed rats have revealed prominent analyte peaks with little to no background noise (Figure 5.6A).

Figure 5.5 Concentration-dependent formation of EB-GII adducts in HT1080 cells treated with increasing amounts of EB (0.5-10 μM).

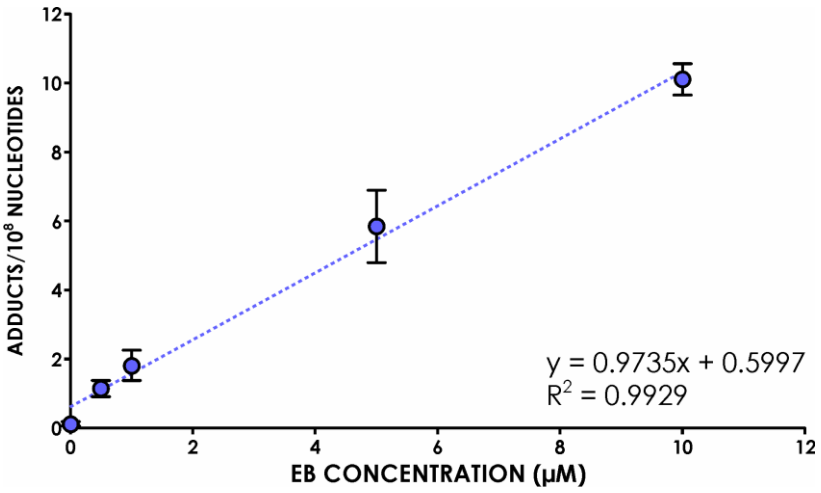

Figure 5.6 A. Representative extracted ion chromatogram for nano-HPLC-nanoESI^{+}-HRMS^{3} analysis of EB-GII adducts in liver DNA of a laboratory rat exposed to 1.0 ppm BD by inhalation for 2 weeks. Liver DNA (53.3 μg) was spiked with $^{15}N_5$-EB-GII (internal standard for quantitation) and subjected to neutral thermal hydrolysis, sample processing, and nano-HPLC-nanoESI^{+}-HRMS^{3} analysis on an Obitrap Velos mass spectrometer. B. Concentration-dependent formation of EB-GII adducts in liver DNA of laboratory rats exposed to low ppm (0.5, 1.0, 1.5 ppm) concentrations of BD.

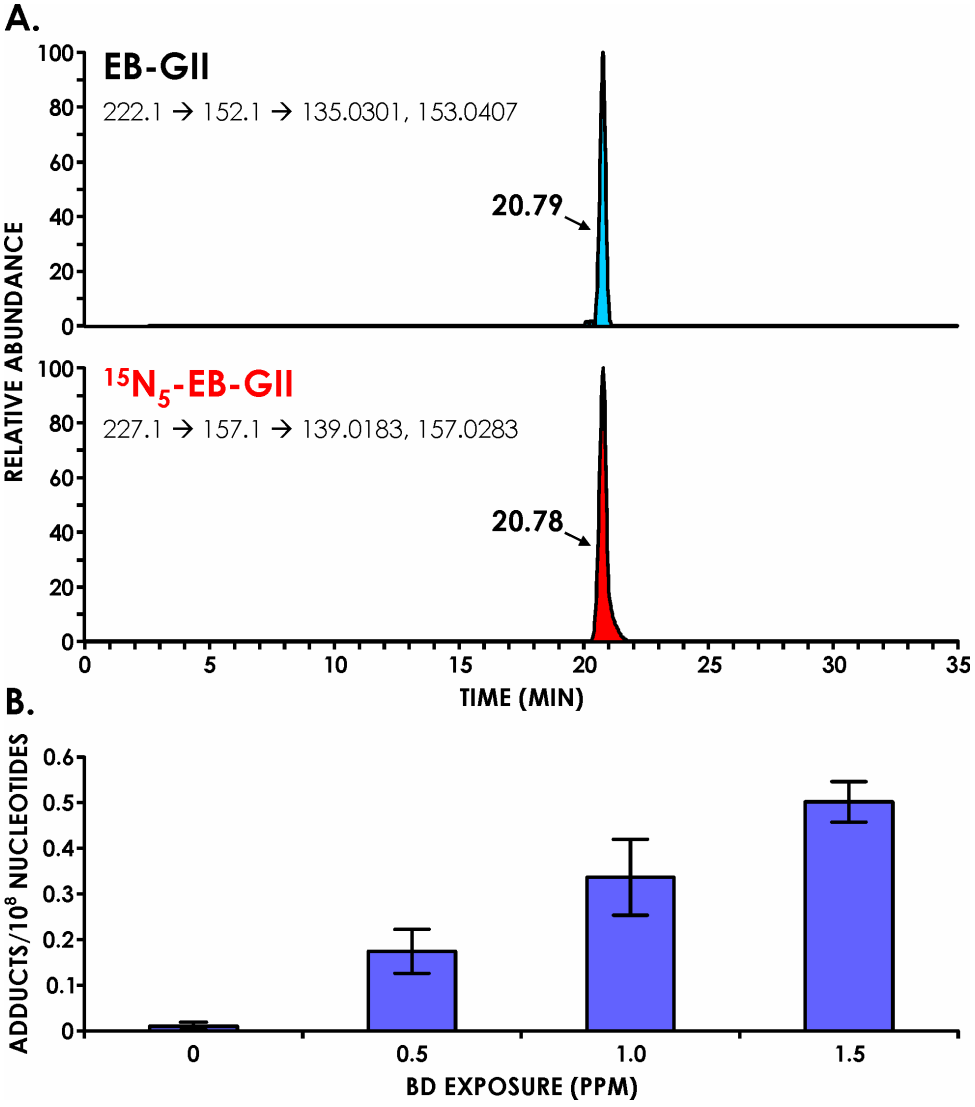

A dose dependent increase in adduct amounts was observed in animals treated with higher BD concentrations, with EB-GII numbers changing from 0.17 ± 0.05 adducts/10^8 nucleotides following 0.5 ppm exposure to 0.33 ± 0.08 adducts/10^8 nucleotides following 1.0 ppm exposure, and further to 0.50 ± 0.04 adducts/10^8 nucleotides following exposure to 1.5 ppm BD (Figure 5.6B). No EB-GII adducts were detected in control animals exposed to ambient air only. The new method was further applied to determine the *in vivo* half-lives of EB-GII adducts in liver of laboratory rats exposed to 1250 ppm BD. Only 7 µg of DNA was used in this case due to the high adduct levels in these samples. EB-GII adduct concentrations in rat tissues gradually decreased 1, 3 and 6 days post exposure to BD (Figure 5.7A). Data processing via first order kinetics analysis yielded the EB-GII half-life in rat liver DNA as 2.20 ± 0.12 days (Figure 5.7B), which is significantly shorter than the half-life of structurally analogous N7-THBG adducts *in vivo* ($t_{1/2}$ = 3.6-4.0 days) *(75)*.

5.3.5 Attempted EB –GII quantitation in human blood leukocyte DNA

To test the ability of the new method to detect BD-DNA adducts in humans, it was applied to blood leukocyte DNA of confirmed smokers (N = 8). Smokers are exposed to BD due to its relatively high concentrations in cigarette smoke (8.5-48.2 µg/cigarette) *(289)*. Although we were able to successfully detect EB-GII adducts in human DNA (Figure 5.8), adduct amounts were below the limit of quantitation of our method (0.4 adducts/10^9 nucleotides). Unfortunately, DNA amounts could not be increased due to the limited human sample availability. Furthermore, our *in vivo* persistence data (Figure 5.7) suggest that EB-GII adducts are rapidly released from the DNA backbone by spontaneous hydrolysis and/or active repair. Our current efforts are to

develop a nanoLC/ESI$^+$-HRMS^3 methodology for EB-GII adducts in human urine, which is readily available, but will require additional sample cleanup steps to remove salts and other polar matrix compounds prior to analysis. Our final goal is to develop analytical methodology that has adequate sensitivity, accuracy, and precision for quantitation of EB-G II adducts in human populations.

Figure 5.7 Persistence of EB-GII adducts in liver DNA of rats exposed to1250 ppm BD by inhalation (A) and first order kinetic analysis for estimation of adduct half-life *in vivo* (B).

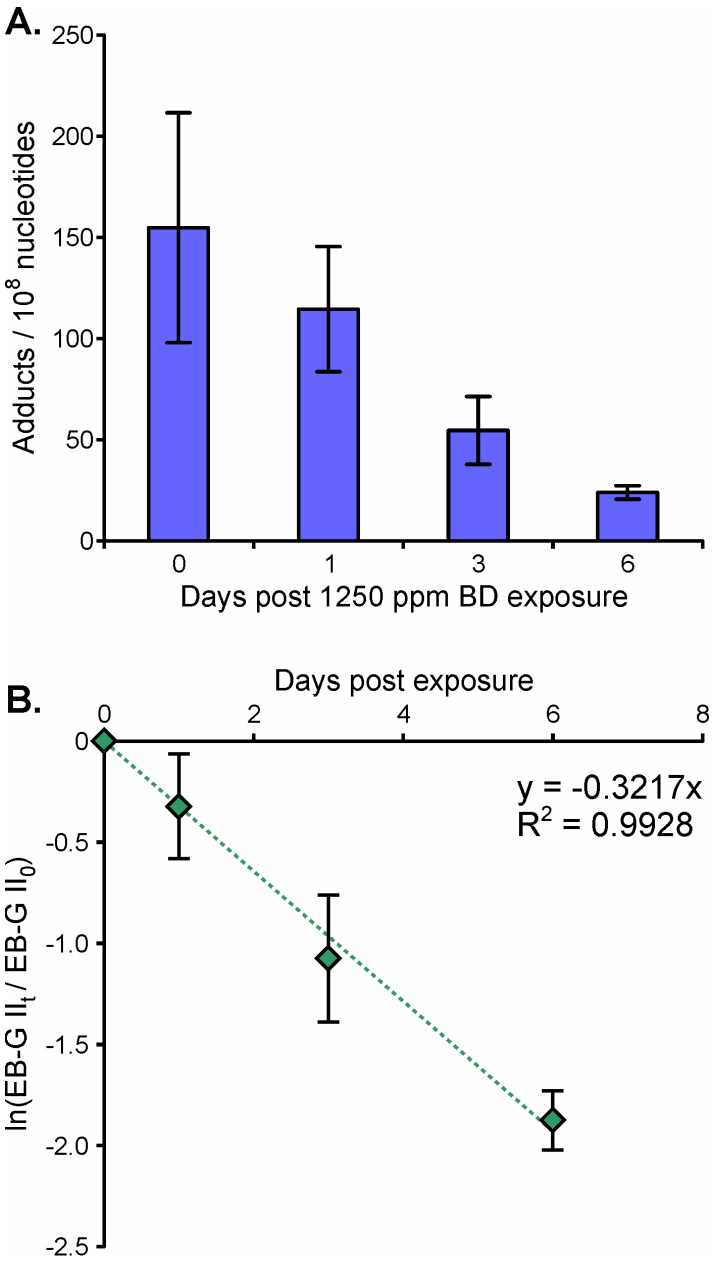

Figure 5.8 Representative extracted ion chromatogram for nanoLC/ESI$^+$ HRMS^3 analysis of EB-GII adducts in blood leukocyte DNA of a smoker. DNA (71 μg) was spiked with $^{15}N_5$-EB-GII (internal standard) and subjected to neutral thermal hydrolysis, sample processing, and analysis on an Obitrap Velos mass spectrometer.

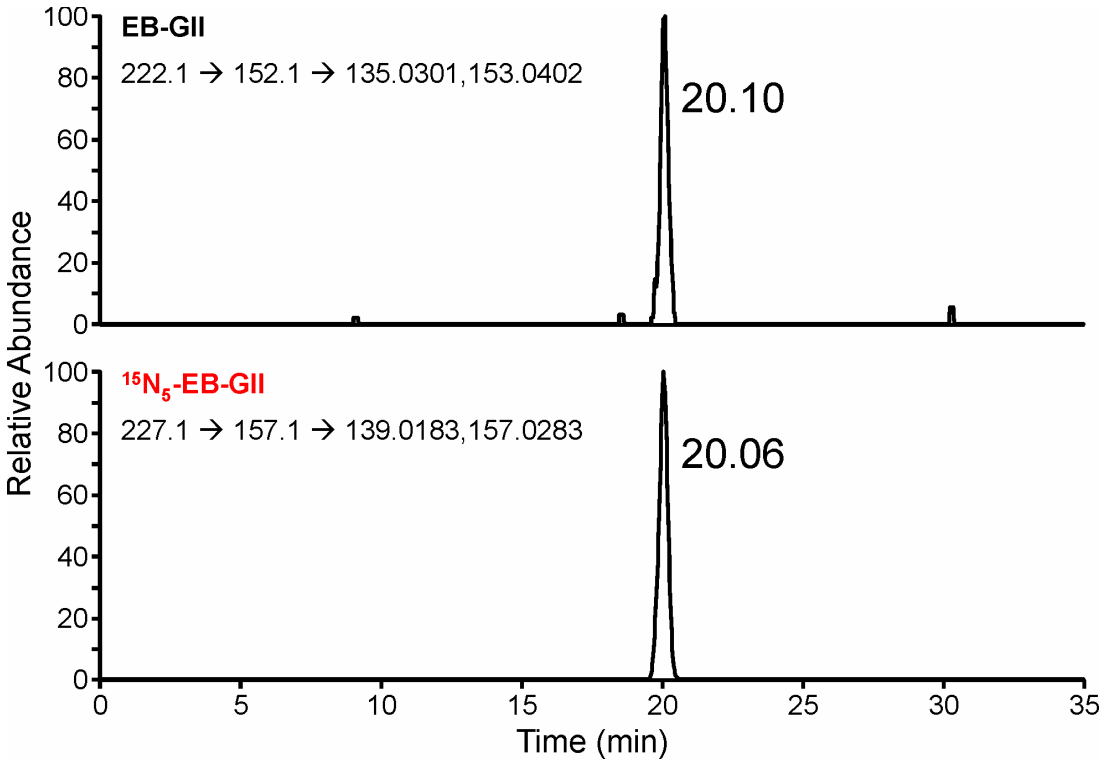

In conclusion, sensitive, accurate, and specific nanoLC/ESI$^+$-HRMS^3 isotope dilution methodology has been developed for accurate and precise quantitation of BD-specific EB-GII adducts *in vivo*. The applicability of this method was demonstrated by quantitation of EB-GII adducts in human fibrosarcoma cells exposed to low micromolar concentrations of EB and in liver DNA of laboratory rats exposed to sub-ppm concentration of BD, which mimic occupational exposure in humans. The method had adequate sensitivity to quantify EB-GII DNA adducts in human leukocyte DNA, provided that that adequate DNA amounts are available for analysis. We conclude that nanoLC/ESI$^+$-HRMS^3 methodology holds a great promise in quantitative analyses of trace levels of DNA adducts in human and animal samples due to an increased sensitivity, specificity, and detailed structural confirmation from MS^3 spectra.

VI. ISOTOPE DILUTION NANO LC/ESI$^+$ HRMS^3 QUANTITATION OF URINARY N-7-(1-HYDROXY-3-BUTEN-2-YL) GUANINE ADDUCTS AS BIOMARKERS OF HUMAN EXPOSURE TO 1,3-BUTADIENE

6.1 Introduction

1,3-Butadiene (BD) is a carcinogenic gas abundant in cigarette smoke, automobile emissions, and in wood smoke from forest fires *(300)*. Human exposure to BD can also occur in occupational settings in styrene-butadiene polymer industries and synthetic rubber production facilities *(216;274)*. BD undergoes cytochrome P450 2E1-mediated metabolic activation to epoxide metabolites such as 3,4-epoxy-1-butene (EB) (Scheme 6.1) *(92;93)*. EB is mutagenic in cultured human lymphoblasts *(95)* and is carcinogenic in laboratory animals, especially in mice *(84;85;114)*.

EB reacts with nucleophilic N7 positions of guanine bases of DNA to form regioisomeric N7-(2-hydroxy-3-buten-1-yl) guanine (EB-GI) and N7-(1-hydroxy-3-buten-2-yl) guanine (EB-GII) adducts (Scheme 6.1) *(75;103)*. These adducts are hydrolytically labile due to the positive charge generated upon alkylation of the N-7 position of guanine, resulting in their spontananeous depurination over time ($t_{1/2}$, 2.20 ± 0.12 days) *(278;282)*. EB-GI ad EB-GII have been previously detected in EB-treated calf thymus DNA *(265)*, in EB-treated human cells in culture *(104)*, and in tissues of laboratory rats and mice exposed to BD by inhalation *(70;75)*. Liver DNA of F344 rats exposed to 20 - 625 ppm BD for 6 h/day, 5 days/week for 4 weeks contained 0.1-1.2 EB-GI and 0.2-0.9 EB-GII adducts per 10^6 guanine bases, respectively. Liver DNA of BD-exposed B6C3F1 mice exposed to same BD concentrations contained higher adduct levels (0.2-3.0 EB-GI and 0.1-2.4 EB-GII adducts per 10^6 guanine bases) due to more

efficient formation of EB in this species *(70;75)*. Quantitation of EB-G adducts in humans exposed to BD from occupational or environmental sources is a challenging task due to their low levels (< 1 per 10^8 guanine bases), requiring an ultra-sensitive methodologies. Recently, we reported a quantitative isotope dilution nanoLC/ESI^+ $HRMS^3$ methodology for EB-G adducts in human blood leukocyte DNA *(70)*. Although our method had excellent sensitivity (LOQ, 0.4 adducts/10^9 nucleotides, we were unable to accurately quantify EB-GII in human DNA because of their low concentrations in humans (< 0.2 adducts/10^9 nucleotides) and limited human blood sample availability.

In the present study, we evaluated the possibility of quantifying EB-GII in human urine as biomarkers of BD exposure and metabolism to DNA-reactive epoxides. N7-alkylguanine adducts are excreted in urine following their spontaneous hydrolysis and/or active repair *(301)*. We utilized isotope dilution mass spectrometric nanoLC-high resolution tandem mass spectrometry (nanoLC/ESI^+-$HRMS^3$) methodology on an Orbitrap Velos mass spectrometer for sensitive and specific quantitation of EB-GII in human urine. Following full validation, the new methodology was used to quantify EB-GII in rats exposed to BD, occupationally exposed workers, nonsmokers, and smokers of African American and European American ethnicity.

Scheme 6.1 Partial metabolic scheme of BD showing DNA adduct formation, hydrolysis and urinary excretion. EH, epoxide hydrolase; EB-GI, N-7-(2-hydroxy-3-buten-1-yl) guanine; EB-GII, N-7-(1-hydroxy-3-buten-2-yl) guanine.

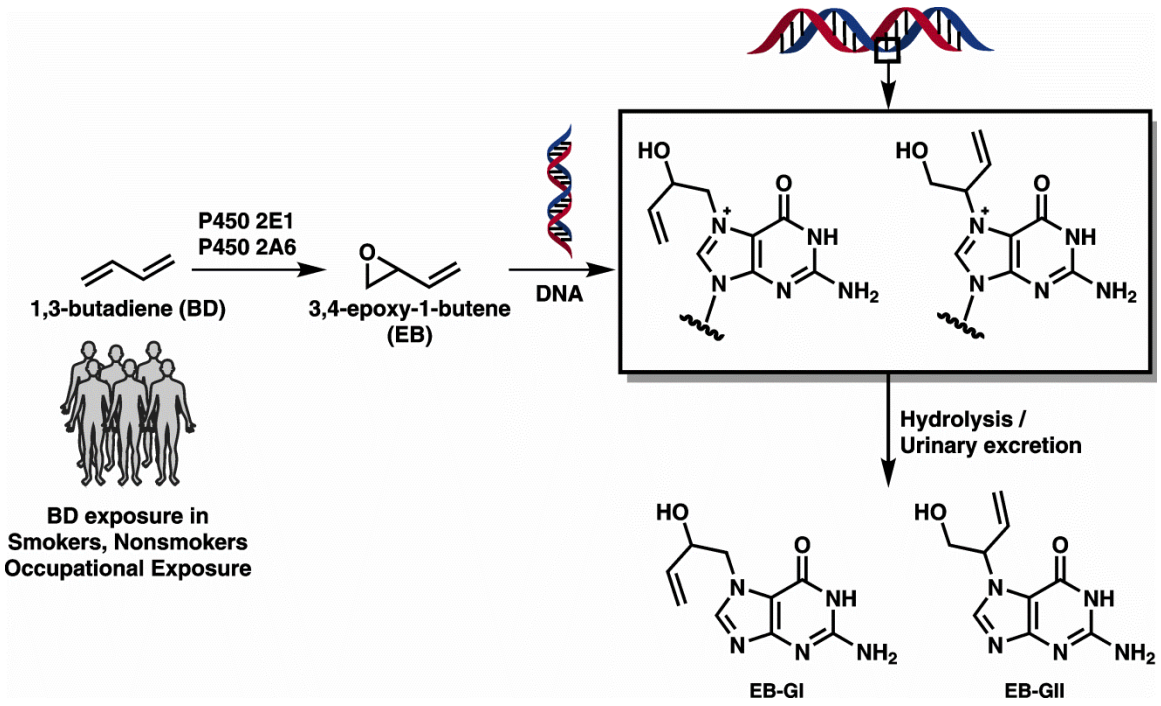

6.2 Materials and Methods

Note: *EB is a known carcinogen and, should be handled with adequate safety precautions following specific material safety data sheet.*

Materials

LC-MS grade water, methanol, and acetonitrile were purchased from Fisher Scientific (Pittsburgh, PA). All other chemicals and solvents were obtained from Sigma-Aldrich (Millwaukee, WI, St. Louis, MO). Strata X polymeric reversed phase SPE cartridges (30 mg/ 1 mL) were obtained from Phenomenex (Torrance, CA). EB-GII and $^{15}N_5$-EB-GII standards were prepared as previously reported *(265;294)*. Molar concentrations of EB-GII and $^{15}N_5$-EB-GII standard solutions were determined by UV spectrophotometry using the molar extinction coefficient (ε) of 8030 M^{-1} cm^{-1} at 284 nm at neutral pH *(294)*. Isotopic purity of $^{15}N_5$-EB-GII as determined by mass spectrometry was 99.93 %. Stock solutions of EB-GII and $^{15}N_5$-EB-GII were prepared in water and stored at −20 °C.

Animals and Treatment

Male and female F344 rats (N = 3 per group) were exposed to 62.5 or 200 ppm for 2 weeks (6 h/day, 5 days/week) using whole-body exposure chambers at the Environmental Exposure and Inhalation Health Facility at the University of Texas Medical Branch at Galveston as reported previously *(135)*. Control rats were exposed to filtered air only. Urine was collected using metabolic chambers and stored at -80 °C until analysis as described previously *(135)*.

Human study subjects

Spot urine samples were collected from occupationally exposed human subjects (N = 23) in BD production facility and control administrative workers (28 per group) *(125;132;155)*. BD exposures were determined by personal monitoring for 8-h work shifts on 10 separate occasions over an interval of 4 months for each study subject. The details of the occupational exposure study have been reported previously *(125;132;155)*. This work was approved by the Institutional Review Boards at Regional Institute of Hygiene of Central Bohemia and the University of Vermont. The archived urine samples were shipped to the University of Minnesota on dry ice and stored at −80 °C until analysis.

Nonsmoker urine samples (N = 28) were obtained from the Tobacco Research Biorepository Facility at the Masonic Cancer Center, University of Minnesota. Nonsmoker human subjects were at least of age 19 years or older (mean age; 33 ± 12 years) and were not pregnant or breast feeding. They consumed less than 21 alcoholic drinks per week and were in good physical and mental health. Nonsmokers smoked less than 100 cigarettes in their lifetime and were not using any tobacco products

24 hour urine samples from male (N = 86) and female (N = 82) current smokers of African American (N = 86) and European American (N = 80) ancestry were collected. This study was approved by the University of Minnesota Institutional Review Board (Study # 1007M85757). Male (age: 42 ± 11) and female (age: 44 ± 11) smokers who smoked average of 17 cigarettes per day for at least one year were recruited. Overall mean CO levels in smokers were 16 ± 7 ppm for males and 20 ± 10 ppm for females. Subjects were asked to collect a 24 h urine sample and bring it to the Tobacco Research

Programs Clinic at the University of Minnesota. Urine samples were stored at -20 °C before analysis.

Urine sample processing and EB-GII adduct enrichment (Scheme 6.2)

Urine (10 μL for rat samples, 200 μL for human samples) was centrifuged at 10,000g for 15 min to remove any particulate matter. The supernatants were spiked with $^{15}N_5$-EB-GII (5 fmol, internal standard for mass spectrometry) and subjected to solid phase extraction on Strata X cartridges (30 mg/1 mL, Phenomenex, Torrance, CA). SPE cartridges were conditioned with 2 mL of methanol, followed by 2 mL of MilliQ water. Urine samples (10 – 200 μL) were loaded on to prepared cartridges, and the cartridges were washed with 1 mL of water, followed by 1 mL of 10% methanol in water. EB-GII and its internal standard were eluted with 60% methanol in water, dried under vacuum, and reconstituted with 200 μL of water containing dT retention time marker (0.1 mg/mL). Offline HPLC purification was conducted on an Agilent 1100 series HPLC system equipped with a UV detector and an automated fraction collector (Agilent Technologies, Palo Alto, CA) *(70)*. A Zorbax Eclipse XDB-C18 column (4.6 × 150 mm, 5 μm, from Agilent Technologies, Palo Alto, CA) was eluted at flow rate of 1 mL/min with a gradient of 0.4% formic acid in Milli-Q water (A) and HPLC grade acetonitrile (B). Solvent composition was maintained at 0% B for 5 min and then linearly increased to 3% B in 10 min and further to 40% B in 5 min. The solvent composition was returned to 0% acetonitrile in 5 min and held at 0% for 15 min for column equilibration. UV absorbance was monitored at 254 nm. 2′-deoxythymidine (dT, 2.06 nmol on column) was used as a retention time marker, which typically eluted at 18.3 min. EB-GII eluted at ~16.6 min.

Scheme 6.2 Sample preparation procedure for isotope dilution nanoLC/ESI$^+$ HRMS^3 analysis of EB-GII in urine.

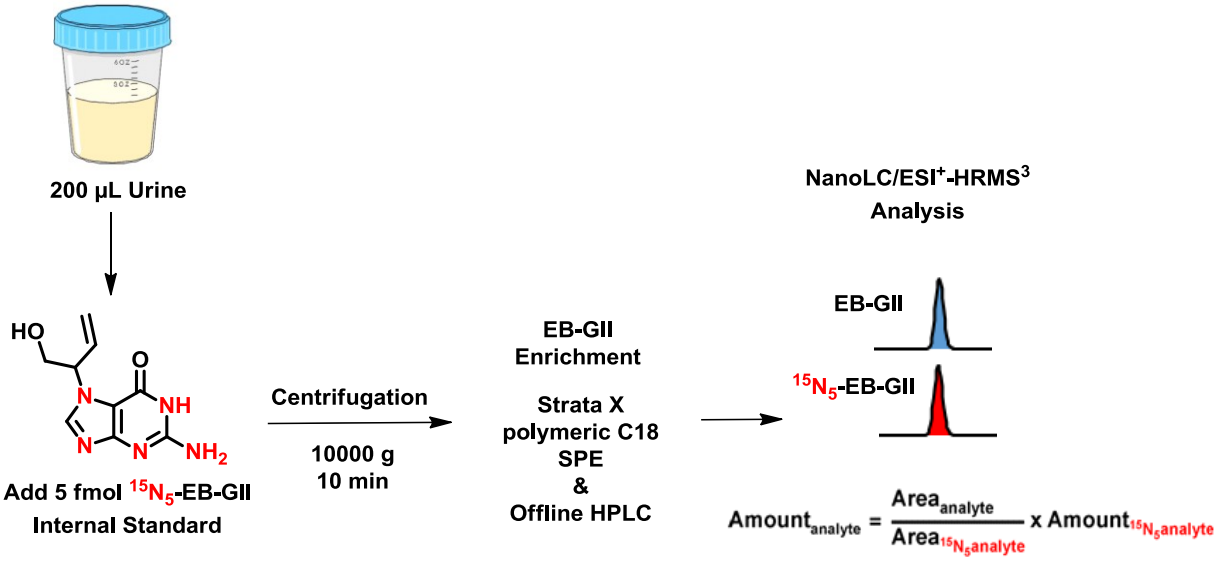

HPLC fractions containing EB-GII and its internal standard (16.0 – 18.0 min, 1 mL each) were collected in 1.2 mL MS total recovery vials (Thermo Fischer Scientific, Waltham, MA), concentrated under vacuum, and re-dissolved in LC-MS grade water (10 µL) for nano-HPLC-nanoESI$^+$-HRMS^3 analysis. Typical injection volume was 5 µL. HPLC blanks containing 200 µL of water with 5 fmol of $^{15}N_5$-EB-GII internal standard and dT retention time marker were periodically injected to detect any potential carryover during the offline HPLC clean up procedure.

NanoLC/ESI$^+$-HRMS^3 analysis of urinary EB–GII

All nanoLC/ESI$^+$-HRMS^3 analyses were conducted Nano2D-LC HPLC system (Eksigent, Dublin, CA) fitted with 5 µL injection loop and interfaced to an LTQ Orbitrap Velos instrument equipped with a nanospray source (Thermo Fisher Scientific Corp., Waltham, MA). Gradient elution was achieved using LC-MS grade water containing 0.01% acetic acid (A) and LC-MS grade acetonitrile containing 0.02% acetic acid (B). Samples were loaded onto a trapping column (Symmetry C18 nanoAcquity, 0.18 × 20 mm, Waters Corp., Millford, MA), which was connected in line with a nano-LC column (0.075× 200 mm) manually packed with Synergi Hydro-RP, 80Å, 4 µm chromatographic packing (Phenomenex, Torrance, CA). The initial HPLC flow was maintained at 2% B, 1 µL/min, for 5.5 min to enable sample loading onto the trapping column, followed by flow rate decrease to 300 nL/min at 2% B for 0.5 min. The percentage of solvent B was linearly increased to 25% B in 19 min and further to 50% B in 10 min, returned to 2% B in 2 min, and equilibrated for 7 min. Under these conditions, EB-GII eluted as a sharp peak at 20 min.

The mass spectrometry analysis was performed by fragmenting $[M + H]^+$ ions of EB-GII (*m/z* 222.1) via collision induced dissociation (CID) in the linear ion trap using the collision energy (CE) at 25 units and the isolation width of 1.0 amu. MS/MS fragment ions at *m/z* 152.1 $[Gua + H]^+$ were subjected to further fragmentation in the high collision dissociation (HCD) cell using nitrogen as a collision gas (CE = 75 units, IW = 1.0 amu). The resulting MS^3 fragment ions were detected in the mass range of *m/z* 50 to *m/z* 270 using the Orbitrap mass analyzer (HRMS) at a resolution of ~ 25,000. EB-GII was quantified using extracted ion chromatograms from the combined signals of *m/z* 135.0301 ($[Gua - NH_3]^+$) and *m/z* 153.0411 ($[Gua - NH_3 + H_2O]^+$), at a mass tolerance of 5 ppm. The $^{15}N_5$ labeled internal standard ($[^{15}N_5]$-EB-GII) was quantified using an analogous MS^3 scan event consisting of fragmentation of *m/z* 227.1 ($[M + H]^+$) to *m/z* 157.1 $[^{15}N_5$-Gua + $H]^+$ and further to *m/z* 139.0183 ($[^{15}N_5$-Gua – $NH_3]^+$). Extracted ion chromatograms corresponding to the sum of *m/z* 139.0183 ($[^{15}N_5$-Gua – $NH_3]^+$) and *m/z* 157.0283 ($[^{15}N_5$-Gua – $NH_3 + H_2O]^+$) at 5 ppm were generated and used for quantitation. A full scan event was also performed over the mass range of *m/z* 100-500 at a resolution of 15000 to monitor for any co-eluting matrix components. EB-GII amounts were determined by comparing the areas of the nanoLC/ESI^+-$HRMS^3$ peaks corresponding to the analyte and its internal standard.

Method validation

Standard curves were constructed by analyzing aqueous solutions containing fixed amounts of $^{15}N_5$-EB-GII (5 fmol) and increasing amounts of EB-GII (0.1 - 10.0 fmol, in triplicate), followed by regression analysis of the actual and the observed amounts of EB-GII. Method validation curves were constructed by spiking control

nonsmoker urine or artificial urine (200 μL) with 0.1 - 10 fmol of EB-GII and 5 fmol of $^{15}N_5$-EB-GII internal standard (in triplicate), followed by sample processing and nanoLC/ESI$^+$-HRMS^3 analysis as described above. The observed EB-GII amounts were plotted against the theoretical values, followed by standard regression analysis.

The limit of detection (LOD) of the new method was determined by spiking synthetic urine (200 μL) with EB-GII (0.05, 0.1, 0.2, or 0.5 fmol) and $^{15}N_5$-EB-GII internal standard (5 fmol). The fortified urine samples were processed and analyzed as described above. The method's limit of quantification (LOQ) was determined by spiking (200 μL) control nonsmoker urine described above with 0.1- 0.5 fmol of EB-GII and 5 fmol of $^{15}N_5$-EB-GII internal standard (in triplicate), followed by sample processing and nanoLC/ESI$^+$-HRMS^3 analysis by standard methods. The LOQ value was determined as EB-GII amount which consistently gave a signal to noise ratio (S/N) greater than 10 and % CV < 15% , while LOD of the method was determined as EB-GII amounts that resulted in S/N ratio > 3.

Intra/inter day precision and accuracy of the analytical method was determined by spiking control nonsmoker urine (200 μL) with 0.2 fmol of EB-GII and 5.0 fmol of $^{15}N_5$-EB-GII internal standard, followed by sample preparation and analysis as described above, three times per day on three consecutive days. The relative standard deviations between these measurements were calculated and reported as intra-day and inter-day precision, while the method accuracy range was determined from the equation ($A_m/A_a \times 100\%$), where A_m is the measured amount of EB-GII and A_a is the actual analyte amount added.

SPE recovery was determined by adding $^{15}N_5$-EB-GII (5 fmol) to synthetic urine (200 μL) and sample processing by standard methods as described above (in triplicate). Unlabeled EB-GII standard (4.2 fmol) was added immediately prior to nanoLC/ESI$^+$-HRMS^3 analysis, and the recovery was determined by comparing the theoretical and the observed $^{15}N_5$-EB-GII:EB-GII peak area ratios. Analyte signal suppression in urine matrix was evaluated from the ratio of peak area of EB-GII (4.2 fmol) spiked into artificial urine matrix post sample processing, and the corresponding peak area of the EB-GII obtained by nanoLC/ESI$^+$-HRMS^3 analysis of a pure standard in water (N = 3).

The stability of EB-GII in human urine matrix was determined using a smoker urine sample. The urine was frozen for 24 hours at -20 °C and thawed for 2 hour at room temperature (freeze-thaw cycle 1), after which it was processed and analyzed in duplicates. This procedure was repeated for two additional freeze-thaw cycles, followed by sample processing and analysis. Freeze-thaw cycle variability was determined using %CV within and between cycles.

6.3 Results

6.3.1 NanoLC/ESI$^+$-HRMS^3 method development for EB-GII in human urine

Human urine it is a highly complex and variable biological matrix containing many polar metabolites, bile salts, and other small molecules which can adversely affect urinary DNA adduct analysis due to ESI signal suppression *(302;303)*. Therefore, analyte-selective enrichment strategies such as solid phase extraction (SPE) and/or offline HPLC fractionation are typically required for trace level analyses of DNA adducts in urine *(304;305)*. Our experimental approach for quantitation of EB-GII in human urine is summarized in Scheme 6.2. Our methodology employs 200 µL of human urine. Following centrifugation to remove any particulate matter, the supernatant is spiked with $^{15}N_5$-EB-GII internal standard (5 fmol). The use of isotopically labeled internal standard accounts for any analyte loss during sample enrichment and allows for absolute quantitation. The spiked samples are subjected to solid phase extraction on Strata X cartridges (30 mg/ 1mL) to eliminate the bulk of impurities, followed by further sample enrichment by offline HPLC and quantitative analysis via nanoLC/ESI$^+$-HRMS^3 (Scheme 6.2).

During initial stages of method development, several SPE solid phases were tested for EB-GII isolation form urine matrix, including Strata X (Phenomenex), Oasis HLB (Waters Corp.), and Isolute ENV+ (Biotage). Among these, Strata X was the most effective in respect to elimination of co-eluting impurities and analyte recovery. Strata X SPE method was further optimized, resulting in SPE recovery of 56.6 ± 1.72 % in spiked urine samples.

Our initial experiments established that SPE alone did not afford sufficient sample purity for nanoLC-MS analysis of EB-GII because of the presence of co-eluting impurities (results not shown). Therefore, SPE enriched fractions were subjected to additional enrichment by offline HPLC *(70)*. HPLC fractions containing EB-GII and its internal standard (retention time, 16-17 min) were collected, concentrated under vacuum, and reconstituted with 10 μL of water for nanoLC/ESI^+-$HRMS^3$ analysis. HPLC blanks were periodically injected to determine analyte carryover during offline HPLC clean up procedure.

NanoLC/ESI^+-$HRMS^3$ analysis was performed using an Orbitrap Velos mass spectrometer *(70)*. We took advantage of accurate mass capabilities of the instrument in order to maximize the specificity and sensitivity of EB-GII detection in human samples. The use of MS^3 mode provided an increased specificity and a reduced background noise, leading to excellent signal to noise ratios. Analysis of standard solutions containing 0.1-10.0 fmol of EB-GII and 5.0 fmol of $^{15}N_5$-EB-GII each in 25 μL of water (5 μL on column) resulted in linear standard curves ($y = 1.0044x$, $R^2 = 0.9984$).

The nanoLC/ESI^+-$HRMS^3$ method was further validated by analyzing EB-GII (0.1-10 fmol) and $^{15}N_5$-EB-GII (5 fmol) standards spiked either into artificial urine or nonsmoker urine (200 μL), followed by sample processing and analysis by standard methodologies. A linear correlation was observed between the spiked and the observed amounts of EB-GII in urine matrix ($y = 1.0042x$, $R^2 = 0.992$ for nonsmoker urine and $y = 0.9649x$, $R^2 = 0.994$ for artificial urine) (Figures 6.1). No EB-GII was detected in this particular non-smoker (data not shown).

Figure 6.1 NanoLC/ESI^{+}-HRMS^{3} method validation: correlation between the spiked and the observed amounts of EB-GII spiked into 200 µL of nonsmoker urine. Spiked amounts were 0, 0.1, 0.2, 0.5, 1, 5, or 10 fmol of EB-GII and 5 fmol of $^{15}N_5$- EB-GII (internal standard), followed by sample processing and MS analysis.

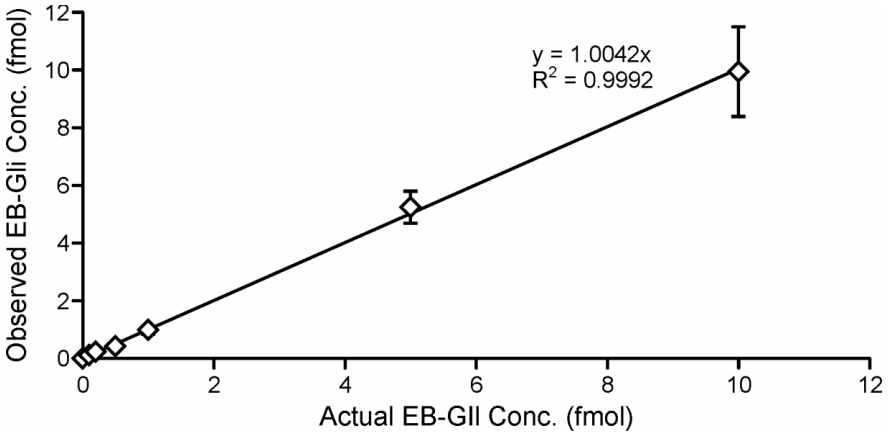

Method LOD and LOQ values determined from analysis of spiked samples were 0.25 fmol/mL and 0.5 fmol/mL artificial urine and nonsmoker urine, respectively. Intraday and interday assay precision (% coefficient of variance) determined by repeated analysis of EB-GII (0.2 fmol) spiked into either nonsmoker urine (200 μL) was 13.1 % (Table 6.1). Minimal signal suppression (<25 %) was observed upon comparison of nanoLC/ESI^{+}-HRMS^{3} peak areas in the presence and in the absence of urine matrix (post-SPE). Method accuracy was determined to be 109.9 ± 10.4% when 0.2 fmol of EB-GII was spiked into 200 μL of nonsmoker urine, along with 5 fmol of $^{15}N_5$-EB-GII (N = 5) . Freeze-thaw stability studies of a smoker urine sample (200 μL, 2.45 ± 0.34 fmol) showed low variability (< 15% RSD).

Table 6-1 Accuracy and precision results for NanoLC/ESI$^+$ HRMS^3 analysis of EB-GII (0.2 fmol) spiked into 200 μL of nonsmoker urine.

Day	Parameter	value
Day 1	Mean	0.19
	RSD (%)	13.1
	Accuracy (%)	96.4
	N	3
Day 2	Mean	0.19
	RSD (%)	11.7
	Accuracy (%)	97.5
	N	3
Day 3	Mean	0.21
	RSD (%)	9.9
	Accuracy (%)	103.5
	N	3
Interday	Mean	0.19
	RSD (%)	10.6
	Accuracy (%)	99.2
	N	9

6.3.2 Quantitation of EB-GII in urine of F344 rats exposed to BD by inhalation

The validated nanoLC/ESI$^+$-HRMS^3 method was initially used to quantify EB-GII in urine of F344 rats (n = 3 each) treated with 0, 62.5 or 200 ppm BD by inhalation for 2 weeks (6 h/day, 5 days/week). Urinary EB-GII amounts increased in a concentration-dependent manner (Figure 6.2). Low but detectable amounts of EB-GII (14.5 – 87.0 pg/mL) were found in urine of control rats exposed to filtered air only (Figure 6.2). This is consistent with previous studies that detected EB-specific urinary metabolites of BD, 2-(N-acetyl-L-cystein-S-yl)-1-hydroxybut-3-ene and 1-(N-acetyl-L-cystein-S-yl)-2-hydroxy-but-3-ene (MHBMA), in unexposed animals and in non-smoker human subjects *(135)*. Mean concentrations of EB-GII in urine of male F344 rats urine exposed to 62.5 or 200 p.p.m. BD were 679.3 ± 86.3 pg/mL and 1567.4 ± 401.5 pg/mL urine, respectively ($p = 0.06$, unpaired two sample t-test, Figure 6.2). Interestingly, urinary EB-GII concentrations were 1.5 times higher in female rats ($p = 0.15$, unpaired two sample t-test) as compared to males, with 1311.7 ± 413.9 pg/mL and 2672.4 ± 1005.69 pg/mL ($p = 0.12$, unpaired two sample t-test) present following exposure to 62.5 and 200 ppm BD, respectively (Figure 6.2), suggesting possible gender differences in BD, metabolism/urinary DNA adduct formation.

6.3.3 Quantification of EB-GII in urine of smokers, nonsmokers, and occupationally exposed workers

We next employed nanoLC/ESI$^+$-HRMS^3 to determine urinary EB-GII concentrations in confirmed nonsmokers (N = 28), smokers (N = 29), administrative control workers (N = 29), and occupationally BD exposed workers from a BD production facility (N = 24).

Figure 6.2 Concentration-dependent formation of EB-GII adducts in F344 male and female rats treated with increasing amounts of EB (0, 62.5, 200 ppm).

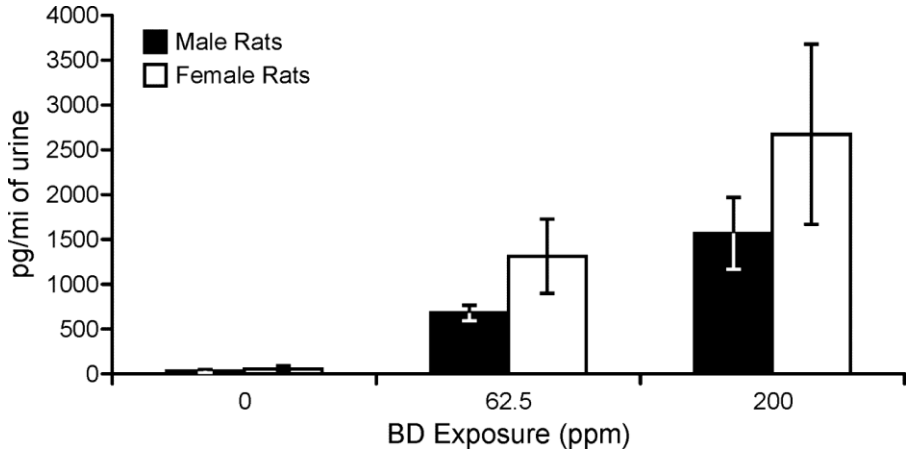

Smokers included in this study were between the ages of 19-44 and smoked at least 20 ± 7 cigarettes/day, with mean CO concentration levels of 20 ± 7 ppm. Nonsmokers smoked less than 10 cigarettes in their life time with age range between 19 and 44. NanoLC/ESI^+-$HRMS^3$ analyses have revealed clear EB-GII signals in most human urine samples analyzed (see examples in Figure 6.3A, B) with good S/N ratios and excellent chromatographic peak shapes. In contrast, we were unable to quantify the EB-GI regioisomer due to a co-eluting peak which interfered with its analysis *(70)*. The co-eluting impurity peak with *m/z* of 222.1681 has different MS/MS fragmentation pattern than EB-G adducts of interest, but shared the same major fragment ion at *m/z* 152.0566, which interfered with accurate quantitation of EB-GI in human sample. Since our efforts to separate EB-GI from this contaminant by modifying HPLC conditions were unsuccessful, we focused on the EB-GII isomer only. Mean concentrations of EB-GII in urine of nonsmokers and smokers were 1.24 ± 2.31 and 1.78 ± 2.81 pg/mg creatinine, respectively. These differences were not statistically significant, probably because of the limited group size (p = 0.08, group t-test) (Figure 6.4A). In contrast, urinary concentrations of EB-GII in urine of occupationally exposed workers (N = 23, exposed to 0.1–2.2 ppm BD) were significantly higher than in urine of administrative controls (N = 28) exposed to <0.01 ppm BD (2.94 ± 3.54 pg/mg creatinine and 0.93 ± 1.85 and pg/mg creatinine, , respectively, see Figure 6.4B) (p = 0.0051, Group t-test).

Figure 6.3 Representative extracted ion chromatogram for nanoLC/ESI$^+$-HRMS^3 analysis of EB-GII adducts in smoker (A, C), occupationally exposed BD worker urine (B, D) (200 µL each) spiked with $^{15}N_5$-EB-GII (internal standard for quantitation) and subjected to sample processing, and nanoLC/ESI$^+$-HRMS^3 analysis on an Obitrap Velos mass spectrometer.

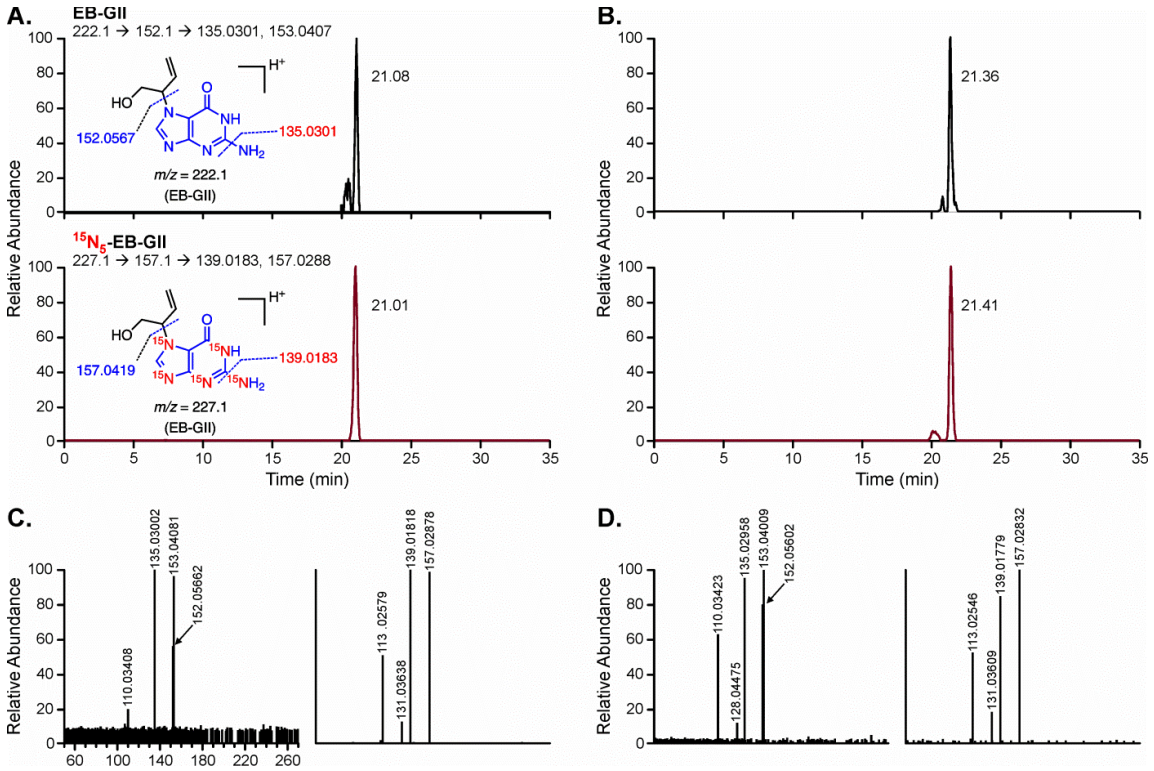

Figure 6.4 Box plots showing urinary EB-GII adducts levels showing statistically significant differences between administrative worker controls and occupationally exposed BD workers (A) and no significant differences between smokers and nonsmokers (B).

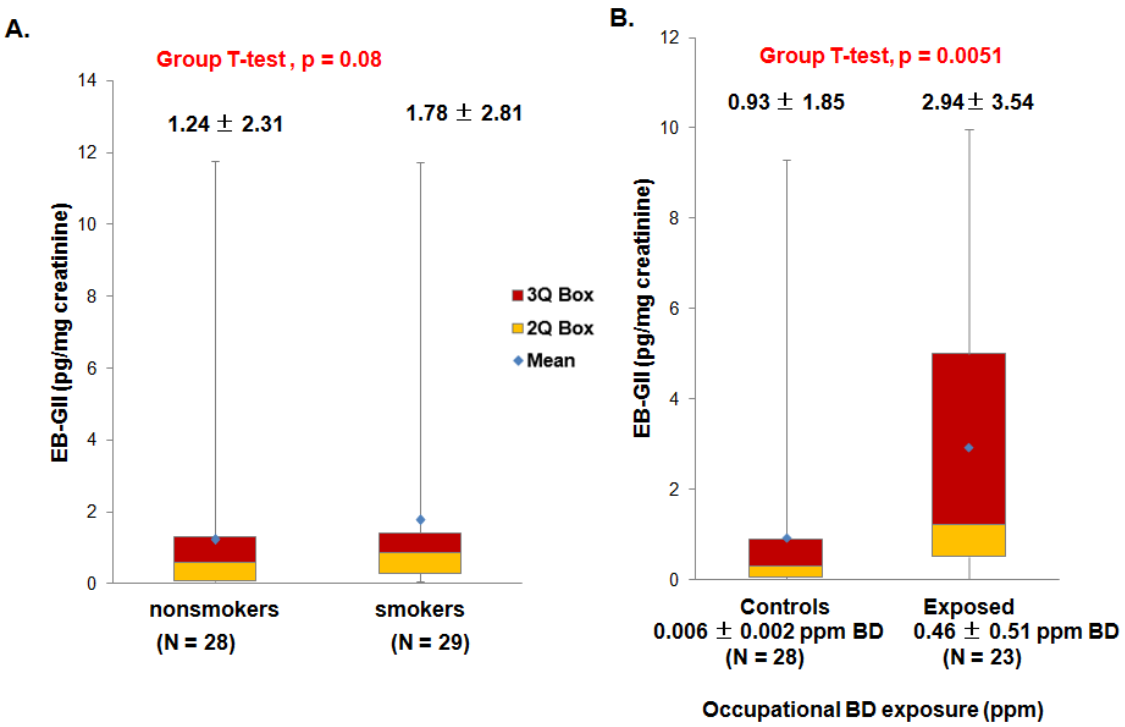

We next investigated urinary BD-DNA adducts in smokers belonging to two different ethnic groups. Urinary EB-GII concentrations in African American and European American smokers (male and female, total number = 166) were quantified (Table 6.2). No statistically differences in urinary EB-GII adduct levels were observed between male and female smokers in the multi ethnic study. We also did not observe any correlation between EB-GII levels and smokers' age, exhaled carbon monoxide, and cigarettes pet day. However, highly significant ethnic differences were observed between EB-GII excretion by African American and European American smokers, with European American smokers excreting 4-fold more EB-G II than African Americans (Table 6.2).

Table 6.2: Urinary EB-GII levels in African American (N = 86) and European American smokers (N = 80).

Smokers (N = 168)	**Males (N = 86)**	**Females (N = 82)**
Age (years)	42 ± 11	44 ± 11
CO levels (ppm)	16 ± 7	20 ± 10
Cigarettes smoked per day (CPD)	17 ± 7	17 ± 7
pg EB-GII/mg creatinine, Average ± SD	0.81 ± 1.97	0.76 ± 1.34
pg EB-GII/mg creatinine, Range, (Median)	0.005 – 13.64 (0.31)	0.005 – 9.82 (0.36)

EB-GII (pg/mg Creatinine)				
Smokers Ethnicity	**N**	**Unadjusted Mean ± SD**	**Geometric Mean ± SD ***	**Adjusted P-value ***
Afr.Am.	86	0.32 ± 0.31	0.14 ± 0.02	**<0.0001**
Eur.Am.	80	1.31 ± 2.33	0.52 ± 0.09	

**The geometric means on the log transformed variables and the p-values are adjusted for age and sex*

6.4 Discussion

Urinary DNA adducts represent useful biomarkers of carcinogen exposure and metabolic activation to electrophilic species. DNA adducts can be released from the DNA backbone and excreted in urine as free nucleobases as a result of their spontaneous depurination *(278;306)* or their active repair via base excision repair pathways *(307)*. Previous studies have detected urinary nucleobase adducts induced by estrogens *(308)*, lipid peroxidation products *(309)*, *N*-ethyl-*N*-nitrosourea *(306)*, and reactive metabolites of environmental chemicals such as polyaromatic hydrocarbons *(310)* and styrene *(311)*. In contrast, urinary DNA adducts of the important environmental, industrial, and cigarette smoke carcinogen 1,3-butadiene have not been previously investigated. Covalent BD-nucleobase adducts within genomic DNA have been widely utilized as biologically relevant biomarkers of BD exposure and metabolic activation to reactive epoxides *(69;74;114;115;295)*. However, human DNA is not always available from large epidemiological studies due to the invasive nature of blood and tissue collection.

In our earlier study, we have reported mass-spectrometry based quantitation of N-7-(1-hydroxy-3-buten-2-yl) guanine (EB-GII) adducts induced by 3,4-epoxy-1-butene (EB) in DNA isolated from peripheral blood leukocytes of smokers, nonsmokers and occupationally exposed BD workers *(70)*. Athough EB-GII was detectable in blood DNA of most human subjects, its concentrations were below the LOQ of the method (0.4 adducts/10^9 nucleotides or 0.2 fmol/ 150 μg of DNA) due to relatively low levels of human exposure to BD, limited amounts of blood sample available, and spontaneous hydrolysis of EB-GII adducts. N7-guanine adducts such as those induced by BD-derived epoxides are hydrolytically unstable due to the presence of positive charge on N-7

position of the alkylated base and are spontaneously released from the DNA backbone over time *(75;115;295)*.

We therefore decided to develop a qantitative method for EB-GII adducts in human urine, which is readily available in quantity and is easier to collect. Since urine is a highly complex and variable biological matrix as compared to DNA, advanced sample enrichment procedures (SPE, offline HPLC) were used to isolate urinary adducts of interest, followed by sensitive and specific analysis by nanoLC/ESI^+-HRMS.[3] EB-GII adducts were first quantified in urine of male and female F344 rats exposed to BD by inhalation (Figure 6.2). We found that BD adduct numbers correlated with BD exposure concentrations, with higher numbers of adducts formed in female rats as compared to males. However, these gender differences were not statistically significant ($p = 0.15$) *(213;277)*. This is consistent with the previous reports where no differences in EB levels were found between male and female Sprague-Dawley rats exposed to BD *(150;312)*.

Background of levels EB-GII (14.5 – 87.0 pg/mL) were detected in urine of control rats which had not been exposed to BD (Figure 6.2), suggesting that there might be an endogenous source for this adduct *(129)*. This finding in accord with a previous report where EB specific urinary mercapturic acid metabolite 2-(N-acetyl-L-cystein-S-yl)-1-hydroxybut-3-ene/1-(N-acetyl-L-cystein-S-yl)-2-hydroxybut-3-ene(MHBMA) was detected in the urine of control F344 rats *(142)*. Furthermore, significant quantities of the corresponding EB specific-hemoglobin adduct N-(2-hydroxy-3-butenyl)–valine (HB-Val) were found in unexposed F344 rats *(118)*. It has been hypothesized that MHBMA and other four carbon chain metabolites can originate from lipid peroxidation pathways or catabolism of carbohydrates *(133;134;142)*.

EB-GII adducts were readily detectable in human urine (Figure 6.3), with adduct concentrations ranging between 1.1 to 4.0 pg/mg creatinine. The use of accurate mass MS^3 methodology on an Orbitrap mass spectrometer has allowed us to obtain MS^3 spectra of urinary EB-GII from human samples, which matched that of an authentic standard (Figures 6.3). Accurate quantitation was achieved by using isotope dilution with the corresponding ^{15}N-labeled standard. The validated NanoLC/ESI^+-$HRMS^3$ method has an accuracy of 109.9 ± 10.4% and intra/inter day precision (%CV) less than 13% for 0.2 fmol spiked in 200 µL of nonsmoker urine. A comparison of EB-GII adducts levels in urine of occupationally exposed workers and control administrative workers (Figure 6.4B) provides evidence for an increased adduct numbers in exposed individuals (Group t-test, $p = 0.0051$), consistent with differences in BD exposure. This finding indicates that urinary EB-GII adduct levels can be used as mechanism-based biomarkers of BD exposure in humans. In contrast, EB-GII adduct levels were not statistically different between confirmed smokers and nonsmokers (group t-test, $p = 0.08$ Figure 6.4A). BD is produced in cigarette smoke by thermal cracking process due to the combustion of complex molecules such as carbohydrates, amino acids, phytosterols, paraffins, and other tobacco components, which is known to vary according to the type of tobacco, its curing process, and its carbohydratecontent *(160;313;314)*. Although smokers are generally exposed to higher concentrations of BD than nonsmokers, these differences were not reflected in our study that was limited to a small number of subjects N = 28/group).

Determination of true amounts of BD exposure in smokers is difficult due to the variability factors such as puff volume, duration, interpuff interval, number of puffs per cigarette which is again based on the extent of nicotine addiction *(315;316)*. Lya G et al.

estimated that smokers consuming on an average of 20 cigarettes/day are exposed to 0.01 mg BD/kg/day, considering BD amounts per cigarette (76.4–259.6 µg/cigarette), the amount that reaches alveoli (70%), and the extent of alveolar absorption (50%). For a 70 kg individual, the total amount of BD consumption would be 0.7 mg BD/day *(161)*. In the case of occupational BD exposure (1.0 ppm or 2.21 mg/m^3 OHSA exposure limit, 1 ppm BD = 2.21 mg/m^3) *(216)* and considering average human inhalation volume of 20 m^3/day, BD occupational human exposure is around 44.2 mg/day, which is on average 60 fold higher than the amount inhaled by smoker *(161)*. Average BD urinary metabolite concentrations of monohydroxybutenyl-mercapturic acid (MHBMA), N-acetyl-S-(3,4-dihydroxybutyl)-L-cysteine (DHBMA), and 4-(N-acetyl-L-cystein-S-yl)-1,2,3-trihydroxybutane (THBMA) in occupationally exposed workers were 82 ± 138, 3094 ± 4162 and 157 ± 158 ng/mg creatinine, respectively *(135)*. In smokers, the corresponding concentrations were 11 ± 12, 631 ± 452 and 31 ± 20 ng/mg creatinine respectively *(135)*. It is possible that our inability to detect differences in urinary EB-GII levels between smokers and nonsmokers (Figure 6.4A) is due to relatively low BD exposures in case of smoking as compared to occupational exposure, environmental sources of BD, and endogenous formation of BD metabolites. Nonsmokers included in our study might have been exposed to low levels of environmental BD exposure from automobile exhaust (0.1-10 ppb) *(284)*, second hand smoke (5.0-8.6 ppb) *(161)* and wood burning *(290)*.

In contrast, workers employed at BD monomer and polymer industries can be exposed to much greater (up to 60 fold) amounts of BD and thus excrete significantly higher EB-GII concentrations in their urine. Although smoking is a major risk factor for lung cancer, only 1 out of 10 smokers develop lung cancer. Smokers belonging to various ethnic

groups have different risk of lung cancer development, with the relative risk highest among African American and Native Hawaiian smokers followed by European American, Japanese American and Latino smokers *(167)*. According to another independent five year study by National Cancer Institute, lung cancer incidence rates were highest in African Americans, followed by European Americans and others ethnic groups *(157;158)*.We hypothesized that the differences in the lung cancer risk was attributed to varied metabolic enzymes/pathways involved in the metabolism of carcinogens present in cigarette smoke. As BD is one of the carcinogens present in cigarette smoke we intended to use urinary BD-DNA adducts to provide a sensitive, non-invasive biomarkers of carcinogen exposure, metabolic activation, human cancer risk and explain the differences in lung cancer risk among African American (N = 86) and European American smokers (N = 80). We found that there are significant inter ethnic differences in BD metabolism and urinary EB-GII levels between African American (0.32 ± 0.31 pg/mg creatinine, N = 86) and European American smokers (1.31 ± 2.33 pg/mg creatinine, N = 80) (P-value = <0.0001 adjusted for age and sex). Urinary EB-GII levels represent the concentration of BD DNA adducts released from DNA due to hydrolysis or DNA adduct repair. Increased concentration of urinary EB-GII adducts in European American Smokers then African American Smokers might represent efficient removal of EB-GII adducts in DNA hence explaining the relatively decreased risk of BD induced DNA damage and cancer in European American Smokers as compared to African American Smokers. But further studies involving smokers from other ethnic groups such as Latino, Japanese and Native Hawaiians along with European American

and African American Smokers with increased population size should be used for this study to confirm this result.

In summary, we have developed and validated an isotope dilution nanoLC/ESI^+-$HRMS^3$ method for urinary EB-GII adducts of BD in humans. This method has excellent sensitivity, accuracy and selectivity. Although nucleobase adducts found in urine may have sources other than DNA (for example, they can be formed from RNA or cellular nucleoside pools), urinary EB-GII can serve as biomarkers of BD exposure and metabolic activation in future epidemiological studies.

VII. SUMMARY AND CONCLUSIONS

Human exposure to 1,3-butadiene (BD) is widespread because of its widespread presence in automobile exhaust *(284)*, cigarette smoke *(90)*, forest and wood fires *(290)*, and occupational settings such as synthetic rubber and plastic polymer production industries *(274)*. Among various carcinogens present in cigarette smoke, 1,3-butadiene (BD) has a very high cancer risk index *(159)* and is likely to contribute to the induction of smoking-mediated lung cancer in smokers *(157)*. Hence, it is important to determine the extent of BD exposure in humans. One of the best ways to monitor human exposure to a carcinogen is to quantify carcinogen specific biomarkers such as urinary metabolites, protein adducts, and DNA adducts *(279)*. Among various biomarkers of carcinogen exposure, DNA adducts directly correlate to cancer risk because of their ability to cause cancer causing mutations (Scheme 1.1) *(293)*.

BD is metabolically activated by cytochrome P450 monooxygenases CYP2E1 and CYP2A6 to form electrophilic epoxide metabolites (EB, EBD, and DEB), which react with nucleophilic bases in DNA to form covalent adducts (Scheme 1.8) *(92;152)*. Apart from reacting with DNA, BD metabolites also alkylate cellular proteins such as hemoglobin to form protein adducts (Scheme 1.9) *(125;128)* or are detoxified by hydrolysis and conjugation with glutathione to form BD-mercapturic acids, which are excreted in urine (Scheme 1.10) *(120;125)*. BD-protein adducts and BD-mercapturic acids have been previously used as biomarkers of human exposure to BD *(125)*. In contrast, to our knowledge, BD-DNA adducts had not been previously detected in humans.

Several BD-specific DNA adducts had been identified from studies in laboratory rats and mice exposed to relatively high concentrations of BD by inhalation (6.25-625 ppm) *(116)* (Schemes 1.7 and 1.8). By comparison, BD exposures in humans range between 1 to 3 ppm BD in an occupational exposure settings *(274)* and low ppb levels in cigarette smoke and environmental sources *(161)*, giving rise to very low amounts of BD DNA adducts (< 1-3 adducts/10^8 nucleotides). In this Thesis, ultra-sensitive mass spectrometric methods have been developed for the quantitation of BD-DNA adducts in humans exposed to BD from smoking and occupational sources.

In Chapter 2 of this Thesis, isotope dilution nanoLC/ESI^+-SRM methods were developed for quantitation of diepoxybutane specific DNA-DNA crosslinks (*bis*-N7G-BD) in liver DNA of laboratory mice exposed to sub-ppm levels of BD (0.5-1.5 ppm) (Scheme 2.1) *(69)*. We employed an offline HPLC analyte enrichment procedure coupled with nanospray HPLC-ESI^+- MS/MS to achieve excellent sensitivity for *bis*-N7G-BD in genomic DNA (LOQ, 1.0 fmol in 100 μg DNA, corresponding to 0.03 adducts per 10^7 nucleotides) (Scheme 2.2). Using this bioanalytical methodology, we successfully quantified *bis*-N7G-BD adducts in liver DNA of B6C3F1 mice exposed to 0, 0.5, 1.0, 1.5 ppm BD for 2 weeks (6 h/day, 5 days/week). We observed an increase in *bis*-N7G-BD numbers with BD exposure, giving rise to 5.7 ± 3.3, 9.2 ± 1.5, and 18.6 ± 6.9 adducts per 10^9 nucleotides in animals exposed to 0.5, 1.0 and 1.5 ppm BD, respectively (Figure 2.5). Higher efficiency of adduct formation (*bis*-N7G-BD adducts/10^7 nucleotides/ppm of BD) was observed at concentrations of BD less than 6.25 ppm, which are close to human occupational exposure concentrations (Figure 2.6) *(216)*. We concluded that it important to quantify BD specific DNA adducts at sub ppm concentrations which are more relevant

to human occupational exposures, environmental exposure, and cigarette smoking. However, we have been not able to detect *bis*-N7G-BD adducts in human blood DNA samples using this method. This is likely because *bis*-N7G-BD adduct levels in humans are below the limit of quantitation of our method as a result of an inefficient formation and/or rapid detoxification of DEB in humans *(135)*. This is consistent with our recent observation that DEB specific urinary mercapturic acid (*bis*-BDMA) was not detected in urine of humans occupationally exposed to BD *(135)*. It has been proposed that DEB concentrations in BD-exposed humans are low because of the efficient activity of epoxide hydrolase in human cells (Scheme 1.10) *(135)*.

In Chapter 3 of this Thesis, the mechanisms of repair of intestrand *bis*-N7G-BD cross-links in mammalian cells were investigated. Isogenic Chinese hamster lung fibroblasts cell lines deficient in Fanconi Anemia (FA) and nucleotide excision repair pathways (V-H4 and V-H1) were used in order to test the involvement of these pathways in removal of *bis*-N7G-BD adducts. Cytotoxicity studies in wild type V79 fibroblasts, FA repair deficient V-H4 cells, and NER deficient V-H1 cells have revealed that the repair deficient clones were much more sensitive to DEB-mediated toxicity as compared to the wild type cells (Figure 3.1A, B). Furthermore, *bis*-N7G-BD adduct numbers increased linearly with time upon DEB treatment (10 -100 μM). Importantly higher levels of *bis*-N7G-BD cross-links were observed in V-H1 and V-H4 cells deficient in NER and FA repair pathways as compared to V79 wild type cells (Figure 3.3A, B). The involvement of NER repair in *bis*-N7G-BD removal was further confirmed using NER inhibitor UCN-01 (Figure 3.4). Furthermore, γH2AX immunocytochemistry and alkaline comet assays (Figure 3.5, 3.6) have revealed an exaggerated formation of DNA double strand breaks

(DSBs) during the repair of DNA-DNA crosslinks *(245;270)*. In summary, we have shown that DEB exposure leads to increased cytotoxicity and accumulation of *bis*-N7G-BD crosslinks and DSBs in NER- and FA repair deficient cells, suggesting the involvement of these pathways in the repair of BD induced *bis*-N7G-BD adducts. FA repair pathway appears to be more important for protecting human cells against DEB-mediated toxicity as compared to NER.

The third goal of this thesis was the development of ultra-sensitive isotope dilution HPLC-ESI$^+$-HRMS/MS methodologies for quantification of BD-DNA adducts in humans. We initially focused on N7-THBG because it is formed from the most abundant BD epoxide (EBD) (Scheme 4.1). We took advantage of the high mass resolution capabilities of the Orbitrap Velos mass spectrometer, affording excellent LOD values for N7-THBG (0.3 adducts/10^9 nucleotides). Using this methodology, N7-THBG adducts were quantified in blood leukocyte DNA of smokers and non-smokers. Unexpectedly, N7-THBG concentrations were similar in DNA of smokers and non-smokers (8.21 ± 5.12 vs 7.08 ± 5.29 adducts /10^9 nucleotides, respectively; P = 0.60) (Table 4.2) and remained unchanged upon smoking cessation, suggesting that N7-THBG adduct levels in human leukocytes might not be related to smoking (Figure 4.6). Our observation of N7-THBG adducts in nonsmokers may be a result of environmental exposure to BD and/or endogenous sources of N7-THBG. In contrast, N7-THBG levels were significantly increased in leukocyte DNA of occupationally exposed individuals (9.73 ± 3.80 adducts/ 10^9 nucleotides, 1.51 ± 1.12 ppm BD) as compared to matched administrative controls (3.07 ± 2.15 adducts/ 10^9 nucleotides, 0.009 ± 0.012 ppm) (Table 4.3). Our validated

mass spectrometry method for N7-THBG has adequate accuracy and sensitivity for future human biomonitoring studies.

In an attempt to identify a biomarker of BD exposure that is related to smoking, we developed a nanoLC/ESI$^+$-HRMS^3 method for quantification of N-7-(1-hydroxy-3-buten-2-yl) guanine (EB-GII) adducts in human blood leukocyte DNA (Chapter 4, Scheme 5.1). Since EB-GII are induced by less abundant BD epoxide, 3,4-epoxy-1-butene (EB), the added sensitivity of nanospray HPLC and high resolution HRMS^3 on an Orbitrap Velos mass spectrometer was necessary (Scheme 5.2). The EB-GII adducts were released by thermal hydrolysis and enriched by offline HPLC purification. Following method validation, EB-GII were quantified in liver DNA of laboratory rats exposed to sub-ppm concentrations of BD (0, 0.5, 1.0, 1.5 ppm) by inhalation. A linear increase in EB-GII concentrations were observed, with 0.17 ± 0.05, 0.33 ± 0.08, and 0.50 ± 0.04 adducts per 10^8 nucleotides in liver DNA of F344 rats exposed to 0.5, 1.0 and 1.5 ppm BD, respectively (Figure 5.6B). We also determined the *in vivo* half-life of EB-GII adducts (2.20 ± 0.12 days) in rat liver DNA (Figure 5.7B). Finally the new methodology was applied to analyze EB-GII in blood leukocyte DNA of smokers and nonsmokers. Although EB-GII adducts were detected in human DNA of BD exposed individuals, their amounts were below the limit of quantitation of our method (0.4 adducts/10^9 nucleotides, 0.2 fmol in 150 μg of DNA). Unfortunately, DNA amounts could not be increased due to limited blood sample volumes available. *In vivo* persistence data suggested that EB-GII adducts were rapidly released from the DNA backbone by spontaneous hydrolysis and/or active repair. Therefore, we focused our efforts on developing a sensitive mass

spectrometric methodology for EB-GII adducts in human urine, which is more readily available than blood.

Sensitive nanoLC/ESI$^+$-HRMS^3 method was developed for quantitation of EB-GII in urine of human subjects exposed to BD (Chapter 5). As urine is a more complex biological matrix as compared to DNA hydrolysates, an additional solid phase extraction step for EB-GII analyte enrichment was incorporated prior to offline HPLC cleanup, followed by nanoLC/ESI$^+$-HRMS^3 analysis (Scheme 6.2). Our quantitative method for urinary EB-GII adducts was extensively validated for accuracy, intra/interday precision, LOD (0.25 fmol/mL urine), LOQ (1 fmol/mL urine) and freeze-thaw stability. Following validation, the method was applied to quantify EB-GII in urine of male and female F344 rats exposed to BD (0, 62.5 and 200 ppm). A concentration-dependent increase in urinary EB-GII adduct excretion was observed (Figure 6.2). Although female animals excreted 1.5 times higher levels of EB-GII than males, the difference was not statistically significant ($p > 0.15$, unpaired two sample t-test). This method was then applied to quantify EB-GII levels in urine samples of smokers, nonsmokers, and occupationally exposed workers (Figure 6.4). Although urinary levels of EB-GII were higher in smokers as compared to nonsmokers (1.78 ± 2.81 pg/mg vs 1.24 ± 2.31 creatinine, respectively) this difference was not statistically significant ($p = 0.08$, group t-test). In contrast, average urinary concentrations of EB-GII adducts in occupationally exposed workers (2.94 ± 3.54 pg/mg creatinine following 0.1–2.2 ppm BD exposure) were significantly higher than in urine of matched administrative controls (0.93 ± 1.85 pg/mg creatinine , < 0.01 ppm BD exposure). This can be explained by lower BD concentrations in mainstream cigarette smoke (76.4-259.6 µg/cigarette, low ppb levels of BD exposure)

(161) as compared to occupational exposure to BD (0.5-1.0 ppm BD) *(216)*. Furthermore, statistically significant differences were observed in urinary EB-GII excretion between European American and African American smokers (Eur. Am. 1.31 ± 2.33 pg/mg creatinine Afr. Am. 0.32 ± 0.31 pg/mg creatinine, $p = <0.0001$).

In summary, the research described in this Thesis has led to the development of novel isotope dilution mass spectrometric methods for sensitive quantitation of BD-induced *bis*-N7G-BD, N7-THBG, EB-GII adducts *in vivo*. All three adducts were quantified in tissues of BD-exposed laboratory animals, while N7-THBG, EB-GII adducts were also measured in humans exposed to BD from cigarette smoke and occupationally exposed workers. The new methodology has adequate sensitivity, accuracy, and precision to be used for future human BD exposure biomonitoring studies.

VIII. FUTURE DIRECTIONS

8.1 BD DNA adductomics strategies to quantify genome wide DNA damage upon BD exposure

As described in the Introduction (Chapter 1), DNA adductomics is a top down approach to detect and quantify global DNA damage *(199)*. BD-DNA adducts studied so far were investigated by a bottom up approach, where the structure of the target quantified nucleobase adduct is pre-determined. Hence, some important BD induced DNA adducts might have been missed in these targeted studies. By using triple quadrupole mass spectrometry, multistage ion trap scanning ($LC–MS^n$), or accurate mass spectrometry HR-MS^n type scanning, it is possible to detect novel BD-DNA adducts by monitoring a neutral loss of sugar (116 amu) from structurally modified nucleosides. To facilitate the identification of novel BD-DNA adducts, laboratory animals can be exposed to a mixture of BD isotopomers, $^{13}C_2$-BD, and $^{2}H_6$-BD by inhalation. Any BD-DNA adducts formed will display a characteristic isotope pattern with 2 and 6 mass units apart, thus providing a unique way to identify novel BD-DNA adducts and global DNA damage induced by BD (Figure 8.1 A). We hypothesize that these studies will discover novel BD-DNA adducts arising from other DNA bases such as cytosine, thymine, adenine, and guanine which might be useful as novel BD specific biomarkers. Furthermore, they may explain the mutational spectra of BD which is dominated by A→T transversions, although the majority of adducts identified so far are formed at guanine *(96)*.

In a separate study, we propose to investigate global BD-DNA damage in workers occupationally exposed to BD (BD polymer industries) known to be at an increased risk for leukemia. The results can be compared to controls using comprehensive DNA

adductomics methodology (figure 8.1B) *(199;205)*. A differential analysis between BD exposed and control workers using results from DNA adductomics methodology can identify global BD adducts likely responsible for the observed increase in cancer risk.

Figure 8.1(A) Stable isotope labeling-facilitated DNA adductomics that can be used to identify novel BD-DNA adducts.

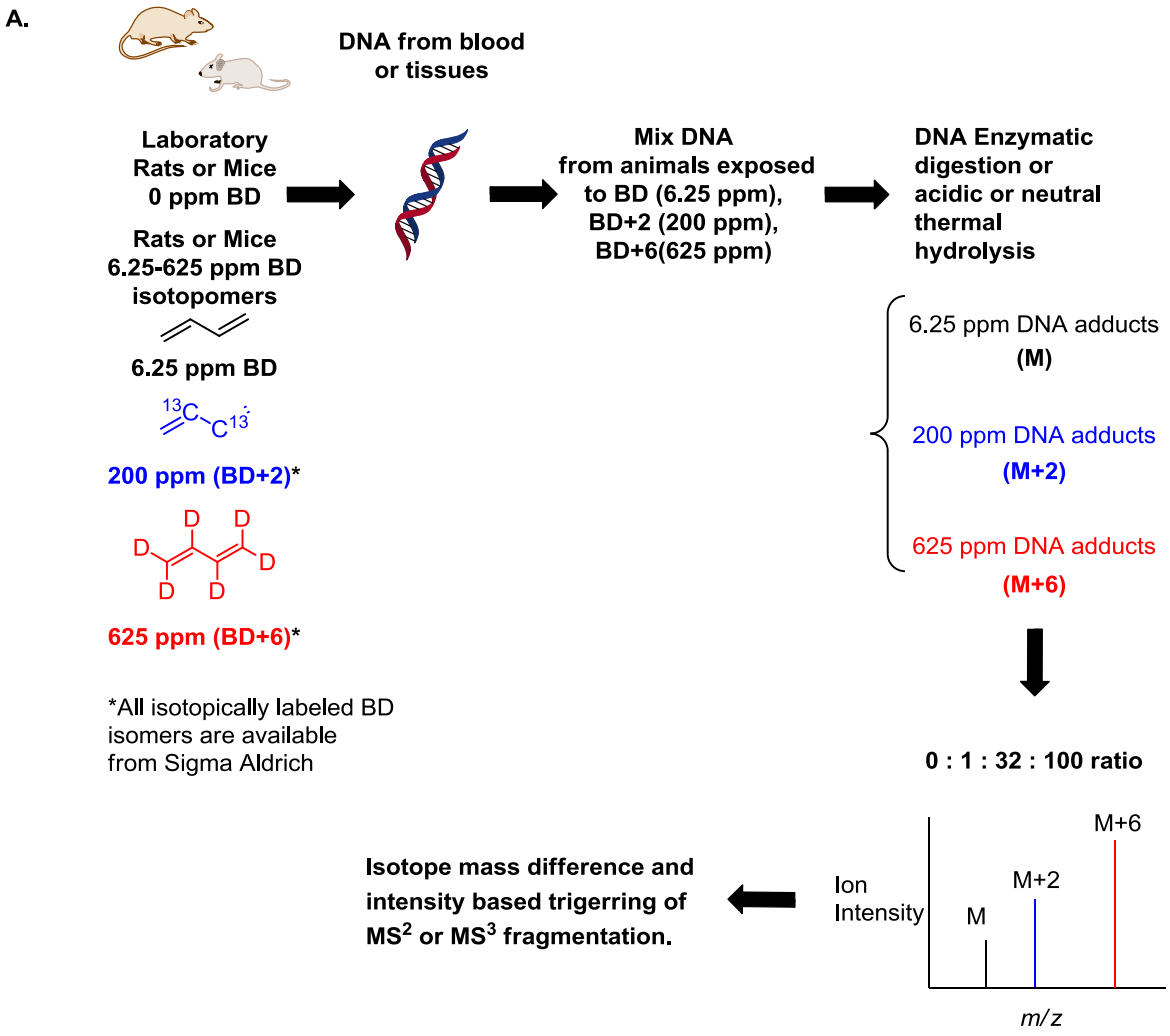

(B) Constant neutral loss of deoxyribose sugar (116 amu) can be used for data dependent scanning to identify unknown adducts in DNA of individuals occupationally exposed to BD *(199;205)*.

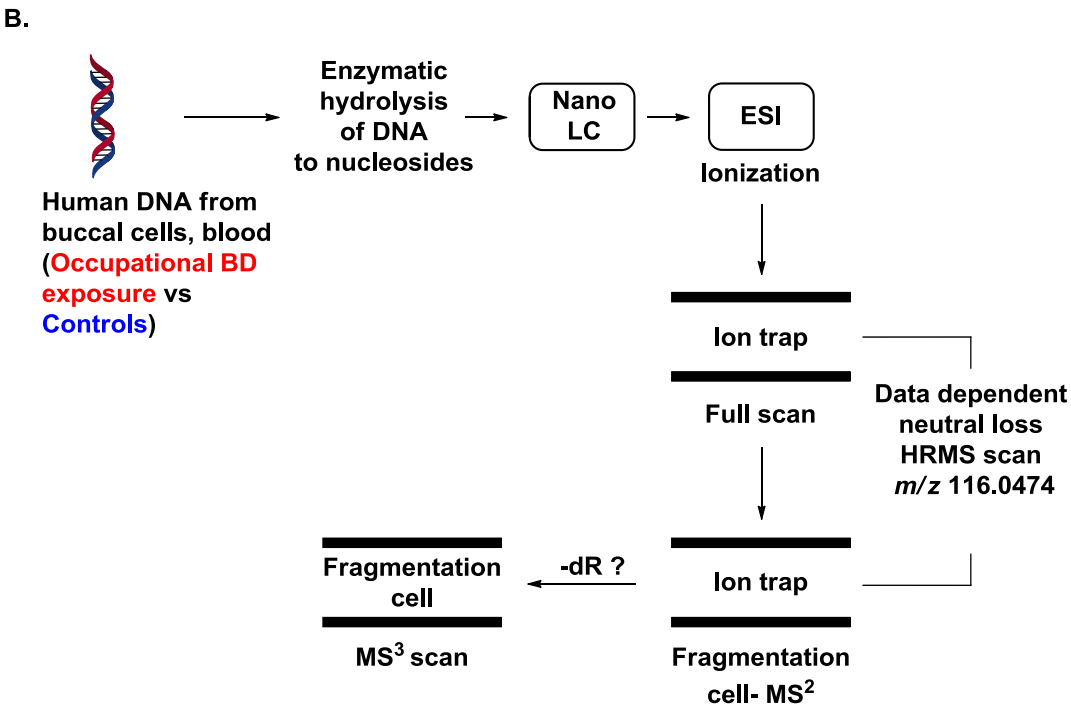

8.2 Investigation of Fanconi Anemia (FA) pathway in the repair DNA-DNA crosslinks induced by DEB.

Fanconi Anemia (FA) pathway is important for repair of DNA-DNA crosslinks induced by various carcinogens and drugs *(189;195)*. In Chapter 2 of this Thesis, we investigated the involvement of the FA pathway in repair of DEB-induced *bis*-N7G-BD crosslinks. An increased accumulation of *bis*-N7G-BD adducts was observed in FA repair pathway deficient V-H4 Chinese hamster cells. V-H4 cells are known to be ultra-sensitive to DNA damage induced by DNA cross-linking agents such as mitomycinC (MMC), cisplatin (cis-DDP), and DEB *(251)*. In fact, DEB is commonly used to diagnose FA *(317)*. V-H4 clones show phenotypic features similar to human patients with Fanconi Anemia *(251)*. However, V-H4 cells are not genetically very well characterized for FA repair pathway *(251)*. Furthermore, Chinese hamster lung fibroblasts are genetically different from human cells, so it would be beneficial to study FA repair pathway in human cell culture.

The FA pathway is a complex DNA repair pathway with at least 8 complementation group proteins FANCA, B, C, D1, D2, E, F and G. It is important to understand the role of particular proteins in the repair of *bis*-N7G-BD adducts induced by BD. We also wish to identify the minimal core FA complex essential for the repair of *bis*-N7G-BD. This information can provide insights into tolerable genetic deficiencies in human FA genes corresponding to certain proteins in the FA core complex. Several human lymphocyte and fibroblast cell lines deficient in specific FA proteins are available from the Coriell Institute Cell Repositories. Some of them are listed in the Table 8.1 below. *bis*-N7G-BD repair studies will be conducted in these cell lines to study the

cytotoxicity, double strand break formation, and the rate of *bis*-N7G-BD adduct formation and removal as compared to wild type cells treated with DEB. DEB induced DNA damage studies in specific FA protein repair deficient cells can provide insights into tolerable genetic deficiencies in human FA genes corresponding to certain proteins in the FA core complex.

Table 8-1 Human cell lines deficient in FA repair pathway

Catalog ID	**Decription**	**Human Cell type**
GM16756 GM16633	Fanconi Anemia Complementation Group, (FANC) FANCD2	B-Lymphocyte Fibroblast
GM13020 GM00449	FANCC	B-Lymphocyte Fibroblast
GM16632 GM13022	FANCA	Fibroblast B-Lymphocyte
GM13023	FANCD1	B-Lymphocyte
GM16757	FANCF	B-Lymphocyte

8.3 Improved analytical methods for N7-(2, 3, 4-trihydroxybut-1-yl) guanine (N7-THBG)

N7-THBG is a DNA adduct formed from the most abundant BD epoxide, 3,4-epoxy-1,2-butanediol (EBD) (Scheme 4.1). Owing to its three hydroxyl groups, N7-THBG is a very polar molecule and does not retain well on standard reverse phase HPLC columns. Commercially available 3-(dansylamino)phenylboronic acid (DPBA) can be used for derivatization of diol functionality of N7-THBG (Scheme 8.1). Since limited stability in water is a common problem with boronic acid esters derivatives, organic mobile phases can be employed for HPLC retention and elution of DPBA-N7-THBMA derivatives *(318)*. The resulting boronic acid ester will be analyzed by isotope dilution reverse phase nanospray HPLC-ESI-MS/MS.

Alternatively, nanospray liquid chromatography coupled to inductively coupled plasma tandem mass spectrometry (nanoLC-ICP-MS/MS) technique can also be used to detect and quantify element boron in derivatizated N7-THBG boronic acid ester to quantify trace levels in parts per trillion range *(319)*. Although isotope dilution is not possible in ICP-MS, another boron containing compound with similar structure can be used as an internal standard *(320)*.

Alternatively, underivatized N7-THBG can be retained using boronate affinity chromatography using specific columns packed with boronic acid stationary phases which is known as online derivatization to retain diols *(321)*.

Scheme 8.1 Proposed derivatization of N7-THBG with 3-(dansylamino) phenylboronic acid (DPBA)

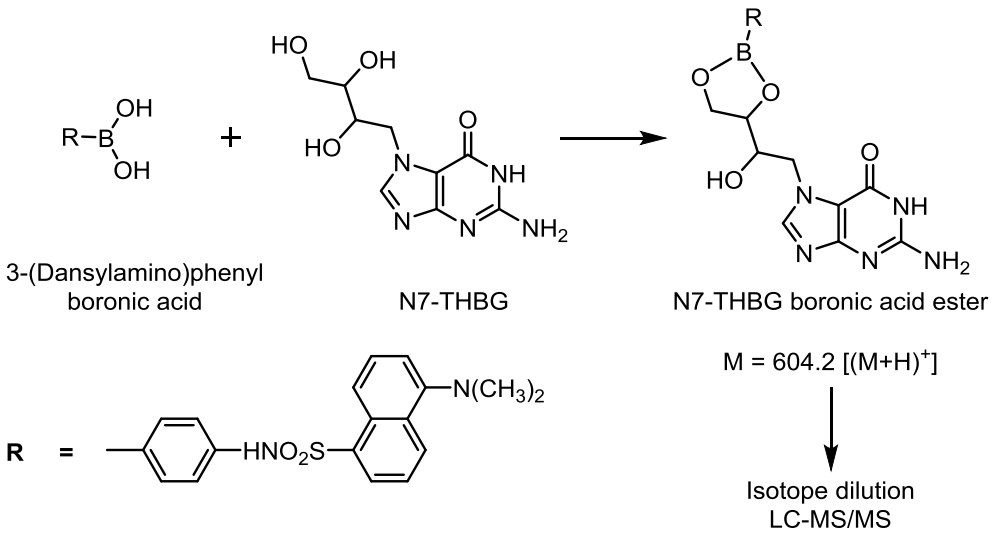

8.4 Quantification of BD-DNA adducts in smokers belonging to different ethnic groups.

In studies described in Chapter 6, we quantified urinary BD DNA adducts (EB-guanine II (EB-GII)) in samples from smokers belonging to two ethnic groups (European American and African Americans, 80 samples per group) and observed 3-fold greater urinary levels of EB-GII in European Americans (Table 6.2). Ethnic differences in BD-DNA adduct formation and urinary excretion may be caused by genetic polymorphisms in drug metabolism genes such as CYP2E1, glutathione-S-transferases GSTM1, GSTT1, and epoxide hydrolase (EH), or in DNA repair genes involved in adduct removal. To further explore ethnic/racial differences in BD metabolism, we propose to expand this study to a large multi-ethnic cohort involving Native Hawaiian, Japanese American, European American, Latino, and African American smokers (450 per group). This will enable us to correlate the observed differences in BD-DNA adducts with specific genetic polymorphisms (Figure 8.2). In the same study, it would be useful to include smokers that develop lung cancer, so that the relationship with lung cancer risk can be evaluated. We hypothesize that genetic polymorphisms in BD metabolizing enzyme CYP2E1 may lead to low enzyme activity, reduced concentrations of BD epoxides, decreased levels of BD-DNA adducts, and reduced lung cancer risk. In contrast, genetic polymorphisms in BD epoxides detoxifying enzymes such as epoxide hydrolase (EH) and glutathione -S-transferase (GSTT1, M1) may lead to lower detoxification activity than normal, resulting in accumulation of BD epoxides and the corresponding adducts and an increased lung cancer risk. The levels of BD-DNA adducts can also be mediated by polymorphisms in DNA repair proteins such as those involved in FA and NER pathways.

Figure 8.2 Multi ethnic cohort study design for the correlation of BD metabolic enzyme genetic polymorphisms with urinary BD-DNA adducts.

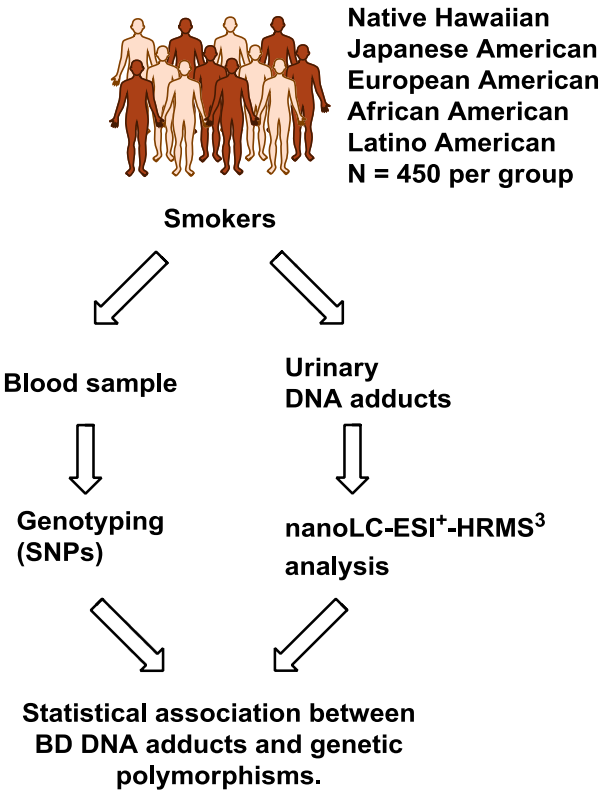

8.5 Measurement of BD induced DNA adducts in a mouse model of cigarette smoke exposure.

In our studies described in Chapters 4-6, we did not observe statistical differences between the concentrations of BD-DNA adducts in smokers and nonsmokers. It is important to determine whether smoking increases the levels of BD-DNA adducts above endogenous levels. We propose to use an animal model of cigarette smoke exposure. In the literature, there are several mouse models of smoking induced chronic obstructive pulmonary disease (COPD) including whole body exposure and nose only exposure models *(322-325)*. Although these models differ in type of mice strains used and commercial brands of cigarette smoke *(323)*, they can be used to evaluate the extent of 1,3-butadiene exposure from cigarette smoke and levels of BD DNA adducts formed upon smoking. The dose of cigarette smoke can be standardized based on nicotine and CO levels simulating human exposure to mainstream and side stream smoke *(326)*.

Although many previous studies have investigated BD-DNA adducts in laboratory animals exposed to BD gas *(137)*, we hypothesize that other carcinogens and co-carcinogens present in cigarette smoke may influence its metabolism. Metabolic differences are expected to be observed between direct exposure to BD by inhalation and BD exposure along with cigarette smoke constituents due to metabolic enzyme induction and inhibition *(327;328)*. For example, CYP2E1 monooxygenase has been reported to be induced by cigarette smoke, which should lead to increased metabolic activation of BD to its DNA-reactive epoxides *(328)*.

8.6 Development of a high throughput mass spectrometric method for simultaneous quantitation of *bis*-N7G-BD, N7-THBG and EB-Gua II.

In our current methodology, *bis*-N7G-BD, N7-THBG, and EB-guanine II are analyzed separately using adduct-specific enrichment and detection strategies. It is our long term goal to develop a single method for simultaneous quantitation of all three BD DNA adducts in biological matrices such as DNA or urine. Since all three adducts are to the N7 position of guanine and are structurally related, it should be possible to develop MS methodology for simultaneous quantitation of all three adducts in a single analysis. As indicated by calculated partition coefficients (miLogP, Scheme 8.2) *(329;330)* the three analytes have variable hydrophobic properties and are expected to behave differently on reverse phase HPLC. However, all three are N7-guanine adducts leading to reduced stability of N-glycosidic bond. Hence, all three adducts can be selectively released from DNA using neutral thermal hydrolysis. Following their release from DNA, ultrafiltration will be used to remove partially hydrolyzed DNA. Final enrichment can be performed by offline HPLC clean up using fraction collection of adduct specific fractions. Urinary adduct analysis may require additional solid phase extraction enrichment. For isotope dilution mass spectrometric quantitation, use of optimized nanospray reverse phase LC is preferred over other methods due to increased ionization leading to improved sensitivity. Accurate mass and high resolution MS is preferred over conventional triple quadrupole MS because of improved signal to noise ratio leading to increased sensitivity. This simplified procedure will save time and resources as all three lesions can be quantified in a single analysis.

Scheme 8.2 BD-DNA adducts induced by epoxide metabolites of BD. miLogP values were calculated using molinspiration cheminformatics tool *(329)*.

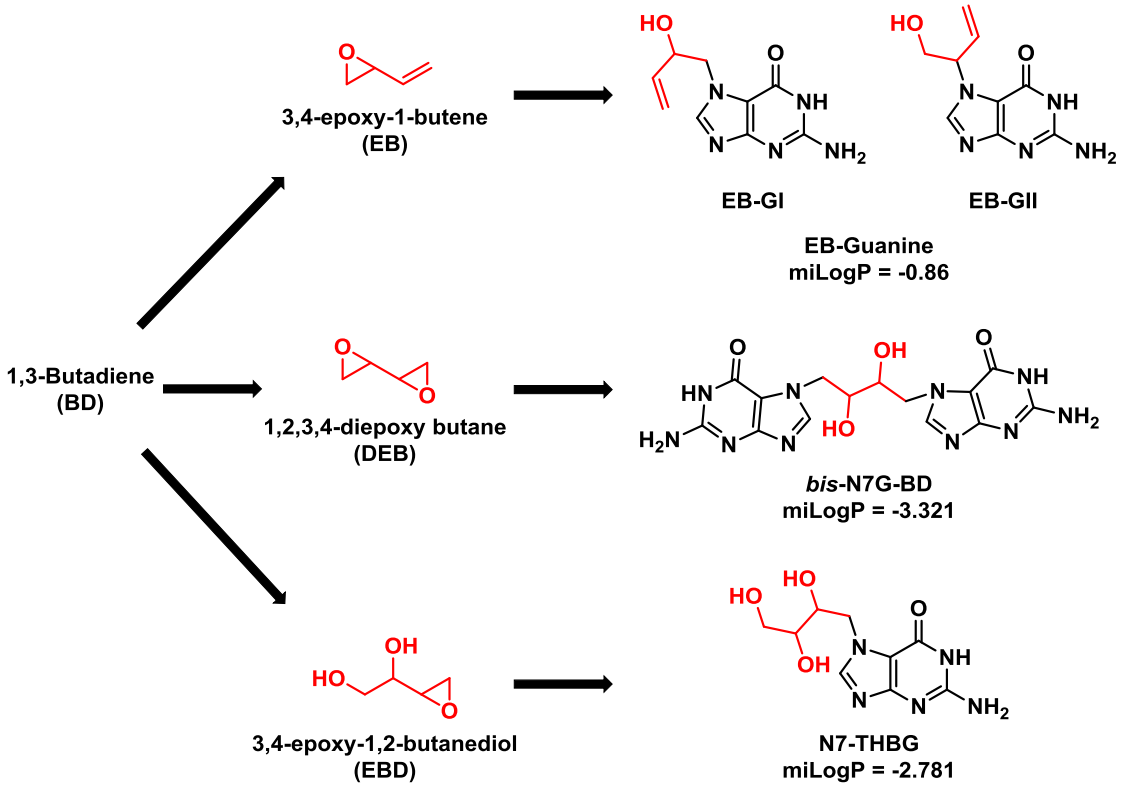

8.7 Quantitation of BD DNA adducts induced by wood burning, second hand smoke, and endogenous sources.

In addition to cigarette smoking, BD is known to be produced from incomplete combustion of wood burning such as in forest fires *(276;331)*. It is important to quantify BD exposure specific biomarkers such as DNA adducts, hemoglobin adducts and urinary metabolites in human populations exposed to BD from various sources such as forest and house fires. Specific human populations of interest are fire workers and people living in areas affected by forest fires. Other human populations of interest for quantitation of BD exposure biomarkers would be people exposed to second hand smoke from various sources such as cigarette smoke filled bars (0.81 to 8.6 ppb) and casinos *(90;332)*.

In our studies described in Chapter 5 and 6, BD-DNA adducts were detected in nonsmokers with no known exposure to BD. These adducts may be formed as a result of environmental BD exposure or may originate from an endogenous source *(134;141)*. Similarly, urinary mercapturic acids formed from HMVK and EBD have been detected in control rats *(135)*. Very low levels of BD epoxide, 3,4-epoxy-1-butene (EB) specific DNA adduct EB-GII was detected in the urine of control rats exposed to filtered air (14.5 – 87.0 pg/mL, Chapter 6). It has been proposed that EB-diol, the common precursor to HMVK and EBD, can be formed during the carbohydrate catabolism *(129)*. To differentiate the endogenous and exogenous BD exposure specific BD-DNA adduct formation, animals can be exposed with $^{13}C_2$-1,3-butadiene or $^{2}H_6$-1,3-butadiene (2 weeks, 6 h/day, 5 days/week). At the end of the exposure period, urinary BD DNA EB-GII adducts ($^{13}C_2$-EB-GII or $^{2}H_6$-EB-GII versus unlabeled EB-GII formed endogenously) can be quantified by the methods described in Chapters 4, 5 and 6. Comparison of $^{13}C_2$-

EB-GII or $^{2}H_{6}$-EB-GII with unlabeled EB-GII would provide information on the relative contributions of exogenous and exogenous BD-DNA adducts.

IX. BIBLIOGRAPHY

1. Lewtas, J. (1993) Airborne Carcinogens. *Pharmacology & Toxicology 72*, S55-S63.

2. Dayan, A. D. (1993) Carcinogenicity and drinking water. *Pharmacol. Toxicol. 72 Suppl 1*, 108-115.

3. Abnet, C. C. (2007) Carcinogenic food contaminants. *Cancer Investigation 25*, 189-196.

4. Hussain, S. P. and Harris, C. C. (2000) Molecular epidemiology and carcinogenesis: endogenous and exogenous carcinogens. *Mutat. Res. 462*, 311-322.

5. Burcham, P. C. (1998) Genotoxic lipid peroxidation products: their DNA damaging properties and role in formation of endogenous DNA adducts. *Mutagenesis 13*, 287-305.

6. Miller, J. A. (1970) Carcinogenesis by chemicals: an overview--G. H. A. Clowes memorial lecture. *Cancer Res. 30*, 559-576.

7. Rajski, S. R. and Williams, R. M. (1998) DNA Cross-Linking Agents as Antitumor Drugs. *Chem. Rev. 98*, 2723-2796.

8. Guengerich, F. P. (2000) Metabolism of chemical carcinogens. *Carcinogenesis 21*, 345-351.

9. Guengerich, F. P. (2000) Metabolism of chemical carcinogens. *Carcinogenesis 21*, 345-351.

10. Hemminki, K. (1993) DNA adducts, mutations and cancer. *Carcinogenesis 14*, 2007-2012.

11. Goggin, M., Sangaraju, D., Walker, V. E., Wickliffe, J., Swenberg, J. A., and Tretyakova, N. (2011) Persistence and repair of bifunctional DNA adducts in tissues of laboratory animals exposed to 1,3-butadiene by inhalation. *Chem. Res. Toxicol. 24*, 809-817.

12. Sancar, A., Lindsey-Boltz, L. A., Unsal-Kacmaz, K., and Linn, S. (2004) Molecular mechanisms of mammalian DNA repair and the DNA damage checkpoints. *Annu. Rev. Biochem. 73*, 39-85.

13. Minca, E. C. and Kowalski, D. (2011) Replication fork stalling by bulky DNA damage: localization at active origins and checkpoint modulation. *Nucleic Acids Res. 39*, 2610-2623.

14. Kotapati, S., Maddukuri, L., Wickramaratne, S., Seneviratne, U., Goggin, M., Pence, M. G., Villalta, P., Guengerich, F. P., Marnett, L., and Tretyakova, N. (2012) Translesion synthesis across 1,N6-(2-hydroxy-3-hydroxymethylpropan-1,3-diyl)-2'-deoxyadenosine (1,N6-gamma-HMHP-dA) adducts by human and archebacterial DNA polymerases. *J. Biol. Chem. 287*, 38800-38811.

15. Hockenbery, D. (1995) Defining apoptosis. *Am. J. Pathol. 146*, 16-19.

16. Kure, E. H., Ryberg, D., Hewer, A., Phillips, D. H., Skaug, V., Baera, R., and Haugen, A. (1996) p53 mutations in lung tumours: relationship to gender and lung DNA adduct levels. *Carcinogenesis 17*, 2201-2205.

17. Tretyakova, N., Matter, B., Jones, R., and Shallop, A. (2002) Formation of benzo[a]pyrene diol epoxide-DNA adducts at specific guanines within K-ras and p53 gene sequences: stable isotope-labeling mass spectrometry approach. *Biochemistry 41*, 9535-9544.

18. Rundle, A. (2006) Carcinogen-DNA adducts as a biomarker for cancer risk. *Mutat. Res. 600*, 23-36.

19. Essigmann, J. M., Croy, R. G., Nadzan, A. M., Busby, W. F., Jr., Reinhold, V. N., Buchi, G., and Wogan, G. N. (1977) Structural identification of the major DNA adduct formed by aflatoxin B1 in vitro. *Proc. Natl. Acad. Sci. U. S. A 74*, 1870-1874.

20. Peterson, L. A. (2010) Formation, repair, and genotoxic properties of bulky DNA adducts formed from tobacco-specific nitrosamines. *J. Nucleic Acids 2010*.

21. Geacintov, N. E., Yoshida, H., Ibanez, V., Jacobs, S. A., and Harvey, R. G. (1984) Conformations of adducts and kinetics of binding to DNA of the optically pure enantiomers of anti-benzo(a)pyrene diol epoxide. *Biochem. Biophys. Res. Commun. 122*, 33-39.

22. Schut, H. A. and Snyderwine, E. G. (1999) DNA adducts of heterocyclic amine food mutagens: implications for mutagenesis and carcinogenesis. *Carcinogenesis 20*, 353-368.

23. Zhang, S., Balbo, S., Wang, M., and Hecht, S. S. (2011) Analysis of acrolein-derived 1,N2-propanodeoxyguanosine adducts in human leukocyte DNA from smokers and nonsmokers. *Chem. Res. Toxicol. 24*, 119-124.

24. Blommaert, F. A., Floot, B. G., Dijk-Knijnenburg, H. C., Berends, F., Baan, R. A., Schornagel, J. H., den Engelse, L., and Fichtinger-Schepman, A. M. (1998) The formation and repair of cisplatin-DNA adducts in wild-type and cisplatin-resistant L1210 cells: comparison of immunocytochemical determination with detection in isolated DNA. *Chem. Biol. Interact. 108*, 209-225.

25. Tentori, L. and Graziani, G. (2009) Recent approaches to improve the antitumor efficacy of temozolomide. *Curr. Med. Chem. 16*, 245-257.

26. Maccubbin, A. E., Caballes, L., Riordan, J. M., Huang, D. H., and Gurtoo, H. L. (1991) A cyclophosphamide/DNA phosphoester adduct formed in vitro and in vivo. *Cancer Res. 51*, 886-892.

27. Oyama, T., Kagawa, N., Kunugita, N., Kitagawa, K., Ogawa, M., Yamaguchi, T., Suzuki, R., Kinaga, T., Yashima, Y., Ozaki, S., Isse, T., Kim, Y. D., Kim, H., and Kawamoto, T. (2004) Expression of cytochrome P450 in tumor tissues and its association with cancer development. *Front Biosci. 9*, 1967-1976.

28. De Bont, R. and van Larebeke, N. (2004) Endogenous DNA damage in humans: a review of quantitative data. *Mutagenesis 19*, 169-185.

29. Klaunig, J. E. and Kamendulis, L. M. (2004) The role of oxidative stress in carcinogenesis. *Annu. Rev. Pharmacol. Toxicol. 44*, 239-267.

30. Bartsch, H. and Nair, J. (2000) Ultrasensitive and specific detection methods for exocylic DNA adducts: markers for lipid peroxidation and oxidative stress. *Toxicology 153*, 105-114.

31. Dwivedy, I., Devanesan, P., Cremonesi, P., Rogan, E., and Cavalieri, E. (1992) Synthesis and characterization of estrogen 2,3- and 3,4-quinones. Comparison of DNA adducts formed by the quinones versus horseradish peroxidase-activated catechol estrogens. *Chem. Res. Toxicol. 5*, 828-833.

32. De Bont, R. and van Larebeke, N. (2004) Endogenous DNA damage in humans: a review of quantitative data. *Mutagenesis 19*, 169-185.

33. Guengerich, F. P. (2000) Metabolism of chemical carcinogens. *Carcinogenesis 21*, 345-351.

34. Farmer, P. B. (2004) DNA and protein adducts as markers of genotoxicity. *Toxicol. Lett. 149*, 3-9.

35. Prestera, T., Holtzclaw, W. D., Zhang, Y., and Talalay, P. (1993) Chemical and molecular regulation of enzymes that detoxify carcinogens. *Proc. Natl. Acad. Sci. U. S. A 90*, 2965-2969.

36. Trushin, N., Alam, S., El Bayoumy, K., Krzeminski, J., Amin, S. G., Gullett, J., Meyers, C., and Prokopczyk, B. (2012) Comparative metabolism of benzo[a]pyrene by human keratinocytes infected with high-risk human papillomavirus types 16 and 18 as episomal or integrated genomes. *J. Carcinog. 11*, 1.

37. Yang, Y., Rafter, J., Gustafsson, J. A., Sjovall, J., and Griffiths, W. J. (1998) Analysis of the major mercapturic acid pathway metabolites of benzo[a]pyrene found in rat urine by nano-electrospray mass spectrometry. *Rapid Commun. Mass Spectrom. 12*, 465-471.

38. Zheng, Z., Fang, J. L., and Lazarus, P. (2002) Glucuronidation: an important mechanism for detoxification of benzo[a]pyrene metabolites in aerodigestive tract tissues. *Drug Metab Dispos. 30*, 397-403.

39. Guengerich, F. P. (2000) Metabolism of chemical carcinogens. *Carcinogenesis 21*, 345-351.

40. Malayappan, B., Johnson, L., Nie, B., Panchal, D., Matter, B., Jacobson, P., and Tretyakova, N. (2010) Quantitative high-performance liquid chromatography-electrospray ionization tandem mass spectrometry analysis of bis-N7-guanine DNA-DNA cross-links in white blood cells of cancer patients receiving cyclophosphamide therapy. *Anal. Chem. 82*, 3650-3658.

41. Perera, F. P., Motzer, R. J., Tang, D., Reed, E., Parker, R., Warburton, D., O'Neill, P., Albertini, R., Bigbee, W. L., Jensen, R. H., and . (1992) Multiple

biological markers in germ cell tumor patients treated with platinum-based chemotherapy. *Cancer Res. 52*, 3558-3565.

42. Harrison, K. L., Wood, M., Lees, N. P., Hall, C. N., Margison, G. P., and Povey, A. C. (2001) Development and application of a sensitive and rapid immunoassay for the quantitation of N7-methyldeoxyguanosine in DNA samples. *Chem. Res. Toxicol. 14*, 295-301.

43. Hemminki, K., Rajaniemi, H., Lindahl, B., and Moberger, B. (1996) Tamoxifen-induced DNA adducts in endometrial samples from breast cancer patients. *Cancer Res. 56*, 4374-4377.

44. Hernandez-Ramon, E. E., Sandoval, N. A., John, K., Cline, J. M., Wood, C. E., Woodward, R. A., and Poirier, M. C. (2014) Tamoxifen-DNA adduct formation in monkey and human reproductive organs. *Carcinogenesis 35*, 1172-1176.

45. Yun, B. H., Rosenquist, T. A., Sidorenko, V., Iden, C. R., Chen, C. H., Pu, Y. S., Bonala, R., Johnson, F., Dickman, K. G., Grollman, A. P., and Turesky, R. J. (2012) Biomonitoring of aristolactam-DNA adducts in human tissues using ultra-performance liquid chromatography/ion-trap mass spectrometry. *Chem. Res. Toxicol. 25*, 1119-1131.

46. Campbell, T. C. (1994) Correspondence re: G-S. Qian, et al., A follow-up study of urinary markers of aflatoxin exposure and liver cancer risk in Shanghai, People's Republic of China. Cancer Epidemiol., Biomarkers & Prev., 3:3-10, 1994, and C.C. Harris, Solving the viral-chemical puzzle of human liver

carcinogenesis. Cancer Epidemiol., Biomarkers & Prev., 3:1-2, 1994. *Cancer Epidemiol. Biomarkers Prev. 3*, 519-521.

47. Qian, G. S., Ross, R. K., Yu, M. C., Yuan, J. M., Gao, Y. T., Henderson, B. E., Wogan, G. N., and Groopman, J. D. (1994) A follow-up study of urinary markers of aflatoxin exposure and liver cancer risk in Shanghai, People's Republic of China. *Cancer Epidemiol. Biomarkers Prev. 3*, 3-10.

48. Nath, R. G., Ocando, J. E., Guttenplan, J. B., and Chung, F. L. (1998) 1,N2-propanodeoxyguanosine adducts: potential new biomarkers of smoking-induced DNA damage in human oral tissue. *Cancer Res. 58*, 581-584.

49. Poirier, M. C. and Beland, F. A. (1992) DNA adduct measurements and tumor incidence during chronic carcinogen exposure in animal models: implications for DNA adduct-based human cancer risk assessment. *Chem. Res. Toxicol. 5*, 749-755.

50. Otteneder, M. and Lutz, W. K. (1999) Correlation of DNA adduct levels with tumor incidence: carcinogenic potency of DNA adducts. *Mutat. Res. 424*, 237-247.

51. Tretyakova, N., Goggin, M., Sangaraju, D., and Janis, G. (2012) Quantitation of DNA adducts by stable isotope dilution mass spectrometry. *Chem. Res. Toxicol. 25*, 2007-2035.

52. Chen, L., Wang, M., Villalta, P. W., Luo, X., Feuer, R., Jensen, J., Hatsukami, D. K., and Hecht, S. S. (2007) Quantitation of an acetaldehyde adduct in human

leukocyte DNA and the effect of smoking cessation. *Chem. Res. Toxicol. 20*, 108-113.

53. Wang, M., Cheng, G., Balbo, S., Carmella, S. G., Villalta, P. W., and Hecht, S. S. (2009) Clear differences in levels of a formaldehyde-DNA adduct in leukocytes of smokers and nonsmokers. *Cancer Res. 69*, 7170-7174.

54. Stepanov, I., Muzic, J., Le, C. T., Sebero, E., Villalta, P., Ma, B., Jensen, J., Hatsukami, D., and Hecht, S. S. (2013) Analysis of 4-hydroxy-1-(3-pyridyl)-1-butanone (HPB)-releasing DNA adducts in human exfoliated oral mucosa cells by liquid chromatography-electrospray ionization-tandem mass spectrometry. *Chem. Res. Toxicol. 26*, 37-45.

55. Bessette, E. E., Spivack, S. D., Goodenough, A. K., Wang, T., Pinto, S., Kadlubar, F. F., and Turesky, R. J. (2010) Identification of carcinogen DNA adducts in human saliva by linear quadrupole ion trap/multistage tandem mass spectrometry. *Chem. Res. Toxicol. 23*, 1234-1244.

56. Gorlewska-Roberts, K., Green, B., Fares, M., Ambrosone, C. B., and Kadlubar, F. F. (2002) Carcinogen-DNA adducts in human breast epithelial cells. *Environ. Mol. Mutagen. 39*, 184-192.

57. Talaska, G., Schamer, M., Skipper, P., Tannenbaum, S., Caporaso, N., Unruh, L., Kadlubar, F. F., Bartsch, H., Malaveille, C., and Vineis, P. (1991) Detection of carcinogen-DNA adducts in exfoliated urothelial cells of cigarette smokers:

association with smoking, hemoglobin adducts, and urinary mutagenicity. *Cancer Epidemiol. Biomarkers Prev. 1*, 61-66.

58. Groopman, J. D., Wild, C. P., Hasler, J., Junshi, C., Wogan, G. N., and Kensler, T. W. (1993) Molecular epidemiology of aflatoxin exposures: validation of aflatoxin-N7-guanine levels in urine as a biomarker in experimental rat models and humans. *Environ. Health Perspect. 99*, 107-113.

59. Bransfield, L. A., Rennie, A., Visvanathan, K., Odwin, S. A., Kensler, T. W., Yager, J. D., Friesen, M. D., and Groopman, J. D. (2008) Formation of two novel estrogen guanine adducts and HPLC/MS detection of 4-hydroxyestradiol-N7-guanine in human urine. *Chem. Res. Toxicol. 21*, 1622-1630.

60. Tarun, M. and Rusling, J. F. (2005) Measuring DNA nucleobase adducts using neutral hydrolysis and liquid chromatography-mass spectrometry. *Crit Rev. Eukaryot. Gene Expr. 15*, 295-316.

61. Hah, S. S., Mundt, J. M., Kim, H. M., Sumbad, R. A., Turteltaub, K. W., and Henderson, P. T. (2007) Measurement of 7,8-dihydro-8-oxo-2'-deoxyguanosine metabolism in MCF-7 cells at low concentrations using accelerator mass spectrometry. *Proc. Natl. Acad. Sci. U. S. A 104*, 11203-11208.

62. Chetsanga, C. J., Polidori, G., and Mainwaring, M. (1982) Analysis and excision of ring-opened phosphoramide mustard-deoxyguanine adducts in DNA. *Cancer Res. 42*, 2616-2621.

63. Jaruga, P., Kirkali, G., and Dizdaroglu, M. (2008) Measurement of formamidopyrimidines in DNA. *Free Radic. Biol. Med. 45*, 1601-1609.

64. Upadhyaya, P., Lindgren, B. R., and Hecht, S. S. (2009) Comparative levels of O6-methylguanine, pyridyloxobutyl-, and pyridylhydroxybutyl-DNA adducts in lung and liver of rats treated chronically with the tobacco-specific carcinogen 4-(methylnitrosamino)-1-(3-pyridyl)-1-butanone. *Drug Metab Dispos. 37*, 1147-1151.

65. Goggin, M., Seneviratne, U., Swenberg, J. A., Walker, V. E., and Tretyakova, N. (2010) Column switching HPLC-ESI(+)-MS/MS methods for quantitative analysis of exocyclic dA adducts in the DNA of laboratory animals exposed to 1,3-butadiene. *Chem. Res. Toxicol. 23*, 808-812.

66. Schumacher, F., Herrmann, K., Florian, S., Engst, W., and Glatt, H. (2013) Optimized enzymatic hydrolysis of DNA for LC-MS/MS analyses of adducts of 1-methoxy-3-indolylmethyl glucosinolate and methyleugenol. *Anal. Biochem. 434*, 4-11.

67. Chan, W., Zheng, Y., and Cai, Z. (2007) Liquid chromatography-tandem mass spectrometry analysis of the DNA adducts of aristolochic acids. *J. Am. Soc. Mass Spectrom. 18*, 642-650.

68. Koc, H. and Swenberg, J. A. (2002) Applications of mass spectrometry for quantitation of DNA adducts. *J. Chromatogr. B Analyt. Technol. Biomed. Life Sci. 778*, 323-343.

69. Sangaraju, D., Goggin, M., Walker, V., Swenberg, J., and Tretyakova, N. (2012) NanoHPLC-nanoESI(+)-MS/MS quantitation of bis-N7-guanine DNA-DNA cross-links in tissues of B6C3F1 mice exposed to subppm levels of 1,3-butadiene. *Anal. Chem. 84*, 1732-1739.

70. Sangaraju, D., Villalta, P. W., Wickramaratne, S., Swenberg, J., and Tretyakova, N. (2014) NanoLC/ESI(+) HRMS (3) Quantitation of DNA Adducts Induced by 1,3-Butadiene. *J. Am. Soc. Mass Spectrom. 25*, 1124-1135.

71. Ho, C. S., Lam, C. W., Chan, M. H., Cheung, R. C., Law, L. K., Lit, L. C., Ng, K. F., Suen, M. W., and Tai, H. L. (2003) Electrospray ionisation mass spectrometry: principles and clinical applications. *Clin. Biochem. Rev. 24*, 3-12.

72. Frischmann, M., Bidmon, C., Angerer, J., and Pischetsrieder, M. (2005) Identification of DNA adducts of methylglyoxal. *Chem. Res. Toxicol. 18*, 1586-1592.

73. Iijima, H., Patrzyc, H. B., Dawidzik, J. B., Budzinski, E. E., Cheng, H. C., Freund, H. G., and Box, H. C. (2004) Measurement of DNA adducts in cells exposed to cisplatin. *Anal. Biochem. 333*, 65-71.

74. Goggin, M., Loeber, R., Park, S., Walker, V., Wickliffe, J., and Tretyakova, N. (2007) HPLC-ESI+-MS/MS analysis of N7-guanine-N7-guanine DNA cross-links in tissues of mice exposed to 1,3-butadiene. *Chem. Res. Toxicol. 20*, 839-847.

75. Koc, H., Tretyakova, N. Y., Walker, V. E., Henderson, R. F., and Swenberg, J. A. (1999) Molecular dosimetry of N-7 guanine adduct formation in mice and rats exposed to 1,3-butadiene. *Chem. Res. Toxicol. 12*, 566-574.

76. Chen, H. J. and Lin, W. P. (2009) Simultaneous quantification of 1,N2-propano-2'-deoxyguanosine adducts derived from acrolein and crotonaldehyde in human placenta and leukocytes by isotope dilution nanoflow LC nanospray ionization tandem mass spectrometry. *Anal. Chem. 81*, 9812-9818.

77. Chen, H. J., Wang, Y. C., and Lin, W. P. (2012) Analysis of ethylated thymidine adducts in human leukocyte DNA by stable isotope dilution nanoflow liquid chromatography-nanospray ionization tandem mass spectrometry. *Anal. Chem. 84*, 2521-2527.

78. Page, J. S., Kelly, R. T., Tang, K., and Smith, R. D. (2007) Ionization and transmission efficiency in an electrospray ionization-mass spectrometry interface. *J. Am. Soc. Mass Spectrom. 18*, 1582-1590.

79. Marshall, A. G., Hendrickson, C. L., and Shi, S. D. (2002) Scaling MS plateaus with high-resolution FT-ICRMS. *Anal. Chem. 74*, 252A-259A.

80. Hu, Q., Noll, R. J., Li, H., Makarov, A., Hardman, M., and Graham, C. R. (2005) The Orbitrap: a new mass spectrometer. *J. Mass Spectrom. 40*, 430-443.

81. Zhang, N. R., Yu, S., Tiller, P., Yeh, S., Mahan, E., and Emary, W. B. (2009) Quantitation of small molecules using high-resolution accurate mass

spectrometers - a different approach for analysis of biological samples. *Rapid Commun. Mass Spectrom. 23*, 1085-1094.

82. Olsen, J. V., Macek, B., Lange, O., Makarov, A., Horning, S., and Mann, M. (2007) Higher-energy C-trap dissociation for peptide modification analysis. *Nat. Methods 4*, 709-712.

83. White, W. C. (2007) Butadiene production process overview. *Chem. Biol. Interact. 166*, 10-14.

84. Melnick, R. L., Huff, J., Chou, B. J., and Miller, R. A. (1990) Carcinogenicity of 1,3-butadiene in C57BL/6 x C3H F1 mice at low exposure concentrations. *Cancer Res. 50*, 6592-6599.

85. Owen, P. E., Glaister, J. R., Gaunt, I. F., and Pullinger, D. H. (1987) Inhalation toxicity studies with 1,3-butadiene. 3. Two year toxicity/carcinogenicity study in rats. *Am. Ind. Hyg. Assoc. J. 48*, 407-413.

86. Sathiakumar, N., Graff, J., Macaluso, M., Maldonado, G., Matthews, R., and Delzell, E. (2005) An updated study of mortality among North American synthetic rubber industry workers. *Occup. Environ. Med. 62*, 822-829.

87. Delzell, E., Sathiakumar, N., Hovinga, M., Macaluso, M., Julian, J., Larson, R., Cole, P., and Muir, D. C. (1996) A follow-up study of synthetic rubber workers. *Toxicology 113*, 182-189.

88. Ward, E. M., Fajen, J. M., Ruder, A. M., Rinsky, R. A., Halperin, W. E., and Fessler-Flesch, C. A. (1996) Mortality study of workers employed in 1,3-butadiene production units identified from a large chemical workers cohort. *Toxicology 113*, 157-168.

89. Kagawa, J. (2002) Health effects of diesel exhaust emissions--a mixture of air pollutants of worldwide concern. *Toxicology 181-182*, 349-353.

90. Brunnemann, K. D., Kagan, M. R., Cox, J. E., and Hoffmann, D. (1990) Analysis of 1,3-butadiene and other selected gas-phase components in cigarette mainstream and sidestream smoke by gas chromatography-mass selective detection. *Carcinogenesis 11*, 1863-1868.

91. Himmelstein, M. W., Acquavella, J. F., Recio, L., Medinsky, M. A., and Bond, J. A. (1997) Toxicology and epidemiology of 1,3-butadiene. *Crit Rev. Toxicol. 27*, 1-108.

92. Duescher, R. J. and Elfarra, A. A. (1994) Human liver microsomes are efficient catalysts of 1,3-butadiene oxidation: evidence for major roles by cytochromes P450 2A6 and 2E1. *Arch. Biochem. Biophys. 311*, 342-349.

93. Csanady, G. A., Guengerich, F. P., and Bond, J. A. (1992) Comparison of the biotransformation of 1,3-butadiene and its metabolite, butadiene monoepoxide, by hepatic and pulmonary tissues from humans, rats and mice. *Carcinogenesis 13*, 1143-1153.

94. Krause, R. J., Sharer, J. E., and Elfarra, A. A. (1997) Epoxide hydrolase-dependent metabolism of butadiene monoxide to 3-butene-1,2-diol in mouse, rat, and human liver. *Drug Metab Dispos. 25*, 1013-1015.

95. Cochrane, J. E. and Skopek, T. R. (1994) Mutagenicity of butadiene and its epoxide metabolites: I. Mutagenic potential of 1,2-epoxybutene, 1,2,3,4-diepoxybutane and 3,4-epoxy-1,2-butanediol in cultured human lymphoblasts. *Carcinogenesis 15*, 713-717.

96. Recio, L., Steen, A. M., Pluta, L. J., Meyer, K. G., and Saranko, C. J. (2001) Mutational spectrum of 1,3-butadiene and metabolites 1,2-epoxybutene and 1,2,3,4-diepoxybutane to assess mutagenic mechanisms. *Chem. Biol. Interact. 135-136*, 325-341.

97. Meng, Q., Redetzke, D. L., Hackfeld, L. C., Hodge, R. P., Walker, D. M., and Walker, V. E. (2007) Mutagenicity of stereochemical configurations of 1,2-epoxybutene and 1,2:3,4-diepoxybutane in human lymphblastoid cells. *Chem. Biol. Interact. 166*, 207-218.

98. Steen, A. M., Meyer, K. G., and Recio, L. (1997) Analysis of hprt mutations occurring in human TK6 lymphoblastoid cells following exposure to 1,2,3,4-diepoxybutane. *Mutagenesis 12*, 61-67.

99. Liu, S., Ao, L., Du, B., Zhou, Y., Yuan, J., Bai, Y., Zhou, Z., and Cao, J. (2008) HPRT mutations in lymphocytes from 1,3-butadiene-exposed workers in China. *Environ. Health Perspect. 116*, 203-208.

100. Ma, H., Wood, T. G., Ammenheuser, M. M., Rosenblatt, J. I., and Ward, J. B., Jr. (2000) Molecular analysis of hprt mutant lymphocytes from 1, 3-butadiene-exposed workers. *Environ. Mol. Mutagen. 36*, 59-71.

101. Hayes, R. B., Xi, L., Bechtold, W. E., Rothman, N., Yao, M., Henderson, R., Zhang, L., Smith, M. T., Zhang, D., Wiemels, J., Dosemeci, M., Yin, S., and O'Neill, J. P. (1996) hprt mutation frequency among workers exposed to 1,3-butadiene in China. *Toxicology 113*, 100-105.

102. Tates, A. D., van Dam, F. J., de Zwart, F. A., Darroudi, F., Natarajan, A. T., Rossner, P., Peterkova, K., Peltonen, K., Demopoulos, N. A., Stephanou, G., Vlachodimitropoulos, D., and Sram, R. J. (1996) Biological effect monitoring in industrial workers from the Czech Republic exposed to low levels of butadiene. *Toxicology 113*, 91-99.

103. Tretyakova, N. Y., Lin, Y. P., Upton, P. B., Sangaiah, R., and Swenberg, J. A. (1996) Macromolecular adducts of butadiene. *Toxicology 113*, 70-76.

104. Tretyakova, N. Y., Chiang, S. Y., Walker, V. E., and Swenberg, J. A. (1998) Quantitative analysis of 1,3-butadiene-induced DNA adducts in vivo and in vitro using liquid chromatography electrospray ionization tandem mass spectrometry. *J. Mass Spectrom. 33*, 363-376.

105. Park, S., Anderson, C., Loeber, R., Seetharaman, M., Jones, R., and Tretyakova, N. (2005) Interstrand and intrastrand DNA-DNA cross-linking by 1,2,3,4-diepoxybutane: role of stereochemistry. *J. Am. Chem. Soc. 127*, 14355-14365.

106. Park, S., Hodge, J., Anderson, C., and Tretyakova, N. (2004) Guanine-adenine DNA cross-linking by 1,2,3,4-diepoxybutane: potential basis for biological activity. *Chem. Res. Toxicol. 17*, 1638-1651.

107. Seneviratne, U., Antsypovich, S., Goggin, M., Dorr, D. Q., Guza, R., Moser, A., Thompson, C., York, D. M., and Tretyakova, N. (2010) Exocyclic deoxyadenosine adducts of 1,2,3,4-diepoxybutane: synthesis, structural elucidation, and mechanistic studies. *Chem. Res. Toxicol. 23*, 118-133.

108. Koivisto, P., Kilpelainen, I., Rasanen, I., Adler, I. D., Pacchierotti, F., and Peltonen, K. (1999) Butadiene diolepoxide- and diepoxybutane-derived DNA adducts at N7-guanine: a high occurrence of diolepoxide-derived adducts in mouse lung after 1,3-butadiene exposure. *Carcinogenesis 20*, 1253-1259.

109. Koivisto, P., Adler, I. D., Pacchierotti, F., and Peltonen, K. (1998) DNA adducts in mouse testis and lung after inhalation exposure to 1,3-butadiene. *Mutat. Res. 397*, 3-10.

110. Koivisto, P., Adler, I. D., Sorsa, M., and Peltonen, K. (1996) Inhalation exposure of rats and mice to 1,3-butadiene induces N6-adenine adducts of epoxybutene detected by 32P-postlabeling and HPLC. *Environ. Health Perspect. 104 Suppl 3*, 655-657.

111. Koivisto, P. and Peltonen, K. (2001) N7-guanine adducts of the epoxy metabolites of 1,3-butadiene in mice lung. *Chem. Biol. Interact. 135-136*, 363-372.

112. Zhao, C., Vodicka, P., Sram1 RJ, and Hemminki, K. (2000) Human DNA adducts of 1,3-butadiene, an important environmental carcinogen. *Carcinogenesis 21*, 107-111.

113. Goggin, M., Anderson, C., Park, S., Swenberg, J., Walker, V., and Tretyakova, N. (2008) Quantitative high-performance liquid chromatography-electrospray ionization-tandem mass spectrometry analysis of the adenine-guanine cross-links of 1,2,3,4-diepoxybutane in tissues of butadiene-exposed B6C3F1 mice. *Chem. Res. Toxicol. 21*, 1163-1170.

114. Goggin, M., Swenberg, J. A., Walker, V. E., and Tretyakova, N. (2009) Molecular dosimetry of 1,2,3,4-diepoxybutane-induced DNA-DNA cross-links in B6C3F1 mice and F344 rats exposed to 1,3-butadiene by inhalation. *Cancer Res. 69*, 2479-2486.

115. Goggin, M., Sangaraju, D., Walker, V. E., Wickliffe, J., Swenberg, J. A., and Tretyakova, N. (2011) Persistence and repair of bifunctional DNA adducts in tissues of laboratory animals exposed to 1,3-butadiene by inhalation. *Chem. Res. Toxicol. 24*, 809-817.

116. Swenberg, J. A., Bordeerat, N. K., Boysen, G., Carro, S., Georgieva, N. I., Nakamura, J., Troutman, J. M., Upton, P. B., Albertini, R. J., Vacek, P. M., Walker, V. E., Sram, R. J., Goggin, M., and Tretyakova, N. (2011) 1,3-Butadiene: Biomarkers and application to risk assessment. *Chem. Biol. Interact. 192*, 150-154.

117. Perez, H. L., Lahdetie, J., Landin, H., Kilpelainen, I., Koivisto, P., Peltonen, K., and Osterman-Golkar, S. (1997) Haemoglobin adducts of epoxybutanediol from exposure to 1,3-butadiene or butadiene epoxides. *Chem. Biol. Interact. 105*, 181-198.

118. Boysen, G., Georgieva, N. I., Upton, P. B., Walker, V. E., and Swenberg, J. A. (2007) N-terminal globin adducts as biomarkers for formation of butadiene derived epoxides. *Chem. Biol. Interact. 166*, 84-92.

119. Swenberg, J. A., Christova-Gueorguieva, N. I., Upton, P. B., Ranasinghe, A., Scheller, N., Wu, K. Y., Yen, T. Y., and Hayes, R. (2000) 1,3-butadiene: cancer, mutations, and adducts. Part V: Hemoglobin adducts as biomarkers of 1,3-butadiene exposure and metabolism. *Res. Rep. Health Eff. Inst.*191-210.

120. Boogaard, P. J., van Sittert, N. J., and Megens, H. J. (2001) Urinary metabolites and haemoglobin adducts as biomarkers of exposure to 1,3-butadiene: a basis for 1,3-butadiene cancer risk assessment. *Chem. Biol. Interact. 135-136*, 695-701.

121. Kautiainen, A., Fred, C., Rydberg, P., and Tornqvist, M. (2000) A liquid chromatography tandem mass spectrometric method for in vivo dose monitoring of diepoxybutane, a metabolite of butadiene. *Rapid Commun. Mass Spectrom. 14*, 1848-1853.

122. Osterman-Golkar, S., Kautiainen, A., Bergmark, E., Hakansson, K., and Maki-Paakkanen, J. (1991) Hemoglobin adducts and urinary mercapturic acids in rats as biological indicators of butadiene exposure. *Chem. Biol. Interact. 80*, 291-302.

123. Osterman-Golkar, S. M., Bond, J. A., Ward, J. B., Jr., and Legator, M. S. (1993) Use of haemoglobin adducts for biomonitoring exposure to 1,3-butadiene. *IARC Sci. Publ.*127-134.

124. Fred, C., Kautiainen, A., Athanassiadis, I., and Tornqvist, M. (2004) Hemoglobin adduct levels in rat and mouse treated with 1,2:3,4-diepoxybutane. *Chem. Res. Toxicol. 17*, 785-794.

125. Albertini, R. J., Sram, R. J., Vacek, P. M., Lynch, J., Wright, M., Nicklas, J. A., Boogaard, P. J., Henderson, R. F., Swenberg, J. A., Tates, A. D., and Ward, J. B., Jr. (2001) Biomarkers for assessing occupational exposures to 1,3-butadiene. *Chem. Biol. Interact. 135-136*, 429-453.

126. Albertini, R. J., Sram, R. J., Vacek, P. M., Lynch, J., Nicklas, J. A., van Sittert, N. J., Boogaard, P. J., Henderson, R. F., Swenberg, J. A., Tates, A. D., Ward, J. B., Jr., Wright, M., Ammenheuser, M. M., Binkova, B., Blackwell, W., de Zwart, F. A., Krako, D., Krone, J., Megens, H., Musilova, P., Rajska, G., Ranasinghe, A., Rosenblatt, J. I., Rossner, P., Rubes, J., Sullivan, L., Upton, P., and Zwinderman, A. H. (2003) Biomarkers in Czech workers exposed to 1,3-butadiene: a transitional epidemiologic study. *Res. Rep. Health Eff. Inst.*1-141.

127. Vacek, P. M., Albertini, R. J., Sram, R. J., Upton, P., and Swenberg, J. A. (2010) Hemoglobin adducts in 1,3-butadiene exposed Czech workers: female-male comparisons. *Chem. Biol. Interact. 188*, 668-676.

128. Begemann, P., Upton, P. B., Ranasinghe, A., Swenberg, J. A., Soleo, L., Vimercati, L., Gelormini, A., Fustinoni, S., Zwirner-Baier, I., and Neumann, H. G. (2001) Hemoglobin adducts as biomarkers of 1,3-butadiene in occupationally low exposed Italian workers and a few diesel-exposed miners. *Chem. Biol. Interact. 135-136*, 675-678.

129. Fustinoni, S., Soleo, L., Warholm, M., Begemann, P., Rannug, A., Neumann, H. G., Swenberg, J. A., Vimercati, L., and Colombi, A. (2002) Influence of metabolic genotypes on biomarkers of exposure to 1,3-butadiene in humans. *Cancer Epidemiol. Biomarkers Prev. 11*, 1082-1090.

130. Boysen, G., Georgieva, N. I., Upton, P. B., Jayaraj, K., Li, Y., Walker, V. E., and Swenberg, J. A. (2004) Analysis of diepoxide-specific cyclic N-terminal globin adducts in mice and rats after inhalation exposure to 1,3-butadiene. *Cancer Res. 64*, 8517-8520.

131. Georgieva, N. I., Boysen, G., Bordeerat, N., Walker, V. E., and Swenberg, J. A. (2010) Exposure-response of 1,2:3,4-diepoxybutane-specific N-terminal valine adducts in mice and rats after inhalation exposure to 1,3-butadiene. *Toxicol. Sci. 115*, 322-329.

132. Boysen, G., Georgieva, N. I., Bordeerat, N. K., Sram, R. J., Vacek, P., Albertini, R. J., and Swenberg, J. A. (2012) Formation of 1,2:3,4-diepoxybutane-specific hemoglobin adducts in 1,3-butadiene exposed workers. *Toxicol. Sci. 125*, 30-40.

133. Urban, M., Gilch, G., Schepers, G., van Miert, E., and Scherer, G. (2003) Determination of the major mercapturic acids of 1,3-butadiene in human and rat urine using liquid chromatography with tandem mass spectrometry. *J. Chromatogr. B Analyt. Technol. Biomed. Life Sci. 796*, 131-140.

134. Kotapati, S., Matter, B. A., Grant, A. L., and Tretyakova, N. Y. (2011) Quantitative analysis of trihydroxybutyl mercapturic acid, a urinary metabolite of 1,3-butadiene, in humans. *Chem. Res. Toxicol. 24*, 1516-1526.

135. Kotapati, S., Sangaraju, D., Esades, A., Hallberg, L., Walker, V. E., Swenberg, J. A., and Tretyakova, N. Y. (2014) Bis-butanediol-mercapturic acid (bis-BDMA) as a urinary biomarker of metabolic activation of butadiene to its ultimate carcinogenic species. *Carcinogenesis*.

136. Sabourin, P. J., Burka, L. T., Bechtold, W. E., Dahl, A. R., Hoover, M. D., Chang, I. Y., and Henderson, R. F. (1992) Species differences in urinary butadiene metabolites; identification of 1,2-dihydroxy-4-(N-acetylcysteinyl)butane, a novel metabolite of butadiene. *Carcinogenesis 13*, 1633-1638.

137. Bechtold, W. E., Strunk, M. R., Chang, I. Y., Ward, J. B., Jr., and Henderson, R. F. (1994) Species differences in urinary butadiene metabolites: comparisons of metabolite ratios between mice, rats, and humans. *Toxicol. Appl. Pharmacol. 127*, 44-49.

138. Richardson, K. A., Peters, M. M., Wong, B. A., Megens, R. H., van Elburg, P. A., Booth, E. D., Boogaard, P. J., Bond, J. A., Medinsky, M. A., Watson, W. P., and

van Sittert, N. J. (1999) Quantitative and qualitative differences in the metabolism of 14C-1,3-butadiene in rats and mice: relevance to cancer susceptibility. *Toxicol. Sci. 49*, 186-201.

139. Boogaard, P. J., Sumner, S. C., and Bond, J. A. (1996) Glutathione conjugation of 1,2:3,4- diepoxybutane in human liver and rat and mouse liver and lung in vitro. *Toxicol. Appl. Pharmacol. 136*, 307-316.

140. van Sittert, N. J., Megens, H. J., Watson, W. P., and Boogaard, P. J. (2000) Biomarkers of exposure to 1,3-butadiene as a basis for cancer risk assessment. *Toxicol. Sci. 56*, 189-202.

141. Carmella, S. G., Chen, M., Han, S., Briggs, A., Jensen, J., Hatsukami, D. K., and Hecht, S. S. (2009) Effects of smoking cessation on eight urinary tobacco carcinogen and toxicant biomarkers. *Chem. Res. Toxicol. 22*, 734-741.

142. McDonald, J. D., Bechtold, W. E., Krone, J. R., Blackwell, W. B., Kracko, D. A., and Henderson, R. F. (2004) Analysis of butadiene urinary metabolites by liquid chromatography-triple quadrupole mass spectrometry. *J. Anal. Toxicol. 28*, 168-173.

143. Schettgen, T., Musiol, A., Alt, A., Ochsmann, E., and Kraus, T. (2009) A method for the quantification of biomarkers of exposure to acrylonitrile and 1,3-butadiene in human urine by column-switching liquid chromatography-tandem mass spectrometry. *Anal. Bioanal. Chem. 393*, 969-981.

144. Ding, Y. S., Blount, B. C., Valentin-Blasini, L., Applewhite, H. S., Xia, Y., Watson, C. H., and Ashley, D. L. (2009) Simultaneous determination of six mercapturic acid metabolites of volatile organic compounds in human urine. *Chem. Res. Toxicol. 22*, 1018-1025.

145. Roethig, H. J., Munjal, S., Feng, S., Liang, Q., Sarkar, M., Walk, R. A., and Mendes, P. E. (2009) Population estimates for biomarkers of exposure to cigarette smoke in adult U.S. cigarette smokers. *Nicotine. Tob. Res. 11*, 1216-1225.

146. Sarkar, M., Muhammad-Kah, R., Liang, Q., Kapur, S., Feng, S., and Roethig, H. (2013) Evaluation of spot urine as an alternative to 24h urine collection for determination of biomarkers of exposure to cigarette smoke in adult smokers. *Environ. Toxicol. Pharmacol. 36*, 108-114.

147. Sapkota, A., Halden, R. U., Dominici, F., Groopman, J. D., and Buckley, T. J. (2006) Urinary biomarkers of 1,3-butadiene in environmental settings using liquid chromatography isotope dilution tandem mass spectrometry. *Chem. Biol. Interact. 160*, 70-79.

148. Arayasiri, M., Mahidol, C., Navasumrit, P., Autrup, H., and Ruchirawat, M. (2010) Biomonitoring of benzene and 1,3-butadiene exposure and early biological effects in traffic policemen. *Sci. Total Environ. 408*, 4855-4862.

149. Thornton-Manning, J. R., Dahl, A. R., Bechtold, W. E., Griffith, W. C., Jr., and Henderson, R. F. (1997) Comparison of the disposition of butadiene epoxides in

Sprague-Dawley rats and B6C3F1 mice following a single and repeated exposures to 1,3-butadiene via inhalation. *Toxicology 123*, 125-134.

150. Thornton-Manning, J. R., Dahl, A. R., Bechtold, W. E., and Henderson, R. F. (1996) Gender and species differences in the metabolism of 1,3-butadiene to butadiene monoepoxide and butadiene diepoxide in rodents following low-level inhalation exposures. *Toxicology 113*, 322-325.

151. Krause, R. J. and Elfarra, A. A. (1997) Oxidation of butadiene monoxide to meso- and (+/-)-diepoxybutane by cDNA-expressed human cytochrome P450s and by mouse, rat, and human liver microsomes: evidence for preferential hydration of meso-diepoxybutane in rat and human liver microsomes. *Arch. Biochem. Biophys. 337*, 176-184.

152. Seaton, M. J., Follansbee, M. H., and Bond, J. A. (1995) Oxidation of 1,2-epoxy-3-butene to 1,2:3,4-diepoxybutane by cDNA-expressed human cytochromes P450 2E1 and 3A4 and human, mouse and rat liver microsomes. *Carcinogenesis 16*, 2287-2293.

153. Oesch-Bartlomowicz, B., Padma, P. R., Becker, R., Richter, B., Hengstler, J. G., Freeman, J. E., Wolf, C. R., and Oesch, F. (1998) Differential modulation of CYP2E1 activity by cAMP-dependent protein kinase upon Ser129 replacement. *Exp. Cell Res. 242*, 294-302.

154. Boysen, G., Scarlett, C. O., Temple, B., Combs, T. P., Brooks, N. L., Borchers, C. H., and Swenberg, J. A. (2007) Identification of covalent modifications in P450 2E1 by 1,2-epoxy-3-butene in vitro. *Chem. Biol. Interact. 166*, 170-175.

155. Albertini, R. J., Sram, R. J., Vacek, P. M., Lynch, J., Rossner, P., Nicklas, J. A., McDonald, J. D., Boysen, G., Georgieva, N., and Swenberg, J. A. (2007) Molecular epidemiological studies in 1,3-butadiene exposed Czech workers: female-male comparisons. *Chem. Biol. Interact. 166*, 63-77.

156. Jemal, A., Bray, F., Center, M. M., Ferlay, J., Ward, E., and Forman, D. (2011) Global cancer statistics. *CA Cancer J. Clin. 61*, 69-90.

157. American Cancer Society Cancer Facts & Figures 2013, *http://www.cancer.org/acs/groups/content/@epidemiologysurveilance/documents/document/acspc-036845.pdf (Accessed August 3rd, 2014)* .

158. (2014) National Cancer Institute.Bethesda, M. (2013) SEER Cancer Statistics Review 1975-2010. *http://seer.cancer.gov/statfacts/html/lungb.html (accessed August 04, 2014)* .

159. Fowles, J. and Dybing, E. (2003) Application of toxicological risk assessment principles to the chemical constituents of cigarette smoke. *Tob. Control 12*, 424-430.

160. Smith, C. J., Perfetti, T. A., Rumple, M. A., Rodgman, A., and Doolittle, D. J. (2000) "IARC group 2A Carcinogens" reported in cigarette mainstream smoke. *Food Chem. Toxicol. 38*, 371-383.

161. Soeteman-Hernandez, L. G., Bos, P. M., and Talhout, R. (2013) Tobacco smoke-related health effects induced by 1,3-butadiene and strategies for risk reduction. *Toxicol. Sci. 136*, 566-580.

162. Le Marchand, L., Wilkens, L. R., and Kolonel, L. N. (1992) Ethnic differences in the lung cancer risk associated with smoking. *Cancer Epidemiol. Biomarkers Prev. 1*, 103-107.

163. Hinds, M. W., Stemmermann, G. N., Yang, H. Y., Kolonel, L. N., Lee, J., and Wegner, E. (1981) Differences in lung cancer risk from smoking among Japanese, Chinese and Hawaiian women in Hawaii. *Int. J. Cancer 27*, 297-302.

164. Schwartz, A. G. and Swanson, G. M. (1997) Lung carcinoma in African Americans and whites. A population-based study in metropolitan Detroit, Michigan. *Cancer 79*, 45-52.

165. Stellman, S. D., Takezaki, T., Wang, L., Chen, Y., Citron, M. L., Djordjevic, M. V., Harlap, S., Muscat, J. E., Neugut, A. I., Wynder, E. L., Ogawa, H., Tajima, K., and Aoki, K. (2001) Smoking and lung cancer risk in American and Japanese men: an international case-control study. *Cancer Epidemiol. Biomarkers Prev. 10*, 1193-1199.

166. Stellman, S. D., Chen, Y., Muscat, J. E., Djordjevic, M. V., Richie, J. P., Jr., Lazarus, P., Thompson, S., Altorki, N., Berwick, M., Citron, M. L., Harlap, S., Kaur, T. B., Neugut, A. I., Olson, S., Travaline, J. M., Witorsch, P., and Zhang, Z.

F. (2003) Lung cancer risk in white and black Americans. *Ann. Epidemiol. 13*, 294-302.

167. Haiman, C. A., Stram, D. O., Wilkens, L. R., Pike, M. C., Kolonel, L. N., Henderson, B. E., and Le Marchand, L. (2006) Ethnic and racial differences in the smoking-related risk of lung cancer. *N. Engl. J. Med. 354*, 333-342.

168. Niture, S. K., Rao, U. S., and Srivenugopal, K. S. (2006) Chemopreventative strategies targeting the MGMT repair protein: augmented expression in human lymphocytes and tumor cells by ethanolic and aqueous extracts of several Indian medicinal plants. *Int. J. Oncol. 29*, 1269-1278.

169. Schmitt, M. W., Matsumoto, Y., and Loeb, L. A. (2009) High fidelity and lesion bypass capability of human DNA polymerase delta. *Biochimie 91*, 1163-1172.

170. Yang, W. (2000) Structure and function of mismatch repair proteins. *Mutat. Res. 460*, 245-256.

171. Preston, T. J., Henderson, J. T., McCallum, G. P., and Wells, P. G. (2009) Base excision repair of reactive oxygen species-initiated 7,8-dihydro-8-oxo-2'-deoxyguanosine inhibits the cytotoxicity of platinum anticancer drugs. *Mol. Cancer Ther. 8*, 2015-2026.

172. Lindahl, T. (1974) An N-glycosidase from Escherichia coli that releases free uracil from DNA containing deaminated cytosine residues. *Proc. Natl. Acad. Sci. U. S. A 71*, 3649-3653.

173. Coste, F., Ober, M., Le Bihan, Y. V., Izquierdo, M. A., Hervouet, N., Mueller, H., Carell, T., and Castaing, B. (2008) Bacterial base excision repair enzyme Fpg recognizes bulky N7-substituted-FapydG lesion via unproductive binding mode. *Chem. Biol. 15*, 706-717.

174. Couve-Privat, S., Mace, G., Rosselli, F., and Saparbaev, M. K. (2007) Psoralen-induced DNA adducts are substrates for the base excision repair pathway in human cells. *Nucleic Acids Res. 35*, 5672-5682.

175. Lukina, M. V., Popov, A. V., Koval, V. V., Vorobjev, Y. N., Fedorova, O. S., and Zharkov, D. O. (2013) DNA damage processing by human 8-oxoguanine-DNA glycosylase mutants with the occluded active site. *J. Biol. Chem. 288*, 28936-28947.

176. Yin, Z. B., Hua, R. X., Li, J. H., Sun, C., Zhu, J. H., Su, X., Ji, C., Xiang, Q., and Hua, Z. M. (2014) Smoking and hOGG1 Ser326Cys polymorphism contribute to lung cancer risk: evidence from a meta-analysis. *Tumour. Biol. 35*, 1609-1618.

177. Lu, M., Sun, L., Zhou, J., and Zhang, J. (2014) Assessment of the association between hOGG1 C8069G polymorphism and colorectal cancer. *Tumour. Biol. 35*, 2373-2377.

178. Singer, B. and Hang, B. (1997) What structural features determine repair enzyme specificity and mechanism in chemically modified DNA? *Chem. Res. Toxicol. 10*, 713-732.

179. Tchou, J., Bodepudi, V., Shibutani, S., Antoshechkin, I., Miller, J., Grollman, A. P., and Johnson, F. (1994) Substrate specificity of Fpg protein. Recognition and cleavage of oxidatively damaged DNA. *J. Biol. Chem. 269*, 15318-15324.

180. Lindahl, T. and Wood, R. D. (1999) Quality control by DNA repair. *Science 286*, 1897-1905.

181. Srivastava, D. K., Berg, B. J., Prasad, R., Molina, J. T., Beard, W. A., Tomkinson, A. E., and Wilson, S. H. (1998) Mammalian abasic site base excision repair. Identification of the reaction sequence and rate-determining steps. *J. Biol. Chem. 273*, 21203-21209.

182. Ouzounis, C. A. and Blencowe, B. J. (1991) Bacterial DNA replication initiation factor priA is related to proteins belonging to the 'DEAD-box' family. *Nucleic Acids Res. 19*, 6953.

183. Sancar, A. (1995) Excision repair in mammalian cells. *J. Biol. Chem. 270*, 15915-15918.

184. Grossman, L. and Thiagalingam, S. (1993) Nucleotide excision repair, a tracking mechanism in search of damage. *J. Biol. Chem. 268*, 16871-16874.

185. Hoeijmakers, J. H. (1994) Human nucleotide excision repair syndromes: molecular clues to unexpected intricacies. *Eur. J. Cancer 30A*, 1912-1921.

186. Huang, J. C., Hsu, D. S., Kazantsev, A., and Sancar, A. (1994) Substrate spectrum of human excinuclease: repair of abasic sites, methylated bases, mismatches, and bulky adducts. *Proc. Natl. Acad. Sci. U. S. A 91*, 12213-12217.

187. You, J. S., Wang, M., and Lee, S. H. (2003) Biochemical analysis of the damage recognition process in nucleotide excision repair. *J. Biol. Chem. 278*, 7476-7485.

188. Hanawalt, P. C. (2002) Subpathways of nucleotide excision repair and their regulation. *Oncogene 21*, 8949-8956.

189. Zhang, N., Liu, X., Li, L., and Legerski, R. (2007) Double-strand breaks induce homologous recombinational repair of interstrand cross-links via cooperation of MSH2, ERCC1-XPF, REV3, and the Fanconi anemia pathway. *DNA Repair (Amst) 6*, 1670-1678.

190. Li, X. and Heyer, W. D. (2008) Homologous recombination in DNA repair and DNA damage tolerance. *Cell Res. 18*, 99-113.

191. Moore, J. K. and Haber, J. E. (1996) Cell cycle and genetic requirements of two pathways of nonhomologous end-joining repair of double-strand breaks in Saccharomyces cerevisiae. *Mol. Cell Biol. 16*, 2164-2173.

192. Wang, H., Perrault, A. R., Takeda, Y., Qin, W., Wang, H., and Iliakis, G. (2003) Biochemical evidence for Ku-independent backup pathways of NHEJ. *Nucleic Acids Res. 31*, 5377-5388.

193. Moldovan, G. L. and D'Andrea, A. D. (2009) How the fanconi anemia pathway guards the genome. *Annu. Rev. Genet. 43*, 223-249.

194. Niedzwiedz, W., Mosedale, G., Johnson, M., Ong, C. Y., Pace, P., and Patel, K. J. (2004) The Fanconi anaemia gene FANCC promotes homologous recombination and error-prone DNA repair. *Mol. Cell 15*, 607-620.

195. Sasaki, M. S. (1975) Is Fanconi's anaemia defective in a process essential to the repair of DNA cross links? *Nature 257*, 501-503.

196. Dunn, J., Potter, M., Rees, A., and Runger, T. M. (2006) Activation of the Fanconi anemia/BRCA pathway and recombination repair in the cellular response to solar ultraviolet light. *Cancer Res. 66*, 11140-11147.

197. Taniguchi, T., Garcia-Higuera, I., Andreassen, P. R., Gregory, R. C., Grompe, M., and D'Andrea, A. D. (2002) S-phase-specific interaction of the Fanconi anemia protein, FANCD2, with BRCA1 and RAD51. *Blood 100*, 2414-2420.

198. Tretyakova, N., Villalta, P. W., and Kotapati, S. (2013) Mass spectrometry of structurally modified DNA. *Chem. Rev. 113*, 2395-2436.

199. Balbo, S., Turesky, R. J., and Villalta, P. W. (2014) DNA adductomics. *Chem. Res. Toxicol. 27*, 356-366.

200. Singh, R., Teichert, F., Seidel, A., Roach, J., Cordell, R., Cheng, M. K., Frank, H., Steward, W. P., Manson, M. M., and Farmer, P. B. (2010) Development of a targeted adductomic method for the determination of polycyclic aromatic

hydrocarbon DNA adducts using online column-switching liquid chromatography/tandem mass spectrometry. *Rapid Commun. Mass Spectrom. 24*, 2329-2340.

201. Kanaly, R. A., Matsui, S., Hanaoka, T., and Matsuda, T. (2007) Application of the adductome approach to assess intertissue DNA damage variations in human lung and esophagus. *Mutat. Res. 625*, 83-93.

202. Spilsberg, B., Rundberget, T., Johannessen, L. E., Kristoffersen, A. B., Holst-Jensen, A., and Berdal, K. G. (2010) Detection of food-derived damaged nucleosides with possible adverse effects on human health using a global adductomics approach. *J. Agric. Food Chem. 58*, 6370-6375.

203. Van den, D. B., Van Dongen, W., Lemiere, F., and Esmans, E. L. (2004) Implementation of data-dependent acquisitions in the study of melphalan DNA adducts by miniaturized liquid chromatography coupled to electrospray tandem mass spectrometry. *Rapid Commun. Mass Spectrom. 18*, 2001-2007.

204. Bessette, E. E., Goodenough, A. K., Langouet, S., Yasa, I., Kozekov, I. D., Spivack, S. D., and Turesky, R. J. (2009) Screening for DNA adducts by data-dependent constant neutral loss-triple stage mass spectrometry with a linear quadrupole ion trap mass spectrometer. *Anal. Chem. 81*, 809-819.

205. Balbo, S., Hecht, S. S., Upadhyaya, P., and Villalta, P. W. (2014) Application of a high-resolution mass-spectrometry-based DNA adductomics approach for identification of DNA adducts in complex mixtures. *Anal. Chem. 86*, 1744-1752.

206. Pietsch, K. E., van Midwoud, P. M., Villalta, P. W., and Sturla, S. J. (2013) Quantification of acylfulvene- and illudin S-DNA adducts in cells with variable bioactivation capacities. *Chem. Res. Toxicol. 26*, 146-155.

207. Pelz, N., Dempster, N. M., and Shore, P. R. (1990) Analysis of low molecular weight hydrocarbons including 1,3-butadiene in engine exhaust gases using an aluminum oxide porous-layer open-tubular fused-silica column. *J. Chromatogr. Sci. 28*, 230-235.

208. Hecht, S. S. (1999) Tobacco smoke carcinogens and lung cancer. *J. Natl. Cancer Inst. 91*, 1194-1210.

209. Cheng, H., Sathiakumar, N., Graff, J., Matthews, R., and Delzell, E. (2007) 1,3-Butadiene and leukemia among synthetic rubber industry workers: exposure-response relationships. *Chem. Biol. Interact. 166*, 15-24.

210. Kirman, C. R., Albertini, R. A., and Gargas, M. L. (2010) 1,3-Butadiene: III. Assessing carcinogenic modes of action. *Crit Rev. Toxicol. 40 Suppl 1*, 74-92.

211. Meng, Q., Henderson, R. F., Walker, D. M., Bauer, M. J., Reilly, A. A., and Walker, V. E. (1999) Mutagenicity of the racemic mixtures of butadiene monoepoxide and butadiene diepoxide at the Hprt locus of T-lymphocytes following inhalation exposures of female mice and rats. *Mutat. Res. 429*, 127-140.

212. Jelitto, B., Vangala, R. R., and Laib, R. J. (1989) Species differences in DNA damage by butadiene: role of diepoxybutane. *Arch. Toxicol. Suppl 13*, 246-249.

213. Henderson, R. F., Thornton-Manning, J. R., Bechtold, W. E., and Dahl, A. R. (1996) Metabolism of 1,3-butadiene: species differences. *Toxicology 113*, 17-22.

214. Henderson, R. F., Barr, E. B., Belinsky, S. A., Benson, J. M., Hahn, F. F., and Menache, M. G. (2000) 1,3-butadiene: cancer, mutations, and adducts. Part I: Carcinogenicity of 1,2,3,4-diepoxybutane. *Res. Rep. Health Eff. Inst.*11-43.

215. Park, S. and Tretyakova, N. (2004) Structural characterization of the major DNA-DNA cross-link of 1,2,3,4-diepoxybutane. *Chem. Res. Toxicol. 17*, 129-136.

216. United States Department of Labor, Occupational Health and Safety Administration Standards for 1,3-Butadiene Page. https://www.osha.gov/SLTC/butadiene/index.html#standards (accessed Aug 26, 2014).

217. Michaelson-Richie, E. D., Ming, X., Codreanu, S. G., Loeber, R. L., Liebler, D. C., Campbell, C., and Tretyakova, N. Y. (2011) Mechlorethamine-induced DNA--protein cross-linking in human fibrosarcoma (HT1080) cells. *J. Proteome. Res. 10*, 2785-2796.

218. Karas, M., Bahr, U., and Dulcks, T. (2000) Nano-electrospray ionization mass spectrometry: addressing analytical problems beyond routine. *Fresenius. J. Anal. Chem. 366*, 669-676.

219. Lim, C. K. and Lord, G. (2002) Current developments in LC-MS for pharmaceutical analysis. *Biol. Pharm. Bull. 25*, 547-557.

220. Ramanathan, R., Zhong, R., Blumenkrantz, N., Chowdhury, S. K., and Alton, K. B. (2007) Response normalized liquid chromatography nanospray ionization mass spectrometry. *J. Am. Soc. Mass Spectrom. 18*, 1891-1899.

221. Chen, H. J. and Lin, W. P. (2011) Quantitative analysis of multiple exocyclic DNA adducts in human salivary DNA by stable isotope dilution nanoflow liquid chromatography nanospray ionization tandem mass spectrometry. *Anal. Chem. 83*, 8543-8551.

222. Chen, H. J., Lin, G. J., and Lin, W. P. (2010) Simultaneous quantification of three lipid peroxidation-derived etheno adducts in human DNA by stable isotope dilution nanoflow liquid chromatography nanospray ionization tandem mass spectrometry. *Anal. Chem. 82*, 4486-4493.

223. Balbo, S., Villalta, P. W., and Hecht, S. S. (2011) Quantitation of 7-ethylguanine in leukocyte DNA from smokers and nonsmokers by liquid chromatography-nanoelectrospray-high resolution tandem mass spectrometry. *Chem. Res. Toxicol. 24*, 1729-1734.

224. Zarbl, H., Gallo, M. A., Glick, J., Yeung, K. Y., and Vouros, P. (2010) The vanishing zero revisited: thresholds in the age of genomics. *Chem. Biol. Interact. 184*, 273-278.

225. Covey, T. R. , Devanand, P. (2002) *Nanospray Electrospray Ionization Development: LC/MS, CE/MS Application*. Practical Spectroscopy Series. *32*.

226. Vare, D., Groth, P., Carlsson, R., Johansson, F., Erixon, K., and Jenssen, D. (2012) DNA interstrand crosslinks induce a potent replication block followed by formation and repair of double strand breaks in intact mammalian cells. *DNA Repair (Amst) 11*, 976-985.

227. Deans, A. J. and West, S. C. (2011) DNA interstrand crosslink repair and cancer. *Nat. Rev. Cancer 11*, 467-480.

228. Eastman, A. (1986) Reevaluation of interaction of cis-dichloro(ethylenediamine)platinum(II) with DNA. *Biochemistry 25*, 3912-3915.

229. Gargiulo, D., Kumar, G. S., Musser, S. S., and Tomasz, M. (1995) Structural and function modification of DNA by mitomycin C. Mechanism of the DNA sequence specificity of mitomycins. *Nucleic Acids Symp. Ser.*169-170.

230. Vare, D., Johansson, F., Persson, J. O., Erixon, K., and Jenssen, D. (2014) Quantification and repair of psoralen-induced interstrand crosslinks in human cells. *Toxicol. Lett. 226*, 343-350.

231. Fleer, R. and Brendel, M. (1982) Toxicity, interstrand cross-links and DNA fragmentation induced by 'activated' cyclophosphamide in yeast: comparative studies on 4-hydroperoxy-cyclophosphamide, its monofunctional analogon, acrolein, phosphoramide mustard, and nor-nitrogen mustard. *Chem. Biol. Interact. 39*, 1-15.

232. Kozekov, I. D., Nechev, L. V., Moseley, M. S., Harris, C. M., Rizzo, C. J., Stone, M. P., and Harris, T. M. (2003) DNA interchain cross-links formed by acrolein and crotonaldehyde. *J. Am. Chem. Soc. 125*, 50-61.

233. Stone, M. P., Cho, Y. J., Huang, H., Kim, H. Y., Kozekov, I. D., Kozekova, A., Wang, H., Minko, I. G., Lloyd, R. S., Harris, T. M., and Rizzo, C. J. (2008) Interstrand DNA cross-links induced by alpha,beta-unsaturated aldehydes derived from lipid peroxidation and environmental sources. *Acc. Chem. Res. 41*, 793-804.

234. Lawley, P. D. and Brookes, P. (1967) Interstrand cross-linking of DNA by difunctional alkylating agents. *J. Mol. Biol. 25*, 143-160.

235. Millard, J. T., McGowan, E. E., and Bradley, S. Q. (2012) Diepoxybutane interstrand cross-links induce DNA bending. *Biochimie 94*, 574-577.

236. Guainazzi, A. and Scharer, O. D. (2010) Using synthetic DNA interstrand crosslinks to elucidate repair pathways and identify new therapeutic targets for cancer chemotherapy. *Cell Mol. Life Sci. 67*, 3683-3697.

237. Kim, H. and D'Andrea, A. D. (2012) Regulation of DNA cross-link repair by the Fanconi anemia/BRCA pathway. *Genes Dev. 26*, 1393-1408.

238. Mouw, K. W. and D'Andrea, A. D. (2014) Crosstalk between the nucleotide excision repair and Fanconi anemia/BRCA pathways. *DNA Repair (Amst) 19*, 130-134.

239. Peng, M., Xie, J., Ucher, A., Stavnezer, J., and Cantor, S. B. (2014) Crosstalk between BRCA-Fanconi anemia and mismatch repair pathways prevents MSH2-dependent aberrant DNA damage responses. *EMBO J. 33*, 1698-1712.

240. Clauson, C., Scharer, O. D., and Niedernhofer, L. (2013) Advances in understanding the complex mechanisms of DNA interstrand cross-link repair. *Cold Spring Harb. Perspect. Med. 3*, a012732.

241. Quentin, S., Cuccuini, W., Ceccaldi, R., Nibourel, O., Pondarre, C., Pages, M. P., Vasquez, N., Dubois, d. C., Larghero, J., Peffault, d. L., Rocha, V., Dalle, J. H., Schneider, P., Michallet, M., Michel, G., Baruchel, A., Sigaux, F., Gluckman, E., Leblanc, T., Stoppa-Lyonnet, D., Preudhomme, C., Socie, G., and Soulier, J. (2011) Myelodysplasia and leukemia of Fanconi anemia are associated with a specific pattern of genomic abnormalities that includes cryptic RUNX1/AML1 lesions. *Blood 117*, e161-e170.

242. Nijnik, A., Woodbine, L., Marchetti, C., Dawson, S., Lambe, T., Liu, C., Rodrigues, N. P., Crockford, T. L., Cabuy, E., Vindigni, A., Enver, T., Bell, J. I., Slijepcevic, P., Goodnow, C. C., Jeggo, P. A., and Cornall, R. J. (2007) DNA repair is limiting for haematopoietic stem cells during ageing. *Nature 447*, 686-690.

243. Kutler, D. I., Wreesmann, V. B., Goberdhan, A., Ben Porat, L., Satagopan, J., Ngai, I., Huvos, A. G., Giampietro, P., Levran, O., Pujara, K., Diotti, R., Carlson, D., Huryn, L. A., Auerbach, A. D., and Singh, B. (2003) Human papillomavirus

DNA and p53 polymorphisms in squamous cell carcinomas from Fanconi anemia patients. *J. Natl. Cancer Inst. 95*, 1718-1721.

244. Zhang, J. and Walter, J. C. (2014) Mechanism and regulation of incisions during DNA interstrand cross-link repair. *DNA Repair (Amst) 19*, 135-142.

245. Dudas, A. and Chovanec, M. (2004) DNA double-strand break repair by homologous recombination. *Mutat. Res. 566*, 131-167.

246. Lieber, M. R. (2010) The mechanism of double-strand DNA break repair by the nonhomologous DNA end-joining pathway. *Annu. Rev. Biochem. 79*, 181-211.

247. Niedernhofer, L. J., Odijk, H., Budzowska, M., van Drunen, E., Maas, A., Theil, A. F., de Wit, J., Jaspers, N. G., Beverloo, H. B., Hoeijmakers, J. H., and Kanaar, R. (2004) The structure-specific endonuclease Ercc1-Xpf is required to resolve DNA interstrand cross-link-induced double-strand breaks. *Mol. Cell Biol. 24*, 5776-5787.

248. McNeil, E. M. and Melton, D. W. (2012) DNA repair endonuclease ERCC1-XPF as a novel therapeutic target to overcome chemoresistance in cancer therapy. *Nucleic Acids Res. 40*, 9990-10004.

249. Enoiu, M., Jiricny, J., and Scharer, O. D. (2012) Repair of cisplatin-induced DNA interstrand crosslinks by a replication-independent pathway involving transcription-coupled repair and translesion synthesis. *Nucleic Acids Res. 40*, 8953-8964.

250. Larminat, F., Germanier, M., Papouli, E., and Defais, M. (2004) Impairment of homologous recombination control in a Fanconi anemia-like Chinese hamster cell mutant. *Biol. Cell 96*, 545-552.

251. Zdzienicka, M. Z., Arwert, F., Neuteboom, I., Rooimans, M., and Simons, J. W. (1990) The Chinese hamster V79 cell mutant V-H4 is phenotypically like Fanconi anemia cells. *Somat. Cell Mol. Genet. 16*, 575-581.

252. Studzian, K., Telleman, P., van der Schans, G. P., and Zdzienicka, M. Z. (1994) Mutagenic response and repair of cis-DDP-induced DNA cross-links in the Chinese hamster V79 cell mutant V-H4 which is homologous to Fanconi anemia (group A). *Mutat. Res. 314*, 115-120.

253. Arwert, F., Rooimans, M. A., Westerveld, A., Simons, J. W., and Zdzienicka, M. Z. (1991) The Chinese hamster cell mutant V-H4 is homologous to Fanconi anemia (complementation group A). *Cytogenet. Cell Genet. 56*, 23-26.

254. Kadkhodayan, S., Salazar, E. P., Ramsey, M. J., Takayama, K., Zdzienicka, M. Z., Tucker, J. D., and Weber, C. A. (1997) Molecular analysis of ERCC2 mutations in the repair deficient hamster mutants UVL-1 and V-H1. *Mutat. Res. 385*, 47-57.

255. Yamauchi, T., Keating, M. J., and Plunkett, W. (2002) UCN-01 (7-hydroxystaurosporine) inhibits DNA repair and increases cytotoxicity in normal lymphocytes and chronic lymphocytic leukemia lymphocytes. *Mol. Cancer Ther. 1*, 287-294.

256. Olive, P. L. and Banath, J. P. (2006) The comet assay: a method to measure DNA damage in individual cells. *Nat. Protoc. 1*, 23-29.

257. Kumaravel, T. S., Vilhar, B., Faux, S. P., and Jha, A. N. (2009) Comet Assay measurements: a perspective. *Cell Biol. Toxicol. 25*, 53-64.

258. Clingen, P. H., Wu, J. Y., Miller, J., Mistry, N., Chin, F., Wynne, P., Prise, K. M., and Hartley, J. A. (2008) Histone H2AX phosphorylation as a molecular pharmacological marker for DNA interstrand crosslink cancer chemotherapy. *Biochem. Pharmacol. 76*, 19-27.

259. Franken, N. A., Rodermond, H. M., Stap, J., Haveman, J., and van Bree, C. (2006) Clonogenic assay of cells in vitro. *Nat. Protoc. 1*, 2315-2319.

260. De Silva, I. U., McHugh, P. J., Clingen, P. H., and Hartley, J. A. (2000) Defining the roles of nucleotide excision repair and recombination in the repair of DNA interstrand cross-links in mammalian cells. *Mol. Cell Biol. 20*, 7980-7990.

261. Jones, N. J., Cox, R., and Thacker, J. (1987) Isolation and cross-sensitivity of X-ray-sensitive mutants of V79-4 hamster cells. *Mutat. Res. 183*, 279-286.

262. Kang, S. G., Chung, H., Yoo, Y. D., Lee, J. G., Choi, Y. I., and Yu, Y. S. (2001) Mechanism of growth inhibitory effect of Mitomycin-C on cultured human retinal pigment epithelial cells: apoptosis and cell cycle arrest. *Curr. Eye Res. 22*, 174-181.

263. Seyschab, H., Friedl, R., Sun, Y., Schindler, D., Hoehn, H., Hentze, S., and Schroeder-Kurth, T. (1995) Comparative evaluation of diepoxybutane sensitivity and cell cycle blockage in the diagnosis of Fanconi anemia. *Blood 85*, 2233-2237.

264. Nieto, A., Cabrera, C. M., Catalina, P., Cobo, F., Barnie, A., Cortes, J. L., Barroso, d. J., Montes, R., and Concha, A. (2007) Effect of mitomycin-C on human foreskin fibroblasts used as feeders in human embryonic stem cells: immunocytochemistry MIB1 score and DNA ploidy and apoptosis evaluated by flow cytometry. *Cell Biol. Int. 31*, 269-278.

265. Tretyakova, N., Lin, Y., Sangaiah, R., Upton, P. B., and Swenberg, J. A. (1997) Identification and quantitation of DNA adducts from calf thymus DNA exposed to 3,4-epoxy-1-butene. *Carcinogenesis 18*, 137-147.

266. Gherezghiher, T. B., Ming, X., Villalta, P. W., Campbell, C., and Tretyakova, N. Y. (2013) 1,2,3,4-Diepoxybutane-induced DNA-protein cross-linking in human fibrosarcoma (HT1080) cells. *J. Proteome. Res. 12*, 2151-2164.

267. Oe, T., Kambouris, S. J., Walker, V. E., Meng, Q., Recio, L., Wherli, S., Chaudhary, A. K., and Blair, I. A. (1999) Persistence of N7-(2,3,4-trihydroxybutyl)guanine adducts in the livers of mice and rats exposed to 1,3-butadiene. *Chem. Res. Toxicol. 12*, 247-257.

268. Mitchell, D. L., Zdzienicka, M. Z., van Zeeland, A. A., and Nairn, R. S. (1989) Intermediate (6-4) photoproduct repair in Chinese hamster V79 mutant V-H1

correlates with intermediate levels of DNA incision and repair replication. *Mutat. Res. 226*, 43-47.

269. Wakasugi, M., Sasaki, T., Matsumoto, M., Nagaoka, M., Inoue, K., Inobe, M., Horibata, K., Tanaka, K., and Matsunaga, T. (2014) Nucleotide Excision Repair-dependent DNA Double-strand Break Formation and ATM Signaling Activation in Mammalian Quiescent Cells. *J. Biol. Chem.*

270. Zhang, Y., Rohde, L. H., and Wu, H. (2009) Involvement of nucleotide excision and mismatch repair mechanisms in double strand break repair. *Curr. Genomics 10*, 250-258.

271. Hoy, C. A., Thompson, L. H., Mooney, C. L., and Salazar, E. P. (1985) Defective DNA cross-link removal in Chinese hamster cell mutants hypersensitive to bifunctional alkylating agents. *Cancer Res. 45*, 1737-1743.

272. Andersson, B. S., Sadeghi, T., Siciliano, M. J., Legerski, R., and Murray, D. (1996) Nucleotide excision repair genes as determinants of cellular sensitivity to cyclophosphamide analogs. *Cancer Chemother. Pharmacol. 38*, 406-416.

273. Knipscheer, P., Raschle, M., Smogorzewska, A., Enoiu, M., Ho, T. V., Scharer, O. D., Elledge, S. J., and Walter, J. C. (2009) The Fanconi anemia pathway promotes replication-dependent DNA interstrand cross-link repair. *Science 326*, 1698-1701.

274. Fajen, J. M., Roberts, D. R., Ungers, L. J., and Krishnan, E. R. (1990) Occupational exposure of workers to 1,3-butadiene. *Environmental Health Perspectives 86*, 11-18.

275. Grant, R. L., Leopold, V., McCant, D., and Honeycutt, M. (2007) Spatial and temporal trend evaluation of ambient concentrations of 1,3-butadiene and chloroprene in Texas. *Chem. Biol. Interact. 166*, 44-51.

276. Agency for Toxic Substances and Disease Registry (ATSDR) Public Health Statement for 1,3-Butadiene page, http://www.atsdr.cdc.gov/PHS/PHS.asp?id=457&tid=81 (accessed July 26, 2014).

277. Blair, I. A., Oe, T., Kambouris, S., and Chaudhary, A. K. (2000) 1,3-butadiene: cancer, mutations, and adducts. Part IV: Molecular dosimetry of 1,3-butadiene. *Res. Rep. Health Eff. Inst.*151-190.

278. Gates, K. S., Nooner, T., and Dutta, S. (2004) Biologically relevant chemical reactions of N7-alkylguanine residues in DNA. *Chem. Res. Toxicol. 17*, 839-856.

279. Hecht, S. S. (2003) Tobacco carcinogens, their biomarkers and tobacco-induced cancer. *Nat. Rev. Cancer 3*, 733-744.

280. Rodriguez, D. A., Kowalczyk, A., Ward, J. B., Jr., Harris, C. M., Harris, T. M., and Lloyd, R. S. (2001) Point mutations induced by 1,2-epoxy-3-butene N1 deoxyinosine adducts. *Environ. Mol. Mutagen. 38*, 292-296.

281. Carmical, J. R., Kowalczyk, A., Zou, Y., Van Houten, B., Nechev, L. V., Harris, C. M., Harris, T. M., and Lloyd, R. S. (2000) Butadiene-induced intrastrand DNA cross-links: a possible role in deletion mutagenesis. *J. Biol. Chem. 275*, 19482-19489.

282. Boysen, G., Pachkowski, B. F., Nakamura, J., and Swenberg, J. A. (2009) The formation and biological significance of N7-guanine adducts. *Mutat. Res. 678*, 76-94.

283. Cote, I. L. and Bayard, S. P. (1990) Cancer risk assessment of 1,3-butadiene. *Environ. Health Perspect. 86*, 149-153.

284. NELIGAN, R. E. (1962) Hydrocarbons in the Los Angeles atmosphere. A comparison between the hydrocarbons in automobile exhaust and those found in the Los Angeles atmosphere. *Arch. Environ. Health 5*, 581-591.

285. De Bont, R. and van Larebeke, N. (2004) Endogenous DNA damage in humans: a review of quantitative data. *Mutagenesis 19*, 169-185.

286. Matsuda, T., Tao, H., Goto, M., Yamada, H., Suzuki, M., Wu, Y., Xiao, N., He, Q., Guo, W., Cai, Z., Kurabe, N., Ishino, K., Matsushima, Y., Shinmura, K., Konno, H., Maekawa, M., Wang, Y., and Sugimura, H. (2013) Lipid peroxidation-induced DNA adducts in human gastric mucosa. *Carcinogenesis 34*, 121-127.

287. Nair, J., Carmichael, P. L., Fernando, R. C., Phillips, D. H., Strain, A. J., and Bartsch, H. (1998) Lipid peroxidation-induced etheno-DNA adducts in the liver

of patients with the genetic metal storage disorders Wilson's disease and primary hemochromatosis. *Cancer Epidemiol. Biomarkers Prev. 7*, 435-440.

288. Bartsch, H. (1996) DNA adducts in human carcinogenesis: etiological relevance and structure-activity relationship. *Mutat. Res. 340*, 67-79.

289. Counts, M. E., Hsu, F. S., and Tewes, F. J. (2006) Development of a commercial cigarette "market map" comparison methodology for evaluating new or non-conventional cigarettes. *Regul. Toxicol. Pharmacol. 46*, 225-242.

290. Gustafson, P., Barregard, L., Strandberg, B., and Sallsten, G. (2007) The impact of domestic wood burning on personal, indoor and outdoor levels of 1,3-butadiene, benzene, formaldehyde and acetaldehyde. *J. Environ. Monit. 9*, 23-32.

291. Carmical, J. R., Zhang, M., Nechev, L., Harris, C. M., Harris, T. M., and Lloyd, R. S. (2000) Mutagenic potential of guanine N2 adducts of butadiene mono- and diolepoxide. *Chem. Res. Toxicol. 13*, 18-25.

292. Seo, K. Y., Jelinsky, S. A., and Loechler, E. L. (2000) Factors that influence the mutagenic patterns of DNA adducts from chemical carcinogens. *Mutat. Res. 463*, 215-246.

293. Poirier, M. C. (1997) DNA adducts as exposure biomarkers and indicators of cancer risk. *Environ. Health Perspect. 105 Suppl 4*, 907-912.

294. Citti, L., Gervasi, P. G., Turchi, G., Bellucci, G., and Bianchini, R. (1984) The reaction of 3,4-epoxy-1-butene with deoxyguanosine and DNA in vitro: synthesis and characterization of the main adducts. *Carcinogenesis 5*, 47-52.

295. Sangaraju, D., Villalta, P., Goggin, M., Agunsoye, M. O., Campbell, C., and Tretyakova, N. (2013) Capillary HPLC-Accurate Mass MS/MS Quantitation of N7-(2,3,4-Trihydroxybut-1-yl)-guanine Adducts of 1,3-Butadiene in Human Leukocyte DNA. *Chem. Res. Toxicol. 26*, 1486-1497.

296. Tuytten, R., Lemiere, F., Van Dongen, W., Esmans, E. L., Witters, E., Herrebout, W., Van, D., V, Dudley, E., and Newton, R. P. (2005) Intriguing mass spectrometric behavior of guanosine under low energy collision-induced dissociation: H2O adduct formation and gas-phase reactions in the collision cell. *J. Am. Soc. Mass Spectrom. 16*, 1291-1304.

297. Downs, T. D., Crane, M. M., and Kim, K. W. (1987) Mortality among workers at a butadiene facility. *Am. J. Ind. Med. 12*, 311-329.

298. Smith, R. D., Shen, Y., and Tang, K. (2004) Ultrasensitive and quantitative analyses from combined separations-mass spectrometry for the characterization of proteomes. *Acc. Chem. Res. 37*, 269-278.

299. Bond, J. A., Himmelstein, M. W., Seaton, M., Boogaard, P., and Medinsky, M. A. (1996) Metabolism of butadiene by mice, rats, and humans: a comparison of physiologically based toxicokinetic model predictions and experimental data. *Toxicology 113*, 48-54.

300. (2011) National Toxicology Program and Department of Health and Human Services. *1,3-Butadiene. Report on Carcinogens, Twelfth Edition*. *National Toxicology Program, Research Triangle Park, NC* .

301. Shuker, D. E. and Farmer, P. B. (1992) Relevance of urinary DNA adducts as markers of carcinogen exposure. *Chem. Res. Toxicol. 5*, 450-460.

302. Taylor, P. J. (2005) Matrix effects: the Achilles heel of quantitative high-performance liquid chromatography-electrospray-tandem mass spectrometry. *Clin. Biochem. 38*, 328-334.

303. Annesley, T. M. (2003) Ion suppression in mass spectrometry. *Clin. Chem. 49*, 1041-1044.

304. Bylda, C., Thiele, R., Kobold, U., and Volmer, D. A. (2014) Recent advances in sample preparation techniques to overcome difficulties encountered during quantitative analysis of small molecules from biofluids using LC-MS/MS. *Analyst 139*, 2265-2276.

305. Zhang, H., Xin, B., Caporuscio, C., and Olah, T. V. (2011) Bioanalytical strategies for developing highly sensitive liquid chromatography/tandem mass spectrometry based methods for the peptide GLP-1 agonists in support of discovery PK/PD studies. *Rapid Commun. Mass Spectrom. 25*, 3427-3435.

306. Chen, H. J. and Lin, C. R. (2013) Simultaneous quantification of ethylpurine adducts in human urine by stable isotope dilution nanoflow liquid

chromatography nanospray ionization tandem mass spectrometry. *J. Chromatogr. A 1322*, 69-73.

307. Hang, B. (2010) Formation and repair of tobacco carcinogen-derived bulky DNA adducts. *J. Nucleic Acids 2010*, 709521.

308. Gaikwad, N. W., Yang, L., Weisenburger, D. D., Vose, J., Beseler, C., Rogan, E. G., and Cavalieri, E. L. (2009) Urinary biomarkers suggest that estrogen-DNA adducts may play a role in the aetiology of non-Hodgkin lymphoma. *Biomarkers 14*, 502-512.

309. Nair, J., Nair, U. J., Sun, X., Wang, Y., Arab, K., and Bartsch, H. (2011) Quantifying etheno-DNA adducts in human tissues, white blood cells, and urine by ultrasensitive (32)P-postlabeling and immunohistochemistry. *Methods Mol. Biol. 682*, 189-205.

310. Peters, S., Talaska, G., Jonsson, B. A., Kromhout, H., and Vermeulen, R. (2008) Polycyclic aromatic hydrocarbon exposure, urinary mutagenicity, and DNA adducts in rubber manufacturing workers. *Cancer Epidemiol. Biomarkers Prev. 17*, 1452-1459.

311. Mikes, P., Korinek, M., Linhart, I., Krouzelka, J., Dabrowska, L., Stransky, V., and Mraz, J. (2010) Urinary N3 adenine DNA adducts in humans occupationally exposed to styrene. *Toxicol. Lett. 197*, 183-187.

312. Thornton-Manning, J. R., Dahl, A. R., Bechtold, W. E., Griffith, W. C., Jr., Pei, L., and Henderson, R. F. (1995) Gender differences in the metabolism of 1,3-

butadiene in Sprague-Dawley rats following a low level inhalation exposure. *Carcinogenesis 16*, 2875-2878.

313. Adam, T., Mitschke, S., Streibel, T., Baker, R. R., and Zimmermann, R. (2006) Puff-by-puff resolved characterisation of cigarette mainstream smoke by single photon ionisation (SPI)-time-of-flight mass spectrometry (TOFMS): comparison of the 2R4F research cigarette and pure Burley, Virginia, Oriental and Maryland tobacco cigarettes. *Anal. Chim. Acta 572*, 219-229.

314. Talhout, R., Opperhuizen, A., and van Amsterdam, J. G. (2006) Sugars as tobacco ingredient: Effects on mainstream smoke composition. *Food Chem. Toxicol. 44*, 1789-1798.

315. Marian, C., O'Connor, R. J., Djordjevic, M. V., Rees, V. W., Hatsukami, D. K., and Shields, P. G. (2009) Reconciling human smoking behavior and machine smoking patterns: implications for understanding smoking behavior and the impact on laboratory studies. *Cancer Epidemiol. Biomarkers Prev. 18*, 3305-3320.

316. Burns, D. M., Dybing, E., Gray, N., Hecht, S., Anderson, C., Sanner, T., O'Connor, R., Djordjevic, M., Dresler, C., Hainaut, P., Jarvis, M., Opperhuizen, A., and Straif, K. (2008) Mandated lowering of toxicants in cigarette smoke: a description of the World Health Organization TobReg proposal. *Tob. Control 17*, 132-141.

317. Esmer, C., Sanchez, S., Ramos, S., Molina, B., Frias, S., and Carnevale, A. (2004) DEB test for Fanconi anemia detection in patients with atypical phenotypes. *Am. J. Med. Genet. A 124A*, 35-39.

318. Wu, Q., Wu, D., Shen, Z., Duan, C., and Guan, Y. (2013) Quantification of endogenous brassinosteroids in plant by on-line two-dimensional microscale solid phase extraction-on column derivatization coupled with high performance liquid chromatography-tandem mass spectrometry. *J. Chromatogr. A 1297*, 56-63.

319. Gifford, I., Vreeland, W., Grdanovska, S., Burgett, E., Kalinich, J., Vergara, V., Wang, C. K., Maimon, E., Poster, D., and Al Sheikhly, M. (2014) Liposome-based delivery of a boron-containing cholesteryl ester for high-LET particle-induced damage of prostate cancer cells: a boron neutron capture therapy study. *Int. J. Radiat. Biol. 90*, 480-485.

320. Svantesson, E., Capala, J., Markides, K. E., and Pettersson, J. (2002) Determination of boron-containing compounds in urine and blood plasma from boron neutron capture therapy patients. The importance of using coupled techniques. *Anal. Chem. 74*, 5358-5363.

321. Zhang, Q., Tang, N., Brock, J. W., Mottaz, H. M., Ames, J. M., Baynes, J. W., Smith, R. D., and Metz, T. O. (2007) Enrichment and analysis of nonenzymatically glycated peptides: boronate affinity chromatography coupled with electron-transfer dissociation mass spectrometry. *J. Proteome. Res. 6*, 2323-2330.

322. Wright, J. L. and Churg, A. (2010) Animal models of cigarette smoke-induced chronic obstructive pulmonary disease. *Expert. Rev. Respir. Med. 4*, 723-734.

323. Vlahos, R. and Bozinovski, S. (2014) Recent advances in pre-clinical mouse models of COPD. *Clin. Sci. (Lond) 126*, 253-265.

324. Goldklang, M. P., Marks, S. M., and D'Armiento, J. M. (2013) Second hand smoke and COPD: lessons from animal studies. *Front Physiol 4*, 30.

325. Rinaldi, M., Maes, K., De Vleeschauwer, S., Thomas, D., Verbeken, E. K., Decramer, M., Janssens, W., and Gayan-Ramirez, G. N. (2012) Long-term nose-only cigarette smoke exposure induces emphysema and mild skeletal muscle dysfunction in mice. *Dis. Model. Mech. 5*, 333-341.

326. Jardim, J. R., Bizeto, L., Fleig, M. A., Camelier, A., Rosa, F. W., Oliveira, D., Azevedo, D., Saldiva, P. H., Martins, M. A., Bonassa, J., and Nascimento, O. A. (2010) [An inhalation chamber model for controlled studies of tobacco smoke toxicity in rodents]. *Arch. Bronconeumol. 46*, 455-458.

327. Kalow, W. and Tang, B. K. (1991) Caffeine as a metabolic probe: exploration of the enzyme-inducing effect of cigarette smoking. *Clin. Pharmacol. Ther. 49*, 44-48.

328. Zevin, S. and Benowitz, N. L. (1999) Drug interactions with tobacco smoking. An update. *Clin. Pharmacokinet. 36*, 425-438.

329. Molinspiration cheminformatics online tool for LogP prediction, *http://www.molinspiration.com/cgi-bin/properties (Accessed October 2nd, 2014)*.

330. Pyka, A., Babuska, M., and Zachariasz, M. (2006) A comparison of theoretical methods of calculation of partition coefficients for selected drugs. *Acta Pol. Pharm. 63*, 159-167.

331. (1993) NTP Toxicology and Carcinogenesis Studies of 1,3-Butadiene (CAS No. 106-99-0) in B6C3F1 Mice (Inhalation Studies). *Natl. Toxicol. Program. Tech. Rep. Ser. 434*, 1-389.

332. (2014) Environmental Protection Agency (EPA) Air Resources Board and Office of Environmental Health Hazard Assesment (OEHHA): Proposed Identification of 1,3-Butadiene as a Toxic Air Contaminant, http://oehha.ca.gov/air/toxic_contaminants/html/1,3-Butadiene.htm. (Accessed Sept 29, 2014).